Uniwersytet Łódzki

Wydział Chemii

Katedra Chemii Nieorganicznej i Analitycznej

Zakład Elektroanalizy i Elektrochemii

Zespół Electrochemistry@Soft Interfaces (E@SI)

Reakcje polikondensacji prowadzone na spolaryzowanych granicach fazowych typu ciecz – ciecz

Karolina Anna Kowalewska

ROZPRAWA DOKTORSKA

Promotor: ***dr hab. Łukasz Półtorak, prof. UŁ***

Promotor pomocniczy: ***dr Karolina Kwaczyński***

Łódź 2023

PODZIĘKOWANIA

*Składam serdeczne podziękowania mojemu promotorowi **dr hab. Łukaszowi Półtorakowi, prof. UŁ** za okazaną pomoc naukową, opiekę i poświęcony czas w trakcie moich studiów doktoranckich. Wyrażam głęboką wdzięczność za bezgraniczną wyrozumiałość oraz empatię, dzięki czemu możliwe było dzielenie roli mamy z realizacją pracy doktorskiej. Dodatkowo dziękuję za naukowe inspiracje, cenne wskazówki, motywację i ogromną możliwość rozwoju.*

*Chciałabym również podziękować mojej promotorce pomocniczej **dr Karolinie Kwaczyński** za współpracę naukową, pomoc udzieloną w trakcie przygotowywania niniejszej rozprawy doktorskiej, wszystkie rady, cierpliwość, uśmiech i dodawanie otuchy w trudnych chwilach.*

*Dziękuje **prof. dr hab. Sławomirze Skrzypek** za umożliwienie realizacji studiów doktoranckich z dzieleniem roli mamy, otwartość, życzliwość i wiarę w moje możliwości.*

*Wyrazy podziękowania kieruje również dla całego zespołu **Electrochemistry@Soft Interfaces** (E@SI), w którym miałam zaszczyt pracować. Dziękuję za życzliwość, ciepłą atmosferę i okazaną pomoc.*

*Szczególne podziękowania kieruję mojej rodzinie, bez której nie byłoby możliwe zrealizowanie niniejszej rozprawy doktorskiej. Dziękuję za nieocenioną pomoc w opiece nad moimi dziećmi oraz okazane wsparcie: moim rodzicom **Magdalenie i Tomaszowi,** dziadkom **Annie i Tadeuszowi,** teściom **Beacie i Krzysztofowi** oraz cioci **Stasi**.*

*Dziękuje mojemu mężowi **Damianowi** za miłość, wiarę we mnie, okazane wsparcie, wyrozumiałość i pomoc, na którą zawsze mogę liczyć.*

Niniejszą rozprawę doktorską dedykuję moim wspaniałym synom

Wiktorowi i Szymonowi

SPIS TREŚCI

ABSTRACT

The subject of this doctoral thesis concerns the study and analysis of polycondensation reactions occurring at the polarized liquid-liquid interfaces. Concerned thesis is based on research results published in four scientific articles from the JCR list and one article which is published in chemical repository and also being submitted to the JCR journal. The theoretical part concerning the electrochemistry of soft junctions was prepared on the basis of the author's chapter in the monograph published in the journal Wiadomości Chemiczne.

The subject of this work is focused on possibilities to electrochemical control the interfacial polycondensation reactions at polarized liquid-liquid interfaces, this is, the synthesis of polyamide materials, and their further interfacial (and electrochemically controlled) modification with metallic nanoparticles. In addition, the formation of titanium dioxide at the electrified liquid-liquid interface and electroanalytical studies of interfacial behaviour of five carbosilane dendrimers were tested and described in this work.

The starting point of the experimental part of this work were the studies focused on the electrochemically controlled synthesis of nylon-6,6 at the polarized liquid-liquid interface. This material was successfully obtained in an electrochemically controlled manner, and further modified with silver-based nanoparticles via heterogenous interfacial electron transfer reaction between metal precures from the aqueous phase and electron donor from the organic phase. By developing a general mechanism for the synthesis of polyamides at polarized liquid-liquid interfaces, five other materials were produced in an electrochemically controlled manner. Using the miniaturized ITIES system, the synthesized polyamides were characterized in terms of their molecular screening properties.

Also, the dendrimers were supposed to be used to induce porosity of titanium dioxide during its interfacial polycondensation at the electrified liquid-liquid interface. Unfortunately, the expected results were not achieved. Electrochemical control of the

titanium dioxide formation at the electrified liquid-liquid interface failed. However, interesting results were obtained pertaining to dendrimers electroanalytical behaviour and characterization of the liquid-liquid interface modified with titanium dioxide. Obtained results were published in Analyst, and Materials, respectively.

LISTA SKRÓTÓW

AC – chlorek adypoilu

BDTR-2; BDTR-5 – dendrymer należący do generacji G1; G3

BTPPA^{+}TPBCl^{-} – tetrakis(4-chlorofenylo)boran bis(trifenylofosforanodiylo)amoniowy

1,2-DCE – 1,2-dichloroetan

1,6-DAH – 1,6-heksanodiamina

EDX – spektroskopia rentgenowska z dyspersją energii

IR – spektroskopia w podczerwieni

ITV – woltamperometria przeniesienia jonu

TBOT – tetrabutoksytytan

TMA^{+} - kation tetrametyloamoniowy

TPhAs^{+}TPhB^{-} – tetrafenyloboran tetrafenyloarseniowy

SEM – skaningowa mikroskopia elektronowa

Autoreferat

TEMATYKA, HIPOTEZA I CEL BADAŃ

Tematyka niniejszej pracy doktorskiej dotyczy badania i analizy reakcji polikondensacji międzyfazowej kontrolowanych elektrochemicznie na spolaryzowanych granicach fazowych typu ciecz – ciecz. Postawiono pięć hipotez, które zostały przedstawione w formie schematu na **Rysunku 1**. Wyniki badań uzyskane w trakcie doktoratu pozwoliły na ich weryfikacje tzn. potwierdziły trzy, a pozostałe dwie hipotezy zostały obalone.

Rysunek 1. Hipotezy pracy doktorskiej (✓ - potwierdzone, × - obalone).

Głównym celem pracy było wykorzystanie spolaryzowanych granic cieczowych do elektrochemicznego kontrolowania reakcji polikondensacji międzyfazowej. Pierwszym obiektem badań był popularny w przemyśle tekstylnym Nylon-6,6. Do wytworzenia tego poliamidu zastosowano układ spolaryzowanych granic cieczowych, które wykorzystano do przeprowadzenia reakcji polikondensacji zachodzącej pomiędzy 1,6-heksanodiaminą (1,6-DAH) rozpuszczoną w fazie wodnej

z chlorkiem adypoilu (AC) będącego roztworem 1,2-dichloroetanu (faza organiczna). Uzyskane wyniki posłużyły jako badania wstępne do przygotowania wniosku w konkursie Preludium – 19 organizowanym przez Narodowe Centrum Nauki. Dzięki przyznanemu finansowaniu (UMO-2020/37/N/ST4/00270) możliwe było przeprowadzenie badań mających na celu syntezę innych materiałów poliamidowych na spolaryzowanych granicach cieczowych (w układach makro- i mikroskopowych), a także modyfikowanie syntezowanych poliamidów nanocząstkami metalicznymi.

Dendrymery to polimery, które ze względu na rozgałęzioną budowę cząsteczki zawierającą wiele różnych grup funkcyjnych (np. aminowych), są wykorzystywane np. w medycynie jako nośniki leków. Posiadają one zdolność do enkapsulacji różnych substancji bez wchodzenia z nimi w reakcję chemiczną. W niniejszej pracy zostało przebadanych pięć różnych dendrymerów karbosilanowych na spolaryzowanych granicach cieczowych. Badania te miały umożliwić zastosowanie ich do indukowania porowatości ditlenku tytanu na granicy fazowej typu ciecz – ciecz. W trakcie prowadzonych eksperymentów wykazano, że niemożliwe jest elektrochemiczne kontrolowanie reakcji polikondensacji międzyfazowej ditlenku tytanu ze względu na jego właściwości fotoelektrochemiczne związane z absorpcją światła oraz spontaniczność zachodzących reakcji. Ditlenek tytanu wytwarzany na granicy fazowej typu ciecz-ciecz jak i zachowanie międzyfazowe dendrymerów karbosilanowych zostało scharakteryzowane przy użyciu technik elektrochemicznych.

ELEKTROCHEMIA GRANIC FAZOWYCH TYPU CIECZ - CIECZ

1. Wstęp

Elektrochemia granic fazowych pomiędzy niemieszającymi się roztworami elektrolitów (z ang. Electrochemistry at the **I**nterface between **T**wo **I**mmiscible **E**lectrolyte **S**olutions, **ITIES**) jest działem elektrochemii, w którym ciekłe granice fazowe są polaryzowane w sposób jonowy. Układy te pozwalają na badanie mechanizmów międzyfazowego przejścia jonów, elektronu, adsorpcji jonów i cząsteczek dipolowych, a także wszystkich tych procesów jednocześnie. Układ spolaryzowanych granic cieczowych lub spolaryzowanych granic fazowych typu ciecz – ciecz dostarcza szerokie spektrum możliwości badania zjawisk przenoszenia ładunku przez granicę pomiędzy dwoma niemieszającymi się fazami pod wpływem przyłożonego potencjału. Pierwsze doniesienia literaturowe opisujące tą tematykę badawczą datuje się na lata 70-te ubiegłego wieku, kiedy zespół Calude'a Gavach'a z Francji opublikował pracę opisującą zjawiska zachodzące w obszarze międzyfazowym.[1,2] Praca ta była „iskrą" rozpalającą zainteresowanie kolejnych naukowców tematem miękkich i polaryzowalnych granic fazowych, jak na przykład prof. Koryta (w tych czasach) z Czechosłowacji.[3] Spolaryzowane granice cieczowe do dnia dzisiejszego przyciągają zainteresowanie badaczy, ponieważ uznawane są jako środowisko wolne od defektów mechanicznych, stabilne i odporne na uszkodzenia. Podział związków w układzie ITIES następuje ze względu na ich powinowactwo do danej fazy, a granica faz może przyjmować dowolny kształt w zależności od zastosowanego naczynka pomiarowego. Niewątpliwą zaletą tego układu jest możliwość badania zjawisk międzyfazowych wszystkimi dostępnymi technikami elektrochemicznymi. Spolaryzowane granice fazowe typu ciecz – ciecz znalazły szereg zastosowań m.in w chemii materiałów, analityce chemicznej, naukach o polimerach, farmacji, fizykochemii membran czy w chemii koloidów.

Granica między dwoma niemieszającymi się roztworami elektrolitów jest nazywana również miękką granicą fazową, która posiada charakter molekularny i heterogeniczny, a także umożliwia podział reagentów ze względu na ich lipofilowość.[4]

Tworzy się przez kontakt dwóch faz – hydrofilowej i hydrofobowej. Najczęściej, pierwszą fazę stanowią roztwory wodne soli takich jak np. chlorek sodu (NaCl), chlorek potasu (KCl) czy chlorek litu (LiCl). Natomiast fazę hydrofobową, czyli organiczną tworzą sole takie jak tetrakis(4-chlorofenylo)boran bis(trifenylofosforanodiylo)amoniowy ($BTPPA^+TPBCl^-$) lub tetrafenyloboran tetrafenyloarseniowy ($TPhAs^+TPhB^-$), które rozpuszczone są w polarnym rozpuszczalniku organicznym takim jak np. 1,2-dichloroetan (1,2-DCE), nitrobenzen lub 1,2-dichlorobenzen.[5–7] Przykładowy układ dwóch elektrolitów tworzących ITIES przedstawiony jest na **Rysunku 2**.

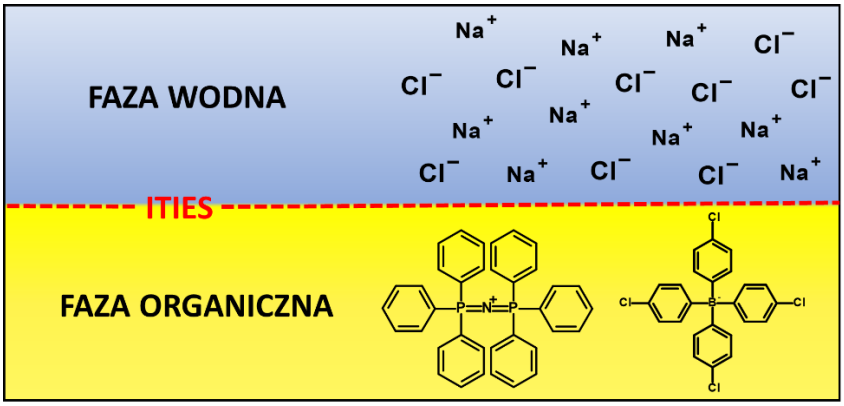

Rysunek 2. Przykład utworzenia ITIES poprzez kontakt wodnego roztworu NaCl i soli $BTPPA^+TPBCl^-$ rozpuszczonej w fazie organicznej.

2. Zjawiska zachodzące na spolaryzowanej granicy cieczowej

Utworzona spolaryzowana granica cieczowa pozwala na badanie zjawisk, przemian i reakcji chemicznych pod wpływem przyłożonej różnicy potencjału Galvaniego. Wyróżniamy trzy podstawowe typy reakcji przenoszenia ładunku przez granicę faz typu ciecz – ciecz (**Rys. 3**):

a) Transfer jonu A_i^z obecnego w fazie wodnej (*i* = aq) do fazy organicznej (*i* = org) lub z fazy organicznej *(i* = org) do fazy wodnej (*i* = aq).

$$A_{aq}^{+} \leftrightarrow A_{org}^{+}$$

b) Transfer elektronu pomiędzy dwoma parami redoks (hydrofilowa para redoks obecna w fazie wodnej i hydrofobowa para redoks obecna w fazie organicznej):

$$O_{x_1}(aq) + Red_2(org) \leftrightarrow Red_1(aq) + O_{x_2}(org)$$

c) Międzyfazowa wspomagana reakcja przeniesienia jonów – przejście jonu, który posiada zdolność tworzenia kompleksu z ligandem obecnym w tej samej fazie lub oddzielonego przez granicę fazową ciecz – ciecz. Wyróżniamy cztery mechanizmy zachodzące w tym typie reakcji:

- **ACT** (z ang. *Aqueous Complexation followed by Transfer*) – transfer kompleksu utworzonego w fazie wodnej.
- **TOC** (z ang. *Transfer to Organic phase followed by Complexation*) – transfer jonu z fazy wodnej do fazy organicznej, a następnie utworzenie kompleksu.
- **TIC** (z ang. *Transfer by Interfacial Complexation)* – przeniesienie przez kompleksowanie międzyfazowe.
- **TID** (z ang. *Transfer by Interfacial Dissociation)* – przeniesienie jonu z fazy organicznej do wodnej w wyniku dysocjacji kompleksu.[8,9]

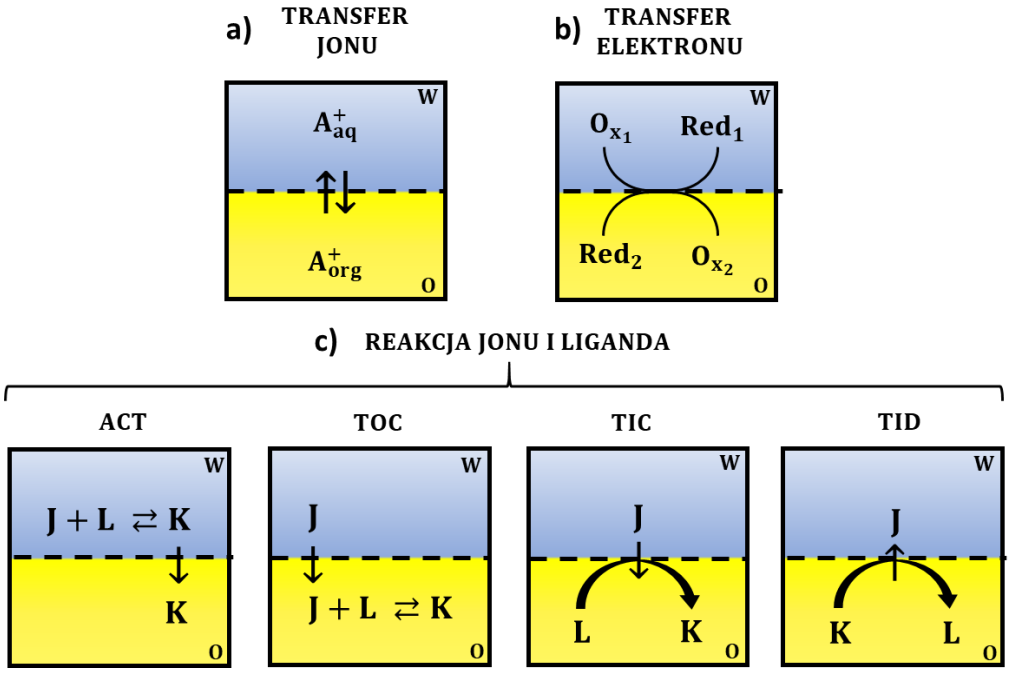

Rysunek 3. Mechanizmy przenoszenia ładunku przez spolaryzowaną granice fazową typu ciecz – ciecz. **W** – faza wodna, **O** – faza organiczna, $A^+_{org/aq}$ - jon obecny w fazie organicznej bądź wodnej, Ox_1, Ox_2, Red_1, Red_2 – dwie pary redoks, **J** – jon, **L** – ligand, **K** – kompleks.

Podstawowym wymiarem ITIES jest skala makroskopowa, gdzie stosuje się roztwory o objętości mililitrów. Badania w tej skali przeprowadza się w przystosowanym

naczynku woltamperometrycznym (**Rys. 5**) wyposażonym w dwie kapilary Ługgina. Stosując układ ITIES możemy również dążyć do wielkości mikro/nanometrycznych. Do ich tworzenia wykorzystuje się szklane kapilary utworzone najczęściej poprzez ciągnięcie rozgrzanych w ogniu palnika szklanych pipet czy kapilar o grubych ściankach z zatopionym drutem metalowym, który następnie rozpuszcza się w odpowiednio dobranej mieszaninie kwasów. Przykładem może być drut np. miedziany, który rozpuszcza się w wodzie królewskiej pozostawiając po sobie otwór (por) o określonej średnicy, który staje się mikro – granicą cieczową. Stosowane są również kapilary z dwoma porami lub z wytworzonymi mikro- i nanogranicami poprzez emulsyfikację w wyniku intensywnego mieszania.[9,10] W celu wytworzenia zminiaturyzowanego systemu ITIES można wykorzystać komercyjnie dostępne kapilary krzemionkowe o średnicy wewnętrznej od 5 do 25 µm zatapiając ją w końcówce od mikropipety automatycznej.[11] Innym rozwiązaniem jest wykorzystanie membran polimerowych czy membran z włókna szklanego. Zminiaturyzowane granice fazowe ciecz – ciecz pociągają za sobą szereg zalet m.in. większa stabilność ITIES w porównaniu do skali makroskopowej oraz małe zużycie toksycznych odczynników chemicznych.

3. Modyfikacje granic fazowych typu ciecz – ciecz

Nie tylko zmiana skali układu ma wpływ na wyniki prowadzonych badań, ale również zastosowana modyfikacja spolaryzowanych granic cieczowych, która otwiera możliwości poszukiwania nowych zastosowań np. w przemyśle czy medycynie. Wyróżniamy trzy główne mechanizmy modyfikacji (**Rys. 4**):

- **Modyfikacja *in situ* (I)**

(**A**) międzyfazowy transfer jonu – pod wpływem przyłożonej różnicy potencjałów kation obecny w fazie organicznej (A^+_{org}) zostaje przeniesiony do fazy wodnej (A^+_{aq}), gdzie w wyniku reakcji z obecnym tam anionem (B^-_{aq}) wytrąca się produkt w postaci osadu (C_{ITIES}). Przykładem takiej reakcji może być krzemionka otrzymana w sposób kontrolowany elektrochemicznie.[12,13]

(**B**) międzyfazowe przeniesienie elektronu prowadzące do otrzymania nanocząstek metalicznych w wyniku reakcji redoks.

(**C**) powstanie na granicy fazowej ciecz – ciecz fizycznego produktu (osad, materiał polimerowy) w wyniku reakcji pomiędzy dwoma reagentami znajdującymi się w odrębnych fazach.

- **Modyfikacja zachodząca na drodze „samoorganizacji" (II)**

Materiały osadzają się na spolaryzowanej granicy faz typu ciecz – ciecz w wyniku ich samoorganizacji. Proces ten jest często kontrolowany również elektrochemicznie.

- **Modyfikacja *ex situ* (III)**

Modyfikatorami spolaryzowanej granicy cieczowej są membrany przygotowane poza układem pomiarowym. Mogą one mieć liczne lub pojedyncze pory o przypadkowym lub uporządkowanym rozmieszczeniu. Najczęściej używane w układzie ITIES są membrany z włókna szklanego, zeolitowe lub polietylenowe.[14]

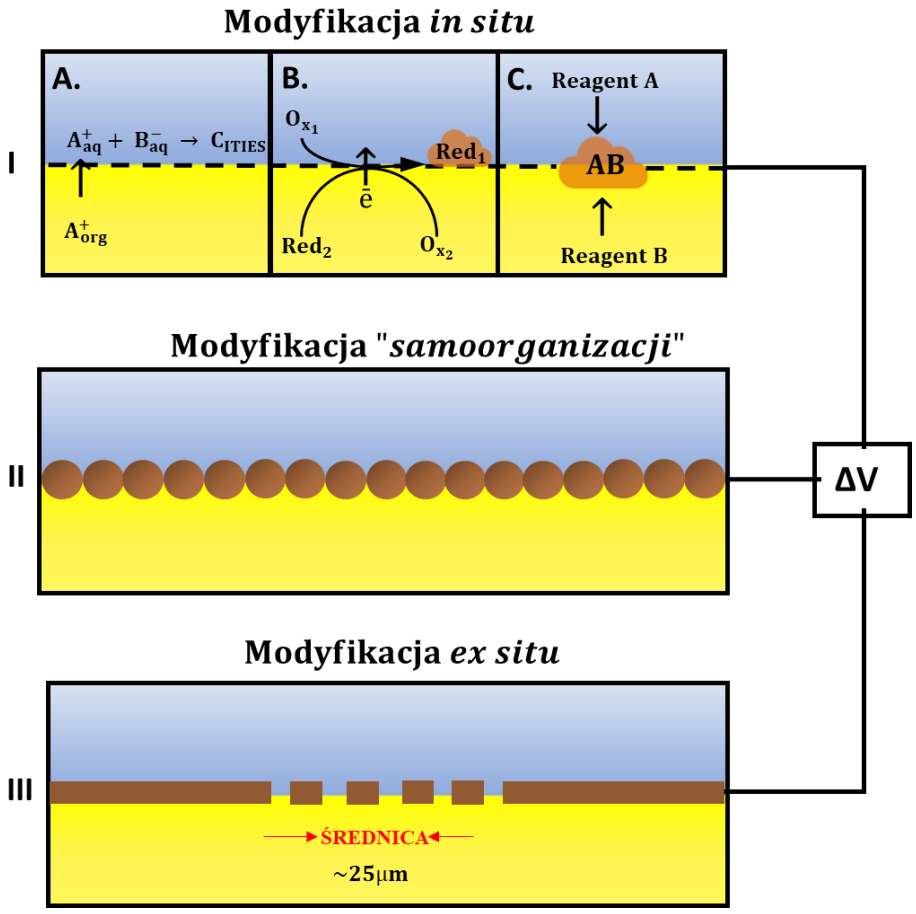

Rysunek 4. Sposoby modyfikacji spolaryzowanych granic cieczowych. $A^+_{org/aq}$ = kation fazy organicznej/wodnej, B^-_{aq} = anion fazy wodnej, C_{ITIES} = modyfikator eLLI, $Ox_{1,2}$ = utleniacz, $Red_{1,2}$= reduktor, AB – wytworzony materiał.

Przykłady literaturowe modyfikacji spolaryzowanych granic cieczowych:

- **Modyfikacje amfifilami**

Amfifile są to długołańcuchowe związki posiadające zdolności powierzchniowo czynne, które są jedną z głównych sił napędowych „samoorganizacji". W swojej budowie posiadają części polarne i niepolarne przez co niecałkowicie rozpuszczają się w dwóch różnych rozpuszczalnikach (wodnym i organicznym) powodując tworzenie się pojedynczych warstw pomiędzy dwoma niemieszającymi się ze sobą fazami lub agregatów w roztworze homogenicznym. Przykładami takich związków są między innymi kwasy tłuszczowe, fosfolipidy czy białka.[15] Nowe właściwości spolaryzowanych granic fazowych typu ciecz – ciecz można uzyskać w sposób elektrochemicznie kontrolowany wykorzystując do tego modyfikację na drodze „samoorganizacji". Przykładem może być międzyfazowe osadzanie białek[16,17], dendrymerów[18], surfaktanów[19] czy fosfolipidów[20], które adsorbują się do granicy cieczowej w wyniku przyłożonej różnicy potencjałów (warunkiem koniecznym jest występowanie badanych związków w postaci jonowej).

- **Modyfikacje polimerami**

Synteza poliamidów na spolaryzowanych granicach fazowych typu ciecz – ciecz wpisuje się w sposób modyfikacji *in situ*. Polimery te powstają na skutek zachodzącej reakcji polikondensacji międzyfazowej, podczas której monomery rozpuszczone w odrębnych fazach reagują ze sobą tworząc produkt na ich styku.[21] Istnieje niewiele doniesień literaturowych z zakresu elektrochemii spolaryzowanych granic cieczowych dotyczących przeprowadzania reakcji polimeryzacji. Zespół prof. Cunnana opublikował kilka prac dotyczących międzyfazowej syntezy oligomerów metylowych i fenylowo-pirolowych oraz elektropolimeryzacji 2,2':5',2''-tertiofenu, gdzie reakcja była każdorazowo zainicjowana elektrochemicznie poprzez międzyfazowy transport elektronu.[22,23]

- **Modyfikacje nanocząstkami metalicznymi**

Synteza nanocząstek metalicznych odbywa się *in situ* w wyniku międzyfazowego przeniesienia elektronu w reakcji redoks. Nanocząstki można otrzymać poprzez redukcję

soli metali rozpuszczonych w fazie wodnej w obecności reduktora w fazie organicznej. Proces ten może być kontrolowany elektrochemicznie przy zastosowaniu spolaryzowanych granic fazowych typu ciecz – ciecz. Przykładem modyfikacji jest osadzanie nanocząstek metali np. palladu, złota czy srebra.[24–26]

STOSOWANA APARATURA I TECHNIKI POMIAROWE

1. Elektrochemiczne układy pomiarowe

UKŁAD MAKROSKOPOWY

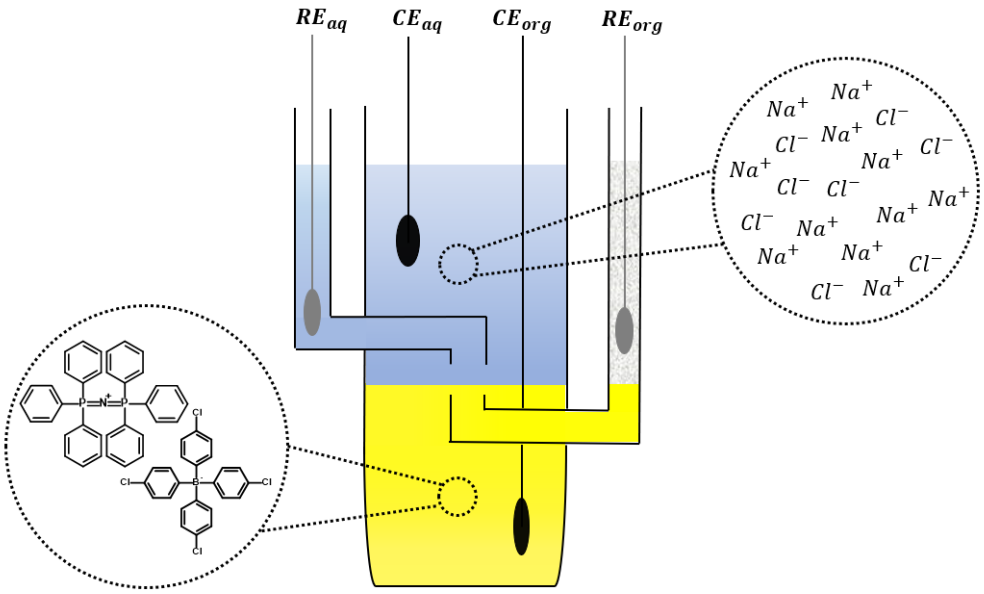

Rysunek 5. Schemat naczynka woltamperometrycznego do badań makroskopowych granic fazowych typu ciecz-ciecz wyposażone w dwa zestawy elektrod. Re_{aq}; Re_{org} – elektrody odniesienia, drucik Ag/AgCl lub Ag/$AgSO_4$; Ce_{aq}; Ce_{org}– elektrody platynowa.

Układem pomiarowym stosowanym do badań makroskopowych granic cieczowych jest naczynko woltamperometryczne (średnica wewnętrzna 0,7 cm) z dwiema kapilarami Ługgina, które przedstawiono na **Rysunku 5**. Wyposażone w zestaw elektrod składających się z dwóch elektrod odniesienia – chlorosrebrowych[27–29] (Ag/AgCl, użyty drut srebrny posiadał czystość wynoszącą 99,99%, Alfa Aesar, Niemcy) lub siarczanowosrebrowych[30] (Ag/$AgSO_4$, użyty drut srebrny posiadał czystość wynoszącą 99,99%, 99,99%, Alfa Aesar, Niemcy), służących do kontrolowania spadku potencjału na styku dwóch faz oraz dwóch elektrod pomocniczych – platynowych (Pt, 99,9%, Sigma Aldrich, Niemcy), przez które przepływa prąd w trakcie trwania pomiarów. Na **Rysunku 5** zaznaczono na żółto fazę organiczną, którą stanowi hydrofobowa sól

rozpuszczona w rozpuszczalniku organicznym, a na niebiesko fazę wodną zawierająca hydrofilową sól.

Taki układ podłączany był do potencjostatu – galwanostatu rejestrującego sygnały elektrochemiczne pochodzące od przejścia aktywnych jonów przez miękką granicę wytworzoną pomiędzy dwoma niemieszającymi się ze sobą fazami.[31]

UKŁAD MIKROSKOPOWY

W badaniach do niniejszej pracy doktorskiej wykorzystano dwa rodzaje układów zminiaturyzowanych granic fazowych typu ciecz – ciecz. Pierwszym z nich jest system opierający się na zastosowaniu szklanej rurki z przyklejoną za pomocą kleju poliamidowego na gorąco odpowiednio dociętej membrany z włókna szklanego (średnica: 47,00mm, grubość: 0,2mm, Ahlstrom Munksjo).[29,30] Po wyschnięciu kleju kapilara została wypełniona fazą organiczną i zanurzona w fazie wodnej. Schemat przygotowania takiego układu przedstawiony jest na **Rysunku 6**. W tym przypadku zminiaturyzowaną granicę fazową ciecz – ciecz stanowiły losowo rozmieszczone pory membrany o wielkościach mikrometrycznych.

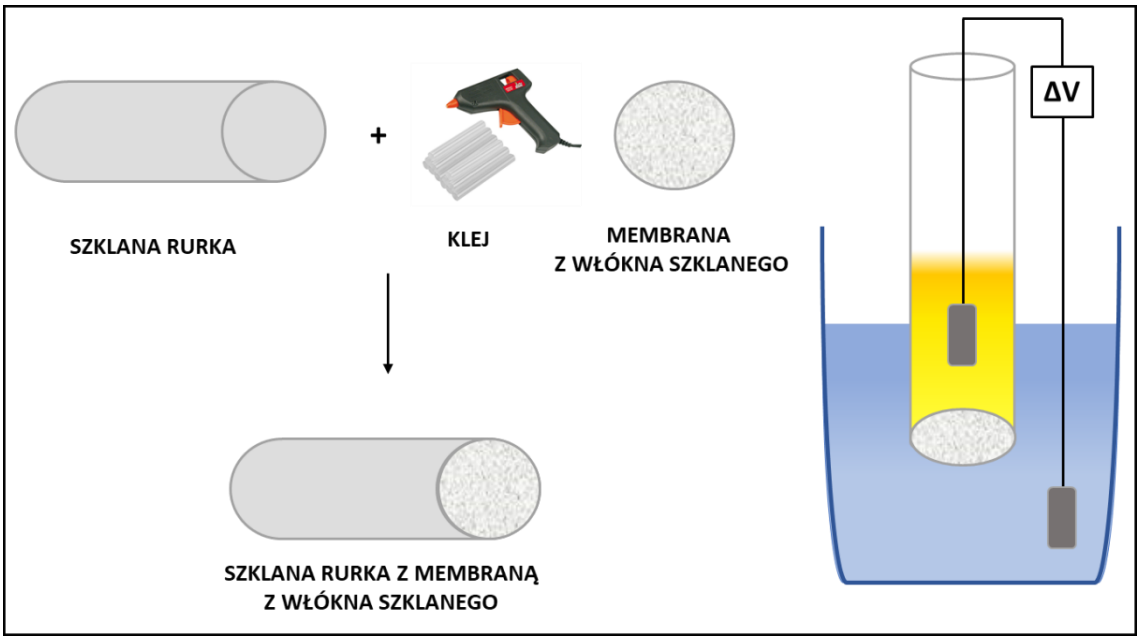

Rysunek 6. Zminiaturyzowana granica cieczowa stworzona przy użyciu szklanek rurki i przyklejonej do jej końca membrany z włókna szklanego.

Drugi układ mikroskopowy wykorzystywany w badaniach został wytworzony przy użyciu końcówki polipropylenowej do mikropipety automatycznej o pojemności 10 µL oraz kapilary krzemionkowej o średnicy 25 µm (VWR).[27,32] Przygotowanie takiego systemu polegało na umieszczeniu niewielkiego kawałka kapilary krzemionkowej odciętej nożykiem ceramicznym w końcówce od mikropipety, a następnie zatopienie jej w płomieniu palnika (**Rys. 7 A**). Po zastygnięciu wystający nadmiar kapilary odcięto przy użyciu nożyka ceramicznego (**Rys. 7 B**). Tak stworzony system wypełniono fazą organiczną i zanurzono w fazie wodnej (**Rys. 7 C**).

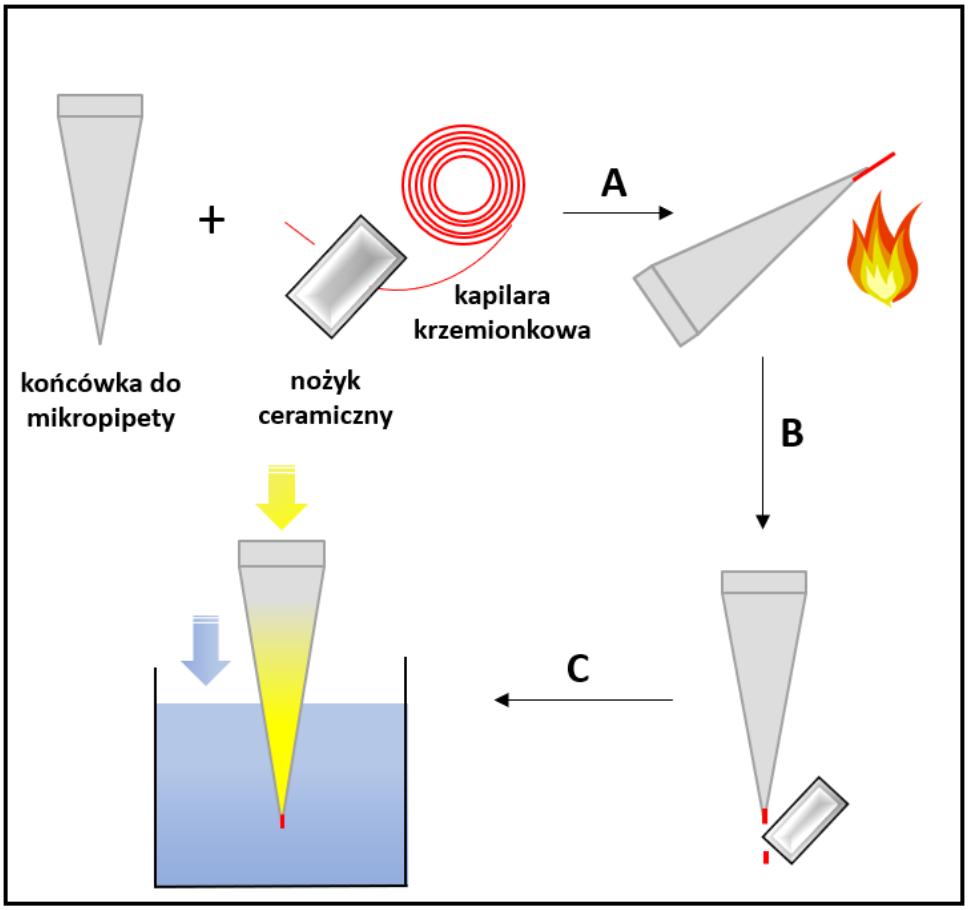

Rysunek 7. Zminiaturyzowana granica cieczowa (mikroITIES) stworzona przy użyciu polipropylenowej końcówki od pipety automatycznej z zatopioną kapilarą krzemionkową.

2. Woltamperometria przeniesienia jonu

Techniką wykorzystaną do badania zjawisk międzyfazowych w układzie ITIES była woltamperometria przeniesienia jonu (ITV – ang. ***I**on **T**ranfer **V**oltammetry*). Różnicę potencjału Galvaniego przy którym jony ulegają przenoszeniu przez spolaryzowaną granicę cieczową oblicza się w oparciu o wzór:

$$\Delta E = \Delta^{aq}_{org}\phi + \Delta^{aq}_{org}\phi^{0}_{TMA^{+}}$$

Gdzie:

ΔE – różnica potencjałów przykładana z zewnętrznego źródła polaryzacji,

$\Delta^{aq}_{org}\phi$ – różnica potencjałów Galvaniego pomiędzy fazą wodną, a fazą organiczną,

$\Delta^{aq}_{org}\phi^{0}_{TMA^{+}}$ – potencjał odniesienia równy standardowemu potencjałowi transferu jonu modelowego TMA^{+} ($\Delta^{aq}_{org}\phi^{0}_{TMA^{+}}$= 160mV).

Opierając się na podstawie powyższej zależności przedstawiono na **Rysunku 8** przykładowy woltamperogram cykliczny zarejestrowany dla jonu modelowego czwartorzędowej tetrametyloaminy (TMA^{+}). Wyróżnia się na nim trzy charakterystyczne obszary: (**I,III**) prądy graniczne i (**II**) okno potencjału, w którym obserwuje się sygnały elektrochemiczne pochodzące od przejścia elektrochemicznie aktywnego jonu przez spolaryzowaną granicę cieczową.

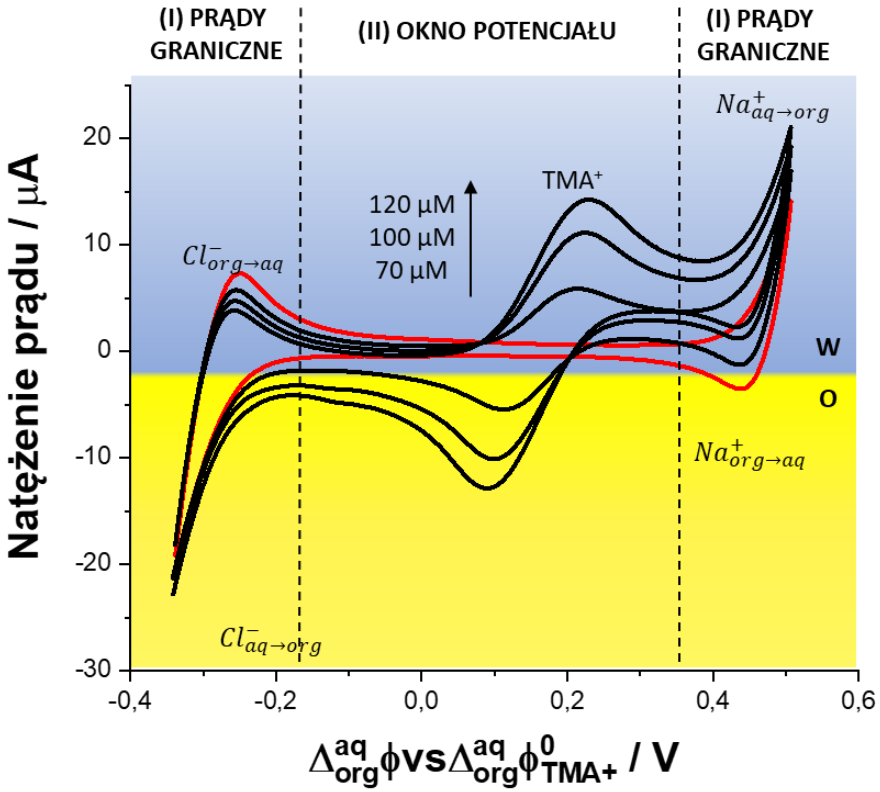

Rysunek 8. Woltamperogram cykliczny zarejestrowany dla wzrastających stężeń jonu modelowego TMA^+. **(W)** Faza wodna: 10 mM NaCl w H_2O **(O)** Faza organiczna: 5 mM $BTPPA^+TPBCl^-$ w 1,2-DCE.

Na powyższym wykresie widoczne są prądy dodatnie i prądy ujemne. Na czerwono została zaznaczona krzywa zarejestrowana dla ślepej próby w 10 mM roztworze NaCl. Prądy dodatnie w obszarze prądów granicznych dla bardziej dodatnich potencjałów dotyczą przeniesienia kationu Na^+ z fazy wodnej do fazy organicznej, natomiast w obszarze prądów granicznych po lewej stronie zestawionego woltamperogramu pochodzą od przejścia anionu Cl^- z fazy organicznej do wodnej. Ujemne prądy, przez analogie, odnoszą się do przejścia kationu Na^+ z fazy organicznej do fazy wodnej (sygnał rejestrowany przy ok 0,4V) i anionu Cl^- z fazy wodnej do organicznej (spadek prądu dla potencjałów niższych od -0,2V). Pomiędzy prądami granicznymi znajduje się okno potencjału, w którym widoczny jest sygnał pochodzący od badanego związku (TMA^+). Dla krzywej czerwonej, zarejestrowane prądy w oknie potencjałów związane są z ładowaniem i rozładowywaniem się podwójnej warstwy elektrycznej występującej po dwóch stronach ITIES.[33]

Do rejestrowania międzyfazowych zjawisk zachodzących na ITIES wykorzystano w badanach:

- potencjostat – galwanostat Autolab302N[30] lub Autolab108[32] (Metrohm) sterowany oprogramowaniem NOVA 1.11. (**Rys. 9 A**)
- potencjostat EmStat3+ wyposażony w wzmacniacz różnicowy PalmSens (Holandia) sterowany oprogramowaniem PSTrace.[27–29] (**Rys. 9 B**)

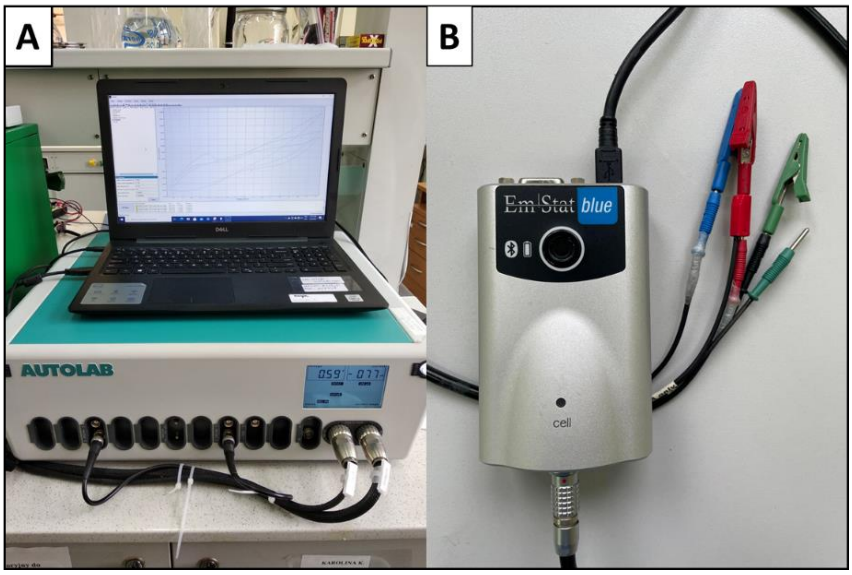

Rysunek 9. Zdjęcia potencjostatów wykorzystanych do realizacji badań.

3. Pomiary spektroskopowe

Materiały poliamidowe otrzymane w klasycznym naczynku woltamperometrycznym podczas eksperymentów z wykorzystaniem spolaryzowanych granic fazowych typu ciecz – ciecz zostały scharakteryzowane przy użyciu następujących technik spektroskopowych:

- Spektroskopia w podczerwieni (spektrometr Nexus FT-IR Thermo Nicolet, USA)[27,29,30].
- Spektroskopia Ramana (Renishaw inVia™ Qontor®, wyposażony w dwa lasery – 532 nm oraz 785nm)[32]

4. Pomiary mikroskopowe

Zmodyfikowane zminiaturyzowane granice cieczowe jak i materiały poliamidowe pochodzące z syntezy w klasycznym układzie pomiarowym ITIES zostały scharakteryzowane przy użyciu następujących instrumentów mikroskopowych:

- Skaningowy mikroskop elektronowy (Phenom G2 Pure, FEI Company, Holandia[27,30] lub Phenom-World BV, Eindhoven, Holandia)[29]
- Skaningowy mikroskop elektronowy (JEOL JMS-IT500HR, JEOL, Japonia) wyposażony w detektor EDX Ultim Max 170 (Oxford instruments, Wielka Brytania).[32]
- Mikroskop FEI Nova NanoSEM 450 (Hillsboro, OR, USA) wyposażony w analizator EDX[29]

CZĘŚĆ EKSPERYMENTALNA

Niniejsza praca doktorska skupia się na (i) badaniu kontrolowanej elektrochemicznie reakcji polikondensacji międzyfazowej, (ii) tworzeniu materiałów poliamidowych na ITIES, (iii) modyfikacji granicy fazowej ciecz – ciecz jak i materiałów poliamidowych nanocząstkami metalicznymi oraz (iv) przeprowadzenia charakterystyki uzyskanych produktów reakcji przy użyciu różnych metod spektroskopowych i mikroskopowych. Na **Rysunku 10** zostały przedstawione struktury związków diamin rozpuszczalnych w fazie wodnej i di- lub tri- chlorków kwasów di- lub tri-karboksylowych rozpuszczalnych w fazie organicznej, które zostały wybrane do badań.

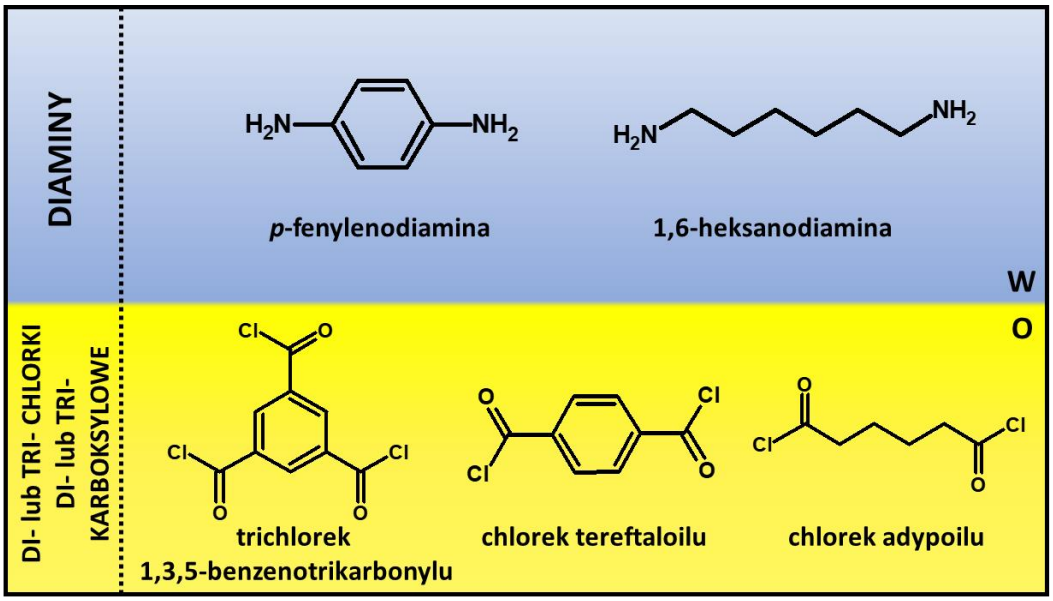

Rysunek 10. Wzory strukturalne diamin rozpuszczalnych w fazie wodnej (**W**) i di- lub trichlorków kwasów di- lub tri-karboksylowych obecnych w fazie organicznej (**O**).

Druga część pracy dotyczy elektrochemicznego badania dendrymerów karbosilanowych przy użyciu spolaryzowanych granic fazowych typu ciecz – ciecz w celu zastosowania ich do indukowania porowatości ditlenku tytanu. Z uwagi na nieudane próby kontrolowania reakcji polikondensacji międzyfazowej ditlenku tytanu, zarówno dendrymery jak i ditlenek tytanu zostały zbadane tylko pod kątem ich elektrochemicznego zachowania na ITIES. W kolejnych podrozdziałach zostaną krótko opisane poszczególne etapy badań eksperymentalnych.

1. Synteza Nylonu-6,6 na spolaryzowanych granicach fazowych typu ciecz – ciecz

Pierwszym etapem badań było zbadanie możliwości elektrochemicznej kontroli syntezy poliamidu Nylonu-6,6 przy użyciu spolaryzowanych granic fazowych typu ciecz – ciecz.[27] Poliamidy są to związki wielkocząsteczkowe posiadające w swojej budowie wiązanie amidowe, zaliczane są do klasy polimerów. Znane są już od prawie stu lat i wciąż budzą zainteresowanie wśród naukowców ze względu na unikalne właściwości oraz szerokie zastosowania komercyjne m.in. w przemyśle tekstylnym. Powstają one m. in. w wyniku reakcji polikondensacji, gdzie z substratów małocząsteczkowych otrzymuje się wielkocząsteczkowe związki polimerów.[34,35] Istnieje kilka metod otrzymywania tych materiałów m.in. poprzez reakcję diamin z chlorkami kwasów di-karboksylowych, polikondensację aminokwasów, polimeryzację w wyniku otwarcia pierścienia laktamów lub reakcję polikondensacji kwasów dikarboksylowych z diaminami.[21,36] W mojej pracy wykorzystywałam syntezę poliamidów w wyniku polikondensacji międzyfazowej kontrolowanej elektrochemicznie w zoptymalizowanych warunkach eksperymentalnych pomiędzy diaminami, a di- lub tri-chlorkami kwasów di- lub tri-karboksylowych.

Nylon-6,6 powstaje w wyniku reakcji pomiędzy 1,6-heksanodiaminą (1,6-DAH) rozpuszczoną w fazie wodnej, a chlorkiem adypoilu (AC) rozpuszczonym w fazie organicznej. Na **Rysunku 11** przedstawiono równanie reakcji syntezy tego poliamidu.

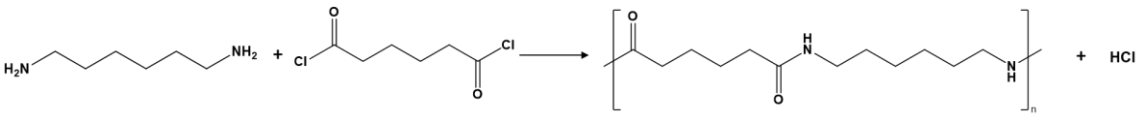

Rysunek 11. Reakcja syntezy Nylonu-6,6.

Ciekawym oraz widowiskowym eksperymentem jest wyciąganie nici Nylonu-6,6 z pomiędzy dwóch faz przy użyciu bagietki. Długość nici uzależniona jest od objętości faz użytych do eksperymentu, a włókna można wyciągać w sposób nieprzerwany, aż do momentu gdy w którejś z faz wyczerpie się reagent.[37] Materiał ten ma szerokie zastosowania komercyjne i można go znaleźć w składzie wielu ubrań, ale również coraz

częściej używany jest do produkcji materiałów ognioodpornych i dywanów. Nici nylonu są bardzo wytrzymałe dlatego poliamid ten wykorzystywany jest do produkcji żyłek wędkarskich, strun do gitary, lin czy spadochronów. Znalazł on również zastosowanie w medycynie, jako nici chirurgiczne. Aby zwiększyć jego wytrzymałość często mieszany jest z bawełną.[38]

Przeprowadzone w ramach rozprawy doktorskiej badania wykazały, że 1,6-heksanodiamina (1,6-DAH) jest aktywna na spolaryzowanych granicach cieczowych, a chlorek adypoilu pozostaje w formie niezjonizowanej w fazie organicznej. Na **Rysunku 12** zostały przedstawione graficzne wzory strukturalne monomerów umieszczone w odpowiednich fazach (**A**) wraz z woltamperogramami cyklicznymi (**B,C**) pokazującymi ich elektrochemiczne zachowanie na ITIES.

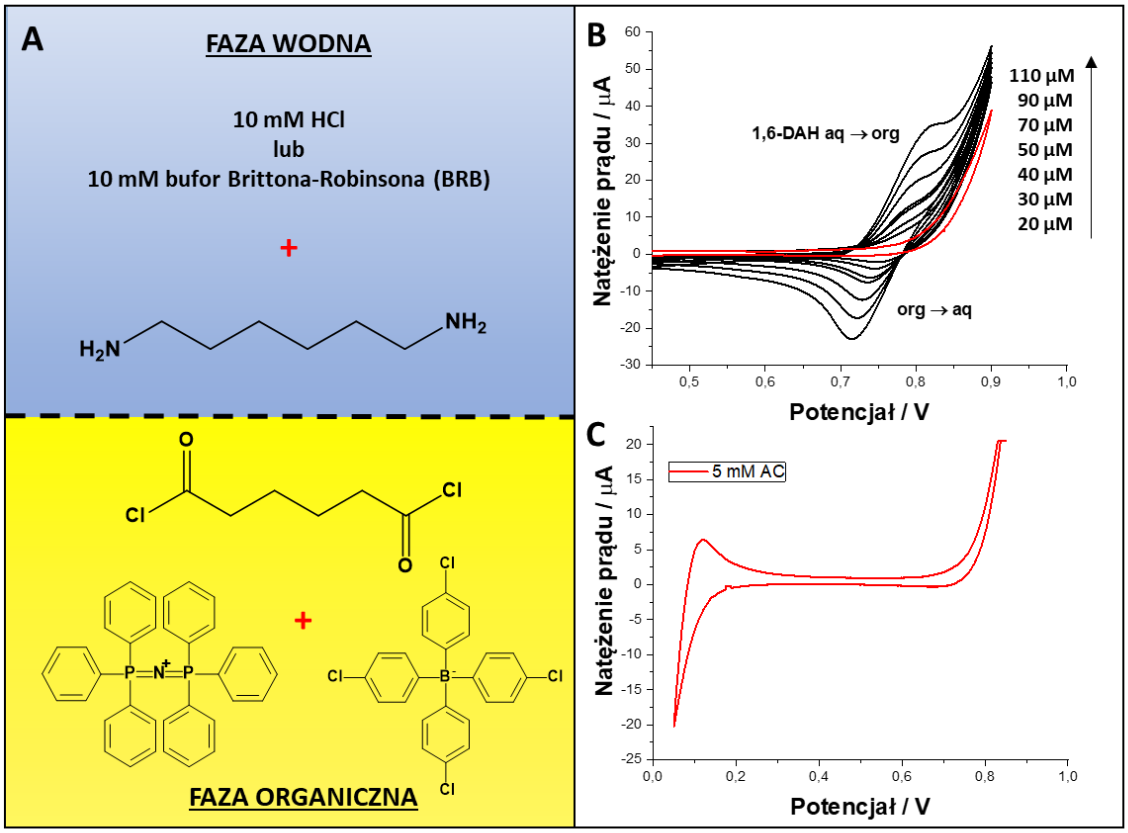

Rysunek 12. Schemat zawierający układ eksperymentalny stosowany do syntezy Nylonu-6,6 (**A**) wraz z woltamperogramami cyklicznymi pokazującymi elektrochemiczną aktywność 1,6-heksanodiaminy (1,6-DAH) i chlorku adypoilu (AC) na spolaryzowanych granicach fazowych typu ciecz – ciecz. (**B, C**).

Kluczem do elektrochemicznej kontroli syntezy Nylonu - 6,6 było dobranie odpowiedniego pH fazy wodnej, w którym diamina występowała w postaci sprotonowanej (jako mono- i di-kation) i niesprotonowanej oraz obecność produktu ubocznego powstającego podczas reakcji otrzymywania poliamidu jakim jest kwas solny. Na **Rysunku 13** zaproponowano mechanizm elektrochemicznie kontrolowanej syntezy poliamidu na spolaryzowanych granicach fazowych typu ciecz – ciecz.

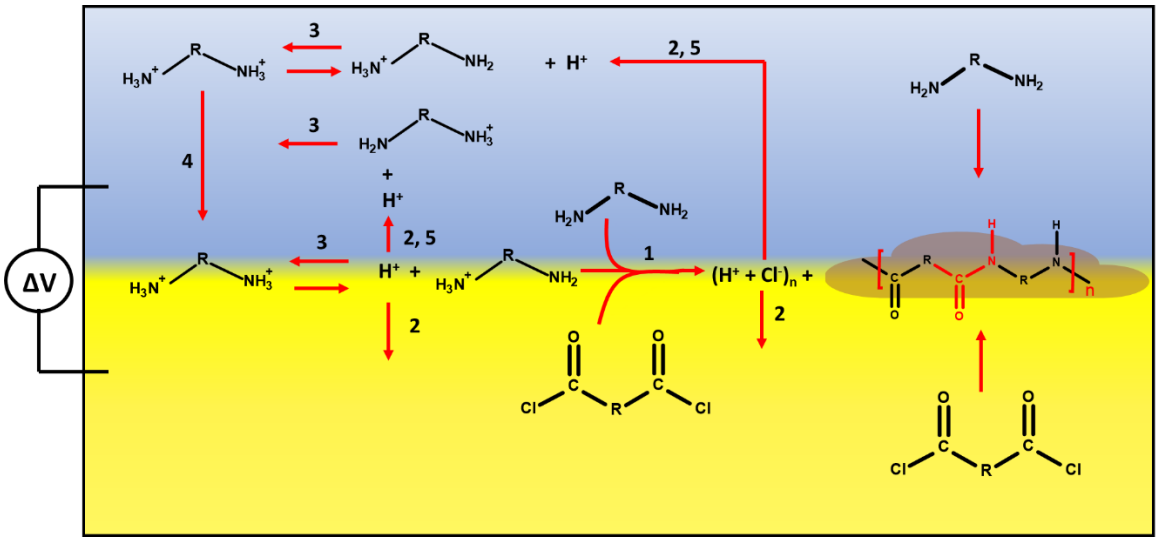

Rysunek 13. Mechanizm elektrochemicznie kontrolowanej syntezy poliamidów na ITIES.

Kwas solny, który jest produktem ubocznym reakcji polikondensacji ulega dysocjacji na spolaryzowanej granicy cieczowej jednocześnie powodując spadek pH fazy wodnej w warstwie elektrolitu dolegającej do granicy fazowej typu ciecz – ciecz. Transport jonu H^+ z jednej fazy do drugiej można kontrolować elektrochemicznie. Obecność nadmiarowej ilości protonów powoduje sprotonowanie grup aminowych (**2,5**) w fazie wodnej przez co wzrasta liczba dodatnio naładowanych diamin, które pod wpływem przyłożonego potencjału można elektrochemicznie przetransportować do fazy organicznej (**4**), gdzie ulegając dysocjacji (**3**) (jeśli takowa zachodzi) reagują z dichlorkiem kwasowym tworząc materiał poliamidowy (**1**).

Materiał Nylonu-6,6 otrzymany w wyniku elektrochemicznie kontrolowanej syntezy zarówno w skali makroskopowej jak i mikroskopowej został scharakteryzowany przy użyciu technik spektroskopowych oraz mikroskopowych. Na **Rysunku 14** podano

przykładowe obrazy tego poliamidu wytworzonego w zminiaturyzowanym systemie ITIES, zarejestrowane przy użyciu skaningowego mikroskopu elektronowego (SEM).

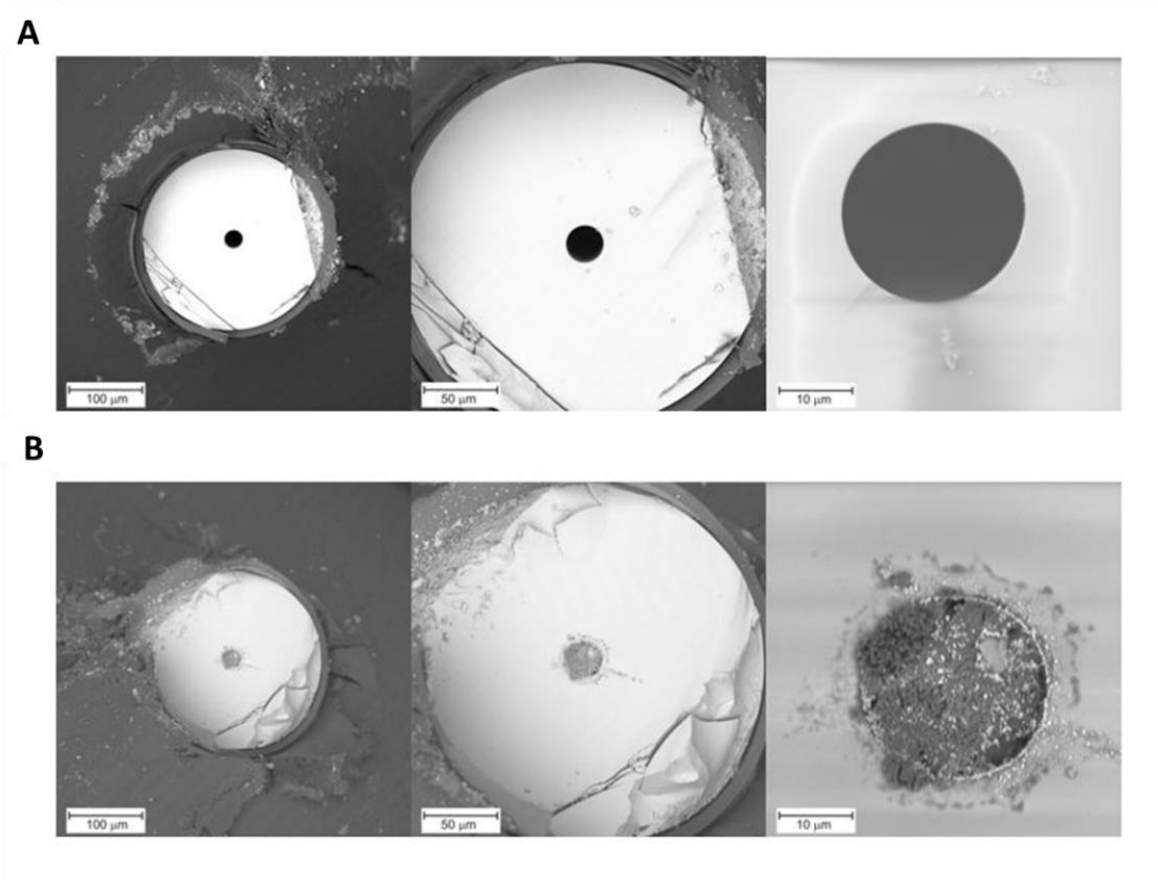

Rysunek 14. Obrazy SEM dla niemodyfikowanych (A) i modyfikowanych Nylonem-6,6 (B) mikrokapilar.

2. Modyfikacja Nylonu–6,6 nanocząstkami na bazie srebra przy zastosowaniu układu ITIES

Kontynuacją badań nad Nylonem–6,6 była jego elektrochemicznie kontrolowana modyfikacja nanocząstkami na bazie srebra. Na **Rysunku 15** przedstawiono zjawiska zachodzące na spolaryzowanej granicy faz typu ciecz – ciecz podczas prowadzonego eksperymentu.

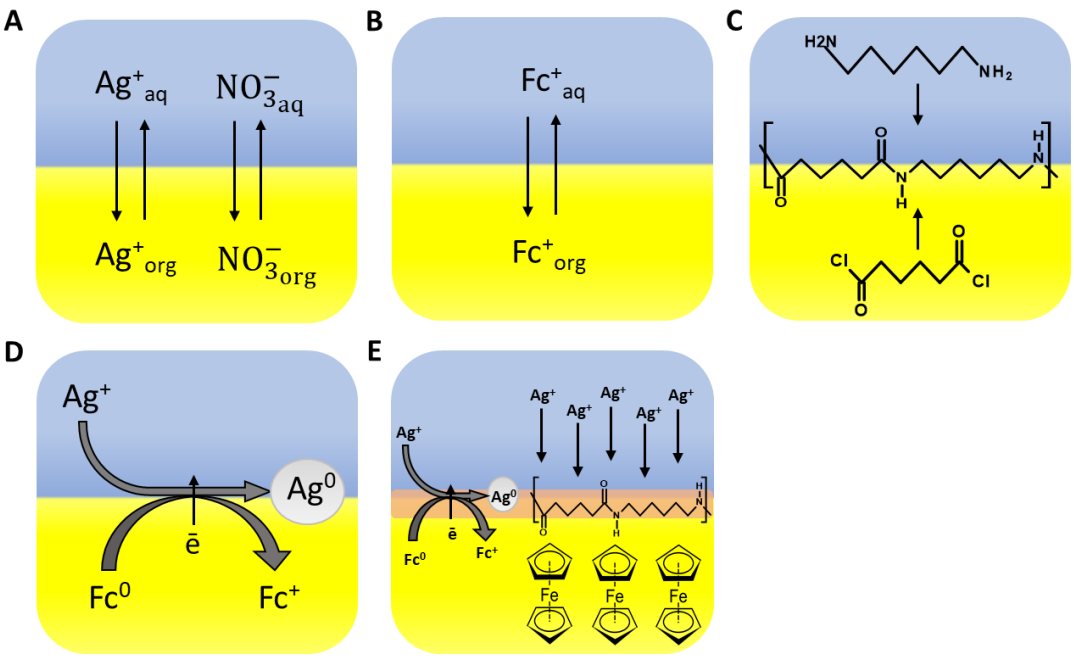

Rysunek 15. Schemat przedstawia zjawiska zachodzące na spolaryzowanej granicy faz typu ciecz – ciecz podczas elektrochemicznie kontrolowanej syntezy Nylonu-6,6 i jego modyfikacji nanocząstkami na bazie srebra. **A** – międzyfazowy transfer jonów Ag^+ i NO_3^-, **B** – międzyfazowy transfer jonu Fc^+, **C** – reakcja polikondensacji międzyfazowej zachodząca pomiędzy 1,6-DAH i AC prowadząca to powstania Nylonu-6,6, **D** – międzyfazowy transfer elektronu z fazy organicznej do wodnej pochodzący z reakcji redoks utleniania jonów ferrocenowych i redukcji jonów Ag^+ do nanocząstek na bazie Ag^0.

Modyfikację przeprowadzono zarówno w układzie makroskopowym jak i mikroskopowym stosując modyfikację *in situ*. Wykorzystano w tym celu membrany z włókna szklanego. Nanocząstki metaliczne otrzymano w wyniku redukcji jonów soli metali rozpuszczonych w fazie wodnej. W eksperymencie tym zaobserwowano cztery różne zjawiska zachodzące na spolaryzowanej granicy fazowej typu ciecz – ciecz: (**A**) międzyfazowy transfer jonów soli srebra i azotanów (V), (**B**) międzyfazowy transfer jonów ferrocenowych, (**C**) reakcja polikondensacji kontrolowana elektrochemiczne oraz (**D**) reakcja redukcji jonów srebra do nanocząstek metalicznych w obecności ferrocenu rozpuszczonego w fazie organicznej (międzyfazowe przeniesienie elektronu). Ze względu na wysokie pH środowiska prowadzonego eksperymentu (pH = 11) oprócz

nanocząstek srebra zaobserwowano wytrącanie się osadu tlenku srebra, który ulegał rozpuszczeniu po dodaniu do roztworu 1,6-heksanodiaminy.

Elektrochemicznie kontrolowana synteza Nylonu-6,6 oraz jego modyfikacja została przeprowadzona na dwa sposoby (**Rys. 16**). Pierwszy sposób (**Rys. 16 A**) polegał na syntezie poliamidu i jego modyfikacji nanocząstkami na bazie srebra w tym samym czasie. Do fazy wodnej jednocześnie dodano 1,6-heksanodiaminę i azotan (V) srebra w wyniku czego wytworzono poliamid kontrolując ten proces elektrochemicznie. Natomiast drugi sposób (**Rys. 16 B**) polegał na tym, iż w pierwszej kolejności elektrochemicznie zsyntetyzowano poliamid, a następnie wytworzony materiał poddano elektrochemicznej modyfikacji dodając do fazy wodnej azotanu (V) srebra.

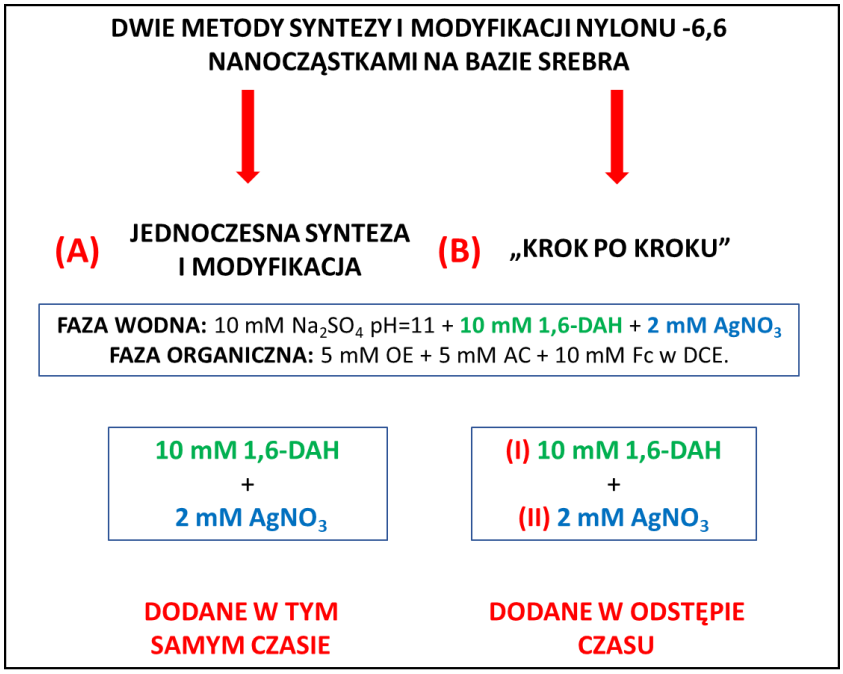

Rysunek 16. Schemat przedstawia dwie metody syntezy i modyfikacji Nylonu–6,6 nanocząstkami na bazie srebra wraz z warunkami prowadzonego eksperymentu. **A** – metoda jednoczesnej syntezy i modyfikacji, **B** – metoda „krok po kroku”.

Poniżej na **Rysunku 17** przedstawiono obrazy SEM zarejestrowane dla materiału otrzymanego w układzie mikroskopowym dla niezmodyfikowanej membrany z włókna szklanego (**A**), zmodyfikowanej membrany wykorzystując metodę jednoczesnej syntezy poliamidu i jego modyfikacji (**B**) oraz (**C**) zmodyfikowanej membrany z włókna szklanego, gdzie zastosowano metodę „krok po kroku”. Na obrazie (**B**) widoczne są liczne

nanoobiekty na bazie srebra, gdzie na obrazie (**C**) widoczny jest głównie materiał poliamidowy, co spowodowane jest prawdopodobnie zablokowaniem reakcji redoks przez wcześniej zsyntetyzowany Nylon-6,6 metodą „krok po kroku”.

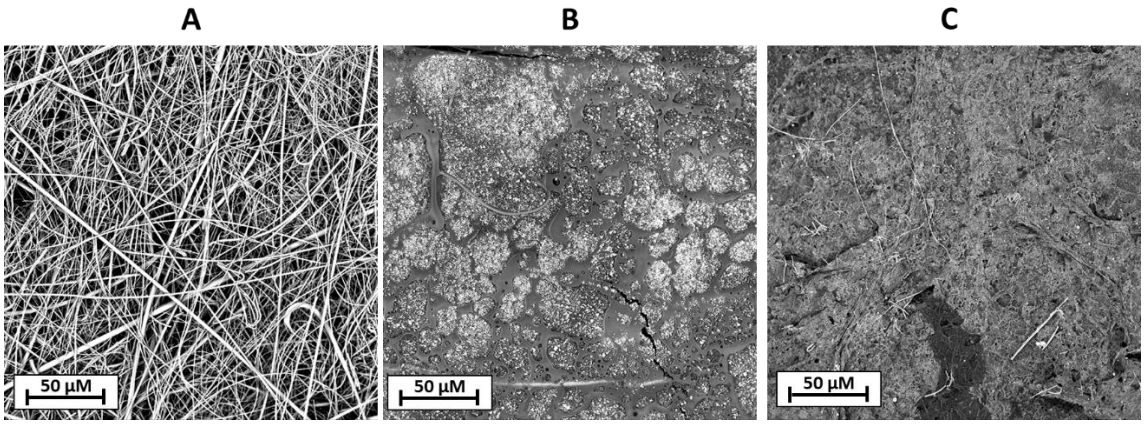

Rysunek 17. Obrazy SEM zarejestrowane dla **A** – niezmodyfikowanej membrany z włókna szklanego, **B** – zmodyfikowanej membrany z włókna szklanego metodą jednoczesnej syntezy i modyfikacji, **C** – zmodyfikowanej membrany z włókna szklanego metodą „krok po kroku”.

Próbki te zostały poddane również analizie spektroskopowej przy użyciu spektroskopii rentgenowskiej z dyspersją energii (EDX), które potwierdziły obecność nanocząstek na bazie srebra na powierzchni wytworzonego materiału poliamidowego. Otrzymane wyniki zostały zebrane w **Tabeli 1.** Na podstawie uzyskanych danych wykazano obecność srebra w próbkach **B**, **C**, **D** co potwierdza skuteczność obu metod elektrochemicznej syntezy nanocząstek. Porównując obie metody wykorzystane do syntezy i modyfikacji Nylonu-6,6 zaobserwowano, że pomimo zbliżonych średnich zawartości srebra w próbkach (**Tabela 1**) to w metodzie jednoczesnej syntezy i modyfikacji największą zawartością srebra jaką wyznaczono było 7.90%, natomiast najwyższa wartość wyznaczona dla materiału otrzymanego metodą „krok po kroku” była mniejsza i wynosiła 6.84%. W tabeli można zauważyć obecność innych pierwiastków takich jak sód czy krzem, które wchodzą w skład membran z włókna szklanego. Pierwiastki sodu czy chloru są jonami obecnymi w roztworach wykorzystanych w eksperymencie, natomiast węgiel, azot i tlen są atomami budulcowymi łańcuch poliamidowy.

Tabela 1. Skład % pierwiastków obecnych w analizowanych próbkach. **A** – niezmodyfikowana membrana z włókna szklanego, **B** – zmodyfikowana membrana metodą jednoczesnej syntezy i modyfikacji, **C** – zmodyfikowana membrana metodą „krok po kroku", **D** – nanocząstki na bazie srebra otrzymane w wyniku redukcji jonów srebra na ITIES, **E** – zmodyfikowana membrana w wyniku elektrochemicznie kontrolowanej syntezy Nylonu–6,6.

	A	B	C	D	E
C	1.67 ± 0.50	56.43 ± 13.38	39.87 ± 13.40	7.96 ± 4.18	42.17 ± 8.62
N	0.00 ± 0.00	4.06 ± 1.49	3.50 ± 1.54	0.69 ± 1.38	3.47 ± 1.61
O	52.26 ± 2.12	20.77 ± 11.19	13.47 ± 10.28	56.59 ± 5.53	28.41 ± 8.53
Ag	0.00 ± 0.00	2.70 ± 2.88	3.11 ± 2.38	5.75 ± 4.77	0.00 ± 0.00
Na	7.65 ± 0.52	2.54 ± 1.28	11.27 ± 9.97	5.46 ± 0.30	4.56 ± 0.77
Si	35.27 ± 2.03	8.27 ± 4.22	8.50 ± 10.06	19.39 ± 3.58	17.44 ± 1.14
Cl	0.00 ± 0.00	3.88 ± 3.23	19.62 ± 16.36	2.75 ± 1.75	2.62 ± 0.77

3. Charakterystyka materiałów poliamidowych otrzymanych w sposób kontrolowany elektrochemicznie

Bazując na zaproponowanym w 1. podrozdziale mechanizmie elektrochemicznie kontrolowanej syntezy poliamidów otrzymano pięć innych materiałów (monomery wybrane do syntezy przedstawiono na **Rys. 10**) na ITIES i przebadano je pod kątem ich właściwości przesiewowych. Do reakcji polikondensacji międzyfazowej użyto zarówno klasycznego układu makroskopowego jak i układu zminiaturyzowanego wykorzystującego polipropylenową końcówkę od mikropipety z zatopioną w jej końcu kapilarą krzemionkową. Materiały poliamidowe wytworzone w klasycznym naczynku woltamperometrycznym zostały poddane charakterystyce przy użyciu technik spektroskopowych i mikroskopowych (SEM, EDX, spektroskopia Ramana). Dodatkowo korzystając z mikroskopowego układu ITIES zbadano zdolności przesiewowe wytworzonych materiałów poliamidowych przy określonej ilości zarejestrowanych cykli

woltamperometrycznych zastosowanych podczas ich syntezy. Następnie po jej zakończeniu badano przepuszczalność wytworzonego materiału przy użyciu jonu modelowego TMA^+. Poniższy opis dotyczy jednej pary monomerów: *p*-fenylenodiaminy i trichlorku 1,3,5-benzenotrikarbonylu, pozostałe wyniki opisano w manuskrypcie będącym częścią niniejszej rozprawy doktorskiej.

Pierwszym etapem eksperymentu było dobranie odpowiedniego pH fazy wodnej oraz zbadanie elektrochemicznego zachowania monomerów biorących udział w reakcji syntezy na spolaryzowanych granicach fazowych typu ciecz – ciecz. Na **Rysunku 18** przedstawiono woltamperogramy elektrochemicznie aktywnej *p*-fenylenodiaminy (**A**), której sygnał rośnie wraz ze wzrostem jej stężenia w fazie wodnej, nieaktywnego elektrochemicznie trichlorku 1,3,5-benzenotrikarbonylu (**B**), diagram ułamka stężenia różnych form diaminy w zależności od pH fazy wodnej (**C**) oraz wykres przedstawiający elektrochemicznie kontrolowaną syntezę poliamidu przy różnych stężeniach diaminy w fazie wodnej (**D**).

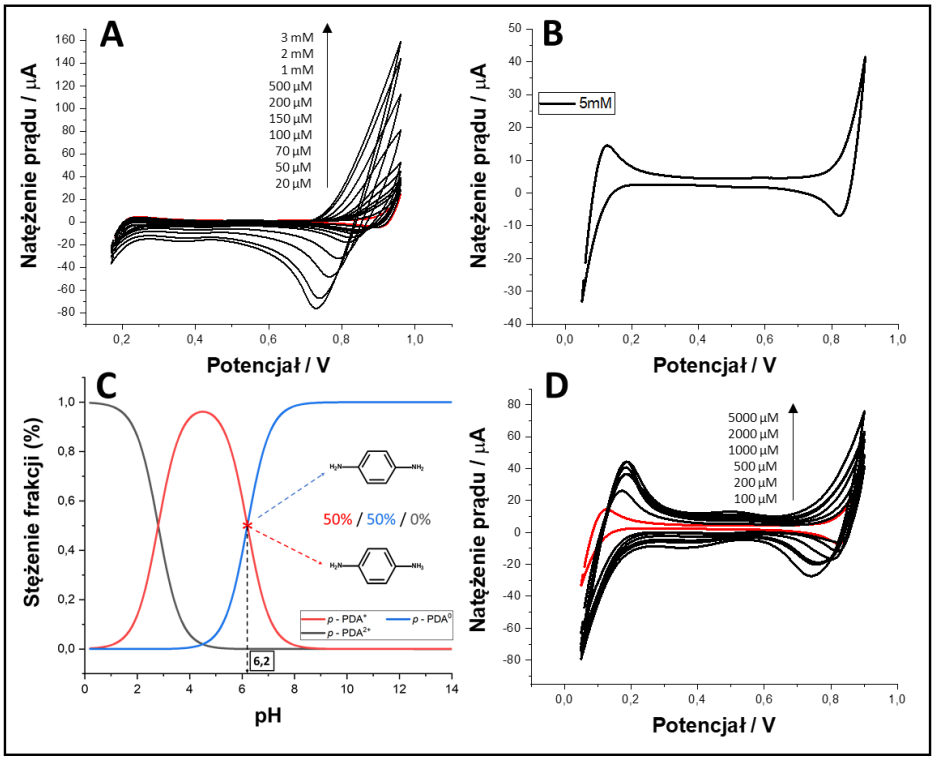

Rysunek 18. Woltamperogramy przedstawiające elektrochemiczną aktywność (**A**) *p*-fenylenodiaminy i (**B**) trichlorku 1,3,5-benzenotrikarbonylu na spolaryzowanej granicy fazowej typu ciecz – ciecz. Dodatkowo sporządzono diagram frakcji stężenia

różnych form diaminy w funkcji pH fazy wodnej (**C**) oraz przedstawiono woltamperogramy elektrochemicznie kontrolowanej syntezy poliamidu przy wzrastającym stężeniu diaminy w fazie wodnej (**D**).

Wykazano, iż najbardziej optymalnym pH fazy wodnej do kontrolowanej elektrochemicznie syntezy poliamidu na spolaryzowanej granicy fazowej typu ciecz – ciecz było pH = 6.2. W tym środowisku formy sprotonowane (A^+) i niesprotonowane (A^0) występują w proporcji 1:1 Obecność formy niesprotonowanej jest niezbędna do zainicjowania reakcji polikondensacji międzyfazowej, ponieważ jest to reakcja samorzutna. Do badań w zminiaturyzowanym układzie ITIES wybrano stężenie 10 mM *p*-fenylenodiaminy. Na **Rysunku 19** przedstawiono wzory strukturalne *p*-fenylenodiaminy i trichlorku 1,3,5-benzenotrikarbonylu rozpuszczonych odpowiednio w fazie wodnej (**A**) i fazie organicznej (**B**). W punktach **C** i **D** widoczne są obrazy SEM w dwóch powiększeniach przedstawiające materiał uzyskany w systemie mikroITIES. Obrazy **E, F, G, H** przedstawiają woltamperogramy zarejestrowane dla zmodyfikowanej mikroukładzie ITIES w obecności jonu modelowego (TMA^+) przy stężeniach 60 lub 180 µM. Kolejne wykresy przedstawiają wyniki otrzymane dla mikroITIES zmodyfikowanego poprzez wzrastającą ilość zarejestrowanych krzywych woltamperometrycznych. Ślepa próba obrazuje woltamperogram zarejestrowany dla zmodyfikowanego układu bez jonu modelowego TMA^+.

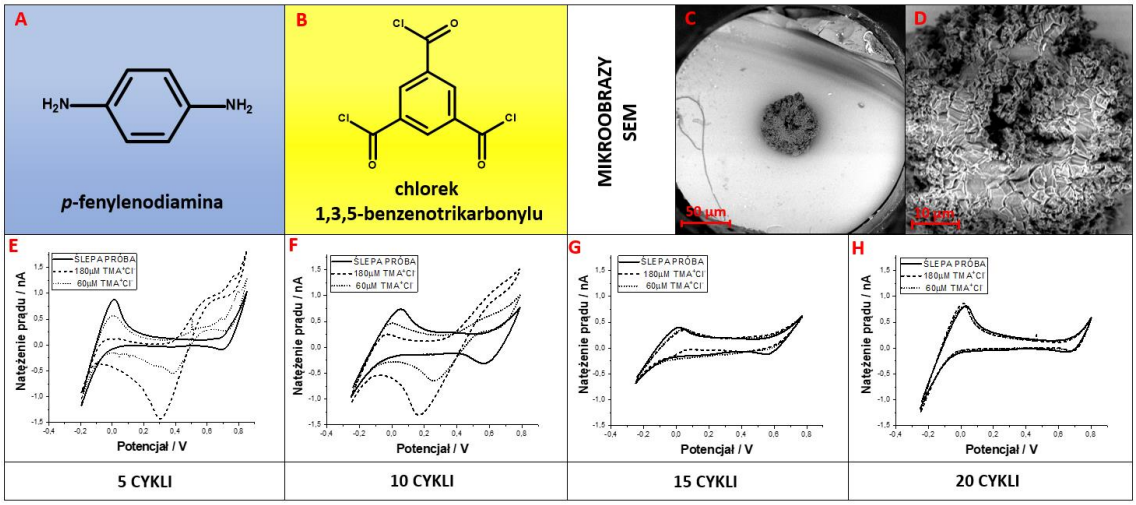

Rysunek 19. Wzory strukturalne *p*-fenylenodiaminy i trichlorku 1,3,5-benzenotrikarbonylu rozpuszczonych w odpowiednich fazach – wodnej (**A**) i organicznej (**B**). **C, D** – obrazy SEM zmodyfikowanego ITIES w różnych powiększeniach. **E, F, G, H** – woltamperogramy dla zmodyfikowanych mikroITIES w obecności jonu modelowego (TMA^+) przy stężeniach 60 lub 180 µM po różnych ilości cykli prowadzenia reakcji polikondensacji.

Na podstawie otrzymanych wyników stwierdzono, że wraz ze wzrostem ilości powtórzonych woltamperogramów cyklicznych zarejestrowanych podczas elektrochemicznie kontrolowanej reakcji polikondensacji międzyfazowej maleje przepuszczalność wytworzonego materiału poliamidowego. Po 15 cyklach syntezy zminiaturyzowana granica cieczowa jest skutecznie zablokowana przez obecny na granicy cieczowej poliamid uniemożliwiając przeniesienie jonu modelowego TMA^+ pomiędzy fazami. Na **Rysunku 20** przedstawiono obrazy SEM innych materiałów poliamidowych otrzymanych w zminiaturyzowanym układzie pomiarowym.

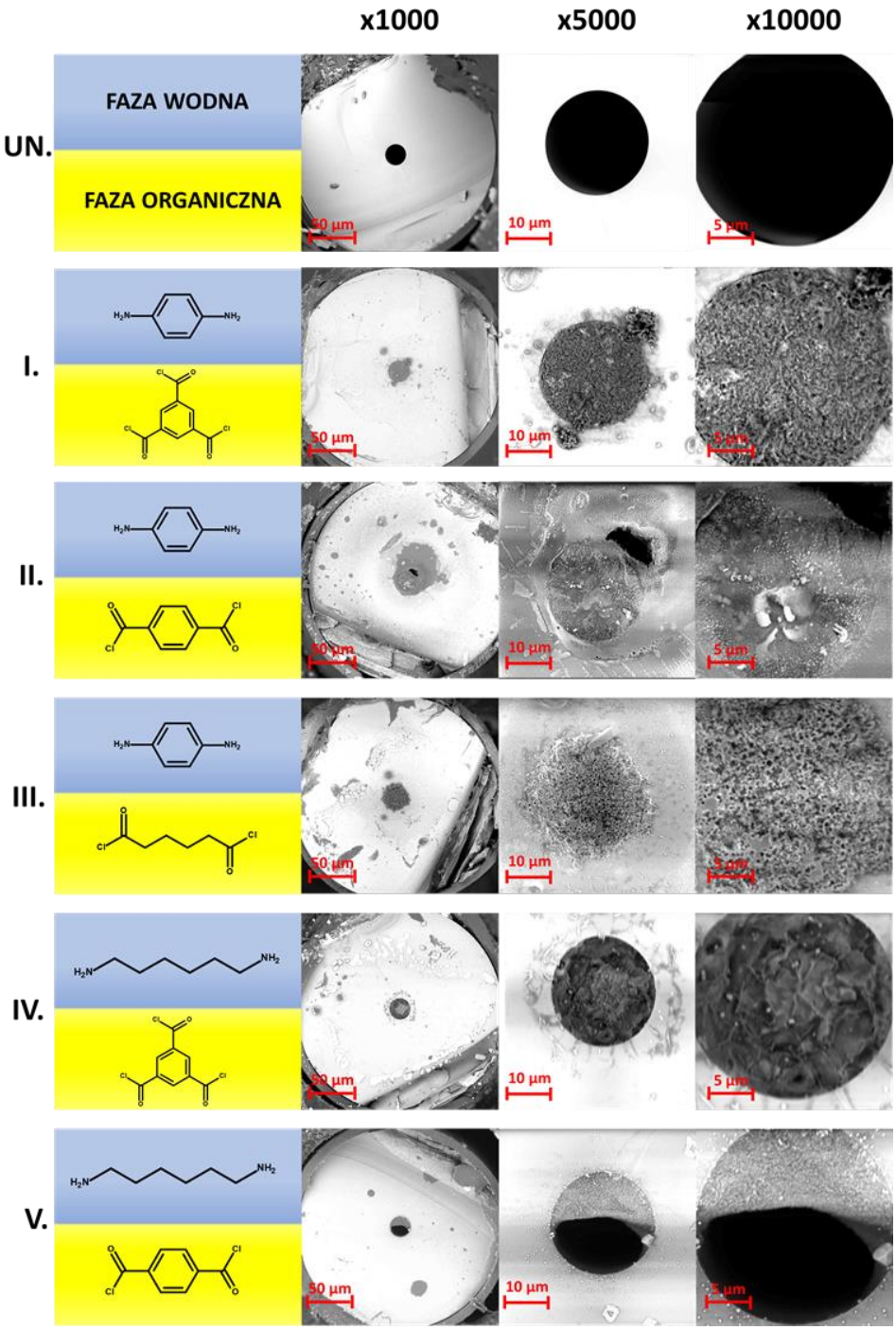

Rysunek 20. Obrazy SEM zarejestrowane dla zmodyfikowanych granic cieczowych materiałami poliamidowymi. **UN** – niezmodyfikowany układ ITIES, **I** – *p*-fenylenodiamina + chlorek 1,3,5-benzenotrikarbonylu, **II** – *p*-fenylenodiamina + chlorek tereftaloilu, **III** – *p*- fenylenodiamina + chlorek adypoilu, **IV** – 1,6-heksanodiamina + chlorek 1,3,5-benzenotrikarbonylu, **V** – 1,6-heksanodiamina + chlorek tereftaloilu, **VI** – 1,6-heksanodiamina + chlorek adypoilu.

4. Elektrochemiczne badania dendrymerów karbosilanowych na spolaryzowanych granicach cieczowych

Dendrymery są to kuliste struktury posiadające rdzeń, rozgałęzienia i wolne przestrzenie wewnętrzne. Liczba rozgałęzień warunkuje przynależność struktury do danej generacji. Ogólny model dendrymeru przedstawiono na **Rysunku 21.**

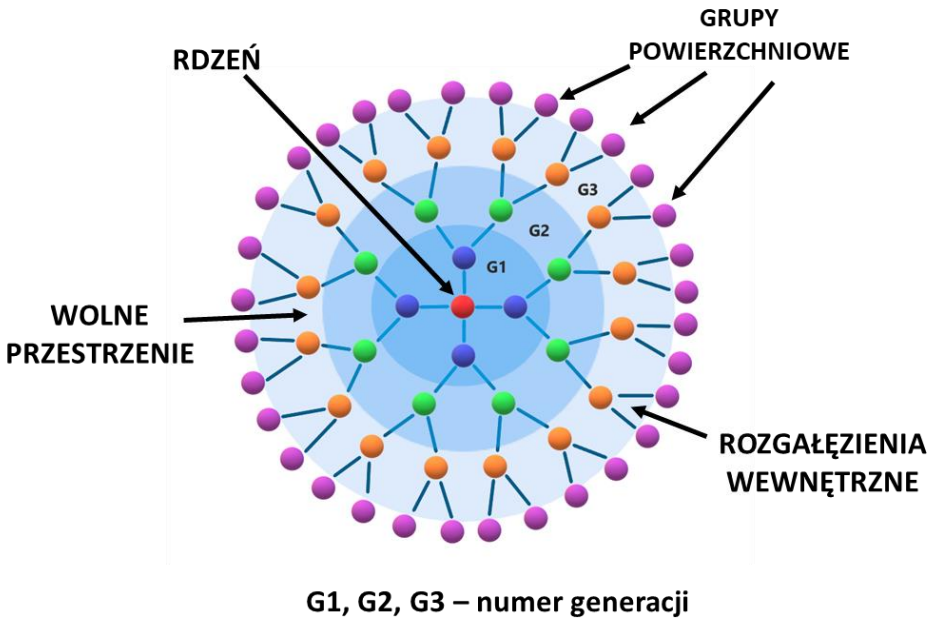

Rysunek 21 . Ogólny model dendrymeru.

Dendrymery posiadają wiele użytecznych właściwości fizykochemicznych, a jedną z najistotniejszych jest zdolność do przenoszenia różnych związków organicznych i nieorganicznych bez wchodzenia z nimi w reakcje. W związku z tym szeroko wykorzystywane są w sektorze medycznym jako transportery leków.[39] Związki te mają wysoki potencjał aplikacyjny w biomedycynie m.in. stosowane są jako biomolekuły w terapii genowej, w terapii nowotworowej, w środkach kontrastowych, leczeniu oparzeń, ale również są wykorzystywane w wysokoczułych urządzeniach analitycznych.[40,41] Struktury przebadanych w pracy elektrochemicznie dendrymerów przedstawiono poniżej (**Rys. 22**).

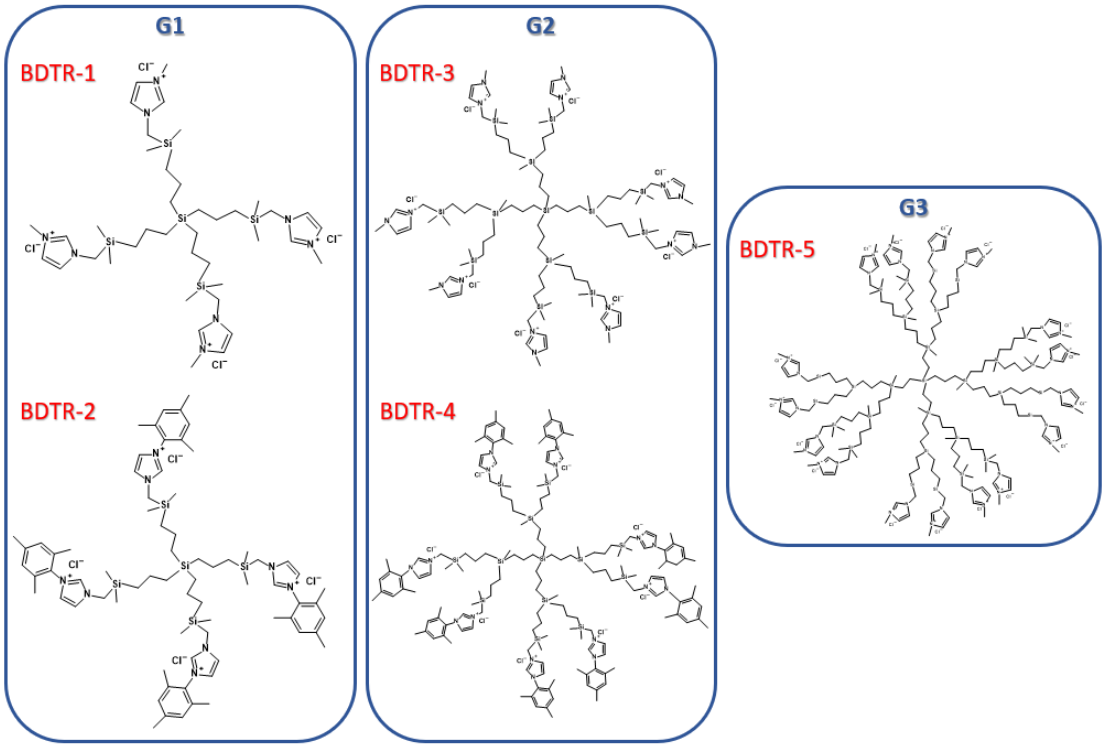

Rysunek 22. Wzory strukturalne badanych dendrymerów karbosilanowych. **G1, G2, G3** – numer generacji; **BDTR-1, BDTR-2, BDTR-3, BDTR-4, BDTR-5** – poszczególne nazwy związków.

Celem tej pracy było zbadanie zachowania pięciu dendrymerów karbosilanowych na spolaryzowanych granicach fazowych typu ciecz – ciecz w celu wykorzystania ich do indukowania porowatości ditlenku tytanu w trakcie zachodzącej reakcji polikondensacji międzyfazowej. Związki badane w niniejszej pracy zostały zsyntetyzowane przez zespół prof. Rafael Gomez Ramirez z University of Alcala. Badania eksperymentalne dotyczyły oceny wpływu stężenia dendrymeru rozpuszczonego w fazie wodnej i zastosowanych parametrów elektroanalitycznych (szybkości przemiatania potencjałem, wpływ wartości przykładanej różnicy potencjałów oraz czas prowadzonego eksperymentu) na rejestrowane sygnały elektrochemiczne, których kształt oraz otrzymane zależności informowały o mechanizmie międzyfazowego przenoszenia ładunku. Poniżej przedstawiono woltamperogramy cykliczne, dla BDTR-2 z generacji G1 i BDTR-5 z generacji G3 (**Rys. 23**).

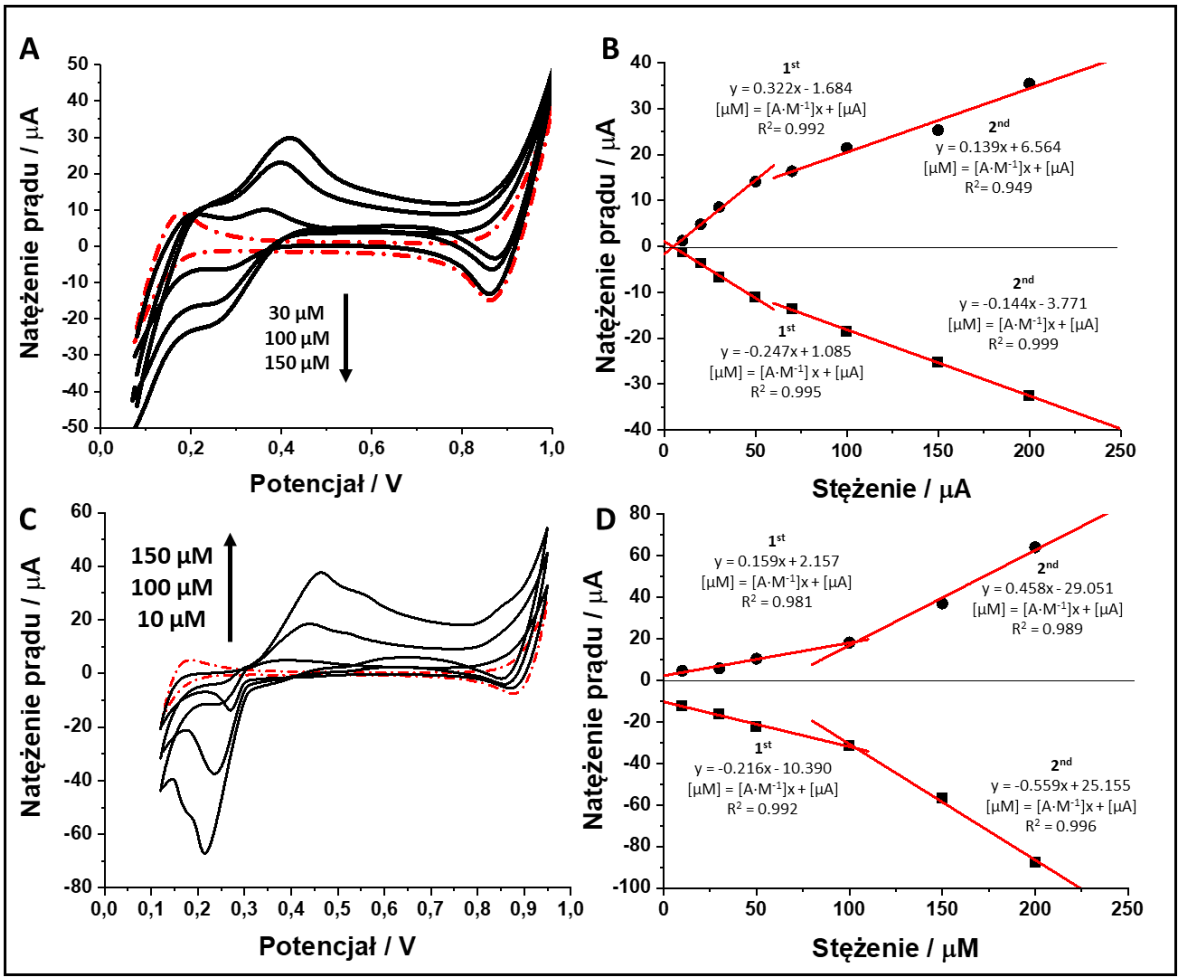

Rysunek 23. Woltamperogramy cykliczne (**A i C**) zarejestrowane dla różnych stężeń dendrymeru. Odpowiadające im krzywe kalibracyjne dla dendrymerów BDTR-2 (**B**) i BDTR-5 (**D**). **A i B** – FAZA WODNA: 10mM NaCl + x µM BDTR-2; **C i D** – FAZA WODNA: 10mM NaCl + x µM BDTR-5; FAZA ORGANICZNA: 5 mM $BTPPA^{+}TPBCl^{-}$ w 1,2-DCE.

Na podstawie zamieszczonych wyżej woltamperogramów stwierdzono, że badane dendrymery są aktywne na spolaryzowanych granicach fazowych typu ciecz – ciecz. Wraz ze wzrostem stężenia dendrymeru obecnego w fazie wodnej rośnie sygnał pochodzący od przejścia jonowej formy badanych związków pomiędzy niemieszającymi się ze sobą fazami. Krzywe kalibracyjne wykreślone na podstawie uzyskanych woltamperogramów cyklicznych w obu przypadkach posiadają dwa zakresy liniowości. Dla dendrymeru BDTR-2 w pierwszej części zaobserwowano większą wartość nachylenia prostej niż w drugiej części co wskazuje prawdopodobnie na adsorpcyjny charakter procesu. Inna sytuacja jest w przypadku dendrymeru BDTR-5, gdzie widoczne są dwa zakresy liniowości o dużym nachyleniu co sugeruje odmienny mechanizm przenoszenia

jonu. Najprawdopodobniej, oprócz adsorbowania się badanego dendrymeru do granicy fazowej typu ciecz – ciecz, mamy do czynienia z jednoczesnym transferem anionu z fazy organicznej do fazy wodnej (reakcja wspomaganego przenoszenia ładunku inicjowana przez zakumulowany ładunek dodatni w warstewce zaadsorbowanego BDTR-5). Na wykresach **Rys. 24 A i B** widoczne są prądy jonowe o wysokiej intensywności przypisane dla pierwszego cyklu skanowania, które charakteryzują się gwałtowanym spadkiem prądowym charakterystycznym dla procesów adsorpcyjnych, co potwierdza wnioski płynące z analizy danych zestawionych na **Rysunku 23**. Zachowanie międzyfazowe badanych dendrymerów jest więc złożone, a zarejestrowane prądy jonowe pochodzą od mieszaniny procesów ograniczonych dyfuzją i adsorpcją międzyfazową, co potwierdzają badania dotyczące wpływu kolejno rejestrowanych cykli woltamperometrycznych. Zaobserwowano, iż w obecności stałych stężeń dendrymerów (**Rys. 24**) otrzymujemy zmienne wartości prądów dodatnich i ujemnych (spadki) pochodzących od międzyfazowego przenoszenia jonu co również przypisano procesom adsorpcyjnym. Dodatkowo przedstawiono wpływ stężenia elektrolitu podstawowego fazy organicznej na wartości prądów dodatnich oraz prądów ujemnych rejestrowanych w obecności stałego stężenia dendrymerów rozpuszczonych w fazie wodnej (**Rys. 24 C-F**). Otrzymane wyniki potwierdziły iż na znaczące fluktuacje wartość prądu jonowego, który przypisano obecności badanego dendrymeru BDTR-5, wpływa stężenie hydrofobowych kationów i anionów z fazy organicznej co potwierdziło występowanie mechanizmu wspomaganego przenoszenia jonów.

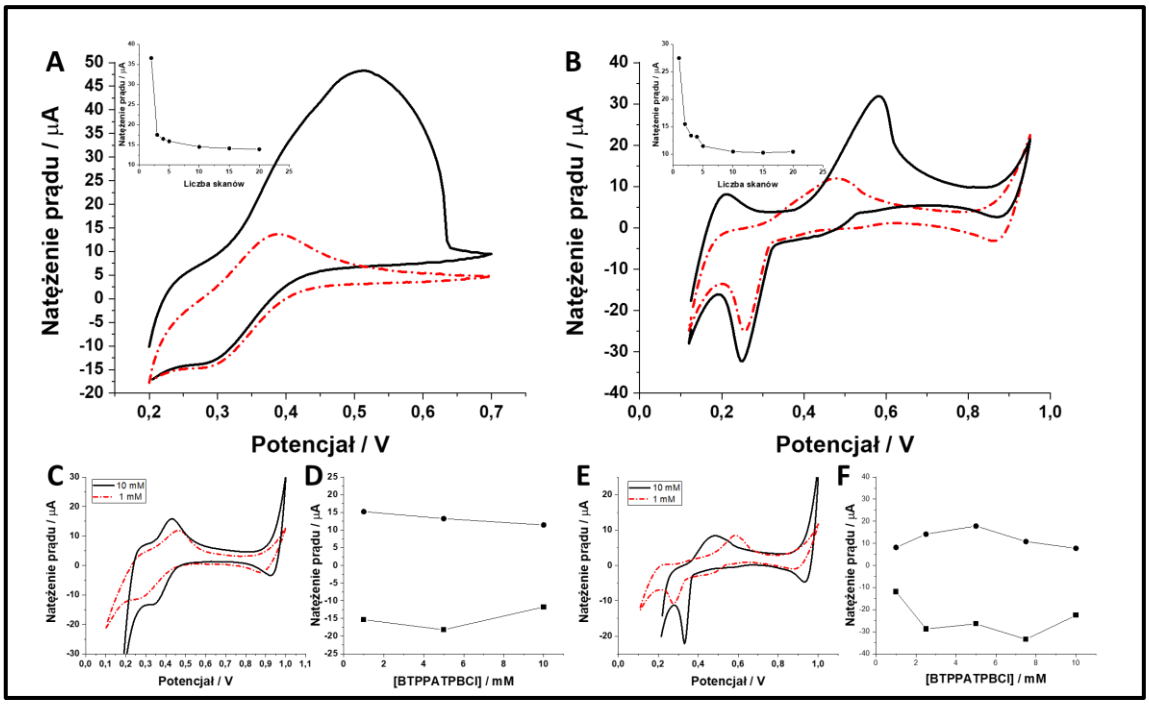

Rysunek 24. A i **B** - wpływ kolejnych cykli woltamperometrycznych dla BDTR-2 i BDTR-5. Czarna ciągła linia przedstawia skan 2 dla BDTR-2 i skan 1 dla BDTR-5. Czerwona przerywana linia to skan 20. **A and B – FAZA WODNA:** 10mM NaCl + 100µM BDTR-2 lub BDTR-5; **FAZA ORGANICZNA:** 5 mM $BTPPA^{+}TPBCl^{-}$ w 1,2-DCE. **C** i **E** przedstawiają woltamperogramy cykliczne zarejestrowane dla różnych stężeń elektrolitu podstawowego w fazie organicznej; **D** i **F** (+) i (-) prądy pików dla różnych stężeń elektrolitu podstawowego $BTPPA^{+}TPBCl^{-}$ w fazie organicznej. **FAZA WODNA:** 10mM NaCl + 100µM BDTR-2 lub 50 µM BDTR-5 **FAZA ORGANICZNA:** 1 mM - 10 mM $BTPPA^{+}TPBCl^{-}$ w 1,2-DCE.

Na podstawie uzyskanych danych wyznaczono parametry elektroanalityczne dla badanych związków, takie jak granica wykrywalności (LOD), czułość detekcji czy współczynniki dyfuzji, które są zamieszczone w załączonej publikacji.[28] Badane związki dendrymerów w przyszłości mogą zostać wykorzystane do charakterystyki spolaryzowanych granic fazowych typu ciecz – ciecz modyfikowanych różnymi materiałami takimi jak np. monowarstwami białek, lipidów czy porowatymi membranami.

5. Ditlenek tytanu na spolaryzowanych granicach cieczowych

Ostatnim obiektem moich badań był ditlenek tytanu (**Rys. 25**) osadzany na granicy fazowej typu ciecz – ciecz na drodze polikondensacji międzyfazowej. TiO_2 jest białym, drobnym proszkiem, który naturalnie występuje w postaci minerałów – anatazu lub rutylu. Jego synteza może być przeprowadzana na wiele różnych sposobów np. metody hydrotermalne, solwotermiczne, oksydacyjne, zol-żel, mikrofalowe oraz w wyniku osadzania chemicznego.[42,43]

Rysunek 25. Wzór strukturalny ditlenku tytanu.

Ditlenek tytanu to związek chemiczny, który stał się bardzo popularny ze względu na swoje obecne lub dawne zastosowanie jako:

- dodatek do żywności (barwnik oznaczany symbolem E171),[44]
- komponent do produkcji tworzyw sztucznych, papieru, lakieru czy farb.[45]
- środek do oczyszczania wody i powietrza,[46]
- komponent powłok stosowanych do tworzenia powierzchni samoczyszczących,[47]
- filtr UV w produktach kosmetycznych,[48]
- barwnik produktów kosmetycznych.[49]

Na podstawie rozporządzenia z 14 stycznia 2022r. ditlenek tytanu uznany jest za związek niebezpieczny dla zdrowia, zwłaszcza w produktach spożywczych. Dodatkowo został on zakwalifikowany jako substancja rakotwórcza kategorii II, co oznacza, że jest toksyczny drogą wziewną, jeżeli występuje w postaci pyłu o wielkości cząsteczki mniejszej niż 10 µm.[50] Jednakże ditlenek tytanu może być nadal stosowany w niektórych farmaceutykach do momentu opracowania odpowiednich alternatyw. Zgoda ta została wydana przez Komisję Europejską po konsultacjach z Europejską Agencją Leków i ma na celu uniknięcie niedoborów farmaceutyków dla osób ich potrzebujących.

Badania zawarte w niniejszej pracy dotyczące ditlenku tytanu koncentrowały się nad możliwością elektrochemicznego kontrolowania jego syntezy w wyniku polikondensacji międzyfazowej zachodzącej na spolaryzowanych granicach fazowych typu ciecz – ciecz. Na **Rysunku 26** przedstawiono mechanizm otrzymywania ditlenku tytanu na spolaryzowanej granicy cieczowej. Fazę wodną stanowił bufor fosforanowy (V) zawierający jony H^+ i OH^- niezbędne do katalizowania reakcji hydrolizy i kondensacji tetrabutoksytytanu (TBOT). Natomiast fazą organiczną była hydrofobowa sól $BTPPA^+TPBCl^-$ rozpuszczona w 1,2-dichloroetanie w stężeniach od 0.01% do 0.1%. W trakcie prowadzenia badań wykazano, że ditlenek tytanu osadza się spontanicznie na granicy cieczowej, a kontrolowanie reakcji jego syntezy jest niemożliwe (lub bardzo trudne) ze względu na fotoelektrochemiczne właściwości tego związku. Elektrochemicznie kontrolowana reakcja polikondensacji równolegle wpływa na reakcję hydrolizy i kondensacji TBOT, które powodują początkowo osadzanie się materiału na granicy cieczowej, a następnie wytrącanie tego związku i/lub sedymentacje do fazy organicznej (**Rys. 26 B**).

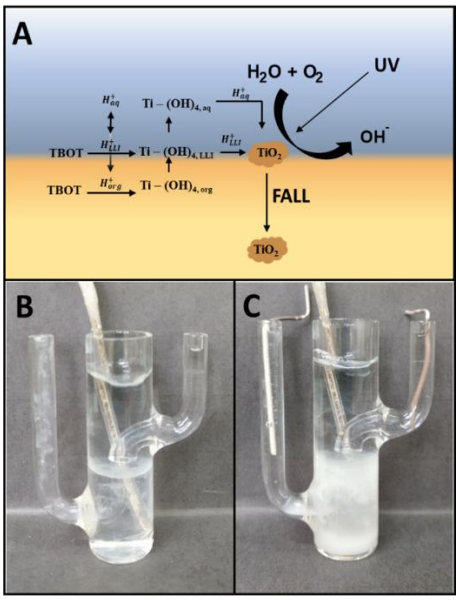

Rysunek 26. (**A**) Reakcje zachodzące podczas wspomaganej elektrochemicznie syntezy TiO_2. Zdjęcia naczynka woltamperometrycznego dla stężenia 0.5% TBOT przed (**B**) i po (**C**) przeprowadzeniu polikondensacji międzyfazowej w warunkach polaryzacji granicy fazowej typu ciecz – ciecz.

W trakcie prowadzonych badań został przebadany wpływ pH fazy wodnej na możliwość elektrochemicznego wytwarzania ditlenku tytanu na ITIES. Dodatkowo, zbadano wpływ czasu osadzania oraz wpływ stężenia TBOT w fazie organicznej (**Rys. 27**) na charakter otrzymanej odpowiedzi prądowo-potencjałowej. Wykazano, że ilość cykli przemiatania potencjałem oraz wzrastające stężenie TBOT wpływa na separację prądów pojemnościowych (wzrost pojemności elektrycznej granicy fazowej typu ciecz-ciecz). Analiza otrzymanych wyników sugeruję iż optymalnym pH fazy wodnej przy którym należy prowadzić reakcję polikondensacji międzyfazowej ditlenku tytanu jest pH = 8.

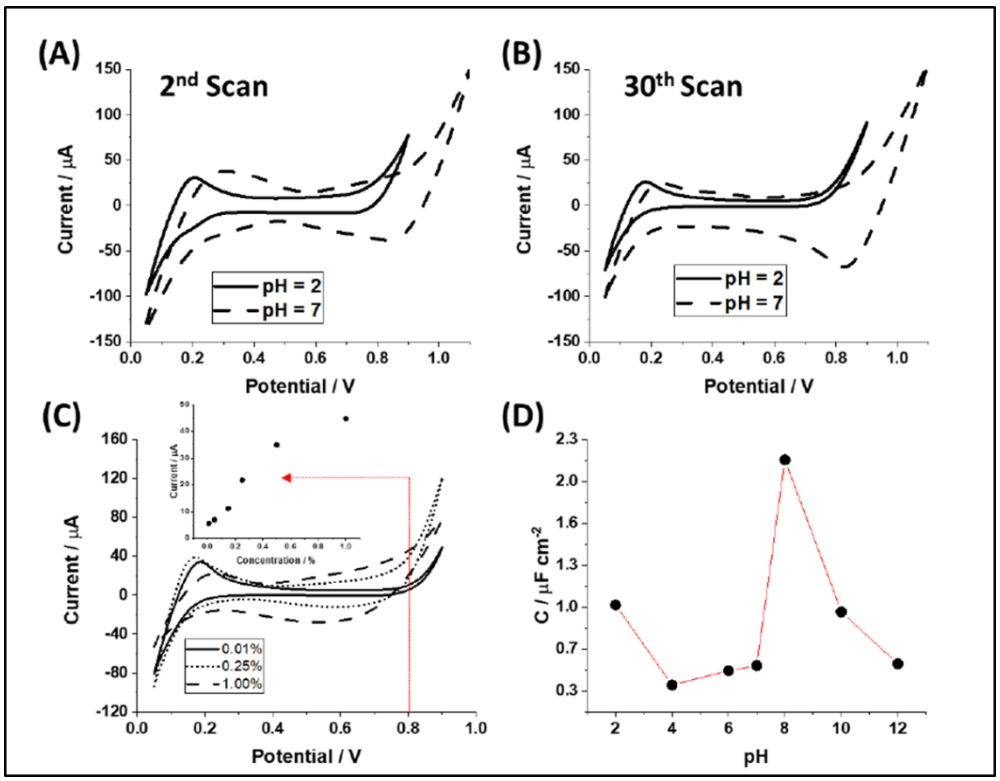

Rysunek 27. Woltamperogramy cykliczne zarejestrowane dla 0.5% TBOT rozpuszczonego w fazie organicznej w kontakcie z fazą wodną o pH = 2 lub pH =7 dla 2 i 30 cyklu przemiatania potencjałem. (**C**) Woltamperogramy cykliczne zarejestrowane dla różnych stężeń TBOT w fazie organicznej oraz krzywa wykreślona dla dodatnich prądów przy potencjalne 0.8 V; pH fazy wodnej = 2. (**D**) Pojemność elektryczna granicy cieczowej zmodyfikowanej ditlenkiem tytanu wykreślona w funkcji pH fazy wodnej.

Kolejnym etapem badań było przeprowadzenie charakterystyki ditlenku tytanu przy użyciu IR oraz SEM-EDX. W tym celu wykorzystano zminiaturyzowany układ ITIES

zbudowany z szklanej rurki z przyklejoną klejem poliamidowym na gorąco membraną z włókna szklanego. Następnie tak stworzone układy zanurzano przez 30 minut w roztworze chlorku sodu o pH = 8. Po tym czasie wypełniono je roztworami fazy organicznej o stężeniach 0.1%, 0.5% i 1% TBOT. Kontakt dwóch faz trwał 5 minut. W kolejnym etapie faza organiczna została usunięta, a systemy pozostawiono do wyschnięcia na powietrzu. Zmodyfikowane ditlenkiem tytanu membrany z włókna szklanego przebadano przy użyciu SEM-EDX (**Rys. 28**).

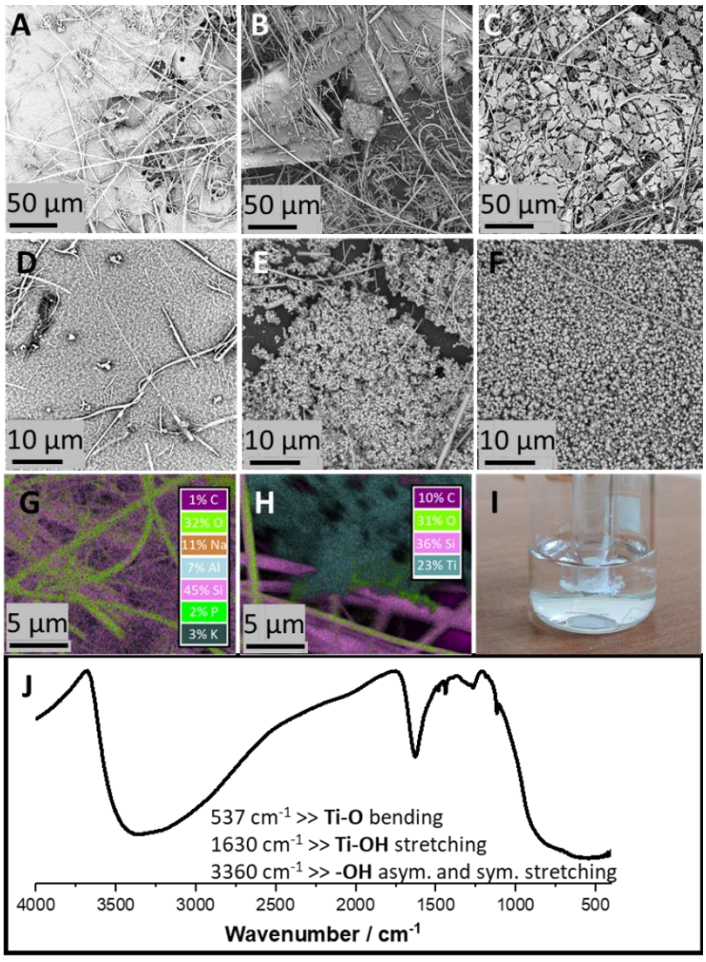

Rysunek 28. (A-F) Obrazy SEM zarejestrowane dla ditlenku tytanu osadzonego na granicy faz typu ciecz – ciecz dla stężeń 0.1%, 0.5% oraz 1.0% TBOT obecnego w fazie organicznej. (**G,H**) Obrazy EDX zarejestrowane dla membran z włókna szklanego odpowiednio przed i po modyfikacji ditlenkiem tytanu. (**I**) Zdjęcie systemu zanurzonego w fazie wodnej. (**J**) Widmo IR zarejestrowane dla materiału pobranego z granicy fazowej typu ciecz – ciecz.

Na podstawie zarejestrowanych obrazów SEM (**Rys. 28**) wykazano, że dla mniejszego stężenia TBOT% w fazie organicznej (0,1%), na granicy faz ciecz – ciecz osadza się TiO_2 w formie porowatego filmu, gdzie przy wyższym stężeniu (0,5%) struktury ditlenku tytanu widoczne są w postaci nanocząstek. Osadzony materiał został poddany analizom EDX oraz IR, które potwierdziły, że badanym materiałem jest TiO_2. Szczegółowy opis eksperymentu znajduje się w załączonej publikacji.[29]

PODSUMOWANIE

Niniejsza rozprawa doktorska oparta jest na wynikach badań opublikowanych w czterech artykułach naukowych z listy JRC oraz jednym artykule naukowym opublikowanym w repozytorium dedykowanym naukom chemicznym. Część teoretyczna dotycząca elektrochemii granic fazowych typu ciecz – ciecz została opracowana na podstawie autorskiej monografii opublikowanej w czasopiśmie Wiadomości Chemiczne[51].

Tematyka badań niniejszej pracy skupiała się na możliwościach elektrochemicznego kontrolowania reakcji polikondensacji międzyfazowej na spolaryzowanych granicach fazowych typu ciecz – ciecz, tworzeniu materiałów poliamidowych, modyfikacji układów ITIES oraz wytworzonych materiałów i analizie ich właściwości z wykorzystaniem technik elektrochemicznych. Dodatkowo przebadano elektrochemicznie ditlenek tytanu oraz pięć dendrymerów karbosilanowych na spolaryzowanych granicach cieczowych w układzie makro- i mikroskopowym.

Punktem wyjściowym części eksperymentalnej niniejszej pracy były badania dotyczące elektrochemicznie kontrolowanej syntezy Nylonu-6,6 na spolaryzowanych granicach fazowych typu ciecz – ciecz. Z sukcesem udało się otrzymać ten materiał w sposób kontrolowany elektrochemicznie, a wytworzony polimer zmodyfikowano przy użyciu nanocząstek na bazie srebra. Dzięki opracowaniu ogólnego mechanizmu syntezy poliamidów na spolaryzowanych granicach fazowych typu ciecz – ciecz udało się wytworzyć pięć innych materiałów polimerowych w sposób kontrolowany elektrochemicznie. Przy użyciu zminiaturyzowanego systemu ITIES scharakteryzowano wytworzone poliamidy pod kątem ich zdolności przesiewania molekularnego.

Kolejnym aspektem tej pracy było wykorzystanie dendrymerów do indukowania porowatości ditlenku tytanu powstającego na granicy fazowej typu ciecz-ciecz w warunkach kontrolowanych elektrochemicznie. Niestety w trakcie prowadzanych eksperymentów wykazano, że nie jest możliwe elektrochemiczne kontrolowanie reakcji syntezy ditlenku tytanu na spolaryzowanych granicach cieczowych co wynikło z bardzo dużej spontaniczności zachodzenia badanej reakcji. W związku z tym eksperymenty

dotyczące ditlenku tytanu i dendrymerów karbosilanowych ograniczyły się do badań elektroanalitycznych.

Założone hipotezy tej pracy zostały przeanalizowane, a następnie potwierdzone lub obalone.

Bibliografia

(1) Girault, H. H. Review Article Two At the Interface Between Electrolyte Solutions. *Electrochim. Acta* **1987**, *32* (3), 383–385.

(2) Gavach, C.; Seta, P.; D'epenoux, B. The Double Layer and Ion Adsorption at the Interface between Two Non Miscible Solutions. Part I. Interfacial Tension Measurements for the Water-Nitrobenzene Tetraalkylammonium Bromide Systems. *J. Electroanal. Chem.* **1977**, *83* (2), 225–235. https://doi.org/10.1016/S0022-0728(77)80168-X.

(3) Koryta, J. Electrochemical Polarization Phenomena at the Interface of Two Immiscible Electrolyte Solutions. *Electrochim. Acta* **1979**, *24* (3), 293–300. https://doi.org/10.1016/0013-4686(79)85048-3.

(4) Su, B.; Girault, H. H.; Samec, Z. Electrocatalysis at Liquid – Liquid. **2011**, 427–451.

(5) Koczorowski, Z.; Figaszewski, Z. A.; Petelska, A. D. *Elektrochemia Cieczowych Granic Fazowych*; Wydawnictwa Uniwersytetu Warszawskiego, 2011. https://doi.org/10.31338/uw.9788323510055.

(6) Girault, H. H. .; Schiffrin, D. J. Thermodymanics of a Polarised Interface between Two Immiscible Electrolyte Solutions. *J. Electroanal. Chem.* **1984**, *170*, 127–141.

(7) Rodgers, A. N. J.; Booth, S. G.; Dryfe, R. A. W. Particle Deposition and Catalysis at the Interface between Two Immiscible Electrolyte Solutions (ITIES): A Mini-Review. *Electrochem. commun.* **2014**, *47*, 17–20. https://doi.org/10.1016/j.elecom.2014.07.009.

(8) Samec, Z. Electrochemistry at the Interface between Two Immiscible Electolyte Solutions (IUPAC Technical Report). *Pure Appl. Chem.* **2004**, *76* (12), 2147–2180. https://doi.org/10.1351/pac200476122147.

(9) Liu, S.; Li, Q.; Shao, Y. Electrochemistry at Micro- and Nanoscopic Liquid/Liquid Interfaces. *Chem. Soc. Rev.* **2011**, *40* (5), 2236–2253. https://doi.org/10.1039/c0cs00168f.

(10) Hu, H.; Xie, S.; Meng, X.; Jing, P.; Zhang, M.; Shen, L.; Zhu, Z.; Li, M.; Zhuang, Q.; Shao, Y. Fabrication and Characterization of Submicrometer- and Nanometer-Sized Double-Barrel Pipets. *Anal. Chem.* **2006**, *78* (19), 7034–7039. https://doi.org/10.1021/ac060773r.

(11) Rudnicki, K.; Poltorak, L.; Skrzypek, S.; Sudhölter, E. J. R. Fused Silica Micro-Capillaries Used for a Simple Miniaturization of the Electrified Liquid – Liquid Interface. *Anal. Chem.* **2018**, *90*, 7112–7116. https://doi.org/10.1021/acs.analchem.8b01351.

(12) Poltorak, L.; Dossot, M.; Herzog, G.; Walcarius, A. Interfacial Processes Studied by Coupling Electrochemistry at the Polarised Liquid-Liquid Interface with in Situ Confocal Raman Spectroscopy. *Phys. Chem. Chem. Phys.* **2014**, *16* (48), 26955–26962. https://doi.org/10.1039/c4cp03254c.

(13) Collins, M. C.; Hébrant, M.; Herzog, G. Ion Transfer at Polarised Liquid-Liquid Interfaces Modified with Adsorbed Silica Nanoparticles. *Electrochim. Acta* **2018**, *282*, 155–162. https://doi.org/10.1016/j.electacta.2018.06.036.

(14) Poltorak, L.; Gamero-quijano, A.; Herzog, G.; Walcarius, A. Decorating Soft Electrified Interfaces : From Molecular Assemblies to Nano-Objects. *Appl. Mater. Today* **2017**, *9*, 533–550. https://doi.org/10.1016/j.apmt.2017.10.001.

(15) Löwik Dennis, W. P. M.; van Hest, J. C. M. Peptide Based Amphiphiles. *Chem. Soc. Rev.* **2004**, *33* (4), 234–245. https://doi.org/10.1039/b212638a.

(16) Arooj, M.; Arrigan, D. W. M.; Mancera, R. L. Characterization of Protein-Facilitated Ion-Transfer Mechanism at a Polarized Aqueous/Organic Interface. *J. Phys. Chem. B* **2019**, *123* (34), 7436–7444. https://doi.org/10.1021/acs.jpcb.9b04746.

(17) Arrigan, D. W. M. Voltammetry of Proteins at Liquid-Liquid Interfaces. *Annu. Reports Prog. Chem. - Sect. C* **2013**, *109*, 167–188. https://doi.org/10.1039/c3pc90007j.

(18) Berduque, A.; Scanlon, D.; Collins, C. J.; Arrigan, D. W. M. Electrochemistry of Non-Redox-Active Poly (Propylenimine) and Poly (Amidoamine) Dendrimers at Liquid - Liquid Interfaces. **2007**, No. 28, 7356–7364.

(19) Viada, B. N.; Juárez, A. V.; Pachón Gómez, E. M.; Fernández, M. A.; Yudi, L. M. Determination of the Critical Micellar Concentration of Perfluorinated Surfactants by Cyclic Voltammetry at Liquid/Liquid Interfaces. *Electrochim. Acta* **2018**, *263*, 499–507. https://doi.org/10.1016/j.electacta.2017.11.053.

(20) Pichot, R.; Watson, R. L.; Norton, I. T. Phospholipids at the Interface: Current Trends and Challenges. *Int. J. Mol. Sci.* **2013**, *14* (6), 11767–11794. https://doi.org/10.3390/ijms140611767.

(21) Piradashvili, K.; Alexandrino, E. M.; Wurm, F. R.; Landfester, K. Reactions and Polymerizations at the Liquid-Liquid Interface. *Chem. Rev.* **2016**, *116* (4), 2141–2169. https://doi.org/10.1021/acs.chemrev.5b00567.

(22) Cunnane, V. J.; Evans, U. Formation of Oligomers of Methyl- and Phenyl-Pyrrole at an Electrified Liquid/Liquid Interface. *Chem. Commun.* **1998**, No. 19, 2163–2164. https://doi.org/10.1039/a806365f.

(23) Gorgy, K.; Fusalba, F.; Evans, U.; Kontturi, K.; Cunnane, V. J. Electropolymerization of 2,2':5',2" Terthiophene at an Electrified Liquid-Liquid Interface. *Synth. Met.* **2001**, *125* (3), 365–373. https://doi.org/10.1016/S0379-6779(01)00474-X.

(24) Smirnov, E.; Peljo, P.; Scanlon, M. D.; Girault, H. H. Gold Nanofilm Redox Catalysis for Oxygen Reduction at Soft Interfaces. *Electrochim. Acta* **2016**, *197*, 362–373. https://doi.org/10.1016/j.electacta.2015.10.104.

(25) Scanlon, M. D.; Smirnov, E.; Stockmann, T. J.; Peljo, P. Gold Nanofilms at Liquid-Liquid Interfaces: An Emerging Platform for Redox Electrocatalysis, Nanoplasmonic Sensors, and Electrovariable Optics. *Chem. Rev.* **2018**, *118* (7), 3722–3751. https://doi.org/10.1021/acs.chemrev.7b00595.

(26) Uehara, A.; Booth, S. G.; Chang, S. Y.; Schroeder, S. L. M.; Imai, T.; Hashimoto, T.; Mosselmans, J. F. W.; Dryfe, R. A. W. Electrochemical Insight into the Brust-Schiffrin Synthesis of Au Nanoparticles. *J. Am. Chem. Soc.* **2015**, *137* (48), 15135–15144. https://doi.org/10.1021/jacs.5b07825.

(27) Kowalewska, K.; Sipa, K.; Leniart, A.; Skrzypek, S.; Poltorak, L. Electrochemistry at the Liquid–Liquid Interface Rediscovers Interfacial Polycondensation of Nylon-6,6. *Electrochem. commun.* **2020**, *115* (April), 106732. https://doi.org/10.1016/j.elecom.2020.106732.

(28) Kowalewska, K.; Rodriguez-Prieto, T.; Skrzypek, S.; Cano, J.; Ramírez, R. G.; Poltorak, L. Electroanalytical Study of Five Carbosilane Dendrimers at the Interface between Two Immiscible Electrolyte Solutions. *Analyst* **2021**, 1376–1385. https://doi.org/10.1039/d0an02101f.

(29) Kowalewska, K.; Sipa, K.; Burnat, B.; Skrzypek, S.; Poltorak, L. Interfacial Deposition of Titanium Dioxide at the Polarized Liquid–Liquid Interface. *Materials (Basel).* **2022**, *15* (6), 2196. https://doi.org/10.3390/ma15062196.

(30) Kowalewska, K.; Sipa, K.; Kaczmarek, K.; Skrzypek, S.; Poltorak, L. Interfacial Synthesis of Nylon-6,6 and Its Modification with Silver-Based Nanoparticles at the Electrified Liquid-Liquid Interface. *ChemElectroChem* **2022**, *9* (18). https://doi.org/10.1002/celc.202200435.

(31) Méndez, M. A.; Partovi-Nia, R.; Hatay, I.; Su, B.; Ge, P.; Olaya, A.; Younan, N.; Hojeij, M.; Girault, H. H. Molecular Electrocatalysis at Soft Interfaces. *Phys. Chem. Chem. Phys.* **2010**, *12* (46), 15163–15171. https://doi.org/10.1039/c0cp00590h.

(32) Kowalewska, K.; Kwaczynski, K.; Tarabet, M.; Sobczak, K.; Leniart, A.; Skrzypek, S.; Dossot, M.; Herzog, G.; Poltorak, L. Characterization of MicroITIES Modified with Polyamides. *Electrochim. Acta* **2023**, *under revi*.

(33) Poltorak, L.; Sudhölter, E. J. R.; de Smet, L. C. P. M. Effect of Charge of Quaternary Ammonium Cations on Lipophilicity and Electroanalytical Parameters: Task for Ion Transfer Voltammetry. *J. Electroanal. Chem.* **2017**, *796* (April), 66–74. https://doi.org/10.1016/j.jelechem.2017.04.051.

(34) Marchildon, K. Polyamides - Still Strong after Seventy Years. *Macromol. React. Eng.* **2011**, *5* (1), 22–54. https://doi.org/10.1002/mren.201000017.

(35) Pielichowski, J.; Puszyński, A. Technologia Tworzyw Sztucznych. *83-204-2831-9* **2003**, 187–188.

(36) Pielichowski, J.; Puszyński, A. Chemia Polimerow. *83-920988-0-3* **2004**, 213.

(37) Kowalewska, K. Nylon Rope Trick. *https://www.youtube.com/watch?v=S6asCwVG8zU&t=14s* **2020**.

(38) Vagholkar, P. K. Nylon (Chemistry , Properties and Uses) Chemistry. **2016**, No. 2277, 349–351.

(39) Fischer, M.; Fritz, V. From Design to Application Dendrimers : From Design to

ApplicationĐA Progress Report. *Angew. Chem. Int. Ed.* **1999**, *38* (7), 884–905.

(40) Cloninger, M. J. Biological Applications of Dendrimers. *Curr. Opin. Chem. Biol.* **2002**, *6* (6), 742–748. https://doi.org/10.1016/S1367-5931(02)00400-3.

(41) Nikzamir, M.; Hanifehpour, Y.; Akbarzadeh, A.; Panahi, Y. Applications of Dendrimers in Nanomedicine and Drug Delivery: A Review. *J. Inorg. Organomet. Polym. Mater.* **2021**, *31* (6), 2246–2261. https://doi.org/10.1007/s10904-021-01925-2.

(42) Chen, X.; Mao, S. S. Titanium Dioxide Nanomaterials: Synthesis, Properties, Modifications and Applications. *Chem. Rev.* **2007**, *107* (7), 2891–2959. https://doi.org/10.1021/cr0500535.

(43) Chen, X. Titanium Dioxide Nanomaterials and Their Energy Applications. *Cuihua Xuebao / Chinese J. Catal.* **2009**, *30* (8), 839–851. https://doi.org/10.1016/s1872-2067(08)60126-6.

(44) Chen, Z.; Han, S.; Zhou, S.; Feng, H.; Liu, Y.; Jia, G. Review of Health Safety Aspects of Titanium Dioxide Nanoparticles in Food Application. *NanoImpact* **2020**, *18* (March), 100224. https://doi.org/10.1016/j.impact.2020.100224.

(45) Guo, M. Z.; Maury-Ramirez, A.; Poon, C. S. Self-Cleaning Ability of Titanium Dioxide Clear Paint Coated Architectural Mortar and Its Potential in Field Application. *J. Clean. Prod.* **2016**, *112*, 3583–3588. https://doi.org/10.1016/j.jclepro.2015.10.079.

(46) Nonami, T.; Hase, H.; Funakoshi, K. Apatite-Coated Titanium Dioxide Photocatalyst for Air Purification. *Catal. Today* **2004**, *96* (3), 113–118. https://doi.org/10.1016/j.cattod.2004.06.112.

(47) Fujishima, A., Rao, T. N., & Tryk, D. A. Titanium Dioxide Photocatalysis. *J. Photochem. Photobiol.* **2000**, *1* (1), 1–21. https://doi.org/10.1016/s1389-5567(00)00002-2.

(48) Catalano, R.; Masion, A.; Ziarelli, F.; Slomberg, D.; Laisney, J.; Unrine, J. M.; Campos, A.; Labille, J. Optimizing the Dispersion of Nanoparticulate TiO2-Based UV Filters in a Non-Polar Medium Used in Sunscreen Formulations – The Roles of Surfactants and Particle Coatings. *Colloids Surfaces A Physicochem. Eng. Asp.* **2020**, *599* (April), 124792. https://doi.org/10.1016/j.colsurfa.2020.124792.

(49) Borges, A. R.; Duarte, Á. T.; Potes, M. da L.; Silva, M. M.; Vale, M. G. R.; Welz, B. Fluorine in Eye Shadow: Development of Method Using High-Resolution Continuum Source Graphite Furnace Molecular Absorption Spectrometry via Calcium Mono-Fluoride with Direct Solid Sample Introduction. *Microchem. J.* **2016**, *124*, 410–415. https://doi.org/10.1016/j.microc.2015.09.025.

(50) Komisja Europejska (UE). Rozporządzenie Komisji (UE) 2022/63. *Dz. Urzędowy Unii Eur.* **2014**, *14* (4), 2014.

(51) Kowalewska, K.; Sipa, K.; Skrzypek, S.; Półtorak, Ł. Poliamidy i Ich Synteza Na Spolaryzowanych Granicach Fazowych Typu Ciecz-Ciecz. **2022**, 9–10. https://doi.org/10.53584/wiadchem.2022.9.4.

Sylwetka autora

Życiorys i przebieg kariery naukowej

Urodziłam się 27 czerwca 1994 roku w Zgierzu (woj. łódzkie). W 2013 roku ukończyłam I Liceum Ogólnokształcące im. Stanisława Staszica w Zgierzu na profilu biologiczno – chemicznym, a następnie zdałam egzamin maturalny. W tym samym roku rozpoczęłam studia I stopnia na Wydziale Chemii Uniwersytetu Łódzkiego na kierunku analityka chemiczna.

Studia licencjackie ukończyłam w 2016 roku otrzymując tytuł licencjata. Swoją pracę zatytułowaną „Wykorzystanie elektrochemicznych zmysłów w chemii analitycznej" wykonałam pod opieką dr Moniki Skowron – Jaskólskiej w Zakładzie Analizy Instrumentalnej Wydziału Chemii UŁ.

W 2018 roku ukończyłam studia II stopnia otrzymując tytuł magistra. Promotorem mojej pracy magisterskiej pt. „Zastosowanie elektrod pastowych na bazie grafitu i grafenu w woltamperometrycznym oznaczaniu pestycydu biksafen" była dr Mariola Brycht. Badania eksperymentalne przeprowadziłam w Zakładzie Elektroanalizy i Elektrochemii Wydziału Chemii UŁ.

Studia doktoranckie rozpoczęłam w październiku 2018 roku. Pierwsze efekty moich badań ukazały się w 2020 roku w czasopiśmie *Electrochemistry Communication*, gdzie opublikowano artykuł dotyczący elektrochemicznie kontrolowanej syntezy Nylonu-6,6 na spolaryzowanych granicach cieczowych. Praca ta posłużyła jako dowód posiadania badań wstępnych przy składaniu wniosku do Narodowego Centrum Nauki w konkursie Preludium – 19. W lutym 2021 roku uzyskałam finansowanie na dalsze badania reakcji polikondensacji międzyfazowej zachodzącej na ITIES. Tytuł projektu badawczego, której jestem kierownikiem to „Elektrochemiczna modyfikacja spolaryzowanych granic cieczowych materiałami poliamidowymi" (DEC-2020/37/N/ST4/00270)". Projekt ten będę realizować do 31-01-2024 roku.

W wyniku współpracy z naukowcami z Hiszpanii w styczniu 2021 roku ukazał się mój drugi artykuł. Został on opublikowany w czasopiśmie *Analyst*. Badania dotyczyły przebadania elektrochemicznego zachowania pięciu dedrymerów karbosilanowych na spolaryzowanej granicy fazowej typu ciecz – ciecz. Dodatkowo związki te chciałam

wykorzystać do indukowania porowatości ditlenku tytanu. Niestety pomimo tego, iż ditlenek tytanu osadzał się na ITIES w wyniku reakcji polikondensacji międzyfazowej jego synteza nie mogła być kontrolowana elektrochemicznie ze względu na wysoką spontaniczność zachodzącego procesu. Materiał ten został przebadany elektroanalitycznie na spolaryzowanych granicach cieczowych, a wyniki badań zostały opublikowane w czasopiśmie *Materials* w 2022 roku.

Następnie moje badania skupiły się na modyfikacji nylonu-6,6 nanoobiektami na bazie srebra w sposób kontrolowany elektrochemicznie na miękkich granicach fazowych. Praca ta zakończyła się sukcesem i opublikowaniem wyników badań w czasopiśmie *ChemElectroChem* w roku ubiegłym.

Ostatnim etapem mojej rozprawy doktorskiej były eksperymenty dotyczące modyfikacji zminiaturyzowanych granic fazowych typu ciecz – ciecz wieloma materiałami poliamidowymi. Wytworzone materiały zostały zbadane pod kątem ich zdolności przesiewowych wykorzystując zminiaturyzowane układy ITIES oraz scharakteryzowane przy użyciu technik spektroskopowych i mikroskopowych. Badania te były prowadzone we współpracy z naukowcami z University of Lorraine w Nancy (Francja), gdzie odbyłam staż naukowy w okresie 14-22 listopada 2022 roku w ramach projektu POLONIUM.

Działalność naukowa, dydaktyczna i organizacyjna

Publikacje wchodzące w skład rozprawy doktorskiej:

1. **Kowalewska, K.**; Sipa, K.; Leniart, A.; Skrzypek, S.; Poltorak, L. *Electrochemistry at the Liquid–Liquid Interface Rediscovers Interfacial Polycondensation of Nylon-6,6,* Electrochem. commun. 2020, 115, 106732.
   DOI: 10.1016/j.elecom.2020.106732.
   IF_{2023}= 4.724 **MNiE= 100**

2. **Kowalewska, K**.; Rodriguez-Prieto, T.; Skrzypek, S.; Cano, J.; Ramírez, R.G., Poltorak, L. *Electroanalytical study of five carbosilane dendrimers at the interface between two immiscible electrolyte solutions*, *Analyst*, 2021, 146, 1376.
   DOI: 10.1039/D0AN02101F
   IF_{2023}= 4.616 **MNiE= 100**

3. **Kowalewska, K.**; Sipa, K.; Burnat, B.; Skrzypek, S.; Poltorak, L. *Interfacial Deposition of Titanium Dioxide at the Polarized Liquid–Liquid Interface,* Materials, 2022, 15, 2196.
   DOI: 10.3390/ma15062196
   IF_{2023}= 3.623 **MNiE= 140**

4. **Kowalewska, K.**; Sipa, K.; Kaczmarek, K.; Skrzypek, S.; Poltorak, L. *Interfacial synthesis of Nylon-6.6 and its modification with silver-based nanoparticles at the electrified liquid – liquid interface*, ChemElectroChem, 2022, 9, 18.
   DOI: 10.1002/celc.202200435
   IF_{2023}= 4.782 **MNiE= 100**

5. **Kowalewska, K.**; Kwaczynski, K.; Tarabet, M.; Sobczak, K.; Leniart, A.; Skrzypek, S.; Dossot, M.; Herzog, G.; Poltorak, L. *Characterization of microITIES modified with polyamides*, 2023, Publikacja opublikowana w repozytorium Zenodo.
   DOI: 10.5281/zenodo.7680292

Publikacje nie wchodzące w skład rozprawy doktorskiej:

A. Czasopisma z listy filadelfijskiej

1. Sipa, K.; **Kowalewska K.**; Leniart, A.; Walcarius A.; Herzog G.; Skrzypek S.; Poltorak, L. *Electrochemically assisted polyamide deposition at three-phase junction*. Electrochem. Commun. 2021, 123, 106910.
   DOI: 10.1016/j.elecom.2020.106910
   IF_{2023}= 4.724 MNiE= 100

2. Brycht, M., **Kowalewska, K.**, Skrzypek, S., Mirčeski V*., Electroanalytical study of fungicide bixafen on paste electrode based on the thermally reduced graphene oxide synthesized in air conditions and its determination in river water samples*, Electroanalysis, 2022, 34, 1 – 11.
   DOI: 10.1002/elan.202200398
   IF_{2023}= 3.223 MNiE= 70

B. Rozdziały w monografiach

1. Kowalewska, K.; Sipa, K.; Skrzypek, S., Półtorak, Ł, *Poliamidy i ich synteza na spolaryzowanych granicach fazowych typu ciecz – ciecz*, Wiadomości Chemiczne, 2022, 9-10.
   DOI: 10.53584/wiadchem.2022.9.4.
   IF_{2023}= brak MNiE= 20

Sumaryczne zestawienie danych bibliograficznych[a]:

Publikacje wchodzące w skład rozprawy doktorskiej	
Liczba publikacji	5*
Sumaryczny IF_{2023}	17,745
Średni IF	4,436**
Punkty MNiSW	440**

Publikacje nie wchodzące w skład rozprawy doktorskiej	
Liczba publikacji	2
Sumaryczny IF_{2023}	7,947
Średni IF	3,9735
Punkty MNiSW	170

Wszystkie publikacje	
Liczba publikacji	7
Sumaryczny IF_{2023}	25,692
Średni IF	4,282**
Punkty MNiSW	610**
Liczba cytowań (bez autocytowania)	10
Liczba cytowań (z autocytowaniem)	15
Indeks Hirsha (H)	2

* Łącznie z publikacją zamieszoną w repozytorium dedykowanym naukom chemicznym.

** Dla publikacji opublikowanych w czasopismach indeksowanych.

Spis doniesień konferencyjnych:

A. Wystąpienia ustne

- w języku polskim:

1. **Karolina Kowalewska**, Mariola Brycht, Sławomira Skrzypek “Zastosowanie nanomateriałów węglowych w analizie woltamperometrycznej nowoczesnego fungicydu biksafen” - Ogólnopolska Konferencja Naukowa "Zrozumieć Naukę" w Łodzi, 29 września 2018, mat. konferencyjne str. 160.

2. **Karolina Kowalewska**, Mariola Brycht, Sławomira Skrzypek „Pastowe elektrody węglowe jako narzędzia do woltamperometrycznego oznaczania pestycydu biksafen”. VII Łódzkie Sympozjum Doktorantów Chemii w Łodzi, 9 maja 2019, mat. konferencyjne str. S02-K05-29.

3. **Karolina Kowalewska**, Karolina Sipa, Andrzej Leniart, Sławomira Skrzypek, Łukasz Półtorak „Synteza nylonu na granicy ciecz-ciecz kontrolowana elektrochemicznie”. I Ogólnopolskie Sympozjum Chemii „UWiedzeni Chemią” w Warszawie, 6 – 8 marca 2020, mat. konferencyjne str. 23.

4. **Karolina Kowalewska**, Sławomira Skrzypek, Łukasz Półtorak „Synteza nylonu na spolaryzowanych granicach cieczowych”. XI Sesja Magistrantów i Doktorantów Łódzkiego Środowiska Chemików w Łodzi, 23 czerwca 2020, mat. konferencyjne str. K-04-8.

5. **Karolina Kowalewska**, Karolina Sipa, Andrzej Leniart, Sławomira Skrzypek, Łukasz Półtorak „Elektrochemia narzędziem do badania reakcji polikondensacji na ITIES”. Kopernikańskie E-seminarium Doktoranckie, 7 września 2020, mat. konferencyjne str. 52.

6. **Karolina Kowalewska,** Magdalena Karpińska, Karolina Sipa, Katarzyna Kaczmarek, Sławomira Skrzypek, Łukasz Półtorak „Modyfikacja Nylonu® nanocząsteczkami srebra za pomocą spolaryzowanych granic cieczowych". XVII Wrocławskie Studenckie Sympozjum Chemiczne, 15-16 maja 2021, mat. konferencyjne str. 18.

7. Weronika Janczak, **Karolina Kowalewska**, Mariola Brycht „Woltamperometryczne oznaczanie fungicydu biksafen za pomocą elektrody pastowej na bazie grafitu", E-Zjazd Wiosenny Sekcji Studenckiej Polskiego Towarzystwa Chemicznego, 27 – 29 maja 2021, mat konferencyjne str**.** 48.

8. Łukasz Półtorak, Paulina Borgul, **Karolina Kowalewska**, Karolina Sobczak, Karolina Sipa, Konrad Rudnicki, Sławomira Skrzypek „Sensory bazujące na spolaryzowanych granicach fazowych typu ciecz-ciecz", 63. Zjazd Naukowy Polskiego Towarzystwa Chemicznego, Łódź, 13 – 17 września 2021, mat. konferencyjne str. 189.

9. **Karolina Kowalewska**, Karolina Sipa, Sławomira Skrzypek, Łukasz Półtorak, „Reakcje polikondensacji międzyfazowej kontrolowane elektrochemicznie", II Ogólnopolska Studencka Konferencja Naukowa „Bliżej Chemii", Kraków, 8 – 9 stycznia 2022, mat. konferencyjne str. 17.

10. **Karolina Kowalewska**, Karolina Sipa, Sławomira Skrzypek, Łukasz Półtorak, Elektrochemicznie kontrolowana polikondensacja międzyfazowa na spolaryzowanych granicach cieczowych, 64 Zjazd Naukowy Polskiego Towarzystwa Chemicznego, 11 – 16 września 2022, Lublin, mat. konferencyjne str. 311.

- w języku angielskim:

1. **Karolina Kowalewska,** Karolina Sipa, Andrzej Leniart, Sławomira Skrzypek, Łukasz Półtorak „Interfacial polycondensation at polarized liquid – liquid interface", I Ogólnopolska Konferencja Online Sekcji Studenckiej Polskiego Towarzystwa Chemicznego, 10 – 12 września 2020, mat. konferencyjne str. 55.

2. Karolina Sipa, **Karolina Kowalewska,** Andrzej Leniart, Sławomira Skrzypek, Łukasz Półtorak „Electrochemically Assisted Polyamide Deposition at Three Phase Junction". 71st Annual Meeting on the International Society of Electrochemistry (ISE), 30 sierpnia – 4 września 2020, Belgrad, Serbia.

3. Lukasz Poltorak, **Karolina Kowalewska**, Karolina Sipa, Andrzej Leniart, Sławomira Skrzypek „ Decoration Of Soft Polarized Junction With Nylon-6,6".71st Annual Meeting on the International Society of Electrochemistry (ISE), 30 sierpnia – 4 września 2020, Belgrad, Serbia.

4. **Karolina Kowalewska,** Tamara Rodriguez-Prieto, Slawomira Skrzypek, Jesús Cano, Rafael Gómez Ramírez, Lukasz Poltorak „Carbosilane dendrimers studied at the polarized liquid – liquid interface", e – zjazd zimowy Sekcji Studenckiej Polskiego Towarzystwa Chemicznego, 19 grudnia 2020, mat. konferencyjne str. 51.

5. **Karolina Kowalewska,** Magdalena Karpińska, Karolina Sipa, Katarzyna Kaczmarek, Sławomira Skrzypek, Łukasz Półtorak „Electrochemical formation of polyamide modified with Ag NPs at the polarized liquid – liquid interface", E-Zjazd Wiosenny Sekcji Studenckiej Polskiego Towarzystwa Chemicznego, 27 – 29 Maja 2021, mat. konferencyjne str**.** 52.

6. **Karolina Kowalewska**, Karolina Sipa, Sławomira Skrzypek, Łukasz Półtorak, Liquid – liquid interfaces modified with polyamides for electroanalytical applications, 27th Young Investigators 'Seminar on Analytical Chemistry, 4 – 7 lipca 2022, Lodz, mat. konferencyjne str. 39.

B. Wystąpienia posterowe

- w języku polskim

1. **Karolina Kowalewska**, Mariola Brycht, Andrzej Leniart, Sławomira Skrzypek "Zastosowanie pastowych elektrod węglowych w analizie woltamperometrycznej wybranego pestycydu" - Zimowy Zjazd SSPTChem w Warszawie, 8 grudnia 2018, mat. konferencyjne str. P70-98.

2. **Karolina Kowalewska**, Tamara Rodriguez-Prieto, Sławomira Skrzypek, Jesús Cano, Rafael Gómez Ramírez, Łukasz Półtorak „Elektrochemiczne badania dendrymerów karbosilanowych na spolaryzowanych granicach cieczowych", Ogólnopolska Studencka Konferencja Naukowa „ Bliżej Chemii, Kraków, 9 – 10 stycznia 2021, mat. konferencyjne str. 68.

3. **Karolina Kowalewska**, Magdalena Karpińska, Karolina Sipa, Katarzyna Kaczmarek, Sławomira Skrzypek, Łukasz Półtorak „Elektrochemicznie kontrolowana modyfikacja Nylonu® nanocząsteczkami srebra" XII Sesja Magistrantów i Doktorantów Łódzkiego Środowiska Chemików, 17 czerwca 2021, mat. konferencyjne str. 21.

4. Weronika Janczak, **Karolina Kowalewska**, Mariola Brycht „Zastosowanie elektrody pastowej na bazie grafenu w analizie woltamperometrycznej fungicydu biksafen" Konferencja naukowa CHEMIA - BIZNES – ŚRODOWISKO (ChemBiŚ), 26 – 27 czerwca 2021, mat. konferencyjne str. 53.

5. **Karolina Kowalewska**, Magdalena Karpińska, Karolina Sipa, Katarzyna Kaczmarek, Sławomira Skrzypek, Łukasz Półtorak „Modyfikacja Nylonu® na spolaryzowanych granicach cieczowych (SGC)" VIII Łódzkie Sympozjum Doktorantów Chemii, Łódź, 24 września 2021.

6. **Karolina Kowalewska**, Karolina Sipa, Sławomira Skrzypek, Łukasz Półtorak, Wytwarzanie poliamidów na zminiaturyzowanych i spolaryzowanych granicach cieczowych, IX Łódzkie Sympozjum Doktorantów Chemii, 19 – 20 maja 2022, Łódź, mat. konferencyjne. P34.

- w języku angielskim:

1. **Karolina Kowalewska**, Sławomira Skrzypek, Łukasz Półtorak „Rediscovering nylon synthesis at the liquid-liquid interface. Electrochemical point of view" – Zimowy Zjazd SSPTChem w Gdańsku, 14 grudnia 2019, mat. konferencyjne str. 137.

2. **Karolina Kowalewska**, Tamara Rodriguez-Prieto, Sławomira Skrzypek, Jesús Cano, Rafael Gómez Ramírez, Łukasz Półtorak „Different generations of carbosilane dendrimers studies at the polarized liquid- liquid interface", International Twitter Conference, 2 – 3 marca 2021.

3. Karolina Sipa, **Karolina Kowalewska**, Andrzej Leniart, Alan Walcarius, Gregoire Herzog, Sławomira Skrzypek, Łukasz Półtorak „Electrochemically assisted nylon film formation at three phase junction", International Twitter Conference, 2 – 3 marca 2021.

4. **Karolina Kowalewska**, Tamara Rodriguez-Prieto, Slawomira Skrzypek, Jesús Cano, Rafael Gómez Ramírez, Lukasz Poltorak „Interfacial behaviour of carbosilane dendrimers at the interface between two immiscible electrolyte solutions", 3rd European BioSensor Symposium, Wildau, ONLINE, 9 – 12 marca 2021, mat konferencyjne str. 131.

5. **Karolina Kowalewska**, Tamara Rodriguez-Prieto, Slawomira Skrzypek, Jesús Cano, Rafael Gómez Ramírez, Lukasz Poltorak, „Carbosilane dendrimers and soft electrochemistry", II Pomorskie Studenckie Sympozjum Chemiczne, 20 – 21 marca 2021, mat. konferencyjne str. 70.

6. **Karolina Kowalewska**, Magdalena Karpińska, Karolina Sipa, Katarzyna Kaczmarek, Sławomira Skrzypek, Łukasz Półtorak „Electrochemically controlled modification of polyamide with nanoparticles of antibacterial properties", Prof. Krzysztof W. Szewczyk IXth Intercollegiate Biotechnology Symposium "Symbioza", 21 – 23 maja 2021, mat. konferencyjne str. 98.

7. **Karolina Kowalewska**, Magdalena Karpińska, Karolina Sipa, Katarzyna Kaczmarek, Sławomira Skrzypek, Łukasz Półtorak „Modification of nylon-6.6 with silver nanoparticles at polarized liquid – liquid interface", 72nd Annual Meeting of the International Society of Electrochemistry, Hybrid Meeting - Jeju Island, Korea/Online, 29 sierpnia – 3 września 2021.

8. Weronika Janczak, Andrzej Leniart, **Karolina Kowalewska**, Mariola Brycht „Preparation and characterization of paste electrode based on reduced graphene oxide, and its application in the voltammetric analysis of bixafen" Ogólnopolska Konferencja Sympozjum Młodych Naukowców, Warszawa, 30 sierpnia – 3 września 2021r., mat. konferencyjne str. 81.

9. **Karolina Kowalewska**, Karolina Sipa, Sławomira Skrzypek, Łukasz Półtorak, Making nylon – 6,6 at the polarized liquid -liquid interface, International Twitter Conference, 1 – 2 marca 2022.

Udział w projektach badawczych:

1. Kierownik projektu badawczego pt." Elektrochemiczna modyfikacja spolaryzowanych granic cieczowych materiałami poliamidowymi" finansowanego przez Narodowe Centrum Nauki w ramach projektu Preludium – 19 ((UMO-2020/37/N/ST4/00270) na lata 2021 – 2024.

Staże naukowe:

1. 14.11 – 22.11.2022 – staż naukowy w ramach projektu PHC POLONIUM NAWA (sgn. BPN/BFR/2021/1/00006) na University of Lorraine, Nancy, Francja.

Nagrody naukowe:

1. Stypendium rektora UŁ dla najlepszych doktorantów (2021 / 2022).
2. Zwiększenie stypendium z dotacji projakościowej w trakcie trwania studiów doktoranckim w roku akademickim 2021/2022 oraz 2022 / 2023.
3. Nagroda Dziekana Wydziału Chemii UŁ za zajęcie I miejsca za wystąpienie posterowe na podstawie badań własnych pt. „Elektrochemicznie kontrolowana modyfikacja Nylonu® nanocząsteczkami srebra" podczas XII Sesji Magistrantów i Doktorantów Łódzkiego Środowiska Chemików, która odbyła się 17 czerwca 2021.
4. Wyróżnienie Komitetu Naukowego za wygłoszony komunikat ustny na podstawie badań własnych pt. „Reakcje polikondensacji międzyfazowej kontrolowane elektrochemicznie" podczas II Ogólnopolskiej Studenckiej Konferencji Naukowej „Bliżej Chemii" , która odbyła się w dniach 8 – 9 stycznia 2022 roku.

Działalność na rzecz Uniwersytetu Łódzkiego:

1. Członek komitetu organizacyjnego VIII Łódzkiego Sympozjum Doktorantów Chemii, Wydział Chemii Uniwersytetu Łódzkiego (2021 rok).
2. Członek komitetu organizacyjnego IX Łódzkiego Sympozjum Doktorantów Chemii, Wydział Chemii Uniwersytetu Łódzkiego (2022 rok).
3. Członek komitetu organizacyjnego 27th Young Investigators 'Seminar on Analytical Chemistry, Wydział Chemii Uniwersytetu Łódzkiego (2022 rok).
4. Przedstawiciel doktorantów w Radzie Wydziału Chemii w kadencji 2020 – 2024.

Działalność dydaktyczna:

W trakcie studiów doktoranckich prowadziłam następujące zajęcia dydaktyczne ze studentami z Wydziału Chemii UŁ oraz Wydziału Biologii i Ochrony Środowiska UŁ:

1. Laboratorium z chemii ogólnej w semestrze letnim w roku akademickim 2018/2019.
2. Laboratorium z chemii ogólnej w semestrze zimowym w roku akademickim 2019/2020.
3. Warsztaty z analizy chemicznej jakościowej (analiza chemiczna jakościowa – analiza mieszanin i stopów) w semestrze letnim w roku akademickim 2019/2020.
4. Laboratorium z chemii nieorganicznej w semestrze letnim w roku akademickim 2019/2020.
5. Laboratorium z chemii ogólnej w semestrze zimowym 2020/2021.
6. Laboratorium z chemii nieorganicznej w semestrze zimowym 2020/2021.
7. Opieka nad dwiema studentkami w ramach prac dyplomowych.

Publikacje stanowiące podstawę rozprawy doktorskiej

Electrochemistry Communications 115 (2020) 106732

Contents lists available at ScienceDirect

Electrochemistry Communications

journal homepage: www.elsevier.com/locate/elecom

Electrochemistry at the liquid–liquid interface rediscovers interfacial polycondensation of nylon-6,6

Karolina Kowalewska[a], Karolina Sipa[a], Andrzej Leniart[a], Sławomira Skrzypek[a], Lukasz Poltorak[a,*]

[a] Department of Inorganic and Analytical Chemistry, Electroanalysis and Electrochemistry Group, Faculty of Chemistry, University of Lodz, Tamka 12, 91-403 Lodz, Poland

ARTICLE INFO

Keywords:
Interfacial polycondensation
ITIES
Miniaturization
Molecular sieving
Polyamide
Interfacial modification

ABSTRACT

The interfacial polymerization of nylon-6,6 is studied at the polarized liquid–liquid interface. The optimal conditions (concentration of reagents in a biphasic system, pH of the water phase, voltammetric cycling) are used to modify the interface, supported by a microcapillary, giving a platform with molecular sieving properties.

1. Introduction

The beauty of the liquid–liquid interface (LLI) lies in its asymmetric properties, which allow the separation of reagents based on their affinity to one or other of the immiscible solvents. This two-phase system provides a unique environment for the preparation of nano/microstructured materials that are difficult or impossible to prepare using other methodologies. The LLI modification can be performed either *ex situ* (the modifier is added to one of the phases) or *in situ* (interfacial decoration follows an interfacial reaction) [1]. In either case, the modifier remains at the interface as the condition for interfacial free energy reduction has to be met. The numerous examples of the reactions that can occur at the LLI are nicely summarized in an elegant review by Piradashvili et al. [2]. The interfacial polycondensation reactions between diamines and diacid chlorides provide an extremely simple way of producing polyamide at the LLI [3]. This reaction, first reported in 1935, not only found commercial success but is also known as a very nice undergraduate experiment – "the nylon rope trick". Other examples placing synthetic chemistry at the LLI may be achieved with the help of "click chemistry", including copper-catalyzed azide–alkyne reactions (e.g. for glycol nanocapsules entrapping oily core creations [4]) or thiol–ene polyaddition (e.g. for the synthesis of chitosan nanocapsules [5]).

Another property of the LLI, frequently coupled to interfacial modification, is the relative ease of operating on different scales, ranging from macroscopic and planar systems down to configurations based on nanodroplets. When placed in a container, the immiscible liquids simply separate to form a continuous and defect-free layer with dimensions defined by its support. Droplets, in turn, can be produced by means of a high energy supply (e.g. sonication) [6], a membrane-based approach [7] or microfluidics [8]. One of the immiscible liquids can be placed in a confined space such as a single nano/micropore or an array of such pores, giving alternative configurations for LLI studies [9–12]. Finally, the LLI can be enriched by another gas or solid phase, forming a multiphase junction. The latter scenario is especially interesting when solid electrodes are employed. Within such a three-phase junction, interdependent electrochemical and chemical reactions can lead to very localized deposition of materials [13–17].

An electrified LLI or interface between two immiscible electrolyte solutions (ITIES) offers electrochemical control during the interfacial modification process. In this respect, a few scenarios can be considered. In the first, a deposit can be formed upon reaction between reactants separated by the LLI (with either one or both having ionic chemical functionality within their structures) where interfacial transfer can be forced via the application of an external potential difference. This methodology was applied to decorate LLI with silica films after adopting a templated sol-gel process [18–21]. LLI polarization may also be used to create floating films of proteins [22–24] or multi-charged species [25,26] electrochemically adsorbed to the soft junction after complex formation with the hydrophobic ions of the organic phase background electrolyte. Finally, the LLI is an environment where heterogeneous redox reactions can proceed. As such, it can be decorated with metallic NPs via the reduction of metal precursors dissolved in one phase (e.g. chloro complexes of Pt or Pd hosted by the water phase)

* Corresponding author.
E-mail address: lukasz.poltorak@chemia.uni.lodz.pl (L. Poltorak).

https://doi.org/10.1016/j.elecom.2020.106732
Received 24 March 2020; Received in revised form 6 April 2020; Accepted 13 April 2020
Available online 15 April 2020

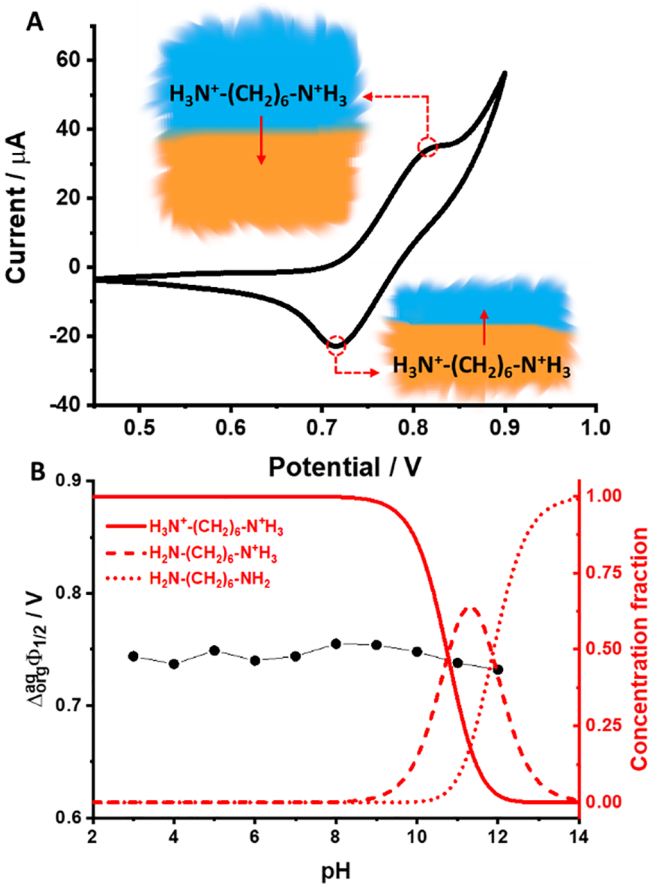

Fig. 1. A Ion transfer voltammogram (ITV) recorded in the presence of 110 μM 1,6-DAH in the water phase (pH ≈ 2, scan rate 10 mV·s^{-1}). The direction of the 1,6-DAH ion transfer is also shown schematically and is attributed to the corresponding signal. **B** The marked points (the line joining them is only a guide for the eye) represent the half-wave potential for the interfacial ion transfer of 1,6-DAH, extracted from voltammograms recorded at different pH values. The red lines represent the distribution diagram of all possible 1,6-DAH species. (For interpretation of the references to colour in this figure legend, the reader is referred to the web version of this article.)

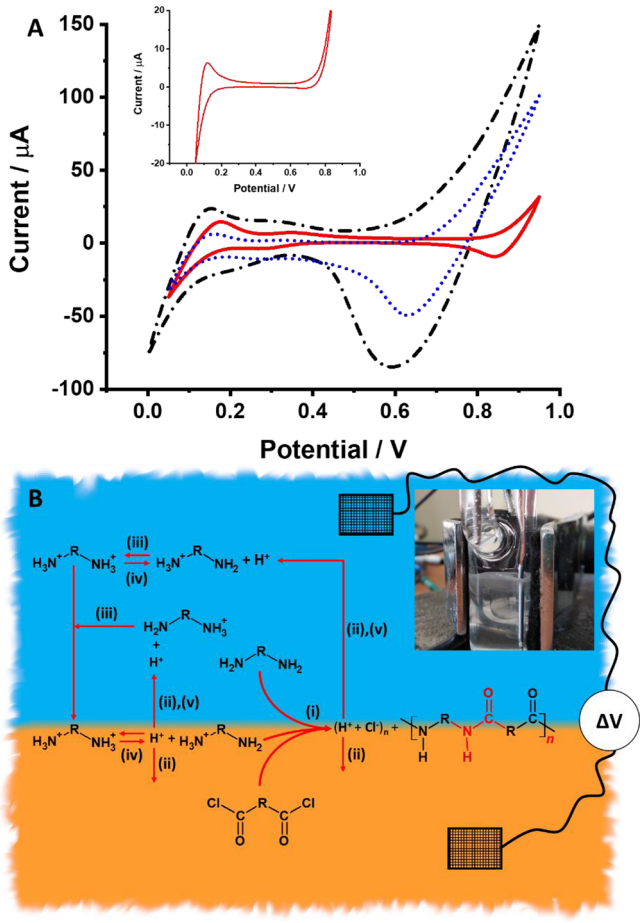

Fig. 2. A ITVs recorded with 5 mM 1,6-DHA in the aqueous phase (dotted blue curve); with 5 mM adipoyl chloride (AC) in the organic phase (solid red curve); and with 5 mM 1,6-DHA in the aqueous phase and 5 mM AC in the organic phase (dot-dash black curve) at a pH equal to 12. The inset shows the voltammogram recorded with 5 mM AC dissolved in the organic phase and the pH of the aqueous phase equal to 2. **B** Proposed mechanism of electrochemically-assisted polyamide formation. A description of the reactions labelled (i) to (v) is given in the text. (For interpretation of the references to colour in this figure legend, the reader is referred to the web version of this article.)

using the electrons from electron donors present in the second phase (e.g. ferrocene derivatives dissolved in the organic solvent) [27–30]. A few examples exist where an electrochemically controlled interfacial electron transfer reaction is used to trigger interfacial polymerization of e.g. polythiophenes [31] or polypyrrole [32,33].

2. Methods and materials

All of the methods, materials and equipment used in this work are described in Section 1 of the electronic Supporting information.

3. Results and discussion

In this work, for the first time, we have used electrochemical control to study nylon-6,6 polycondensation at the polarized water – 1,2-dichloroethane interface. Fig. 1A shows the ion transfer voltammogram (ITV) recorded in the macroscopic electrochemical cell formed upon contacting 110 μM 1,6-diaminohexane (1,6-DAH) dissolved in 10 mM HCl (pH ≈ 2) with 5 mM organic electrolyte solution (for details refer to Supporting information, Section 1.1) dissolved in 1,2-dichloroethane.

Two characteristic signals were recorded and correspond to the interfacial transfer of the charged 1,6-DAH from the aqueous to the organic phase – the positive peak current – and its back transfer from the organic to the aqueous phase, recorded as the negative peak current. The signal originating from the 1,6-DAH appears at around 0.75 V and is partially overlaid with the interfacial transfer of H^+ limiting the potential window on the more positive potential side. Electrochemical characterization of the 1,6-DAH revealed that (i) the corresponding ionic currents can be detected from concentrations as low as 1 μM (see Fig. S1A); (ii) the ratio of the forward and reverse peak current approaches unity, indicating a reversible simple ion-transfer reaction; (iii) the peak-to-peak separation is equal to about 30 mV (within the lower concentration range), which agrees well with the anticipated charge $z = 2$ for pH = 2; (iv) the diffusion coefficient of the 1,6-DAH calculated using the Randles-Sevcik equation is equal to $2.3 \cdot 10^{-6}$ cm^2·s^{-1} and agrees well with the value given in the literature – $1.2 \cdot 10^{-6}$ cm^2·s^{-1} [34] (for details see the Supporting information, Section 2.2). Fig. 1B shows the relation between the half-wave potential of ion transfer for the 1,6-DAH and the pH of the aqueous phase (Britton-Robinson buffer), which is correlated with the fraction of different 1,6-DAH species present in the water phase at different pH values.

The latter data (Fig. 1B in red) were plotted using $pKa_1 = 10.8$ and $pKa_2 = 11.9$ (for details, see Section 2.3 in the Supporting information) [35]. As expected, up to pH 8–9 the potential of 1,6-DAH ion transfer remains largely unaffected as nearly 100% of 1,6-DAH species are fully protonated (each molecule holds two positively charged amine groups –

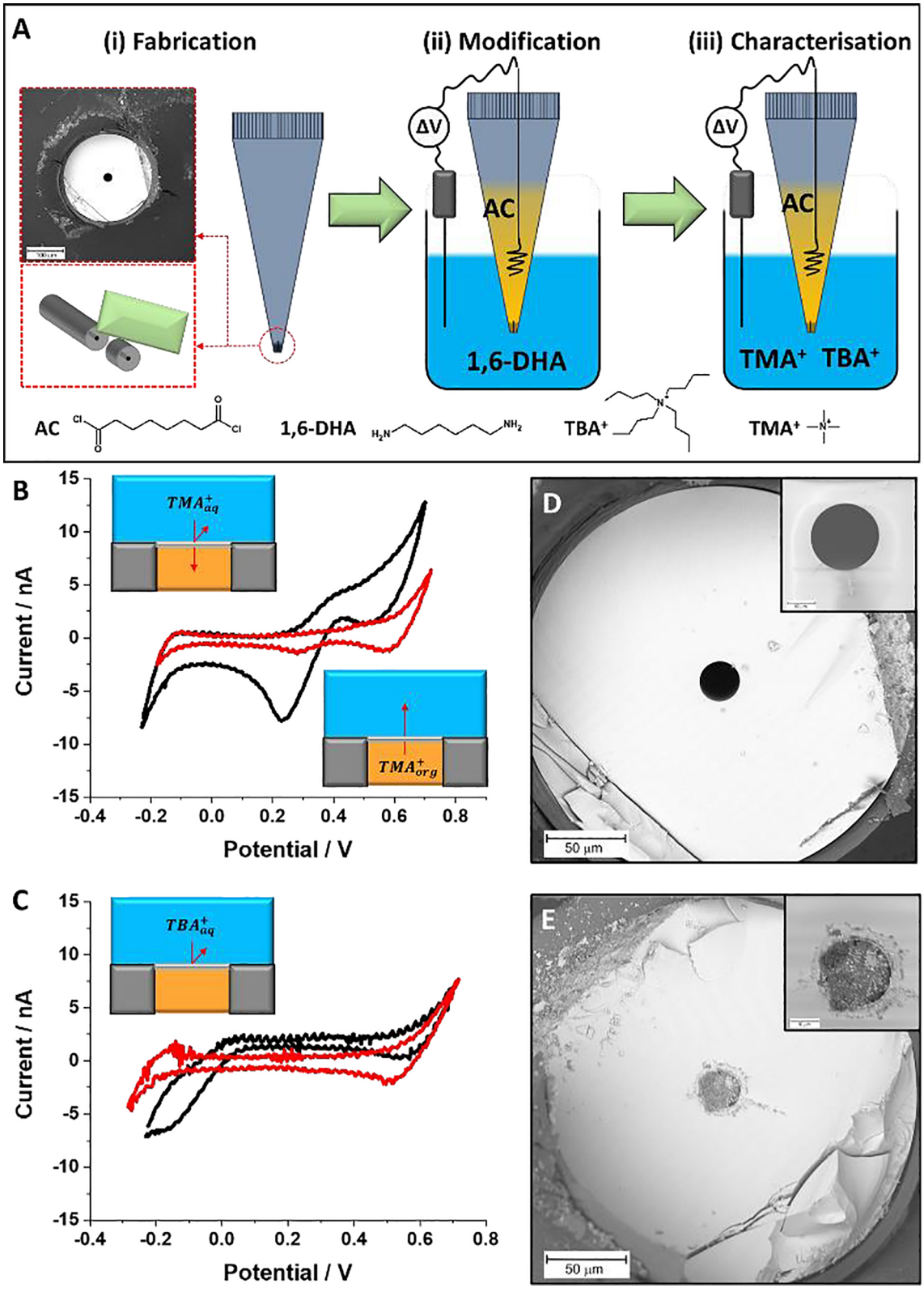

Fig. 3. A – A schematic representation of an experimental protocol involving (i) fabrication of a microscopic ITIES (supported with a piece of silica capillary tubing; the SEM photo shows the capillary embedded in plastic casing), (ii) electrochemical modification of the microscopic ITIES with nylon-6,6; (iii) electrochemical characterization of the modified microscopic ITIES in the presence of TMA^+ and TBA^+. The ITVs show the currents corresponding to the TMA^+ (**B**) and TBA^+ (**C**) initially present in the aqueous phase before and after modification. **D** and **E** (also insets) show SEM micrographics of a fused silica microcapillary before and after modification, respectively.

1,6-DAM^{2+}). A further increase in pH, especially in the pH range from 9 to 13, causes significant fluctuations in the fraction of non- (1,6-DAH^{0}), mono- (1,6-DAM^{+}) and 1,6-DAH^{2+} species. This is also reflected in the position and intensity of the positive and negative peaks attributed to 1,6-DAH ion transfer (see ITVs in Fig. S3). The tentative rule says that the potential of ion transfer can be directly attributed to the hydrophilicity of the molecule under investigation. That is, more hydrophilic cations require a higher portion of the potential applied to the LLI to trigger their interfacial transfer [36]. Consequently, as the concentration of 1,6-DAH^{+} and 1,6-DAH^{0} species (both being slightly more hydrophobic than 1,6-DAH^{2+}) increase, we have observed dropping peak currents and a shift in the transfer potential towards lower potential values. For further experiments involving interfacial polycondensation of nylon-6,6 we have fixed the pH of the aqueous phase at 12, under which conditions 1,6-DAH species exist as the 1,6-DAH^{0} and 1,6-DAH^{+} species in a ratio of about 1:1. A pH optimization study was performed and is summarized in Section 2.4 of the Supporting information. Fig. 2A shows a series of cyclic voltammograms recorded with 5 mM 1,6-DAH in the water phase, 5 mM AC in the organic phase and with both reagents at 5 mM concentration in both the water and the organic phases. Without a permanent charge or ionizable chemical functional group, the AC is electrochemically inactive. The product of its hydrolysis, adipic acid, although probably formed, does not give a signal within the available potential window (ITVs recorded with and without 5 mM AC in the organic phase with the pH of the aqueous phase set to 2 and 12 revealed no differences). A clear signal appears when only 5 mM 1,6-DAH was present in the aqueous phase – Fig. 2A, blue dotted curve. In this particular case, the positive current limiting the potential widow starts increasing 195 mV earlier than the blank and originates from 1,6-DAH^{+} transfer from the water to the organic phase. Further positive polarization eventually triggers Na^{+} transfer from the water to the organic phase. The most interesting situation occurs when both reagents are present in the biphasic system, i.e. 1,6-DAH in the water and AC in the organic phase. First of all, the point at which the positive current starts increasing is further shifted to lower potential values by around 80 mV. Moreover, after just one voltammetric cycle film can be clearly seen with the naked eye at the soft junction (see the photo in the top right-hand corner of Fig. 2B). The material formed at the ITIES contained several absorption bands characteristic of polyamides, as shown using infra-red spectrometry (for details see Section 2.5 in the Supporting information). The blank experiment set in a beaker revealed that for identical conditions but without external polarization, nylon-6,6 film is again formed, but requires more time (2–3 min). The proposed mechanism of electrochemically controlled nylon-6,6 interfacial polymerization is shown schematically in Fig. 2B. Here a number of mutually interconnected reactions can occur. First of all, (i) the 1,6-DAH^{0} can react with AC within the interfacial region giving polyamide and hydrochloric acid which dissociates into H^{+} and Cl^{-}. As the interface is polarized using an external power source, (ii) H^{+} may be transferred to either the organic or the aqueous phase. In the latter case, especially within the interfacial region, (iii) the amine groups of the 1,6-DAH^{0} will be protonated, and hence, the resulting cations may undergo an interfacial ion transfer reaction. (iv) We cannot exclude protonated amine dissociation, especially in the mixed layer region, giving rise to non-protonated amine groups available for reaction with the acyl chloride functional groups and (v) H^{+} further acidifying the aqueous phase layer adjacent to the LLI. All these reactions lead to the formation of a probably partially positively-charged polyamide film that may find applications in size- and charge-sieving-based molecular separation.

To demonstrate the applicability of the developed procedure, we have used electrochemical control to modify the microscopic LLI with nylon-6,6 based films. Firstly, we prepared the microITIES using fused silica capillaries with an internal diameter equal to 25 μm (the protocol of microITIES preparation is described elsewhere) [37]. Electrochemical studies revealed that the location of the ITIES is at the pore ingress and the diameter of the ITIES of 23.2 μm (see Supporting information Section 2.6) agrees very well with the pore diameter measured using SEM (24.8 μm – Fig. 3D). The protocol for the modification of the microITIES with nylon-6,6 is depicted in Fig. 3A. Briefly, the freshly prepared capillaries were filled with the organic phase containing 5 mM AC. Next, these were immersed in a water phase containing 5 mM 1,6-DAH. The electrodes and connections were fixed and five voltammetric cycles were recorded. The SEM micrographs clearly show that a deposit is present within the pore after the electrochemical modification process (Fig. 3E), unlike the unmodified pore (Fig. 3D).

Next, the modified capillary was placed directly into a cell containing either tetramethylammonium (TMA^{+}) or tetrabutylammonium (TBA^{+}) cations. Fig. 3B and C show the ITVs recorded before and after modification in the presence of the specified quaternary ammonium cations in the water phase at a concentration equal to 60 μM. It is nicely shown that the transfer of TBA^{+} is entirely blocked (signal appearing on the negative side of the potential window in Fig. 3C) whereas the faradaic current for TMA^{+} is reduced by 90%. The proposed platform combines a very simple LLI miniaturization approach with an ITIES modification protocol which is equally straightforward. As a whole, the proposed configuration may find applications in sensing, selected molecular recovery or separation.

4. Conclusions

In this work we have shown that the interfacial deposition of polyamide based films can be controlled using electrochemically triggered ion transfer. Precise control of the pH is essential in this respect, as protonation of the amine groups within 1,6-DAH inhibits the reaction with the AC. The resulting polyamide films can be easily removed from the interface, which is of the utmost importance for practical applications. Additionally, micropores with a diameter of 25 μm were used to support the polarized LLI and were further modified under electrochemical control with the polyamide film. The resulting platform exhibited size-sieving properties, being partially permeable to tetramethylammonium cations and entirely inhibiting the interfacial transport of the tetrabutylammonium cation.

Conflicts of interest

There are no conflicts to declare.

CRediT authorship contribution statement

Karolina Kowalewska: Investigation, Formal analysis. **Karolina Sipa:** Investigation, Formal analysis. **Andrzej Leniart:** Investigation, Formal analysis. **Sławomira Skrzypek:** Supervision, Writing - review & editing. **Lukasz Poltorak:** Methodology, Visualization, Supervision, Project administration, Funding acquisition, Writing - review & editing, Writing - original draft.

Acknowledgments

This project was financially supported by the National Science Center (NCN) in Krakow, Poland (Grant no. UMO-2018/31/D/ST4/03259).

Appendix A. Supplementary data

Supplementary data to this article can be found online at https://doi.org/10.1016/j.elecom.2020.106732.

References

[1] L. Poltorak, A. Gamero-Quijano, G. Herzog, A. Walcarius, Decorating soft electrified interfaces: from molecular assemblies to nano-objects, Appl. Mater. Today 9 (2017)

533–550, https://doi.org/10.1016/j.apmt.2017.10.001.
[2] K. Piradashvili, E.M. Alexandrino, F.R. Wurm, K. Landfester, Reactions and polymerizations at the liquid–liquid interface, Chem. Rev. 116 (2016) 2141–2169, https://doi.org/10.1021/acs.chemrev.5b00567.
[3] W.H. Carothers, Linear Polyamides and their Production, US Patent US2130523A, 1938.
[4] R. Roux, L. Sallet, P. Alcouffe, S. Chambert, N. Sintes-Zydowicz, E. Fleury, J. Bernard, Facile and rapid access to glyconanocapsules by CuAAC interfacial polyaddition in miniemulsion conditions, ACS Macro Lett. 1 (2012) 1074–1078, https://doi.org/10.1021/mz300281u.
[5] C.K. Chen, Q. Wang, C.H. Jones, Y. Yu, H. Zhang, W.C. Law, C.K. Lai, Q. Zeng, P.N. Prasad, B.A. Pfeifer, C. Cheng, Synthesis of pH-responsive chitosan nanocapsules for the controlled delivery of doxorubicin, Langmuir 30 (2014) 4111–4119, https://doi.org/10.1021/la4040485.
[6] N. Anton, J.P. Benoit, P. Saulnier, Design and production of nanoparticles formulated from nano-emulsion templates – a review, J. Control. Release 128 (2008) 185–199, https://doi.org/10.1016/j.jconrel.2008.02.007.
[7] G.T. Vladisavljević, R.A. Williams, Recent developments in manufacturing emulsions and particulate products using membranes, Adv. Colloid Interface Sci. 113 (2005) 1–20, https://doi.org/10.1016/j.cis.2004.10.002.
[8] S.Y. Teh, R. Lin, L.H. Hung, A.P. Lee, Droplet microfluidics, Lab. Chip 8 (2008) 198–220, https://doi.org/10.1039/b715524g.
[9] M. Sairi, J. Strutwolf, R.A. Mitchell, D.S. Silvester, D.W.M. Arrigan, Chronoamperometric response at nanoscale liquid–liquid interface arrays, Electrochim. Acta 101 (2013) 177–185, https://doi.org/10.1016/j.electacta.2012.11.062.
[10] Y.H. Lanyon, G. De Marzi, Y.E. Watson, A.J. Quinn, J.P. Gleeson, G. Redmond, D.W.M. Arrigan, Fabrication of nanopore array electrodes by focused ion beam milling, Anal. Chem. 79 (2007) 3048–3055, https://doi.org/10.1021/ac061878x.
[11] M.D. Scanlon, J. Strutwolf, A. Blake, D. Iacopino, A.J. Quinn, D.W.M. Arrigan, Ion-transfer electrochemistry at arrays of nanointerfaces between immiscible electrolyte solutions confined within silicon nitride nanopore membranes, Anal. Chem. 82 (2010) 6115–6123, https://doi.org/10.1021/ac1008282.
[12] R. Zazpe, C. Hibert, J. O'Brien, Y.H. Lanyon, D.W.M. Arrigan, Ion-transfer voltammetry at silicon membrane-based arrays of micro-liquid-liquid interfaces, Lab. Chip 7 (2007) 1732–1737, https://doi.org/10.1039/b712601h.
[13] E. Bak, M. Donten, M. Skompska, Z. Stojek, Electrodeposition of poly(N-vinylcarbazole) at the three-phase junction. Formation of very different polymer structures, J. Phys. Chem. B 110 (2006) 24635–24641, https://doi.org/10.1021/jp063935w.
[14] M. Li, H. Zhu, X. Mao, W. Xiao, D. Wang, Electropolymerization of polypyrrole at the three-phase interline: influence of polymerization conditions, Electrochim. Acta 92 (2013) 108–116, https://doi.org/10.1016/j.electacta.2013.01.016.
[15] I. Kaminska, M. Jonsson-Niedziolka, A. Kaminska, M. Pisarek, R. Hołys, M. Opallo, J. Niedziolka-Jonsson, Electrodeposition of well-adhered multifarious Au particles at a solid|toluene|aqueous electrolyte three-phase junction, J. Phys. Chem. C 116 (2012) 22476–22485, https://doi.org/10.1021/jp307674k.
[16] J. Niedziolka, M. Opallo, Electrochemically assisted sol–gel process at a three phase junction, Electrochem. Commun. 10 (2008) 1445–1447, https://doi.org/10.1016/j.elecom.2008.07.039.
[17] V. Lakshminarayanan, L. Poltorak, D. Bosma, E.J.R. Sudhölter, J.H. van Esch, E. Mendes, Locally pH controlled and directed growth of supramolecular gel microshapes using electrocatalytic nanoparticles, Chem. Commun. 55 (2019) 9092–9095, https://doi.org/10.1039/c9cc04238e.
[18] L. Poltorak, G.G. Herzog, A. Walcarius, Electrochemically assisted generation of silica deposits using a surfactant template at liquid/liquid microinterfaces, Langmuir 30 (2014) 11453–11463, https://doi.org/10.1021/la501938g.
[19] L. Poltorak, K. Morakchi, G. Herzog, A. Walcarius, Electrochemical characterization of liquid-liquid micro-interfaces modified with mesoporous silica, Electrochim. Acta 179 (2015) 9–15, https://doi.org/10.1016/j.electacta.2015.01.129.
[20] L. Poltorak, M. Hébrant, M. Afsharian, M. Etienne, G. Herzog, A. Walcarius, Local pH changes triggered by photoelectrochemistry for silica condensation at the liquid-liquid interface, Electrochim. Acta 188 (2016) 71–77, https://doi.org/10.1016/j.electacta.2015.11.107.
[21] A. Holzinger, G. Neusser, B.J.J. Austen, A. Gamero-Quijano, G. Herzog, D.W.M. Arrigan, A. Ziegler, P. Walther, C. Kranz, Investigation of modified nanopore arrays using FIB/SEM tomography, Faraday Discuss. 210 (2018) 113–130, https://doi.org/10.1039/c8fd00019k.
[22] L. Poltorak, N. van der Meijden, S. Oonk, E.J.R. Sudhölter, M. de Puit, Acid phosphatase behaviour at an electrified soft junction and its interfacial co-deposition with silica, Electrochem. Commun. 94 (2018) 27–30, https://doi.org/10.1016/j.elecom.2018.07.022.
[23] G. Herzog, V. Kam, D.W.M. Arrigan, Electrochemical behaviour of haemoglobin at the liquid/liquid interface, Electrochim. Acta 53 (2008) 7204–7209, https://doi.org/10.1016/j.electacta.2008.04.072.
[24] E. Alvarez de Eulate, S. O'Sullivan, D.W.M. Arrigan, Electrochemically induced formation of cytochrome C oligomers at soft interfaces, ChemElectroChem 4 (2017) 898–904, https://doi.org/10.1002/celc.201600851.
[25] G. Herzog, S. Flynn, C. Johnson, D.W.M. Arrigan, Electroanalytical behavior of poly-L-lysine dendrigrafts at the interface between two immiscible electrolyte solutions, Anal. Chem. 84 (2012) 5693–5699.
[26] A. Berduque, M.D. Scanlon, C.J. Collins, D.W.M. Arrigan, Electrochemistry of non-redox-active poly(propylenimine) and poly(amidoamine) dendrimers at liquid-liquid interfaces, Langmuir 23 (2007) 7356–7364, https://doi.org/10.1021/la063294w.
[27] P.S. Toth, A.N.J. Rodgers, A.K. Rabiu, R.A.W. Dryfe, Electrochemical activity and metal deposition using few-layer graphene and carbon nanotubes assembled at the liquid–liquid interface, Electrochem. Commun. 50 (2015) 6–10, https://doi.org/10.1016/j.elecom.2014.10.010.
[28] Y. Li, O. Zaluzhna, Y.J. Tong, Identification of a source of size polydispersity and its solution in Brust-Schiffrin metal nanoparticle synthesis, Chem. Commun. 47 (2011) 6033–6035, https://doi.org/10.1039/c1cc11642h.
[29] Y. Li, O. Zaluzhna, B. Xu, Y. Gao, J.M. Modest, Y.Y.J. Tong, Mechanistic insights into the Brust-Schiffrin two-phase synthesis of organo-chalcogenate-protected metal nanoparticles, J. Am. Chem. Soc. 133 (2011) 2092–2095, https://doi.org/10.1021/ja1105078.
[30] M. Platt, R.A.W. Dryfe, Structural and electrochemical characterisation of Pt and Pd nanoparticles electrodeposited at the liquid/liquid interface: Part 2, Phys. Chem. Chem. Phys. 7 (2005) 1807–1814 http://www.ncbi.nlm.nih.gov/pubmed/19787942.
[31] U. Evans-Kennedy, J. Clohessy, V.J. Cunnane, Spectroelectrochemical study of 2,2':5',2''-terthiophene polymerization at a liquid / liquid interface controlled by potential-determining ions, Macromolecules 37 (2004) 3630–3634.
[32] P.S. Toth, A.K. Rabiu, R.A.W. Dryfe, Controlled preparation of carbon nanotube-conducting polymer composites at the polarisable organic/water interface, Electrochem. Commun. 60 (2015) 153–157, https://doi.org/10.1016/j.elecom.2015.08.022.
[33] K. Maeda, H. Jänchenová, A. Lhotský, I. Stibor, J. Budka, V. Mareček, Formation of a polymer layer from monomers adsorbed at a liquid | liquid interface, J. Electroanal. Chem. 516 (2001) 103–109, https://doi.org/10.1016/S0022-0728(01)00658-1.
[34] B. Li, Y. Qiao, J. Gu, X. Zhu, X. Yin, Q. Li, Z. Zhu, M. Li, P. Jing, Y. Shao, Electrochemical behaviors of protonated diamines at the micro-water/1,2-dichloroethane interface, J. Electroanal. Chem. 726 (2014) 21–26, https://doi.org/10.1016/j.jelechem.2014.05.007.
[35] D.R. Lide, CRC Handbook of Chemistry and Physics, 84th Edition, 53 (2003) 2616.
[36] A.J. Olaya, M.A. Méndez, F. Cortes-Salazar, H.H. Girault, Voltammetric determination of extreme standard Gibbs ion transfer energy, J. Electroanal. Chem. 644 (2010) 60–66, https://doi.org/10.1016/j.jelechem.2010.03.030.
[37] K. Rudnicki, L. Poltorak, S. Skrzypek, E.J.R. Sudhölter, Fused silica micro-capillaries used for a simple miniaturization of the electrified liquid – liquid interface, Anal. Chem. 90 (2018) 7112–7116, https://doi.org/10.1021/acs.analchem.8b01351.

Supporting Information

Electrochemistry at the liquid–liquid interface rediscovers interfacial polycondensation of nylon-6,6

Karolina Kowalewska,[a] Karolina Sipa,[a] Andrzej Leniart,[a] Sławomira Skrzypek,[a] Lukasz Poltorak[a*]

a. *Department of Inorganic and Analytical Chemistry, Electroanalysis and Electrochemistry Group, Faculty of Chemistry, University of Lodz, Tamka 12, 91-403 Lodz, Poland.*

***Corresponding author:** lukasz.poltorak@chemia.uni.lodz.pl*

Outline:

1. Methods, materials and instrumentation.

1.1. Materials.

Sodium chloride (NaCl, for analysis, ChemPur), acetic acid (CH_3COOH, 99.5 – 99.9%, POCh), phosphoric acid (H_3PO_4, 80%, for analysis, ChemPur), boric acid (H_3BO_3, for analysis, ChemPur), 1,6-diaminohexane (1,6-DAH, ≥99.5%, Acros Organics), adipoyl chloride (AC, 98%, Alfa Aesar), 1,2-dichloroethane (1,2-DCE, for analysis, POCh), tetramethylammonium chloride (TMACl, >98%, Acros Organics), tetrabutylammonium chloride (TBACl, 97%, Apollo Scientific), potassium tetrakis(4-chlorophenyl)borate (KTPBCl, ≥98%, Sigma-Aldrich) and *bis*(*triphenylphosphoranylidene*)*ammonium chloride* (BTPPACl, 97%, Sigma-Aldrich) were used as received. 35-38% hydrochloric acid (HCl, for analysis, ChemPur) and sodium hydroxide (NaOH, for analysis, ChemPur) were used to prepare 1M solution that were further employed for pH adjustment. Britton-Robbinson buffers having different pH values were prepared from the stock solution of 10 mM CH_3COOH, 10 mM H_3PO_4, 10 mM H_3BO_3 and 10 mM NaCl using 1M NaOH. The organic phase background electrolyte (*bis*(*triphenylphosphoranylidene*)*ammonium* tetrakis(4-chlorophenyl)borate (BTPPATPBCl)) was synthetized using BTPPACl and KTPBCl in equimolar amounts according to the protocol reported elsewhere.[1] The methyl deactivated fused silica capillary tubing having the internal diameter equal to 25 µm was purchased from VWR. All experiments were performed using triple distilled water.

1.2. Electrochemical experiments.

The electrochemical experiments involving macroscopic liquid-liquid interface (LLI) (interface radii equal to 0.7 cm) were performed using EmStat3+ from PalmSens. The LLI was polarized in a four electrode configuration. Each phase contained Ag/AgCl and Pt used as the reference and counter electrodes, respectively. The effect of concentration and the scan rate on the 1,6-DAH electrochemical behavior was studied in the following cell:

$$Ag|AgCl|\begin{matrix}10\ mM\ NaCl\\10\ mM\ HCl\\x\ \mu M\ 1{,}6-DAH\ in\ H_2O\end{matrix}\Big|5\ mM\ BTPPATPBCl|\begin{matrix}5\ mM\ BTPPATPBCl\\10\ mM\ NaCl\end{matrix}\Big|AgCl|Ag$$

Cell I

Effect of pH of the aqueous phase on the standard Galvani potential of ion transfer was investigated in cell II:

$$Ag|AgCl|\begin{matrix}10\ mM\ NaCl, 10\ mM\ H_3PO_4,\\10\ mM\ CH_3COOH, 10\ mM\ H_3BO_3\\+\ y\ \mu L\ 1\ M\ NaOH\end{matrix}\Big|5\ mM\ BTPPATPBCl|\begin{matrix}5\ mM\ BTPPATPBCl\\10\ mM\ NaCl\end{matrix}\Big|AgCl|Ag$$

Cell II

Nylon-6,6 electrochemical deposition at the LLI was studied in the cell III:

$$Ag|AgCl|\begin{matrix}10\ mM\ NaCl + y\ \mu L\ 1\ M\ NaOH\\ z\ mM\ 1{,}6-DAH\end{matrix}\Big|\begin{matrix}5\ mM\ BTPPATPBCl\\ 5\ mM\ AC\end{matrix}\Big|\begin{matrix}5\ mM\ BTPPATPBCl\\ 10\ mM\ NaCl\end{matrix}\Big|AgCl|Ag$$

Cell III

The experiments involving microscopic LLI were performed with the Autolab 302N (Metrhom) equipped with the ECD (extreme low currents) module. During experiments the Ag wire covered with the layer of AgTPBCl was used as both the counter and reference electrode, whereas Ag/AgCl and Pt were used as the water phase reference and counter electrode, respectively. The electrochemical cell can be given by:

$$Ag|AgCl|\begin{matrix}10\ mM\ NaCl\\ a\ \mu M\ TMA^+\ or\ b\ \mu M\ TBA^+\ or\\ z\ mM\ 1{,}6-DAH\ in\ H_2O\end{matrix}\Bigg|\begin{matrix}5\ mM\ BTPPATPBCl\\ 5\ mM\ AC\ in\ 1{,}2-DCE\end{matrix}\Bigg|AgTPBCl|Ag$$

Cell IV

1.3. Infra-red spectroscopy.

Nylon-6,6 electrochemically formed at the LLI was collected, dried and further analyzed using KBr pellet method with an infra-red spectrometry (Nexus FT-IR by Thermo Nicolet).

1.4. Scanning Electron Microscopy.

The scanning electron microscopy (SEM, a Phenom G2 Pure, FEI Company, the Netherlands) was used to compare unmodified and nylon-6,6 modified micro-capillaries. SEM images were acquired using a high sensitivity backscatter electron detector (BSD) with an accelerating voltage of 5 kV.

2. Supplementary results.

2.1. Effect of 1,6-DAH concentration on the electrochemical signal.

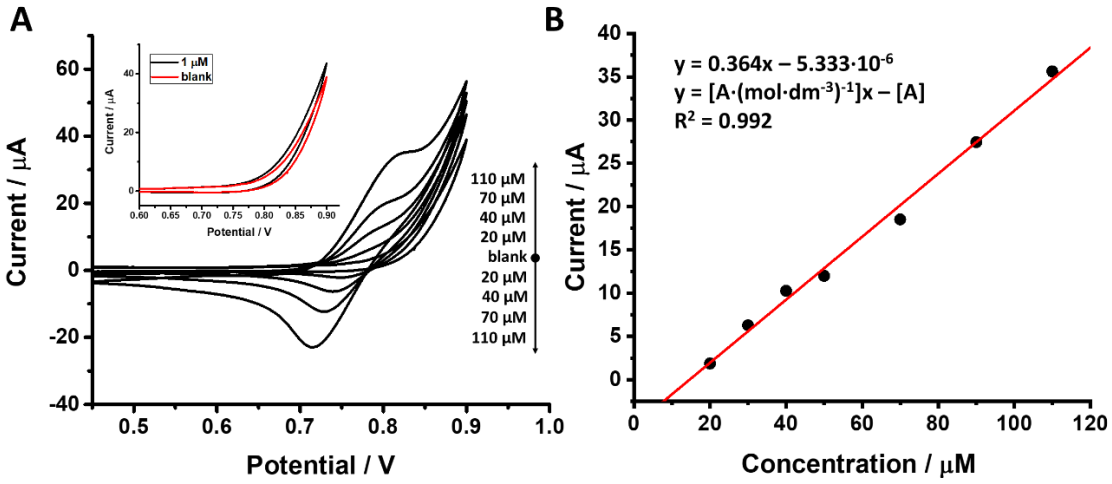

Figure S1. A – the series of ion transfer voltammograms recorded in cell I for increasing concentration of 1,6-DAH (1; 20; 40; 70 and 110 µM). The inset shows the blank (red solid line) together with the voltammogram recorded for [1,6-DAH] = 1 µM. **B** – calibration curve corresponding to the

voltammograms from part A of this figure. Experimental conditions: 10 mM HCl (pH ≈ 2) used as the aqueous phase, scan rate was equal to 10 mV·s^{-1}.

2.2. Effect of scan rate on the 1,6-DAH electrochemical signal.

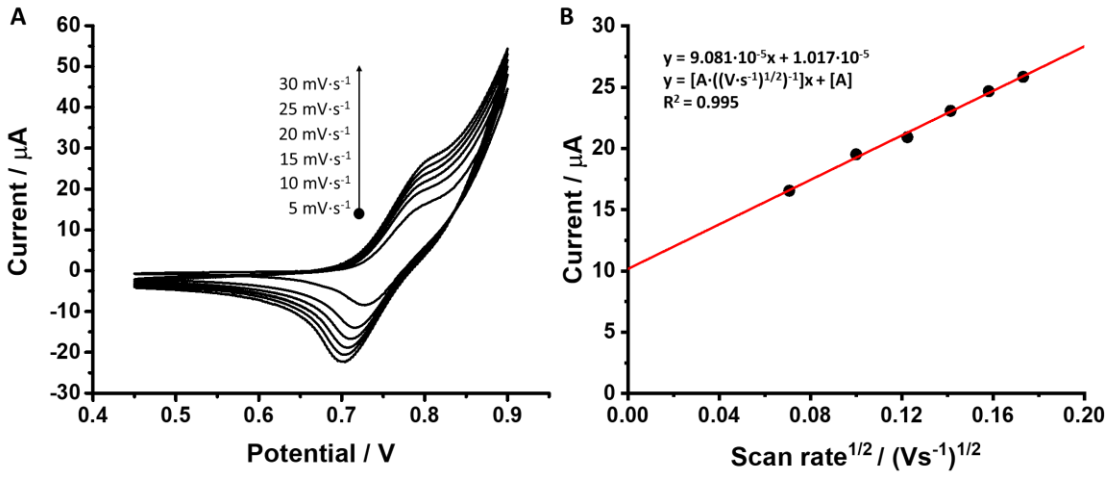

Figure S2. Scan rate dependency experiment. **A** – ion transfer voltammograms recorded for [1,6-DAH] = 70 µM at 5; 10; 15; 20; 25 and 30 mV·s^{-1}. **B** – corresponding dependency of the positive peak current intensity in function of the square root from the scan rate. Experimental conditions: 10 mM HCl (pH ≈ 2) was used as the aqueous phase.

Diffusion coefficient of the 1,6-DAH was calculated using Randles-Sevcik equation:

$$I_+ = 269000 \cdot z^{3/2} \cdot A \cdot D^{1/2} \cdot C \cdot v^{1/2} \qquad \text{eq. S1}$$

where I_+ is the positive peak faradic current; z is the charge of the molecule undergoing interfacial ion transfer reaction (for 1,6-DAH at pH = 2, z = 2); A is the electroactive surface area of the LLI (1.13 cm^2); D is diffusion coefficient (cm^2·s^{-1}); C stands for 1,6-DAH concentration (mol·cm^{-3}) and v is the experimental scan rate (V·s^{-1}). The change of the positive peak current change in function of the square root of the scan rate is given as a slope of linear fitting to the data points from Figure S2-B. Simple rearrangement of eq. 1 and substitution of all experimental data yielded the diffusion coefficient of the 1,6-DAH equal to 2.3·10^{-6} cm^2·s^{-1}.

2.3. Effect of pH on the electrochemical behaviour of 1,6-DAH.

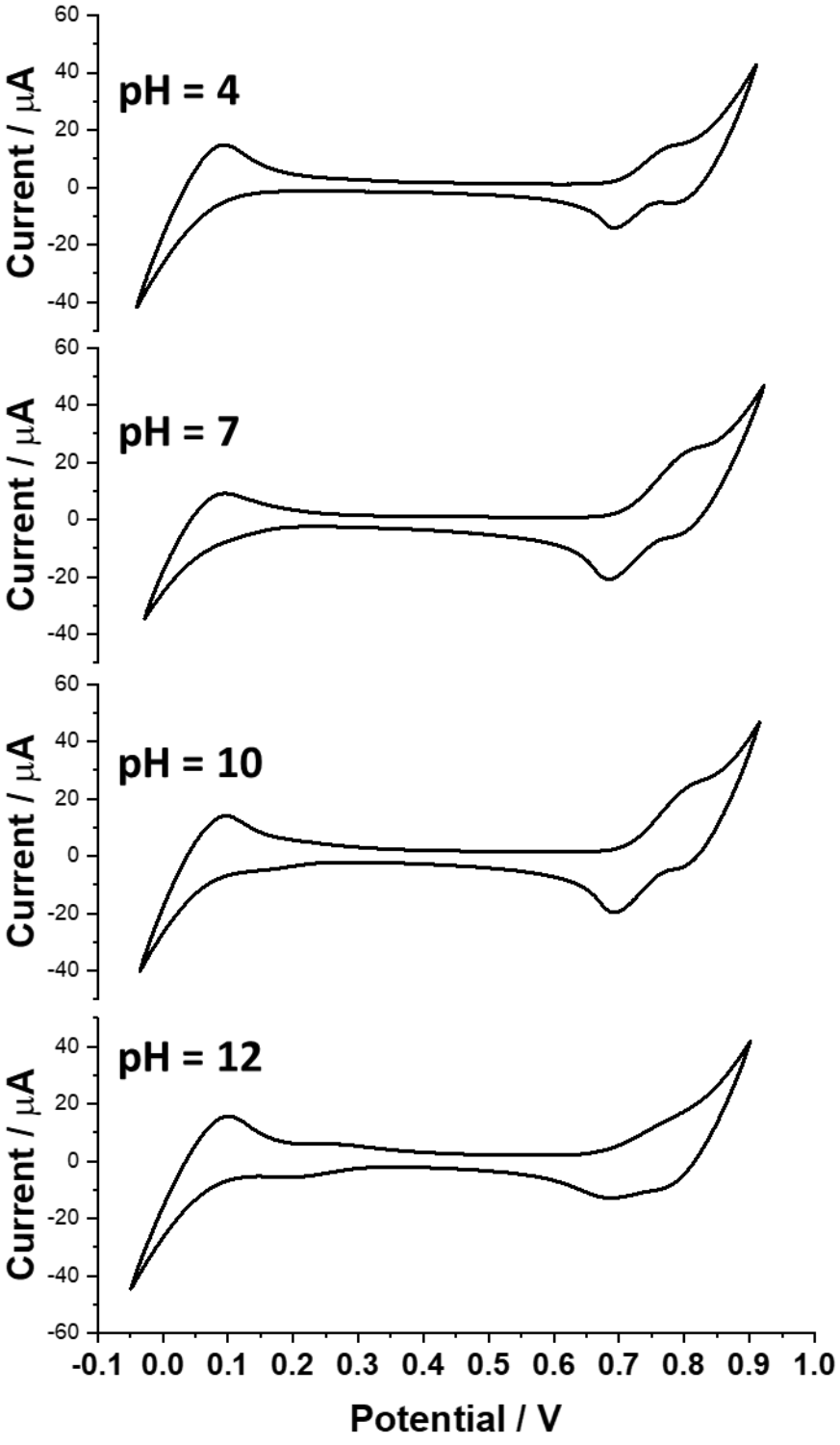

Figure S3. Ion transfer voltammograms recorded in the presence of 70 μM 1,6-DAH at different (indicated on the left) pH values of the aqueous phase.

As a weak base with two primary amine groups the 1,6-DAH can exist in three different forms depending on the pH: non-protonated 1,6-DAH, mono-protonated 1,6-DAH^{+} and di-protonated 1,6-DAH^{2+}. The fraction of each species can be given with the three following equations:

$$f_{1,6-DAH} = \frac{[1,6-DAH]}{[1,6-DAH]+[1,6-DAH^{+}]+[1,6-DAH^{2+}]} \quad \text{eq. S2}$$

$$f_{1,6-DAH^{+}} = \frac{[1,6-DAH^{+}]}{[1,6-DAH]+[1,6-DAH^{+}]+[1,6-DAH^{2+}]} \quad \text{eq. S3}$$

$$f_{1,6-DAH^{2+}} = \frac{[1,6-DAH^{2+}]}{[1,6-DAH]+[1,6-DAH^{+}]+[1,6-DAH^{2+}]} \quad \text{eq. S4}$$

Based on the acid-base equilibria chemical reaction for 1,6-DAH:

$$1,6-DAH^{+} \rightleftarrows 1,6-DAH + H^{+} \quad \text{eq. S5}$$

$$1,6-DAH^{2+} \rightleftarrows 1,6-DAH^{+} + H^{+} \quad \text{eq. S6}$$

we can define the equilibrium constant or the acid dissociation constant, given by:

$$Ka_1 = \frac{[1,6-DAH][H^{+}]}{[1,6-DAH^{+}]} \quad \text{eq. S7}$$

$$Ka_2 = \frac{[1,6-DAH^{+}][H^{+}]}{[1,6-DAH^{2+}]} \quad \text{eq. S8}$$

Finally, the rearrangement and substitution of eq. 2-3, 7 and 8 gives the expressions for the all three 1,6-DAH forms dependent only from the [H^{+}], Ka$_1$ and Ka$_2$.

$$f_{1,6-DAH} = \frac{Ka_1Ka_2}{[H^{+}]^2+Ka_1[H^{+}]+Ka_1Ka_2} \quad \text{eq. S9}$$

$$f_{1,6-DAH^{+}} = \frac{Ka_1[H^{+}]}{[H^{+}]^2+Ka_1[H^{+}]+Ka_1Ka_2} \quad \text{eq. S10}$$

$$f_{1,6-DAH^{2+}} = \frac{[H^{+}]^2}{[H^{+}]^2+Ka_1[H^{+}]+Ka_1Ka_2} \quad \text{eq. S11}$$

Equation S9, S10 and S11 were used to plot concertation fraction diagram shown in Figure 1B in the main text of the manuscript.

2.4. Effect of pH and [1,6-DAH] on the interfacialy formed nylon-6,6 films.

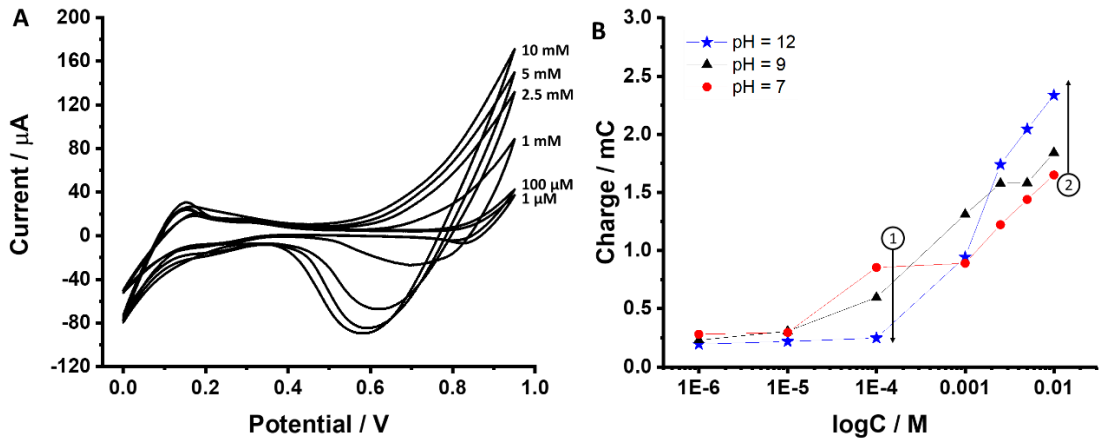

Figure S4. A – series of ion transfer voltammograms recorded in cell III for increasing concentration of 1,6-DAH from 1 µM up to 10 mM at pH = 12. The concertation of AC in the organic phase was fixed and equal to 5 mM. Experimental scan rate was equal to 25 $mV \cdot s^{-1}$. **B –** is the charge over the positive current limiting the potential window on the more positive potential side plotted in function of increasing concentration of 1,6-DAH in the water phase. This experiment was repeated for three pH values marked as red circles (pH = 7), black triangles (pH = 9) and blue stars (pH = 12). Point (1) and (2) correspond to the most prominent changes in the recorded charge transfer.

The results plotted in the Figure S4-A and S4-B aimed at choosing the optimal conditions for the electrochemical deposition of nylon-6,6. Few findings can be inferred for the reported data. (i) For three studied pH values the charge transferring across the LLI increases in function of the increasing concertation of 1,6-DAH. (ii) Interesting tendency was observed for [1,6-DAH] = 100 µM, marked with point (1) in Figure S4-B, since the charge pertaining to the 1,6-DAH transfer from the water to the organic phase decreased in the order 7 > 9 > 12. This indicates that the transfer of di-protonated 1,6-DAH species is a main contribution to the recorded current. (iii) The tendency is reversed (see point (2) in Figure S4-B) for the three last concentration points. Here, it is obvious that the highest amount of charge crossing the interface falls for the highest studied pH values (pH = 12). This in turn, suggest the appearance of additional portion of ions ($1,6\text{-}DAH^{+}$, $1,6\text{-}DAH^{2+}$ and H^{+}) being formed as the interfacial polycondensation reaction occurs. As such, we have chosen pH = 12 as an optimal for further nylon-6,6 interface deposition reaction.

2.5. Infra-red spectra of the nylon-6,6 films collected from the LLI after electrochemical deposition.

Fig. S5A shows the infra-red spectra of the film collected from the electrified liquid-liquid interface. A number of characteristic absorption bands (described in Fig. S5B) confirms that the formed film is a polyamide [2–4]. Almost identical spectra (not shown) was recorded for the film collected from the non-polarized liquid-liquid interface.

A

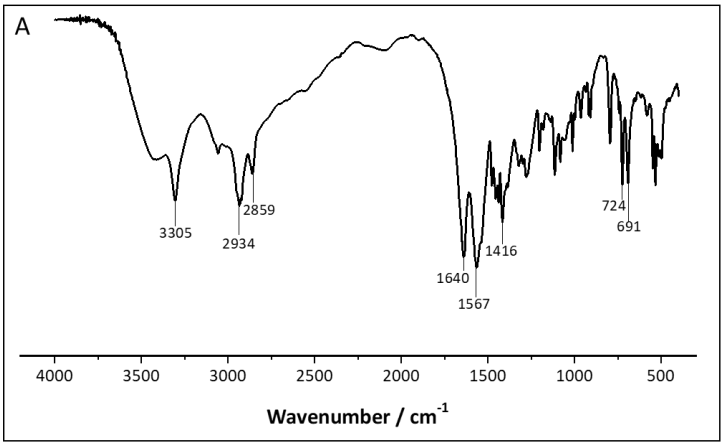

B

Functional group	Vibration type	Vibration frequency [cm^{-1}]
-NH	stretching	3305
$-CH_2$	stretching	2934, 2859
-C=O	stretching	1640
-NH	bending	1567
-C-N	stretching	1416
$-CH_2$	wagging	724, 691

Figure S5. A – infra-red spectrum of the nylon-6,6 collected from the LLI after electrochemical deposition. Experimental conditions: 5 mM 1,6-DAH in water phase, 5 mM AC in the organic phase, pH = 12, 5 voltammetric cycles. **B –** table summarizing main absorption bands for the chemical functional groups located within polyamide structure. Prepared based on ref.[2–4]

2.6. ITIES miniaturization.

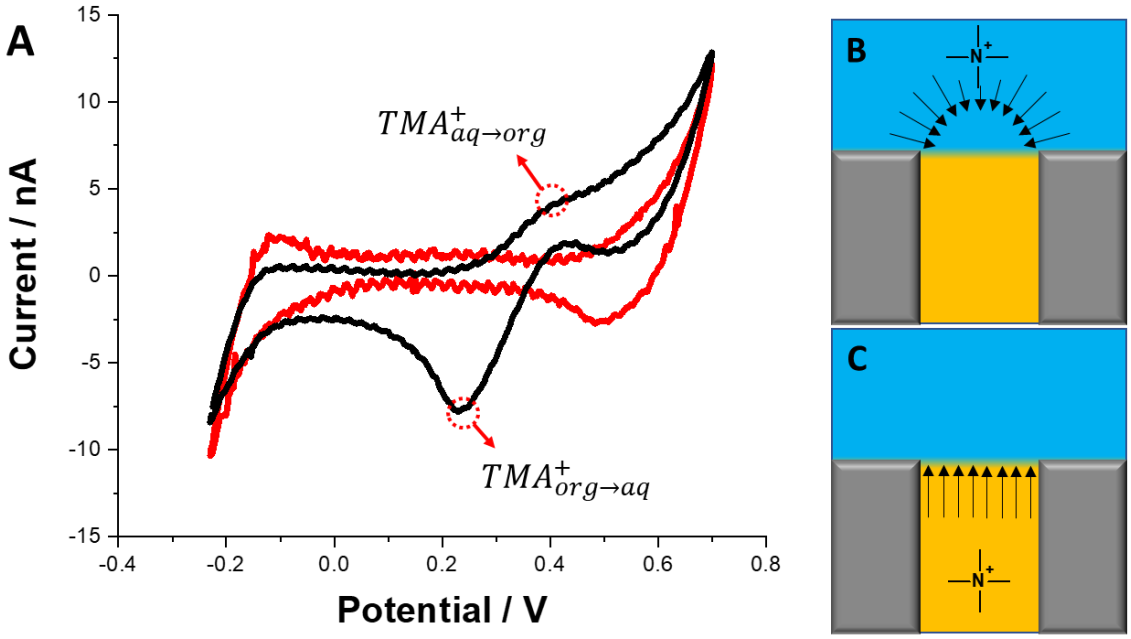

Figure S6. A – Ion transfer voltammograms recorded at the microITIES supported with the silica fused capillary having an internal diameter equal to 25 µm before (black curve) and after (red curve) addition of [TMA^+] = 60 µM to the aqueous phase. The scan rate was 10 $mV \cdot s^{-1}$. B and C are the schematic representations of the hemispherical and linear diffusion zones of the TMA^+ transferring from the aqueous to the organic and from the organic to the aqueous phase, respectively.

The shape of the ion transfer voltammogram shown in Figure S6-A as a black curve is very characteristic for the microITIES supported with the thick walls pore(s) with the LLI located at the pore ingress. Its asymmetry given by the sigmodal positive and peak-like shaped negative signals are in line with the asymmetric diffusion zones established at the water and organic phase side of the LLI. Sigmoidal pattern of the current recorded during forward polarization is a consequence of a hemispherical diffusion zone (Figure S6-B) – ion transfer not-limited by diffusion – of TMA^+ heading towards the organic phase. Negative peak arise from the linear diffusion zone inside the pore of TMA^+ transferring back to the aqueous phase (Figure S6-C).

The electrochemical dimensions of the LLI supported with the microcapillary can be calculated using the value of the steady state current extracted from the ion transfer voltammogram from Figure S6-A recorded in the presence of 60 µM TMA^+. Proper rearrangement of the Saito equation:

$$I_{ss} = 4zFDCr \qquad \text{eq. S12}$$

where I_{ss} is the steady state current equal to 3.7 nA, z is the charge of TMA^+ equal to 1, F is the Faraday constant, D is the TMA^+ diffusion coefficient (13.8 $\mu cm^2 \cdot s^{-1}$),[5] C is the TMA^+ concentration in $mol \cdot cm^{-3}$, allows the calculation of the capillary radius. Obtained value of 11.6 μm is very close to the one measured under SEM (12.4 μm).

3. References.

[1] L. Poltorak, G. Herzog, A. Walcarius, In-situ formation of mesoporous silica films controlled by ion transfer voltammetry at the polarized liquid–liquid interface, Electrochem. Commun. 37 (2013) 76–79. https://doi.org/10.1016/j.elecom.2013.10.018.

[2] T.E. Motaung, M.J. Mochane, Z.L. Linganiso, A.P. Mashigo, In-situ Polymerization of Nylon-Cellulose Nano composite, Polym. Sci. 3 (2017) 1–8. https://doi.org/10.4172/2471-9935.100017.

[3] M. Nasr-Esfahani, M. Mehrabanian, HA/nylon 6,6 porous scaffolds fabricated by salt-leaching/solvent casting technique: effect of nano-sized filler content on scaffold properties, Int. J. Nanomedicine. (2011) 1651. https://doi.org/10.2147/ijn.s21203.

[4] M.C. Tobin, M.J. Carrano, Infrared spectra of polymers. I. Effect of crystallinity on the infrared spectrum of polyethylene and on the infrared spectra of nylon 6 and nylon 11, J. Chem. Phys. 25 (1956) 1044–1052. https://doi.org/10.1063/1.1743095.

[5] L. Poltorak, K. Morakchi, G. Herzog, A. Walcarius, Electrochemical characterization of liquid-liquid micro-interfaces modified with mesoporous silica, Electrochim. Acta. 179 (2015) 9–15. https://doi.org/10.1016/j.electacta.2015.01.129.

Analyst

PAPER

View Article Online
View Journal | View Issue

Cite this: *Analyst*, 2021, **146**, 1376

Electroanalytical study of five carbosilane dendrimers at the interface between two immiscible electrolyte solutions†

Karolina Kowalewska, [a] Tamara Rodriguez-Prieto, [b,c,d] Slawomira Skrzypek, [a] Jesús Cano, [b,c,d] Rafael Gómez Ramírez *[b,c,d] and Lukasz Poltorak *[a]

Received 23rd October 2020,
Accepted 9th December 2020

DOI: 10.1039/d0an02101f

rsc.li/analyst

This work is focused on the electroanalytical study of a family of five imidazolium-terminated carbosilane dendrimers (from generation G1 to G3) at the polarized liquid–liquid interface formed between water and 1,2-dichloroethane solutions. All dendrimers with permanently and positively charged imidazolium groups located at the periphery within the branched carbosilane core were found to be electrochemically active. Based on the concentration and scan rate dependencies we have concluded that these molecules undergo interfacial ion transfer processes accompanied by interfacial adsorption/desorption rather than the electrochemically induced interfacial formation of the macromolecule–anion (tetrakis(4-chlorophenyl)borate) from the organic phase complex. Also, we report several physicochemical and electroanalytical parameters (*e.g.* diffusion coefficients, LODs, and detection sensitivities) for the studied family of dendrimers. Our work aims to contribute to the understating of the interaction between branched macromolecules and biomimetic interfaces.

1. Introduction

Since Flory's report in 1952, hyperbranched polymers have been studied and significantly developed with the aim to be applied in several fields of science.[1–3] In the beginning, just two types of traditional architectures were recognized, which are linear and crosslinked polymers. Branched and dendritic systems were discovered at a later stage.[4] Dendritic systems are one of the most important systems among four classes of polymers holding a number of potential and emerging applications, especially in biomedicine.[3] This is mainly due to their unique properties: (i) unlike other polymers, these chemical species are ideally monodisperse; (ii) dendrimers are nanosized and versatile macromolecules with a noteworthy structural precision; (iii) the organic chemistry toolbox offers a number of existing protocols that allow for the precise control of resulting macromolecule chemical properties, well-defined structures, sizes, and shapes.[5,6] In the dendritic architecture, it is possible to differentiate three parts: the core or focal point, where all the branches emerge; the branches, which determine the size or generation of the dendritic system; and the periphery, where the functional groups are localized. Among the dendrimer typologies available,[7] this work is focused on carbosilane dendrimers,[8] whose structure is based on C–Si bonds that provide chemical and thermal stability and biocompatibility (especially desired when it comes to biomedical applications). Furthermore, the periphery of this family of dendrimers, here reported, is made from imidazolium salts being positively charged within a full conventional pH scale. Normally, the application of the dendrimer is determined by the peripheral groups; however, the core or focal point or the cavities in the internal structure of the dendrimer can also play an important role. Focusing on biomedical applications, anionic dendrimers are deeply studied as antivirals, as these can interact with the virus, avoiding its subsequent infection. Cationic ones are used as potent antibacterial species, damaging the bacterial membrane and provoking the death of the microorganism.[9,10] Dendrimers can also be used as carriers of metals, drugs, or biological molecules, and hence, are extensively studied in *e.g.* anticancer treatment, diagnosis, and gene transfection.[11–14] Imidazolium salts are used in a great variety of biological applications, for instance, anticancer agents, antioxidants, antimicrobials, drug delivery, or biosensors.[15] Therefore, the

[a]*Department of Inorganic and Analytical Chemistry, Electroanalysis and Electrochemistry Group, Faculty of Chemistry, University of Lodz, Tamka 12, 91-403 Lodz, Poland. E-mail: lukasz.poltorak@chemia.uni.lodz.pl*
[b]*Department of Organic and Inorganic Chemistry, Chemical Research Institute "Andrés M. Del Río" (IQAR), University of Alcalá, 28805 Madrid, Spain. E-mail: rafael.gomez@uah.es*
[c]*Ramón y Cajal Health Research Institute (IRYCIS), 28034 Madrid, Spain*
[d]*Networking Research Center on Bioengineering, Biomaterials and Nanomedicine (CIBER-BBN), 28029 Madrid, Spain*

†Electronic supplementary information (ESI) available. See DOI: 10.1039/d0an02101f

inclusion of these groups in the periphery of the dendrimer can result in properties and behaviours, such as multivalence, and needs to be studied. Reaching the full potential of all these applications require a good fundamental understanding on the interaction between dendrimers and bio-interfaces. Model bio-mimicking systems operating under electrochemical control are especially useful in this respect.

Electrified liquid–liquid interfaces (LLIs) have many similarities with the real bio-interfaces (*e.g.* discontinuous properties originating from the existence of contacted hydrophobic and hydrophilic domains, potential drops defined by the ions, and/or intrinsic sieving properties being the result of the size, charge, and chemical nature of studied chemical species). It was proposed already in the 80s that this system can be considered as a model of a half of a lipid bilayer (analogous to a lipid monolayer).[16] As a matter of fact, this belief is still valid to date.[17] Electrified LLIs together with the electrochemical studies devoted to supported[18–20] and black lipid bilayers[21,22] offer an impressive toolbox focused on studying various bio-important interactions.

Polarization of the LLI is possible when contacting phases contain highly hydrophilic (the aqueous phase) and hydrophobic (the organic phase) salts with ideally zero mutual partitioning.[23,24] In such configurations, this system is known as the interface between two immiscible electrolyte solutions (ITIES) which can be electrochemically studied in dedicated glass (and recently 3D printed[25]) cells. This system is especially exciting since in addition to electron transfer reactions between redox couples placed in both phases it allows for the direct electroanalytical probing of the simple ion transfer crossing the ITIES.[26] Correspondingly, chemical species (*e.g.* proteins,[27,28] drugs,[29] biologically important molecules,[30] or polyelectrolytes[31]) with ionizable or permanently charged chemical functional groups are potentially active at the electrified LLI. Due to the still emerging biotechnological applications of dendrimers, these chemical species have attracted significant attention when it comes to the ITIES. Various generations of poly(propylenimine) (DABAM-*n*), poly(amidoamine) (PAMAM),[32] and poly-L-lysine[33,34] dendrimers were found to be electrochemically active (when charged, pH < pK_a) at the polarized water–1,2-dichloroethane interface. It was found that these species undergo interfacial adsorption and facilitate the transfer of hydrophobic anions (usually tetrakis(4-chlorophenyl)borate) initially dissolved in the organic phase rather than undergoing simple interfacial ion transfer reactions.[35] PAMAM dendrimers were also used to study photoinitiated interfacial electron transfer between PAMAM – Zinc(II) porphyrin associates from the aqueous phase and ferrocene dissolved in 1,2-dichloroethane.[36,37] Finally, smaller generations of PAMAM dendrimers (G0 and G1) that may undergo simple ion transfer reactions were used to assess the charge and size sieving properties of silica membranes *in situ* synthesized at the ITIES.[38]

In this work, we show that each member of the studied family (from G1 to G3) of self-synthesized imidazolium terminated carbosilane dendrimers initially dissolved in the aqueous phase gives rise to ionic currents recorded at the ITIES. Based on our results we have concluded that these molecules, rather than facilitating the transfer of the organic phase background electrolyte anion, undergo simple ion transfer accompanied by interfacial adsorption. Our work provides a number of electroanalytical parameters such as detection sensitivities and LOD values. The easiness in size tunability of the studied molecules may give them a new application in the evaluation of the size and charge sieving properties of modified ITIESs.

2. Methods and materials

2.1. Chemicals

BDTR-1, BDTR-2, BDTR-3, BDTR-4, and BDTR-5 were synthesized according to the protocol described below and reported elsewhere.[39] Sodium chloride (NaCl, for analysis, ChemPur) and 1,2-dichloroethane (1,2-DCE, for analysis, POCH) were used as received. The organic phase electrolyte bis(triphenylphosphoranylidene)ammonium tetrakis(4-chlorophenyl)borate ($BTPPA^+TPBCl^-$) was prepared *via* a metathesis reaction between bis(triphenylphosphoranylidene)ammonium chloride ($BTPPA^+Cl^-$, 97%, Sigma-Aldrich) and K^+TPBCl^- potassium tetrakis(4-chlorophenyl)borate (K^+TPBCl^-, >98%, Sigma-Aldrich) salts. The aqueous phase was prepared using water distilled in triplicate.

2.2. Carbosilane dendrimers

In this research, we have studied a self-synthesized new family of spherical carbosilane dendrimers with two types of moieties and generations. BDTR-1, BDTR-3, and BDTR-5 bear a methyl group as the *N*-substituent in the imidazolium fragments, whereas compounds BDTR-2 and BDTR-4 hold a mesityl unit. All compounds used to perform these experiments were prepared by our research group. Briefly, the procedure consists of the *N*-alkylation reaction of the imidazolium salts using iodine-terminated precursor dendrimers under mild conditions.[39] Their characterization included ^1H and ^{13}C NMR spectroscopy performed using a Varian Unity VXR-300 NMR spectrometer at ambient temperature, along with elemental analyses (PerkinElmer 240C) and mass spectrometry (Agilent 6210 spectrometer (ESI) in the positive mode. Data are in agreement with those reported in the literature.

2.3. Electrochemical experiments

Electrochemical characterization of all dendrimers was performed in a macroscopic voltammetric glass cell (the interface radius equals 0.7 cm) equipped with a set of appropriate electrodes (see Fig. 1). Two Ag/AgCl and two Pt wires were used as the reference and counter electrodes, respectively. One pair (Ag/AgCl + Pt) was placed in each phase. All voltammograms were recorded with EmStat3+ (PalmSens) equipped with a differential pulse amplifier or Autolab 302n (Metrohm).

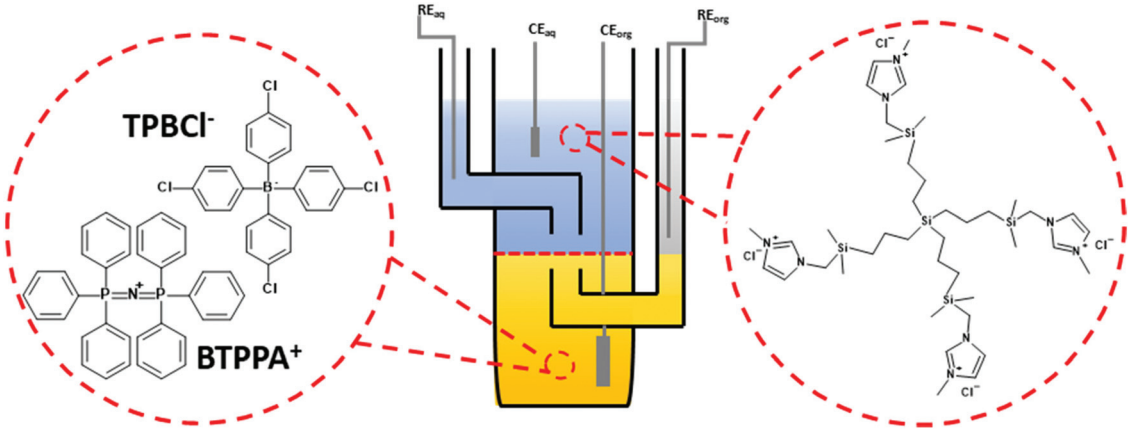

Fig. 1 The electrochemical cell which was used to study the interfacial behavior of imidazolium terminated carbosilane dendrimers. Left: structure of the $BTPPA^{+}TPBCl^{-}$ being the organic phase (bottom phase) background electrolyte. Right: structure of the G1 dendrimer, which similarly to other members of the family, was always initially dissolved in the aqueous phase. RE – reference electrode, CE – counter electrode, aq – the aqueous phase, and org – the organic phase. The red dashed line in between two Luggin capillaries indicates the position of the ITIES.

The following electrochemical cells were applied during experiments:

Cell I:

$$\mathrm{Ag|AgCl}\left|\begin{matrix}x\ \mu\mathrm{M\ BDTR\text{-}1;\ 2;\ 3;\ 4;\ 5}\\ 10\ \mathrm{mM\ NaCl}\end{matrix}\right| \times \left|\begin{matrix}5\ \mathrm{mM\ BTPPATPBCl}\\ \mathrm{in\ 1,2\text{-}DCE}\end{matrix}\right|\begin{matrix}10\ \mathrm{mM\ NaCl}\\ 5\ \mathrm{mM\ BTPPACl}\end{matrix}\mathrm{|AgCl|Ag}$$

Cell II

$$\mathrm{Ag|AgCl}\left|\begin{matrix}100\ \mu\mathrm{M\ BDTR\text{-}2;\ 5}\\ 10\ \mathrm{mM\ NaCl}\end{matrix}\right| \times \left|\begin{matrix}y\ \mathrm{mM\ BTPPATPBCl}\\ \mathrm{in\ 1,2\text{-}DCE}\end{matrix}\right|\begin{matrix}10\ \mathrm{mM\ NaCl}\\ 5\ \mathrm{mM\ BTPPACl}\end{matrix}\mathrm{|AgCl|Ag}$$

Unless otherwise mentioned 20 mV s^{-1} was used to record all voltammograms. The pH of the aqueous phase in all experiments, except for ITVs shown in ESI Fig. 1,† was equal to around 6 (pH of the non-buffered 10 mM NaCl solution affected by the atmospheric CO_2 uptake).

3. Results and discussion

Synthesized dendrimers had the appearance of yellowish oil that was dissolved in 10 mM NaCl aqueous phase, serving as the stock solution. Fig. 2A–E show ion transfer voltammograms recorded before (red dash–dot curves) and after (solid black curves) the addition of the corresponding dendrimers to electrochemical cell I. We have found that the addition of each studied compound to the aqueous phase gave rise to ionic currents. The interfacial activity is expected and governed by the existence of quaternary ammonium cations located within imidazolium groups at the periphery of the carbosilane core, assuring electrochemical activity on the entire conventional pH scale (see ESI Fig. 1†). According to the convention, positive currents are attributed to the positively charged dendrimers transferring from the water to the organic phase, whereas negative currents are recorded on their back transfer from the organic phase to the aqueous phase. Studied molecules differ in size (the hydrodynamic radius grows together with the generation), the number of charges located at the dendrimer periphery (BDTR-1, 4(+); BDTR-2, 4(+); BDTR-3, 8(+); BDTR-4, 8(+); BDTR-5, 16(+)), and the existence of the mesitylene substituent attached to a nitrogen atom located within the imidazolium ring (BDTR-2 and BDTR-4) or methyl substituent for the rest. For the chemical structures refer to Fig. 2 – right section. Molecular hydrophilicity–hydrophobicity can be directly inferred from the voltammetry data. All studied species transfer across the interface, within the less positive side of the potential window indicating their increased hydrophobicity (hydrophilic species require higher applied potential difference values to be transferred from the aqueous to the organic phase).[40] Occasionally, especially lower dendrimer generations gave irregular current patterns similar to those shown in Fig. 2A (second positive peak with a strange geometry). We believe that these signals originate from the phenomenon known as the electrochemical instability[41–43] caused by the surface-active species triggering local changes (gradients) in the interfacial tension upon adsorption to the LLI. Formal Gibbs energy of the ion transfer reaction is directly related to the formal Galvani potential of ion transfer (see eqn (1)).

$$\Delta G_i'^{\mathrm{aq}\rightarrow\mathrm{org}} = -zF\Delta_{\mathrm{org}}^{\mathrm{aq}}\phi'_i \qquad (1)$$

where z is the molecular charge, F is the Faraday constant (96 485 C mol^{-1}) and $\Delta_{\mathrm{org}}^{\mathrm{aq}}\phi'_i$ is the formal Galvani potential difference of the ion transfer reaction. Based on the shape of the recorded irregular ionic currents we concluded that upon interface polarization dendrimers undergo an interfacial ion transfer process accompanied by an interfacial adsorption (this is also discussed later in the manuscript).

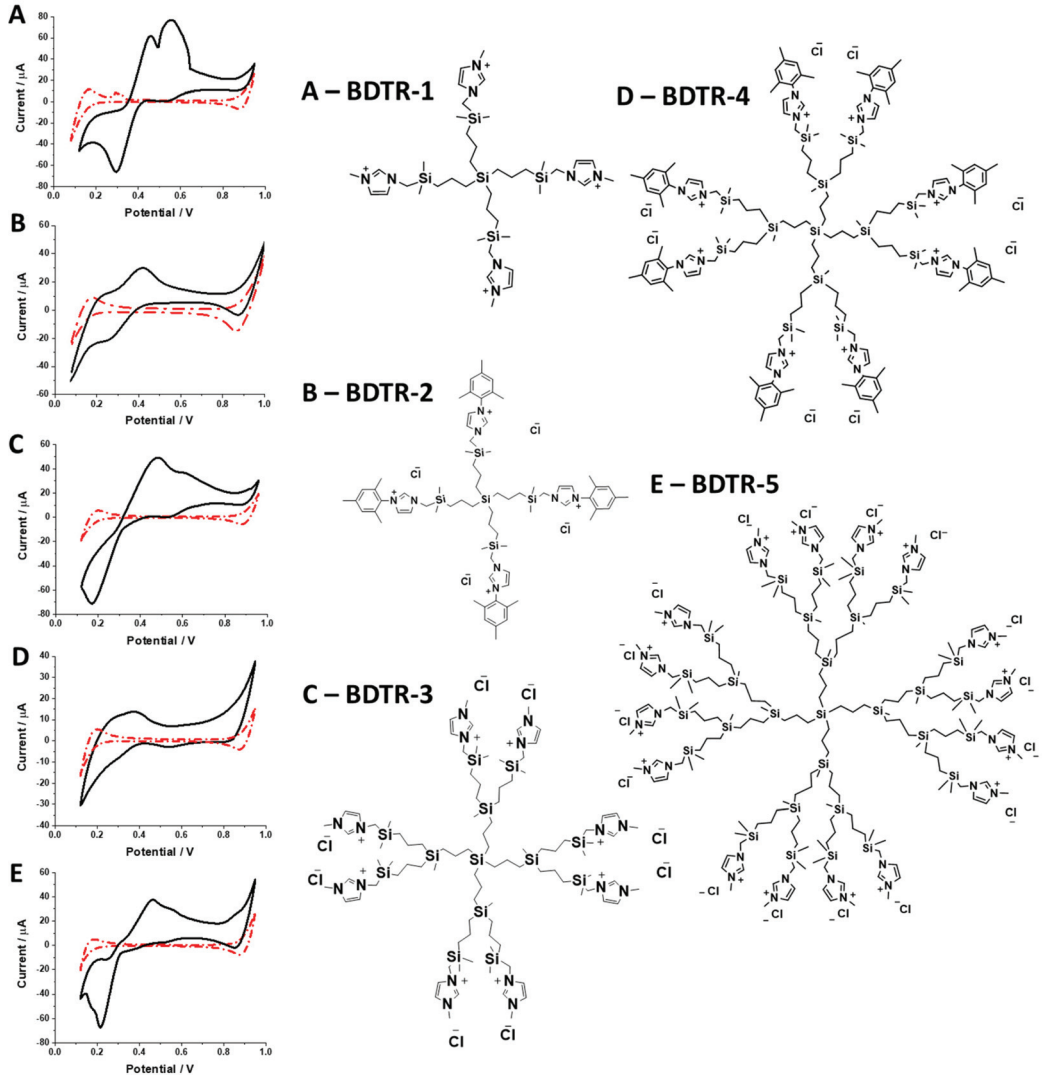

Fig. 2 Ion transfer voltammograms recorded in the left panel correspond to the following dendrimer generations: A – G1 (BDTR-1); B – G2 (BDTR-2); C – G3 (BDTR-3); D – G4 (BDTR-4); E – G5 (BDTR-5). The black solid lines were recorded in cell I for x = 150 μM. The red dash–dot lines correspond to the blank voltammograms recorded in the absence of a dendrimer (10 mM NaCl). The right panel depicts dendrimer structures.

It is therefore difficult to unambiguously determine the $\Delta^{aq}_{org}\phi'_i$ values. However, for evenly charged molecules (for BDTR-1 and BDTR-2 the charge equals 4; for BDTR-3 and BDTR-4 the charge equals 8) we can deduce the change in the free Gibbs energy ($\Delta\Delta G$) according to

$$\Delta\Delta G = -zF\Delta^{aq}_{org}\phi'_{(1)} - \left(-zF\Delta^{aq}_{org}\phi'_{(2)}\right) \quad (2)$$

or

$$\Delta\Delta G = zF\left(\Delta^{aq}_{org}\phi'_{(2)} - \Delta^{aq}_{org}\phi'_{(1)}\right) \quad (3)$$

Since the difference in the formal Galvani potential difference of the ion transfer reaction between evenly charged dendrimers (1 – more hydrophilic and 2 – more hydrophobic) should be equal to the difference in the corresponding forward (or reverse) peak potential values we can simplify eqn (3) to

$$\Delta\Delta G = zF(E^{\text{forward or reveresed}}_{p(2)} - E^{\text{forward or reveresed}}_{p(1)} \quad (4)$$

Like so, we can calculate the additional fraction of energy needed to trigger interfacial ion transfer for evenly charged dendrimers decorated with mesitylene and methyl substituents. In both cases, the presence of mesitylene groups within the structures of dendrimers BDTR-2 and BDTR-4 caused a shift in the recorded peak position towards less positive potential difference values with respect to their structural analogs deprived of this substituent (BDTR-1 and BDTR-3, respectively). According to our calculations (eqn (4)), the $\Delta\Delta G$ between BDTR-1 and BDTR-2 equals around 18.5 kJ mol^{-1}, whereas for BDTR-3 and BDTR-4 it is 53.3 kJ mol^{-1}. If we further divide it by the dendrimer charge, we get similar

values (holding the same order of magnitudes) of 4.6 kJ mol^{-1} and 6.7 kJ mol^{-1} per mesitylene branch for pairs BDTR-1/BDTR-2 and BDTR-3/BDTR-4, respectively.

As shown in Fig. 3 and ESI Fig. 2 (see ESI†) increasing concentration of each dendrimer in the aqueous phase resulted in an increasing recorded peak current. Ionic currents started appearing at dendrimer concentrations equal to around 5–20 μM which agrees well with the calculated limit of detection defined as 3 times the standard deviation of the intercept divided by the slope of the calibration curve (see Table 1, column 11, for details). The calibration curves from Fig. 3B and ESI Fig. 2B, D† recorded for the BDTR-2, BDTR-1 and BDTR-3, respectively, exhibit two linear dynamic ranges. Sensitivity for the first part of the data set (from the first studied concentration to around 50 μM) for the first three studied dendrimer generations was always higher than the sensitivity of the second dynamic range. Surprising is the second part of the calibration curve which levels off stating from [dendrimer] > 50 μM. This most probably indicates an interfacial adsorption process which to some extent affects the simple ion transfer reaction. The pattern of the calibration curve for BDTR-5 is different. This chemical compound exhibits a behaviour that was reported for some of the positively charged macromolecules that were found to be adsorbed to the LLI, further facilitating the transfer of the organic phase anion.[44,45] At this point we can speculate that the interfacial adsorption of BDTR-5, leading to the positive charge accumulation within the interface at higher dendrimer concentration values, may induce the interfacial transfer of $TPBCl^-$ (being the anionic part of the organic phase background electrolyte) from the organic phase to the water phase. This, in turn, may explain the higher than expected recorded ionic currents.

For BDTR-1, BDTR-2, and BDTR-3 the forward and reverse peak current ratio was close to unity, indicating the reversibility of the ion transfer reaction (see Table 1, column 5). Since the transfer of BDTR-4 was severely overlapped with the interfacial transfer of the potential window limiting ion (in that case $Cl^-_{aq\leftrightarrow org}$) we were unable to extract most of its physicochemical and analytical parameters summarized in Table 1. For BDTR-5 the forward and reverse peak current ratio was equal to 0.55. However, the very broad forward (positive current) peak indicates that more than one charge transfer process occurs within the given potential range (from *e.g.* 0.3 to 0.7 V). The integrated area below forward and reverse peak currents equals 0.13 μC and 0.17 μC, respectively, and the corresponding ratio is 0.76. We think that dendrimer BDTR-5 is first adsorbed to the LLI, followed by its gradual transfer to the organic phase, manifested as the complex, and a multistep charge transfer reaction coupled to the interfacial transfer of

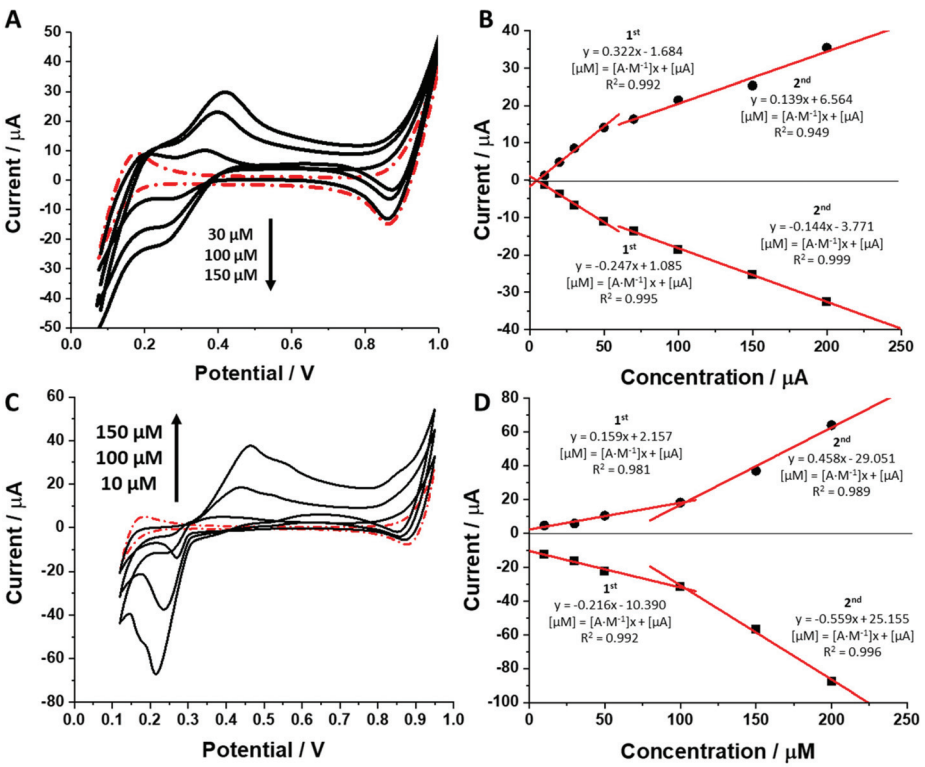

Fig. 3 A and C show the ion transfer voltammograms recorded in the presence of increasing (indicated next to the black arrow) concentrations of BDTR-2 and BDTR-5, respectively. Calibration curves are given as part B (for BDTR-2) and part D (BDTR-5). Red dash–dot lines are the blank readings recorded in the absence of dendrimers. The scan rate was equal to 20 mV s^{-1}. Linear fit equations are displayed next to calibration curves. 1^{st} – corresponds to the first linear dynamic range and 2^{nd} – corresponds to the second linear dynamic range.

Table 1 Electroanalytical parameters for all studied imidazolium terminated carbosilane dendrimers extracted from the voltammetry data. $z^{\text{theor.}}$ – theoretical charge deduced from the dendrimer chemical structure; z^{exp} – charge deduced from the forward and reverse peak to peak separation ΔE_p – forward to reverse peak to peak separation taken from ITVs recorded at [dendrimer] < 100 μM at 2 mV s^{-1} (*for BDTR-3 a broad positive peak was formed in the forward scan, and hence, the positive peak position value is a rough estimation). $D^{z\text{theor.}}$ and $D^{z\text{exp.}}$ – diffusion coefficients calculated using the Randles–Sevcik equation with either $z^{\text{theor.}}$ or $z^{\text{exp.}}$; r – the hydrodynamic radius calculated using the Stokes–Einstein equation; LOD – the limit of detection calculated as 3 times the standard deviation of the intercept divided by the slope of the calibration curve; S_{aq} or S_{org} – the slope of the calibration curve of the forward and reverse signal, respectively. $S_{\log i\ vs.\ \log[v]}$ – the slope of the logarithmic current *versus* logarithmic scan rate dependency. Aq and org stand for the aqueous phase and the organic phase, respectively. (+) and (−) pertain to the positive (forward) and negative (reverse) peak currents, respectively

1 Name	2 $z^{\text{theor.}}$	3 $z^{\text{exp.}}$	4 ΔE_p/mV	5 $\frac{I^+}{I^-}$	6 M/g mol^{-1}	7 $D^{z\text{theor.}}$/$cm^2\ s^{-1}$	8 $D^{z\text{exp.}}$/$cm^2\ s^{-1}$	9 $r^{z\text{theor.}}$/nm	10 $r^{z\text{exp.}}$/nm	11 LOD/μM	12 S_{aq}/A M^{-1}	13 S_{org}/A M^{-1}	14 $S_{\log i\ vs.\ \log[v]}$
BDTR-1	4	2.1	28.1	0.95	955.36	(+) 4.8×10^{-7}	(+) 3.8×10^{-6}	(+) 4.55	(+) 0.6	(+) 2.24	1st 0.576	1st 0.665	(+) 0.56
						(−) 3.1×10^{-7}	(−) 2.5×10^{-6}	(−) 7.0	(−) 0.9	(−) 6.96	2nd 0.317	2nd 0.395	(−) 0.45
BDTR-2	4	1.2	51.0	0.97	1371.97	(+) 7.6×10^{-8}	(+) 1.4×10^{-6}	(+) 28.7	(+) 1.7	(+) 5.36	1st 0.322	1st 0.247	(+) 0.49
						(−) 7.2×10^{-8}	(−) 1.3×10^{-7}	(−) 30.3	(−) 1.8	(−) 4.09	2nd 0.139	2nd 0.144	(−) 0.51
BDTR-3	8	2.9*	20.5	0.92	2223.44	(+) 1.2×10^{-8}	(+) 2.5×10^{-7}	(+) 182.0	(+) 8.7	(+) 17.27	1st 0.508	1st 0.877	(+) 0.54
						(−) 3.9×10^{-8}	(−) 8.3×10^{-7}	(−) 560.0	(−) 26.3	(−) 21.89	2nd 0.265	2nd 0.538	(−) 0.54
BDTR-4	8	—	—	—	3056.66	(+) 7.5×10^{-8}	—	(+) 29.1	—	(+) 5.8	1st 0.082	1st -	(+) 0.58
						(−) -		(−) -		(−) –	2nd -	2nd -	(−) -
BDTR-5	16	—	—	0.55	4756.60	(+) 2.2×10^{-10}	—	(+) 9930	—	(+) 16.98	1st 0.159	1st 0.216	(+) 0.56
						(−) 2.4×10^{-10}		(−) 9100		(−) 11.00	2nd 0.458	2nd 0.559	(−) 0.26

the $TPBCl^-$ ion. On the back transfer, the current is first slightly increased to finally give a sharp and well-defined peak with a characteristic diffusion-limited tail.

For all studied dendrimers we have found that the forward and reverse peak currents, for a fixed dendrimer concentration, increase linearly with the square root of the scan rate (see Fig. 4 and ESI Fig.2†). The rearranged Randles–Sevcik equation

$$\frac{i_p}{v^{1/2}} = 2.69 \cdot 10^5 \cdot A \cdot z^{3/2} \cdot D^{1/2} \cdot C \qquad (5)$$

where $\frac{i_p}{v^{1/2}}$ is the slope of the linear fit equation (see Fig. 4B, D and ESI Fig. 3B, D and F†), 2.69×10^5 is a result of an operation on physicochemical constants (for 25 °C), A is the surface area of the LLI (1.33 cm^2), z is the charge crossing the LLI, and C is the dendrimer concentration (mol cm^{-3}), was used to calculate the diffusion coefficients (D, $cm^2\ s^{-1}$) for studied molecules. The resulting values are summarized in Table 1 (columns 7 and 8). For the calculations, we have used the theoretical number of charges deduced from the chemical structure of each dendrimer and equal to the number of imidazolium groups within the molecular periphery and the charge that was estimated based on the forward and reverse peak to peak separation (Table 1, columns 2 and 3, respectively). When theoretical molecular charge values were substituted in eqn (5) we have obtained diffusion coefficient values 1–2 orders of magnitude lower than expected 10^{-6} $cm^2\ s^{-1}$ for lower and 10^{-7} $cm^2\ s^{-1}$ for higher dendrimer generations.[35,38,46] This means that the interfacial charge transfer reactions recorded in the presence of dendritic molecules are not a one-step process. Reasonable values were obtained, which were 3.8×10^{-6} $cm^2\ s^{-1}$ for BDTR-1, 1.4×10^{-6} $cm^2\ s^{-1}$ for BDTR-2, and 2.5×10^{-7} $cm^2\ s^{-1}$ for BDTR-3, when we performed the charge calculated based on the forward and reverse peak to peak separation taken from ITVs recorded at [dendrimer] < 100 μM at 2 mV s^{-1} (due to uncompensated resistance the peak to peak separation values were increasing during the measurements together with the increasing [dendrimer] and the experimental scan rate). Assuming that the interfacial adsorption processes affect the dendrimer ion transfer to some extent the utility of the Randles–Sevcik equation is most probably limited, and hence, obtained values should be treated as approximations. The calculated $z^{\text{exp.}}$ values were significantly lower than the $z^{\text{theor.}}$. This discrepancy may be due to a few reasons, including sluggish kinetics, the presence of the uncompensated resistance, and/or the occurrence of the interfacial adsorption processes. Diffusion coefficient values for higher generations (which are BDTR-4 and BDTR-5) are not available since we were unable to accurately define the peak to peak separation, and we assumed that these species (especially BDTR-5) do not undergo reversible ion transfer reactions. Also, based on the calculated diffusion coefficients and the Einstein-Stokes equation we have estimated the values of hydrodynamic radii for BDTR-1, BDTR-2, and BDTR-3 which were equal to 0.6, 1.7, and 8.7 nm, respectively. We have found that the first two values are in good agreement (BDTR-1: 0.9 nm and BDTR-2:

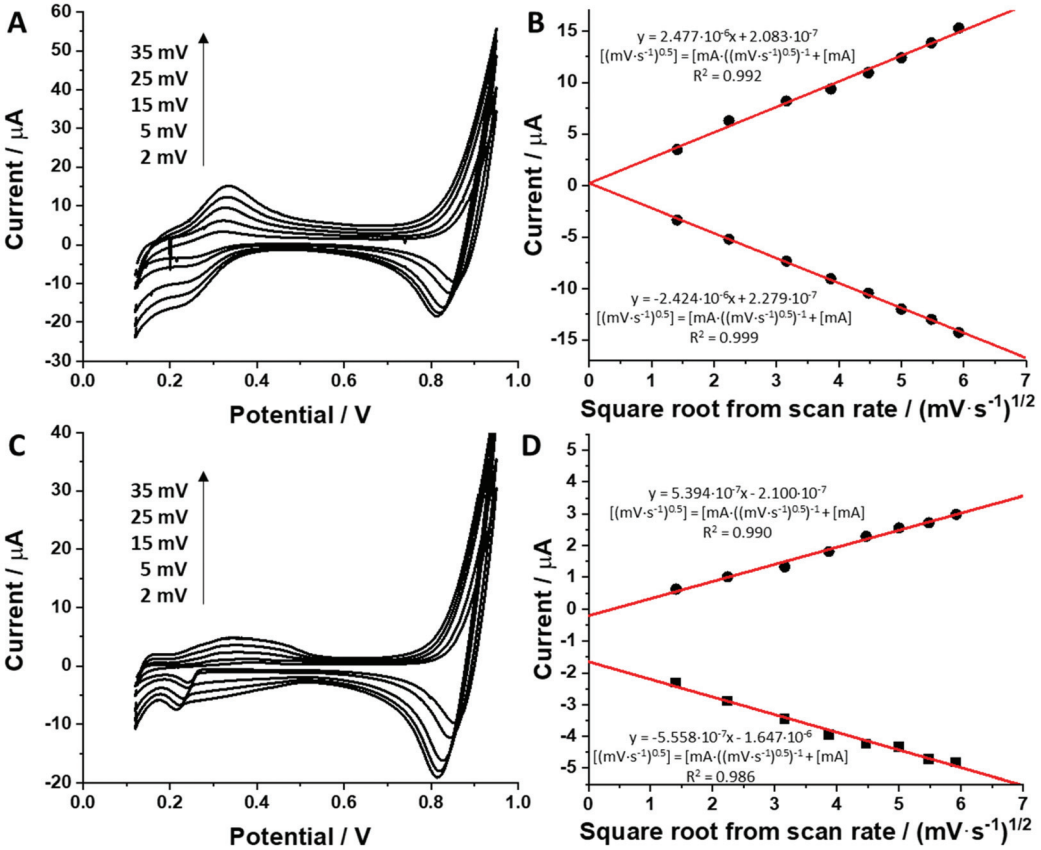

Fig. 4 A and C are ion transfer voltammograms recorded at 2; 5; 15; 25 and 35 mV s^{-1}, whereas B and D show current *versus* square root of the scan rate dependency. Graphs A and B correspond to the BDTR-2 (100 μM) dendrimer. Graphs C and D correspond to the BDTR-5 dendrimer (50 μm). Linear fit equations are displayed next to the corresponding experimental data points.

0.7 nm) with the hydrodynamic radii calculated based on diffusion coefficients measured with diffusion oriented spectroscopy-NMR. The same technique provided the hydrodynamic radius for BDTR-3 equal to 1.7 nm, still within the same order of magnitude (see Table S1 from ESI† for more details) as the value calculated using the electrochemically deduced diffusion coefficient. This underlines that the complex interfacial behaviour of higher dendrimer generations hampers proper evaluation of the charge values crossing the interface during single ion transfer. The values of the slope of the logarithmic dependence of the peak current *versus* experimental scan rate were in the range from 0.45 to 0.58, indicating that the charge transfer reaction is diffusion-limited. Also, we have noticed that BDTR-5, see Fig. 4A and 3C, gave very broad positive and negative peaks (especially for [dendrimer] < 50 μM), which suggests the occurrence of a multistep charge transfer process. At this point, we believe that BDTR-5, to some extent, can facilitate the transfer of $TPBCl^-$ from the organic to the aqueous phase. All these indicate that the voltammetric behavior of all studied dendrimers is complex. The ion transfer reaction for higher generations is surely coupled to the interfacial adsorption/desorption step. This is especially prominent for BDTR-3–BDTR-5 and is in line with other reports.[47]

The behaviour of charged macromolecules (proteins, polyelectrolytes, and dendrimers) at the electrified LLI shares many mechanistic aspects.[32,45,48–50] Upon interfacial polarization, these molecules were found to form a complex with the organic phase anion at the LLI, giving characteristic voltammetric behaviour. (i) Instead of a diffusion-limited current tail, a sharp drop is recorded for the reverse peak current after reaching its maximum (attributed to the partial back transfer of the organic phase anion from the interface to the organic phase). Here, even for the highest dendrimer generation, this behaviour was absent. The complex shape of the (especially) forward peak patterns indicates that the interfacial charge transfer is coupled to the dendrimer adsorption/desorption to/from the LLI. (ii) Macromolecules, upon consecutive voltammetric cycling, tend to form multilayer deposits at the LLI, shown by the increasing forward and reverse peak currents. For all studied dendrimers, the opposite dependency was observed, with the currents dropping over the first few cycles (see the insets of Fig. 5A and B). At this point, we can speculate that the dendrimers studied here (especially smaller molecules) are initially (before LLI polarization) adsorbed to, or in other words pre-concentrated at, the LLI. This could explain the high ionic currents recorded during the first scan, which

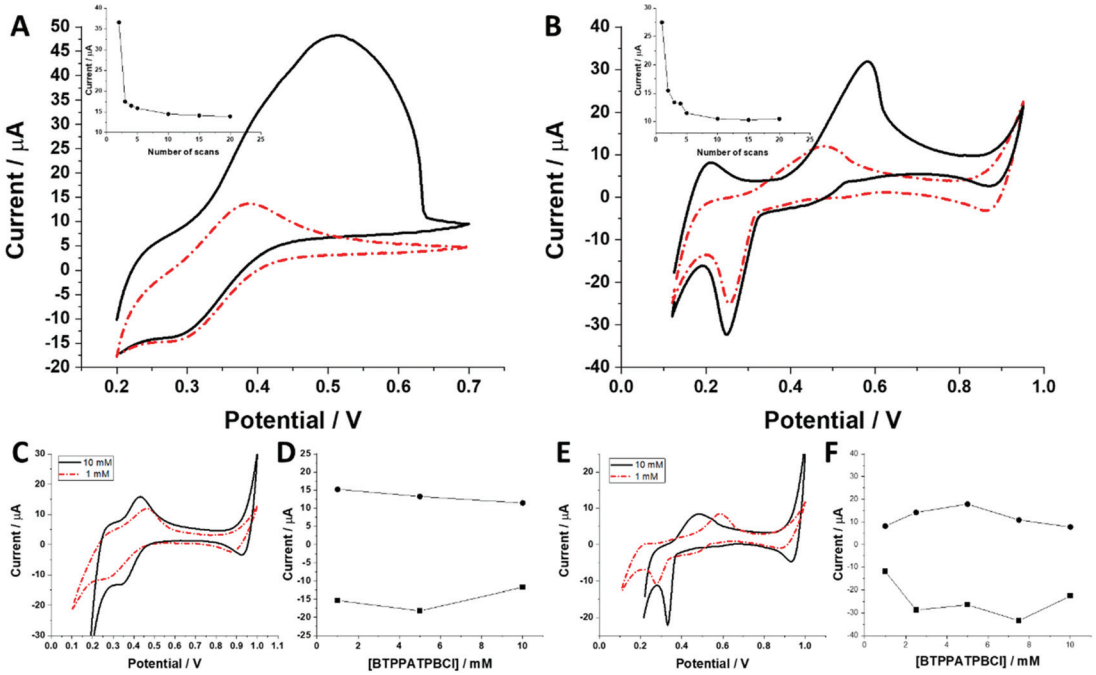

Fig. 5 A and B show the effect of consecutive voltammetric cycling for BDTR-2 and BDTR-5, respectively. Black solid lines represent scan 2 for BDTR-2 and scan 1 for BDTR-5. The red dot–dashed line is scan 20. Insets are the forward peak currents *versus* scan number 1 (or 2 for BDTR-2), 2, 3, 4, 5, 10, 15, and 20. The dendrimer concentration was set to 100 μM, and the scan rate was 20 mV s^{-1}. C (BDTR-2) and E (BDTR-5) are ion transfer voltammograms recorded in cell II with 1 mM (red dot–dash line) and 10 mM (black solid line) BTPPATPBCl in the organic phase. D and F are the corresponding forward and reverse peak current intensities for the varying concentration of the organic phase background electrolyte. The concentration of BDTR-2 was equal to 100 μM and for BDTR-5 it was 50 μM. The scan rate was set to 20 mV s^{-1}. Positive peak currents are given as a result of the signal subtracted from a blank.

may be due to the analyte stripping from the LLI. (iii) The position and intensity of the faradaic signals for interfacially active macromolecules are highly dependent on the nature and concentration of the organic phase background electrolyte anion.[28,51] For the interfacial complex formation (charged macromolecule–hydrophobic anion) it is expected to observe dropping faradaic current signals as a function of the dropping concentration of the background electrolyte. Fig. 5C and E show the ion transfer voltammograms recorded for BDTR-2 and BDTR-5, respectively, in cell II for the organic phase containing either 1 mM or 10 mM BTPPATPBCl in the 1,2-dichloroethane. Fig. 5D and F show the positive and negative peak current intensities for other studied concentrations of the BTPPATPBCl dissolved in the organic phase (ITVs are not shown). We have observed that the decreasing concentration of the organic phase background anion has a minimal effect on the positive and negative peak current intensities for BDTR-2. The increasing forward and reverse peak to peak separation (see the red dash–dotted curve recorded for 1 mM BTPPATPBCl) is due to the increasing uncompensated resistance of the system rather than due to the interaction between BDTR-2 and the anionic part of the organic phase background electrolyte. Based on this and the above observations, we concluded that the interfacial charge transfer reaction for smaller dendrimers is mainly governed by the simple and reversible ion transfer reaction. The positive and negative peak current intensities for BDTR-5, although slightly more scattered, (see Fig. 5F), gave lower peak current values for decreasing concentration of BTPPATPBCl dissolved in the organic phase. As such, we have concluded that branched generations with higher dimensionality undergo interfacial ion transfer coupled to interfacial adsorption (when the direction of the ion transfer is from the aqueous to the organic phase). This is evidenced by (i) broad forward positive peaks, (ii) overlaid signals indicating multistep interfacial charge transfer reactions and (iii) irregular variations in the peak current intensity and forward peak position recorded at different pH values (ESI Fig. 1†). Our study reveals that all five carbosilane dendrimers can cross the LLI under external polarization. In addition to the insight into the interaction between studied macromolecules and the mimetic interface, we think that these molecules can be used to study the permeability of the electrified LLI modified with porous materials that we wish to pursue in the future.

4. Conclusions

In this work, we have studied the behaviour of different generations of carbosilane dendrimers terminated with methyl- (G1–G3) or mesityl-imidazolium (G1–G2) groups. We have found that all studied species are electrochemically active at

the polarized water–1,2-dichloroethane interface. The studied compounds could be detected starting from concentrations equal to around 5–20 μM. Our data indicate that small changes in the molecular structure affecting molecular lipophilicity can be directly visualized using ion transfer voltammetry. The interfacial behaviour of the studied species is complex and recorded ionic currents originate from a diffusion-limited ion transfer reaction coupled to the interfacial adsorption process. The latter was significantly more prominent for higher dendrimer generations. We have excluded the possibility of facilitated transfer of the organic phase anion (usually responsible for interfacial charge transfer phenomena recorded in the presence of positively charged macromolecules) triggered by the BDTR dendrimers (from BDTR-1 to BDTR-3) adsorbed to the liquid–liquid interface. We are convinced that these species can be used in the future for the characterization of liquid–liquid interfaces modified with porous membranes or lipid monolayers.

Conflicts of interest

There are no conflicts to declare.

Acknowledgements

L. P. is grateful for financial support from the National Science Center (NCN) in Krakow, Poland (Grant No. UMO-2018/31/D/ST4/03259). This work was also supported by CTQ2017-86224-P (MINECO) and by a EUROPARTNER: strengthening and spreading international partnership activities of the Faculty of Biology and Environmental Protection for interdisciplinary research and innovation of the University of Lodz Programme: NAWA International Academic Partnership Programme (PPI/APM/2018/1/00007/U/001). CIBER-BBN is an initiative funded by the VI National R&D&i Plan 2008–2011, Iniciativa Ingenio 2010, Consolider Program, CIBER Actions, and financed by the Instituto de Salud Carlos III with assistance from the European Regional Development Fund.

References

1 C. Gao and D. Yan, *Prog. Polym. Sci.*, 2004, **29**, 183–275.
2 C. R. Yates and W. Hayes, *Eur. Polym. J.*, 2004, **40**, 1257–1281.
3 D. A. Tomalia, *Prog. Polym. Sci.*, 2005, **30**, 294–324.
4 M. Seiler, *Fluid Phase Equilib.*, 2006, **241**, 155–174.
5 J. M. Frechet, *Science*, 1994, **263**, 1710–1715.
6 D. A. Tomalia, A. M. Naylor and W. A. Goddard, *Angew. Chem., Int. Ed. Engl.*, 1990, **29**, 138–175.
7 R. S. Ambekar, M. Choudhary and B. Kandasubramanian, *Eur. Polym. J.*, 2020, **126**, 109546.
8 S. W. Krska and D. Seyferth, *J. Am. Chem. Soc.*, 1998, **120**, 3604–3612.
9 D. Maciel, C. Guerrero-Beltrán, R. Ceña-Diez, H. Tomás, M. Á. Muñoz-Fernández and J. Rodrigues, *Nanoscale*, 2019, **11**, 9679–9690.
10 I. Heredero-Bermejo, N. Gómez-Casanova, S. Quintana, J. Soliveri, F. J. de la Mata, J. Pérez-Serrano, J. Sánchez-Nieves and J. L. Copa-Patiño, *Pharmaceutics*, 2020, **12**, 918.
11 N. Weber, P. Ortega, M. I. Clemente, D. Shcharbin, M. Bryszewska, F. J. de la Mata, R. Gómez and M. A. Muñoz-Fernández, *J. Controlled Release*, 2008, **132**, 55–64.
12 E. Pedziwiatr-Werbicka, K. Milowska, V. Dzmitruk, M. Ionov, D. Shcharbin and M. Bryszewska, *Eur. Polym. J.*, 2019, **119**, 61–73.
13 B. Noriega-Luna, L. A. Godínez, F. J. Rodríguez, A. Rodríguez, G. Zaldívar-Lelo de Larrea, C. F. Sosa-Ferreyra, R. F. Mercado-Curiel, J. Manríquez and E. Bustos, *J. Nanomater.*, 2014, **2014**, 507273.
14 P. Kesharwani, K. Jain and N. K. Jain, *Prog. Polym. Sci.*, 2014, **39**, 268–307.
15 L. Zhao, C. Zhang, L. Zhuo, Y. Zhang and J. Y. Ying, *J. Am. Chem. Soc.*, 2008, **130**, 12586–12587.
16 J. Koryta, M. Březina, A. Hofmanová, D. Homolka, L. Q. Hung, W. Khalil, V. Mareček, Z. Samec, S. K. Sen, P. Vanýsek, J. Weber and J. Heyrovský, *Bioelectrochem. Bioenerg.*, 1980, **7**, 61–68.
17 H. A. Santos, V. García-Morales and C. M. Pereira, *ChemPhysChem*, 2010, **11**, 28–41.
18 L. Poltorak, M. L. Verheijden, D. Bosma, P. Jonkheijm, L. C. P. M. de Smet and E. J. R. Sudhölter, *Biochim. Biophys. Acta, Biomembr.*, 2018, **1860**, 2669–2680.
19 O. Purrucker, H. Hillebrandt, K. Adlkofer and M. Tanaka, *Electrochim. Acta*, 2001, **47**, 791–798.
20 C. Steinem, A. Janshoff, H. J. Galla and M. Sieber, *Bioelectrochem. Bioenerg.*, 1997, **42**, 213–220.
21 M. Naumowicz and Z. A. Figaszewski, *J. Membr. Biol.*, 2005, **205**, 29–36.
22 M. Naumowicz and Z. A. Figaszewski, *J. Membr. Biol.*, 2011, **240**, 47–53.
23 P. Vanysek and L. B. Ramirez, *J. Chil. Chem. Soc.*, 2008, **2**, 1455–1464.
24 J. Koryta, *Electrochim. Acta*, 1979, **24**, 293–300.
25 L. Poltorak, K. Rudnicki, V. Kolivoška, T. Sebechlebská, P. Krzyczmonik and S. Skrzypek, *J. Hazard. Mater.*, 2021, **402**, 123411.
26 Z. Samec, *Pure Appl. Chem.*, 2004, **76**, 2147–2180.
27 F. Kivlehan, Y. H. Lanyon and D. W. M. Arrigan, *Langmuir*, 2008, **24**, 9876–9882.
28 H. Sakae, Y. Toda and T. Yokoyama, *Electrochim. Acta*, 2018, **90**, 83–86.
29 J. A. Ribeiro, F. Silva and C. M. Pereira, *Anal. Chem.*, 2013, **85**, 1582–1590.
30 M. D. Scanlon, J. Strutwolf and D. W. M. Arrigan, *Phys. Chem. Chem. Phys.*, 2010, **12**, 10040–10047.
31 J. S. Riva, C. I. Cámara, A. V. Juarez and L. M. Yudi, *J. Appl. Electrochem.*, 2014, **44**, 1381–1392.

32 A. Berduque, M. D. Scanlon, C. J. Collins and D. W. M. Arrigan, *Langmuir*, 2007, **23**, 7356–7364.
33 G. Herzog, S. Flynn and D. W. M. Arrigan, *J. Phys.: Conf. Ser.*, 2011, **307**, 1–6.
34 H. Nagatani, M. Fujisawa and H. Imura, *Langmuir*, 2018, **34**, 3237–3243.
35 H. Nagatani, T. Ueno and T. Sagara, *Electrochim. Acta*, 2008, **53**, 6428–6433.
36 H. Sakae, H. Nagatani, K. Morita and H. Imura, *Langmuir*, 2014, **30**, 937–945.
37 H. Nagatani, H. Sakae, T. Torikai, T. Sagara and H. Imura, *Langmuir*, 2015, **31**, 6237–6244.
38 L. Poltorak, K. Morakchi, G. Herzog and A. Walcarius, *Electrochim. Acta*, 2015, **179**, 9–15.
39 T. Rodríguez-Prieto, A. Fattori, C. Camejo, F. Javier de la Mata, J. Cano, M. Francesca Ottaviani and R. Gómez, *Eur. Polym. J.*, 2020, **133**, 109748.
40 L. Poltorak, I. Eggink, M. Hoitink, M. De Puit, E. J. R. Sudholter and M. De Puit, *Anal. Chem.*, 2018, **90**, 8–13.
41 T. Kakiuchi, M. Chiba, N. Sezaki and M. Nakagawa, *Electrochem. Commun.*, 2002, **4**, 701–704.
42 T. Kakiuchi, *J. Electroanal. Chem.*, 2004, **569**, 287–291.
43 Y. Kitazumi and T. Kakiuchi, *Langmuir*, 2009, **25**, 8062–8068.
44 L. Poltorak, N. Van Der Meijden, S. Oonk, E. J. R. Sudhölter and M. De Puit, *Electrochem. Commun.*, 2018, **94**, 27–30.
45 G. Herzog, V. Kam and D. W. M. Arrigan, *Electrochim. Acta*, 2008, **53**, 7204–7209.
46 M. A. van Dongen, B. G. Orr and M. M. B. Holl, *J. Phys. Chem. C*, 2014, **118**, 7195–7202.
47 D. L. Cheung and P. Carbone, *Soft Matter*, 2013, **9**, 6841–6850.
48 G. Herzog, S. Flynn, C. Johnson and D. W. M. Arrigan, *Anal. Chem.*, 2012, **84**, 5693–5699.
49 E. Alvarez de Eulate and D. W. M. Arrigan, *Anal. Chem.*, 2012, **84**, 2505–2511.
50 S. Ulmeanu, H. J. Lee and H. H. Girault, *Electrochem. Commun.*, 2001, **3**, 539–543.
51 G. Herzog, W. Moujahid, J. Strutwolf and D. W. M. Arrigan, *Analyst*, 2009, **134**, 1608–1613.

materials

MDPI

Communication

Interfacial Deposition of Titanium Dioxide at the Polarized Liquid–Liquid Interface

Karolina Kowalewska, Karolina Sipa, Barbara Burnat, Sławomira Skrzypek and Lukasz Poltorak *

Electroanalysis and Electrochemistry Group, Department of Inorganic and Analytical Chemistry, Faculty of Chemistry, University of Lodz, Tamka 12, 91-403 Lodz, Poland; karolina.kowalewska@chemia.uni.lodz.pl (K.K.); karolina.sipa@chemia.uni.lodz.pl (K.S.); barbara.burnat@chemia.uni.lodz.pl (B.B.); slawomira.skrzypek@chemia.uni.lodz.pl (S.S.)
* Correspondence: lukasz.poltorak@chemia.uni.lodz.pl

Abstract: The interfacial polycondensation of titanium dioxide was studied at the bare and fiberglass membrane supported polarized liquid–liquid interface (LLI). Titanium dioxide synthesis was derived from the titanium (IV) tetrabutoxide (initially dissolved in the 1,2-dichloroethane) interfacial hydrolysis followed by its condensation. Experimental parameters, such as the pH of the aqueous phase and the influence of titanium alkoxide concentration in the organic phase on the electrochemical signal and material morphology, were investigated. The latter was achieved with fiberglass membranes used as the LLI support during TiO_2 interfacial deposition. Cyclic voltammetry was used for the in situ studies, whereas scanning electron microscopy, energy-dispersive X-ray spectroscopy, and infrared spectroscopy were used during ex situ examination. The interfacial polycondensation reaction could be studied using electrified LLI and resulted in the material being a TiO_2 film alone or film decorated with particles.

Keywords: ITIES; interfacial polycondensation; electrochemistry; voltammetry; interfacial modification; titanium dioxide synthesis

Citation: Kowalewska, K.; Sipa, K.; Burnat, B.; Skrzypek, S.; Poltorak, L. Interfacial Deposition of Titanium Dioxide at the Polarized Liquid–Liquid Interface. *Materials* **2022**, *15*, 2196. https://doi.org/10.3390/ma15062196

Academic Editors: Giuseppe Bonura and Catia Cannilla

Received: 11 February 2022
Accepted: 8 March 2022
Published: 16 March 2022

1. Introduction

Titanium dioxide (TiO_2) is a material with a still-expanding list of applications. It can be used, e.g., to purify water and air, as a food additive, in coatings fabrication for self-cleaning surfaces, or as a UV filter in cosmetic products [1–3]. In this respect, TiO_2 nanomaterials have become very popular due to relatively low price, non-toxicity, corrosion resistance, or well-established protocols to tune their surface physico-chemistry (e.g., porosity) [4]. TiO_2 synthesis can be derived from many protocols such as the sol–gel processing, hydrothermal method, solvothermal method, and physical and chemical vapor deposition [5]. TiO_2 thin films processing, with significant potential to be applied in electronic and magneto-electric devices, is challenging. Their formation at the planner liquid–liquid interface (LLI) is an intuitive choice as a free-stating thin film may be obtained. This work aims at providing first insights into electrochemically formed TiO_2 at the LLI.

Electrochemistry at the polarized LLI, alternatively called interface between two immiscible electrolyte solutions (ITIES), finds applications in material science, pharmacochemistry, physicochemistry, and analytical chemistry. ITIES allows the study of the interfacial charge transfer reaction in the form of ions or electrons crossing the soft junction. Polarized LLIs offer properties that are difficult or even impossible to be obtained with conventional electrochemical systems, including (i) the possibility to separate reactive chemical compounds between two immiscible phases, (ii) defect and crack free electrified interface deprived of preferential nucleation sites, or (iii) asymmetric and amphiphilic properties that may be harvested during interfacial deposition reactions. Moreover, electrified LLIs (alone or in the presence of interfacial deposits) can be investigated with all available electrochemical techniques [6].

The placement of TiO_2-based objects at the ITIES is limited to a few examples. In two elegant works, Jensen et al. [7] and later Plana and Fermin [8] showed that preformed TiO_2 nanoparticles self-assembled at the electrified water—1,2-dichloroethane (1,2-DCE) interface could be used to generate photocurrent responses when illuminated with laser light. Another report describes coumarin 343 dye TiO_2 nanoparticles complex interfacial adsorption studied with surface second harmonic generation technique [9]. The intuitive combination between conventional LLI and TiO_2 nanoparticles are Pickering emulsions that can be frequently found in everyday products (e.g., stabilized sun creams) or the scientific literature [10–12]. The sol–gel processing of the TiO_2 can occur at the LLI. Titanium alkoxides are usually dissolved in organic solvent immiscible with water providing self-dissociation reactions products (H_3O^+ or OH^-) catalyzing hydrolysis and condensation reactions happening at the LLI [13–15]. To the best of our knowledge, such reactions have not been investigated at the electrified LLI to date.

This work aims to study TiO_2 interfacial polycondensation at polarized LLI. This project is derived from our experience related to in situ ITIES modification with silica [16] and polyamide-based materials [17]. In this respect, we separated TiO_2 precursor (titanium (IV) butoxide dissolved in the organic phase) from the aqueous phase, which is a solution of a background electrolyte at fixed pH. The following parameters were investigated: pH of the water phase, the effect of titanium (IV) butoxide concentration, and the effect of scan rate on the electrochemical signal. Synthesized material was removed from the interface and characterized using infrared spectroscopy. Finally, we used the fiberglass membranes as the LLI support during TiO_2 synthesis. These were then studied using SEM and EDX. This communication reports on the possibility to form TiO_2 derived from sol–gel processing at the eLLI. After the Materials and Methods section, which lists all chemicals and provides a brief description of the employed methodology, we discussed the possible mechanism governing the electrochemically assisted TiO_2 interfacial polycondensation. We then correlated our understanding of the investigated platform with electrochemical data obtained using ion transfer voltammetry. Finally, we designed the experiment that allowed for the interfacial deposition of TiO_2 over porous support placed within the LLI that was further subjected to comprehensive characterization.

2. Materials and Methods

2.1. Chemicals

Titanium (IV) butoxide ($Ti[O(CH_2)_3CH_3]_4$, reagent grade 97%, Aldrich Chemistry, Germany), sodium chloride (NaCl, for analysis, ChemPur, Poland), 1,2-dichloroethane (1,2-DCE, for analysis, POCH, Poland), 35–38% hydrochloric acid (HCl, for analysis, ChemPur, Poland), sodium hydroxide (NaOH, for analysis, ChemPur, Poland), phosphate buffer made according to appropriate weights of sodium hydrogen phosphate dihydrate ($NaH_2PO_4 \times 2H_2O$, for analysis, ChemPur, Poland), and sodium chloride (NaCl, for analysis, ChemPur, Poland) were used as received. The organic phase electrolyte $BTPPA^+TPBCl^-$ (bis(triphenylphosphoranylidiene)ammonium tetrakis(4-chlorophenylborate)) was synthesized using $BTPPA^+Cl^-$ (bis(triphenylphosphoranylidiene)ammonium chloride, 97% Sigma-Aldrich, Germany) and $KTPB^+Cl^-$ (potassium tetrakis(4-chlorophenyl), 98% Sigma-Aldrich, Germany) salts according to the recipe published elsewhere [18]. The aqueous phase was prepared from the demineralized water (Hydrolab system, Poland).

2.2. Methods

Electrochemical experiments: The TiO_2 synthesis at the ITIES was studied in a dedicated macroscopic voltammetric glass cell (interface radii equal to 0.7 cm) (custom made by glass blower) equipped with a set of four electrodes consisting of two Ag/AgCl reference electrodes (Ag, 99.99%, Alfa Aesar, Germany) and two Pt counter electrodes (Pt, 99.9%, Sigma Aldrich, Germany). The potential interfacial difference was measured between Ag/AgCl wire immersed into the aqueous phase Luggin capillary filled with the aqueous phase with a fixed concentration of Cl^- ions and Ag/AgCl wire present inside the organic

phase Luggin capillary filled with a solution of 10 mM NaCl and 10 mM $BTPPA^+Cl^-$ remaining in direct contact with the 1,2-DCE solution. All experiments were conducted using EmStat3+ equipped with a differential pulse amplifier from PalmSens (The Netherlands). Ion transfer voltammetry (potentiostatic cyclic voltammetry) was used to study the changes in the physicochemical properties of the polarized LLI at different TBOT organic phase % concentrations and different aqueous phase pH. The employed technique allowed for direct insights into ion transfer reactions happening at different polarization directions and interfacial electrical capacitance. The experimental scan rate value was 20 mV s^{-1} unless otherwise stated. Interfacial capacitance was extracted from the ion transfer voltammograms recorded at different potential scan rate values (5; 10; 15; 20; 25; 30 and 35 mV s^{-1}). During all experiments, the LLI was always polarized from less positive to more positive potential values during the forward scan.

Infrared spectroscopy: TiO_2 synthesized at the non-polarized LLI was collected and dried at room temperature. Dry powder was analyzed using the KBr pellet method with a Nexus FT-IR by Thermo Nicolet spectrometer (USA).

Scanning Electron Microscopy: The morphology of the unmodified and titanium dioxide modified glass fiber membranes was examined using Phenom G2 Pure scanning electron microscope (Phenom-World BV, Eindhoven, the Netherlands) operating with an accelerating voltage of 5 kV. The surface elemental composition analysis was performed using FEI Nova NanoSEM 450 microscope (Hillsboro, OR, USA) equipped with an EDS analyzer. Elemental analysis was carried out using an accelerating voltage of 10 kV.

3. Results and Discussion

3.1. TiO_2 Formation at the Electrified Liquid–Liquid Interface—Consideration

The composition of the immiscible phases used for the interfacial deposition of the TiO_2 at the eLLI is shown in Figure 1A. The aqueous phase was the Britton–Robinson buffer providing H^+ or OH^- needed for catalyzing tetrabutoxy titanium (TBOT) hydrolysis and condensation reactions together with other inorganic ions assuring high electric conductivity. The organic phase was the 1,2-DCE solution of the background, hydrophobic electrolyte ($BTPPA^+TPBCl^-$), and TBOT added at different % concentrations ranging from 0.01% to 1%. The interfacial polycondensation reactions occurring at the LLIs provide several routes that may lead to the formation of free-standing materials/films, out-printing the molecular properties of the hydrophobic and hydrophilic phases. As reported in a few elegant works [19,20], TiO_2 can be formed at the LLI followed by sol–gel processing. Substrates, products, and catalysts of the hydrolysis and condensation reaction may undergo partitioning to the contacting phases, and whenever charged, this process is affected by the potential interfacial drops, which may be studied with all techniques offered by the electroanalytical toolbox. Figure 1B and Equations (1)–(11) depicts possible and simplified (100% efficient TBOT hydrolysis is assumed) reactions that may occur spontaneously and/or can be aided electrochemically at the LLI during TBOT hydrolysis and condensation [21,22]. These reactions are simplified to fully hydrolyzed TBOT and are defined based on our understanding of the interfacial region.

$$Ti-(O-R)_{4,\ org}+4H_2O \rightarrow Ti-(OH)_{4,org}+4R-OH \quad (1)$$

$$Ti-(O-R)_{4,\ LLI}+4H_2O \rightarrow Ti-(OH)_{4,LLI}+4R-OH \quad (2)$$

$$Ti-(OH)_{4,org} \rightarrow Ti-(OH)_{4,LLI} \quad (3)$$

$$Ti-(OH)_{4,LLI} \rightarrow Ti-(OH)_{4,aq} \quad (4)$$

$$H^+_{aq} \rightarrow H^+_{org} \quad (5)$$

$$OH^-_{aq} \rightarrow OH^-_{org} \quad (6)$$

$$Ti-(OH)_{4,\ LLI}+Ti-(OH)_{4,\ LLI} \rightarrow (OH)_3-Ti-O-Ti-(OH)_{3,LLI}+H_2O \quad (7)$$

$$Ti-(OH)_{4,\ LLI}+Ti-(OH)_{4,\ aq}\rightarrow(OH)_3-Ti-O-Ti-(OH)_{3,LLI}+H_2O \quad (8)$$

$$Ti-(OH)_{4,\ LLI}+Ti-(OH)_{4,\ org}\rightarrow(OH)_3-Ti-O-Ti-(OH)_{3,LLI}+H_2O \quad (9)$$

$$Ti-(OH)_{4,\ aq}+Ti-(OH)_{4,\ aq}\rightarrow(OH)_3-Ti-O-Ti-(OH)_{3,aq}+H_2O \quad (10)$$

$$(OH)_3-Ti-O-Ti-(OH)_{3,aq}\overset{precipitation}{\rightarrow}(OH)_3-Ti-O-Ti-(OH)_{3,LLI} \quad (11)$$

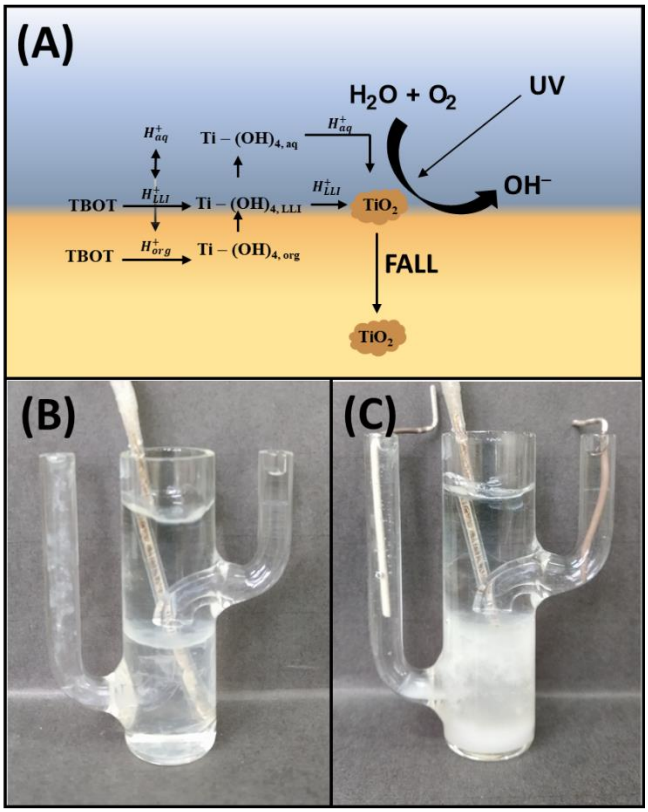

Figure 1. (**A**) Anticipated mechanisms laying behind the interfacial, electrochemically assisted TiO_2 polycondensation. The photo of the electrochemical cell was taken for 0.5% TBOT (**B**) before and (**C**) after LLI polarization.

Hydrophobic TBOT soluble in most organic solvents was initially present in the organic phase where it can undergo hydrolysis (Equation (1)) triggered by the H^+ or OH^- electrochemically transferred from the aqueous to the organic phase (Equations (5) and (6), respectively). Interfacial transfer of ions across the LLI can happen only when the appropriate interfacial potential difference is applied to the interfacial region. The presence of water molecules within the interfacial region is governed not only by the mutual solubility of the employed solvents (reported 1,2-DCE solubility in H_2O is 0.085 mol·dm^{-3} whereas water in 1,2-DCE is 0.11 mol·dm^{-3} [23]) but also can be delivered to the organic phase as the cargo of inorganic ions which are not entirely deprived of the solvation shells when going from the aqueous to the organic phase [20]. This is especially valid for small cationic and anionic species such as Na^+, Li^+, K^+, Cl^-, Br^-, etc. [24–28]. TBOT hydrolysis is also expected to happen within a region defined by the LLI thickness (Equation (2)). For both cases (Equations (1) and (2)), resulting titanium hydroxide species with high hydrophilicity are expected to partition from the organic phase to the interfacial region (Equation (3)) and further to the aqueous phase (Equation (4)) where their subsequent condensation reactions happen (Equation (7)—condensation within the plane of LLI; Equation (8)—condensation between the species from the LLI and the aqueous phase; Equation (9)—condensation between the species from the LLI and the

organic phase; Equation (10)—condensation reactions happening in the aqueous phase). Butanol, which is the side product of the hydrolysis reaction, miscible with H_2O and 1,2-DCE increases the mutual solubility of the concerned solvents, which in turn affects the thickness of the LLI and increases the availability of the substrates of the reaction. The TiO_2 photocatalytic water reduction (caused by the daylight irradiation) leading to the formation of OH^- anions were also expected to contribute to the condensation reactions kinetics. The consequence of the electrochemically controlled ion transfer reaction happening in parallel and affecting the TBOT hydrolysis and condensation reactions initially lead to the interfacial formation of TiO_2 (Figure 1B), which further precipitates into the organic phase (see Figure 1C).

3.2. Voltammetric Insights into Interfacial TiO_2 Formation

The interfacial polycondensation of TiO_2 at the polarized LLI was studied using ion transfer voltammetry. We investigated the effect of the electrochemical processing (the effect of the applied Galvani potential difference, voltammetric cycling, applied sweeping potential scan rate) and the chemical conditions (TBOT % concentration, pH of the aqueous phase) on the experimental output. Figure 2A,B shows the ion transfer voltammograms recorded for the 2nd and 30th cycle, respectively, recorded for two different pH values (2 and 7), assuring high and low concentrations of protons that may be transferred to the organic phase upon interfacial polarization. We observed that subsequent cycling and increasing % concentration of the TBOT in the organic phase affected the separation of the (i) capacitive currents within the available potential window and limiting currents on the (ii) positive and (iii) negative voltammetric scan potential ends. For the latter, both the intensity and the potential at which the background electrolyte ions started crossing the LLI have changed. This observation is in line with the increasing amount of the interfacially formed TiO_2. At low pH values (around 2), the positive end of the potential window is limited by the interfacial transfer of H^+ from the aqueous to the organic (positive current) and from the organic to the aqueous (negative current) phase [28,29]. Protons present within the LLI and in the organic phase were expected to accelerate hydrolysis and condensation reactions. This can be visualized in Figure 3C together with its inset representing the change in the current intensity recorded at 0.8 V. The potential interfacial difference for which an increase in positive current on the more positive potential window end was equal to 5% change, the capacitive current was attributed to the potential difference at which H^+ started transferring from the aqueous to the organic phase [28]. We found that this potential was progressively shifting toward more negative potential values and was equal to 0.76 V for 0.01% TBOT, 0.49 V for 0.25% TBOT, and 0.33 V for 1.00% TBOT. This observation can be attributed to a few interconnected aspects: (i) increasing concertation of TBOT in the organic phase most probably facilitated the transfer of proton to the organic phase (indicated by the negative shift of the limiting current potential); (ii) high TBOT concentration leads to an autocatalytic effect on hydrolysis/condensation reactions as the concertation of protons in the interfacial layer increases (increasing intensities of the limiting current on the positive end—see inset of Figure 2C); (iii) presence of the butanol as a side product of the hydrolysis reaction changes the miscibility of the water and 1,2-DCE, and hence lower free Gibbs energy (energy needed to deprive the transferring ions of the solvation shells) of the proton transfer from the aqueous to the organic phase. Moreover, for high TBOT concentration (1.00%) for the aqueous phase with pH = 2 we observed the cyclic voltammograms with inclined limiting currents (originating from the H^+ transfer on the more positive potential window side and Cl^- anions transfer on the less positive potential window side). This observation is attributed to the formation of a compact TiO_2 based film, making a physical barrier directly existing at the LLI, which increases the resistance of the transferring ions.

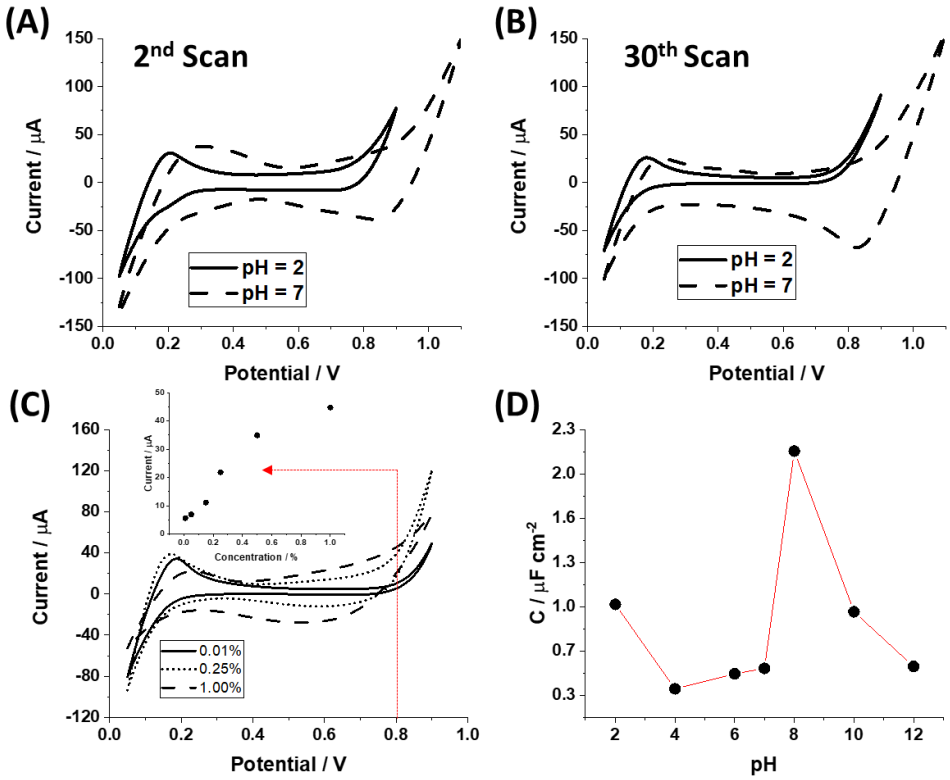

Figure 2. Ion transfer voltammograms (ITVs) recorded for 0.5% TBOT initially dissolved in the organic phase at pH of the aqueous phase equal to 2 (solid line) and 7 (dashed line) for the 2nd (**A**) and 30th (**B**) scan. (**C**) ITVs recorded for TBOT with the organic phase % concentration equal to 0.01% (solid line), 0.25% (dotted line), and 1.00% (dashed line). The second scan is shown. The inset in section (**C**) corresponds to positive ionic current falling for 0.8 V (indicated with the red, horizontal dashed line) recorded for different organic phase TBOT concentrations. pH of the aqueous phase was equal to 2. (**D**) The specific LLI capacitance derived from the voltammetric data plotted in function of the aqueous phase pH.

An interesting observation is provided in Figure 2D showing the interfacial specific capacitance ($\mu F \cdot cm^{-2}$) plotted in function of the aqueous phase pH. The LLI formed between the aqueous phase, which is the Britton–Robinson buffer solution holding a fixed pH value and 0.5% TBOT solution dissolved in 5 mM $BTPPA^{+}TPBCl^{-}$ in 1,2-DCE was polarized at different voltammetric scan rates ranging from 5 to 35 $mV \cdot s^{-1}$. From the obtained voltammograms, we chose the potential difference region where no Faradaic reactions were occurring (data not shown). Next, we plotted the half of the forward and reversed capacitive currents separation in the function of the applied scan rate giving a linear dependency. The slope of the obtained curve with a unit of Farad (F) was further divided by the geometrical area of the cell used to support LLI (ø = 1.25 cm; A = 1.23 cm^2). Finally, we plotted the resulting specific capacitance in the function of pH, providing a very characteristic pattern shown in Figure 2D. The obtained dependency resembles the relative rate of the Si-$(OR)_4$ condensation reactions obtaining maximum values for the acidic environments and pH values falling for the pH range from 8 to 10 [30]. The capacitance of the system should be growing as the amount of interfacially accumulated charge increases. During interfacial condensation of TiO_2, this will mainly originate from the increasing amount of interfacially accumulated charge in the form of background electrolyte salts. Miscibility of both phases, and hence, the thickness of the LLI increases as the condensation proceeds, and butanol is formed as the condensation reaction side products (dielectric properties of the "thick" LLI allow the accumulation of a higher amount of charge). Moreover, the isoelectric point of TiO_2 is reported to be in the pH range from 5 to 7 [31], meaning that beyond this range, it is positively and negatively charged, respectively.

According to the result shown in Figure 2D, most charges was accumulated at the LLI at pH around 8–10 and for pH < 3, which also coincide with the high amount of the deposited TiO_2 material (visual observation). As such, we concluded that the dependency shown in Figure 2D correlate with the titanium alkoxide sol–gel condensation kinetics.

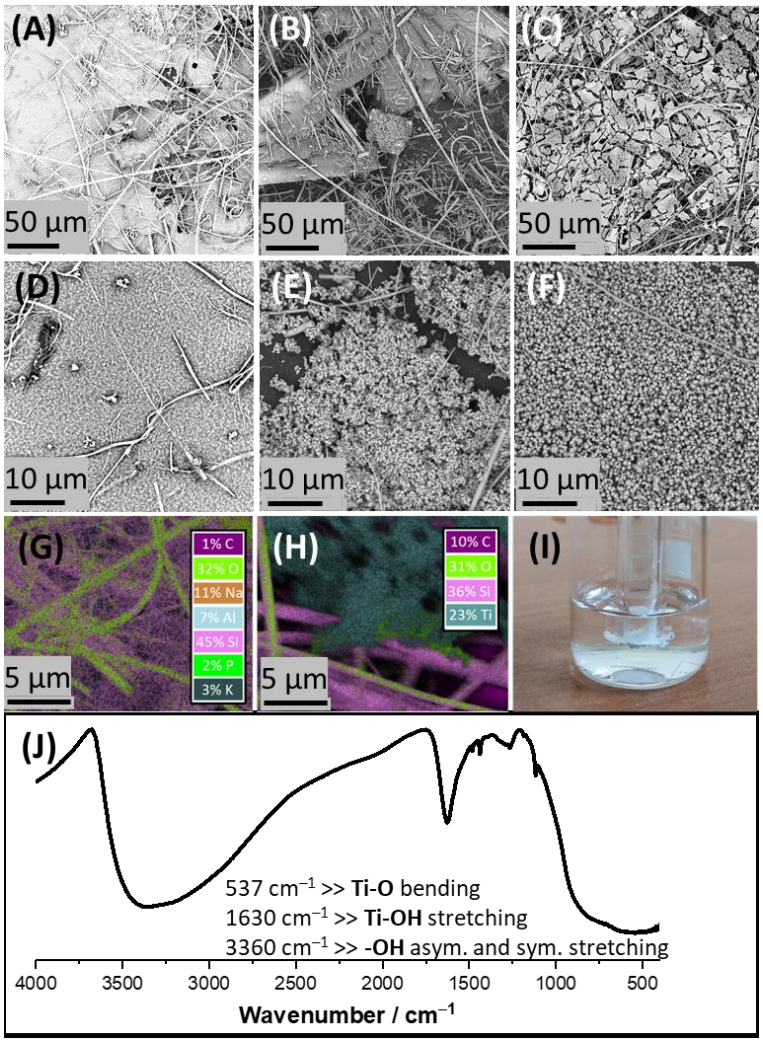

Figure 3. (**A**–**F**) The SEM micrographs recorded for the TiO_2 collected from the LLI with 0.10%, 0.50%, and 1.00% of TBOT initially present in the organic phase; the pH of the aqueous phase was set to 8. (**G**,**H**) The EDS mapping micrographics recorded for the glass fiber membrane before and after modification (1.00% of TBOT in the organic phase) with TiO_2, respectively. (**I**) The photo of a glass fiber membrane fixed to a glass tube. (**J**) The infrared spectrum recorded for the material collected from the LLI (main signals are attributed to the indicted absorption maxima wavenumbers).

3.3. Interfacially Formed TiO_2 Characterization

Figure 3A–F show SEM micrographs that were taken for the fiberglass membranes used as the eLLI support and further modified with TiO_2 derived from the interfacial polycondensation reaction. The image of the cell used during TiO_2 formation is depicted in Figure 3I and shows a beaker filled with the aqueous phase (pH = 8—chosen based on the result provided in Figure 2D), in which we immersed a glass tube filled with the organic phase ended with a fiberglass membrane capillary. The potential drop across such formed interface was defined by the aqueous and the organic phase composition (around 0.4 V). After experimental processing (deposition time was fixed to 30 min; pH of the aqueous phase was 8; the TBOT % concentration in the organic phase was 0.10%; 0.50% or 1.00%), fiberglass membranes were collected and analyzed using SEM and EDS. Figure 3A,D shows

the TiO_2 deposit formed at 0.10% TBOT concentration predominantly existing in the form of a porous film. White fibers, which are visible on all images, are made out of glass and make the volume of the used support (see Figure 3G for the elemental composition). A further increase in TBOT % concentration to 0.50% and 1.00% (see Figure 3B,E and Figure 3C,F, respectively) provided deposits with a shape of a film decorated generously with spherical TiO_2 particles with diameters ranging from few tens to a few hundred nm. The nature of the formed material was studied with EDS (see Figure 3H showing the mapping of the formed flake) and infrared spectroscopy (see Figure 3J), further confirming the presence of TiO_2. For the latter, the presence of the Ti–O bending absorption signal with a center at 537 cm^{-1}; Ti–OH stretching mode with absorption peak maximum falling for 1630 cm^{-1}, and very brad absorption of -OH groups spanning from 2500 to 3700 cm^{-1} confirms the nature of synthesized material [32,33]. This work has delivered the very first proof of concept studies showing the possibility to form TiO_2 at the eLLI. In the future, we plan to improve the proposed methodology further to be able to control TiO2 interfacial polycondensation reactions electrochemically.

4. Conclusions

In this work, we provided the preliminary data confirming the possibility to spontaneously deposit TiO_2 at the polarized LLI. Voltammetry was used to follow the sol–gel processing, whereas the electrochemically controlled interfacial ion transfer reactions (especially the transfer of H^+ from the aqueous to the organic phase) presumably affected the condensation of TBOT hydrolysis products ($Ti(OR)_X(OH)_y$; x + y = 4). The specific capacitance of the LLI calculated from the voltammetric response of a system displayed the highest values falling for the acidic region and the slightly basic pH of the aqueous phase. It is proposed that obtained interfacial capacitance vs. the aqueous pH dependency correlate with the titanium alkoxide condensation reactions kinetics. Finally, we used the fiberglass membranes to support the LLI during TiO_2 sol–gel processing. These platforms helped during formed material post-characterization. We found that interfacially deposited TiO_2 structures range from porous film obtained for low (<0.10%) and films decorated with NPs at high (>0.50%) TBOT % concentrations. The formation of TiO_2 was further confirmed with EDX and infrared spectroscopy. In the future, we plan to investigate the possibility of further controlling the TiO_2 sol–gel processing at the eLLI.

Author Contributions: Conceptualization, K.K. and L.P.; methodology, K.K., L.P. and K.S.; validation, K.K.; formal analysis, K.K., B.B. and K.S.; investigation, K.K., B.B. and K.S.; resources, L.P.; data curation, K.K. and K.S.; writing—original draft preparation, K.K., L.P.; writing—review and editing, L.P., B.B., K.K., K.S. and S.S.; visualization, K.K.; supervision, S.S. and L.P.; project administration, K.K. and L.P.; funding acquisition, K.K. All authors have read and agreed to the published version of the manuscript.

Funding: This research was funded by National Science Centre, Poland, grant number 2020/37/N/ST4/00270.

Institutional Review Board Statement: Not applicable.

Data Availability Statement: Raw data can be found through the link: https://zenodo.org/record/6355563#.YjBZGnrMK3B (accessed on 10 February 2022).

Conflicts of Interest: The authors declare no conflict of interest.

References

1. Catalano, R.; Masion, A.; Ziarelli, F.; Slomberg, D.; Laisney, J.; Unrine, J.M.; Campos, A.; Labille, J. Optimizing the dispersion of nanoparticulate TiO_2-based UV filters in a non-polar medium used in sunscreen formulations—The roles of surfactants and particle coatings. *Coll. Surf. A Physicochem. Eng. Asp.* **2020**, *599*, 124792. [CrossRef]
2. Borges, A.R.; Duarte, Á.T.; Potes, M.D.L.; Silva, M.M.; Vale, M.G.R.; Welz, B. Fluorine in eye shadow: Development of method using high-resolution continuum source graphite furnace molecular absorption spectrometry via calcium mono-fluoride with direct solid sample introduction. *Microchem. J.* **2016**, *124*, 410–415. [CrossRef]

3. Rahimi, N.; Pax, R.A.; Gray, E.M.A. Review of functional titanium oxides. I: TiO_2 and its modifications. *Prog. Solid State Chem.* **2016**, *44*, 86–105. [CrossRef]
4. Bai, J.; Zhou, B. Titanium dioxide nanomaterials for sensor applications. *Chem. Rev.* **2014**, *114*, 10131–10176. [CrossRef] [PubMed]
5. Chen, X.; Mao, S.S. Titanium dioxide nanomaterials: Synthesis, properties, modifications and applications. *Chem. Rev.* **2007**, *107*, 2891–2959. [CrossRef] [PubMed]
6. Poltorak, L.; Gamero-Quijano, A.; Herzog, G.; Walcarius, A. Decorating soft electrified interfaces: From molecular assemblies to nano-objects. *Appl. Mater. Today* **2017**, *9*, 533–550. [CrossRef]
7. Jensen, H.; Fermín, D.; Moser, J.; Girault, H. Organization and reactivity of Nanoparticles at Molecular Interfaces. Part I. Photoelectrochemical Responses Involving TiO_2 Nanoparticles Assembled at Polarizable Water | 1,2-Dichloroethane. *J. Phys. Chem. B* **2002**, *106*, 10908–10914. [CrossRef]
8. Plana, D.; Fermín, D.J. Photoelectrochemical activity of colloidal TiO_2 nanostructures assembled at polarisable liquid/liquid interfaces. *J. Electroanal. Chem.* **2016**, *780*, 373–378. [CrossRef]
9. Pant, D.D.; Joshi, S.; Girault, H.H. Surface second harmonic generation from coumarin 343 dye-attached TiO 2 nanoparticles at liquid-liquid interface. *J. Nanopart. Res.* **2011**, *13*, 7057–7064. [CrossRef]
10. Tan, J.S.J.; Wong, S.L.Y.; Chen, Z. Preparation of Janus Titanium Dioxide Particles via Ultraviolet Irradiation of Pickering Emulsions. *Adv. Mater. Interfaces* **2020**, *7*, 1901961. [CrossRef]
11. Chevalier, Y.; Bolzinger, M.A. Emulsions stabilized with solid nanoparticles: Pickering emulsions. *Coll. Surfaces A Physicochem. Eng. Asp.* **2013**, *439*, 23–34. [CrossRef]
12. Demina, P.A.; Grigoriev, D.O.; Kuz'micheva, G.M.; Bukreeva, T.V. Preparation of pickering-emulsion-based capsules with shells composed of titanium dioxide nanoparticles and polyelectrolyte layers. *Colloid J.* **2017**, *79*, 198–203. [CrossRef]
13. Mori, Y.; Okastu, Y.; Tsujimoto, Y. Titanium dioxide nanoparticles produced in water-in-oil emulsion. *J. Nanopart. Res.* **2001**, *3*, 219–225. [CrossRef]
14. Shimooka, H.; Yamamoto, T.; Takahashi, S.; Kohiki, S. Synthesis of free-standing crystalline barium titanate films at vapor/liquid or liquid/liquid interface. *J. Sol-Gel Sci. Technol.* **2000**, *19*, 749–752. [CrossRef]
15. Tominaga, Y.; Kadota, K.; Shimosaka, A.; Yoshida, M.; Oshima, K.; Shirakawa, Y. The preparation and the sustained release of titanium dioxide hollow particles encapsulating L-ascorbic acid. *J. Cryst. Growth* **2018**, *490*, 11–18. [CrossRef]
16. Poltorak, L.; Herzog, G.; Walcarius, A. In-situ formation of mesoporous silica films controlled by ion transfer voltammetry at the polarized liquid–liquid interface. *Electrochem. Commun.* **2013**, *37*, 76–79. [CrossRef]
17. Kowalewska, K.; Sipa, K.; Leniart, A.; Skrzypek, S.; Poltorak, L. Electrochemistry at the liquid–liquid interface rediscovers interfacial polycondensation of nylon-6,6. *Electrochem. Commun.* **2020**, *115*, 106732. [CrossRef]
18. Poltorak, L.; Morakchi, K.; Herzog, G.; Walcarius, A. Electrochemical characterization of liquid-liquid micro-interfaces modified with mesoporous silica. *Electrochim. Acta* **2015**, *179*, 9–15. [CrossRef]
19. Kadota, K.; Tamura, H.; Shirakawa, Y.; Tozuka, Y.; Shimosaka, A.; Hidaka, J. Interfacial sol–gel processing for preparation of porous titania particles using a piezoelectric inkjet nozzle. *Chem. Eng. Res. Des.* **2014**, *92*, 2461–2469. [CrossRef]
20. Nakashima, T.; Kimizuka, N. Interfacial synthesis of hollow TiO_2 microspheres in ionic liquids. *J. Am. Chem. Soc.* **2003**, *125*, 6386–6387. [CrossRef]
21. Honda, H.; Suzaki, K.; Sugahara, Y. Control of hydrolysis and condensation reactions of titanium tert-butoxide by chemical modification with catechol. *J. Sol-Gel Sci. Technol.* **2001**, *22*, 133–138. [CrossRef]
22. Harris, M.T.; Singhal, A.; Look, J.L.; Smith-Kristensen, J.R.; Lin, J.S.; Toth, L.M. FTIR Spectroscopy, SAXS and Electrical Conductivity Studies of the Hydrolysis and Condensation of Zirconium and Titanium Alkoxides. *J. Sol-Gel Sci. Technol.* **1997**, *8*, 41–47. [CrossRef]
23. Samec, Z. Electrochemistry at the interface between two immiscible electrolyte solutions (IUPAC technical report). *Pure Appl. Chem.* **2004**, *76*, 2147–2180. [CrossRef]
24. Chorny, I.; Benjamin, I. Hydration shell exchange dynamics during ion transfer across the liquid/liquid interface. *J. Phys. Chem. B* **2005**, *109*, 16455–16462. [CrossRef] [PubMed]
25. Osakai, T.; Ebina, K. Non-Bornian theory of the Gibbs energy of ion transfer between two immiscible liquids. *J. Phys. Chem. B* **1998**, *102*, 5691–5698. [CrossRef]
26. Murakami, W.; Eda, K.; Yamamoto, M.; Osakai, T. A revisit to the non-Bornian theory of the Gibbs energy of ion transfer between two immiscible liquids. *J. Electroanal. Chem.* **2013**, *704*, 38–43. [CrossRef]
27. Benjamin, I. Mechanism and dynamics of ion transfer across a liquid-liquid interface. *Science* **1993**, *261*, 1558–1560. [CrossRef] [PubMed]
28. Sánchez, C.; Leiva, E.; Dassie, S.A.; Baruzzi, A.M. Some Theoretical Considerations Concerning Ion Hydration in the Case of Ion Transfer between Water and 1,2-Dichloroethane. *Bull. Chem. Soc. Jpn.* **1998**, *71*, 549–554. [CrossRef]
29. Dryfe, R.A.W.; Hirunpinyopas, W.; Rodgers, A.; Worrall, S.; Bissett, M. Hydrogen Evolution at Liquid | Liquid interfaces catalysed by 2D materials. *ChemNanoMat* **2017**, *3*, 428–435. [CrossRef]
30. Montheil, T.; Echalier, C.; Martinez, J.; Subra, G.; Mehdi, A. Inorganic polymerization: An attractive route to biocompatible hybrid hydrogels. *J. Mater. Chem. B* **2018**, *6*, 3434–3448. [CrossRef]
31. Su, C.; Hong, B.Y.; Tseng, C.M. Sol-gel preparation and photocatalysis of titanium dioxide. *Catal. Today* **2004**, *96*, 119–126. [CrossRef]

32. Cheng, H.H.; Chen, S.S.; Yang, S.Y.; Liu, H.M.; Lin, K.S. Sol-Gel hydrothermal synthesis and visible light photocatalytic degradation performance of Fe/N codoped TiO_2 catalysts. *Materials* **2018**, *11*, 939. [CrossRef] [PubMed]
33. León, A.; Reuquen, P.; Garín, C.; Segura, R.; Vargas, P.; Zapata, P.; Orihuela, P.A. FTIR and raman characterization of TiO_2 nanoparticles coated with polyethylene glycol as carrier for 2-methoxyestradiol. *Appl. Sci.* **2017**, *7*, 49. [CrossRef]

ChemElectroChem

Research Article
doi.org/10.1002/celc.202200435

Chemistry Europe
European Chemical Societies Publishing

www.chemelectrochem.org

Special Collection

Interfacial Synthesis of Nylon-6,6 and Its Modification with Silver-Based Nanoparticles at the Electrified Liquid-Liquid Interface

Karolina Kowalewska, Karolina Sipa, Katarzyna Kaczmarek, Sławomira Skrzypek, and Lukasz Poltorak*[a]

In this work, the synthesis of Nylon-6.6 together with silver nanoparticles (presumably Ag_2O, Ag NPs) was carried out at a polarized liquid-liquid interface (LLI). The reduction of silver ions to Ag-NPs was driven by an electrochemically controlled electron transfer reaction between silver cations initially dissolved in the aqueous phase and ferrocene species present in the organic phase. The formation of Ag_2O is assumed to originate from Ag^+ precipitation to AgOH further converted into Ag_2O. The polyamide formation was derived from the interfacial polycondensation reaction happening between 1,6-diaminohexane and adipoyl chloride. We studied the possibility to form given material simultaneously (interfacial polycondensation and Ag^+ reduction occurring in one step) and sequentially (electrochemical Ag^+ reduction by ferrocene from the organic phase was performed after polyamide deposition). The Ag-based NPs-polyamide material was synthesized at the macroscopic and microscopic LLI. As the support for the latter, fiberglass membranes was used. The resulting material was characterized by infra-red (IR) spectroscopy and scanning electron microscopy (SEM).

Introduction

Electrochemistry at the polarized liquid-liquid interface (LLI), also known as the interface between two immiscible electrolyte solutions (ITIES), allows the study of interfacial charge transfer reactions in the form of ions or electrons crossing soft junctions.[1,2] The defect-free ITIES system is self-healing, renewable, discontinuous, and also modifiable.[3] LLI takes the shape of the support and thanks to its asymmetric properties it can separate the chemical species based on their affinity to adjacent phases. ITIES based systems can be studied with all available electrochemical techniques.[2,4,5] One of the possible directions further exploring these unique systems is the interfacial synthesis of materials. LLI should be used to explore new possibilities allowing the interfacial materials synthesis. When combined with the electrochemical polarization, not only we can control the polycondensation reactions but also further modify the interface with other objects brining desired functionality. Finally, due to asymmetric properties of the biphasic junction we can obtain Janus materials that are very difficult or even impossible to prepare in monophasic systems.

The LLI can exist in different sizes, as defined by Liu et al., the nano-, micro-, and macroscopic scales.[6] The latter can be referred to as a conventional system having at least several millimeters in diameter (e.g. conventional voltammetric cell with two Luggin capillaries defining the position of the soft junction). LLI miniaturization can be achieved with appropriate support (e.g. in a form of membranes or capillaries) or adequate processing (e.g. intensive mixing). The membranes used to create nano- or micro-interfaces are usually made out of patterned supports or materials displaying intrinsic porosity.[7] Single pore ITIES can be prepared from pulled glass capillaries,[8] a pore formed in a glass pipette after dissolving a metal wire embedded within the glass casing,[9] or fused silica microcapillaries.[3] Miniaturized liquid boundaries provide additional stability to the LLI whereas the solid surrounding of the soft junction may serve as the support for the interfacially formed deposits.

The modification of the LLI can be carried out either in-situ or ex-situ. According to the first methodology, the preformed modifier is added to one phase followed by its precipitation at or adsorption to the soft junction. This approach was used to decorate the LLI with a variety of objects such as metallic nanoparticles,[10] carbon nanotubes,[11] silica spheres[12] etc. The in situ modification is derived from the interfacial ion or electron transfer triggering the reaction(s) whose product(s) resided within the interfacial region in a form of solid/soft deposits.[13] In this respect, metallic nanoparticles can be formed within the interface originating from the cationic precursor reduction (initially dissolved in the aqueous phase) by the organic phase soluble electron donor (usually ferrocene and its derivatives).[14–17] Another example is electrochemically controlled interfacial polymerization either derived from the electron[18–21] or ion transfer reaction.[22] Sol-gel processing in a biphasic environment can also be studied or controlled using electroanalytical techniques.[23–26] The modification following ex-

[a] K. Kowalewska, Dr. K. Sipa, K. Kaczmarek, Prof. S. Skrzypek, Dr. L. Poltorak
Department of Inorganic and Analytical Chemistry
Electroanalysis and Electrochemistry Group,
Faculty of Chemistry
University of Lodz
Tamka 12, 91-403 Lodz, Poland
E-mail: lukasz.poltorak@chemia.uni.lodz.pl

Supporting information for this article is available on the WWW under https://doi.org/10.1002/celc.202200435

Special Collection An invited contribution to the Hubert Girault Festschrift.

situ methodology is based on the pre-formed objects or molecular assemblies (metallic particles, carbon-based materials, proteins, surface-active species) that adsorb to the LLI.[11,27–31] Such assemblies found applications in heterogeneous electrocatalysis (especially when metallic nanoparticles are used)[32] and for biomimetic studies (e.g. interfacial behavior of proteins).[33–36]

In this work, for the first time, we have studied the in-situ LLI modification with nylon-6,6 and Ag-based NPs. Interfacial polycondensation of the polyamide was based on our previously reported work whereas the Ag-based NPs were obtained via heterogeneous and electrochemically controlled reduction of Ag-complex (formed in the presence of 1,6-diaminohexane) initially dissolved in the aqueous phase by the electron-donating ferrocene species dissolved in the organic phase and probably chemical reactions (formation of AgOH and Ag_2O) expected to occur at pH = 11. The interfacial formation of both materials (nylon-6,6 and Ag-based NPs) followed two processing methodologies: (i) Ag-based NPs deposition during polyamide formation and (ii) Ag-based NPs deposition after the initial deposition of a polyamide film. The developed material was initially formed at the macroscopic and planar LLI. Further utilization of the soft junction support in the form of the fiberglass membrane facilitated the obtained material processing. Our platform was investigated with cyclic voltammetry, scanning electron microscopy, and infra-red spectroscopy. The aim of this work is to define the possibility to control electrochemically the interfacial polycondensation reactions aiming at the formation of polyamide materials further modified with functional objects (Ag-base NPs display antibacterial properties).

Experimental Section

Chemicals and materials

Sodium sulfate (Na_2SO_4, anhydrous, for analysis, POCh) was used to prepare an aqueous phase at pH = 11. The pH was adjusted with 0.1 M sodium hydroxide (NaOH, for analysis, ChemPur). 1,6-diaminohexane (1,6-DAH, ≥99.5%, Acros Organics), adipoyl chloride (AC, 98%, Alfa Aesar), silver nitrate ($AgNO_3$, ≥99.8%, Fisher Chemical), sodium nitrate ($NaNO_3$, for analysis, ChemPur) and ferrocene (Fc, 98%, Acros Organics) were used as received. The organic phase electrolyte $BTPPA^+TPBCl^-$ (Bis(triphenylphosphoranylidiene)ammonium tetrakis(4-chlorophenylborate)) was synthesized using bis(triphenylphosphoranylidene)ammonium chloride ($BTPPA^+Cl^-$, 97%, Sigma-Aldrich) and potassium tetrakis(4-chlorophenyl)borate ($KTPB^+Cl^-$, ≥98%, Sigma-Aldrich) via methatesis reaction. The organic phase was prepared by dissolving a proper amount of $BTPPA^+TPBCl^-$ in 1,2-dichloroethane (1,2-DCE, for analysis, POCH,). Fiberglass membranes (glass microfiber discs, diameter: 47.0 mm, thickness: 0.2 mm, Ahlstrom Munksjo) glued with silicone to glass tubes were used to create miniaturized liquid-liquid interfaces. All experiments were performed using demineralized water (Hydrolab system, Poland).

Electrochemical experiments

Electrochemically controlled synthesis and modification of polyamide material were performed in a macroscopic voltammetric glass cell (interface radii equal to 0.7 cm) equipped with four electrodes: two $Ag/AgSO_4$ reference electrodes and two Pt counter electrodes. The reference electrodes were prepared by applying anodic potential to the silver wire immersed into 1 M H_2SO_4 solution for 5 minutes. The micro-ITIES systems were prepared by cutting a fiberglass membrane using a scalpel knife. This was then attached to a glass tube with silicone sealant. The created system was filled with the organic phase and immersed in the aqueous phase. Electrode configuration was analogical to macroscopic equivalent. The hardware used during our experiments was Autolab 302 N (Metrohm). The plotted cyclic voltammograms are either given as the current in function of the Galvani potential difference ($\Delta\phi$) or the potential applied using the external power supply – potentiostat. For the latter, the x-axis label reads as "Potential / V". Whenever, the $\Delta\phi$ is given, the x-axis were calibrated using the standard Galvani potential of the TMA^+ cation transfer, equal to 160 mV.[5] Other curves are not calibrated due to the lack of a good internal reference potential difference point. A number of interfacial charge transfer reactions happening in the system overlay (additionally due to high concentration of the reagents), and hence, the common practice relaying on model reference ion addition failed. The iR-compensation was not applied during the experiments.

Infrared spectroscopy

Materials synthesized at the ITIES were collected and analyzed with infra-red spectroscopy (Nexus FT-IR by Thermo Nicolet spectrometer) in transmission mode. Before analysis, all samples were mixed with KBr and the pastille was formed.

Scanning electron microscopy

The scanning electron microscopy (SEM, a Phenom G2 Pure, FEI Company, the Netherlands) was used to examine the surfaces of bare and modified polyamide material extracted from macroscopic cells or being a part of microporous fiberglass membranes used as an ITIES support. During analysis, the samples were fixed on an SEM pin stub using copper tape. SEM images were acquired at a magnification of 250–2500x using a high-sensitivity backscattered electron detector operating at an accelerating voltage of 5 kV.

Result and Discussion

Figure 1a shows the macroscopic cell used during ITIES modification with polyamide film and polyamide film decorated with Ag NPs. On either scale (macroscopic and microscopic), ITIES was polarized using a four-electrode configuration with two platinum counter electrodes one placed in the aqueous and the second in the organic phase. Hydrophilic background electrolyte (Na_2SO_4), $AgNO_3$, and/or diamine were always initially present in the aqueous phase whereas the organic phase was a solution of hydrophobic salt (BTPPATPBCl), adipoyl chloride, and/or ferrocene. In such a configuration we can distinguish a few major reactions governing the interfacial formation of studied deposits. Figure 1b indicates simple ion transfer reactions of Ag^+ and NO_3^- which can be recorded within the available voltammetric potential window. Positive currents will

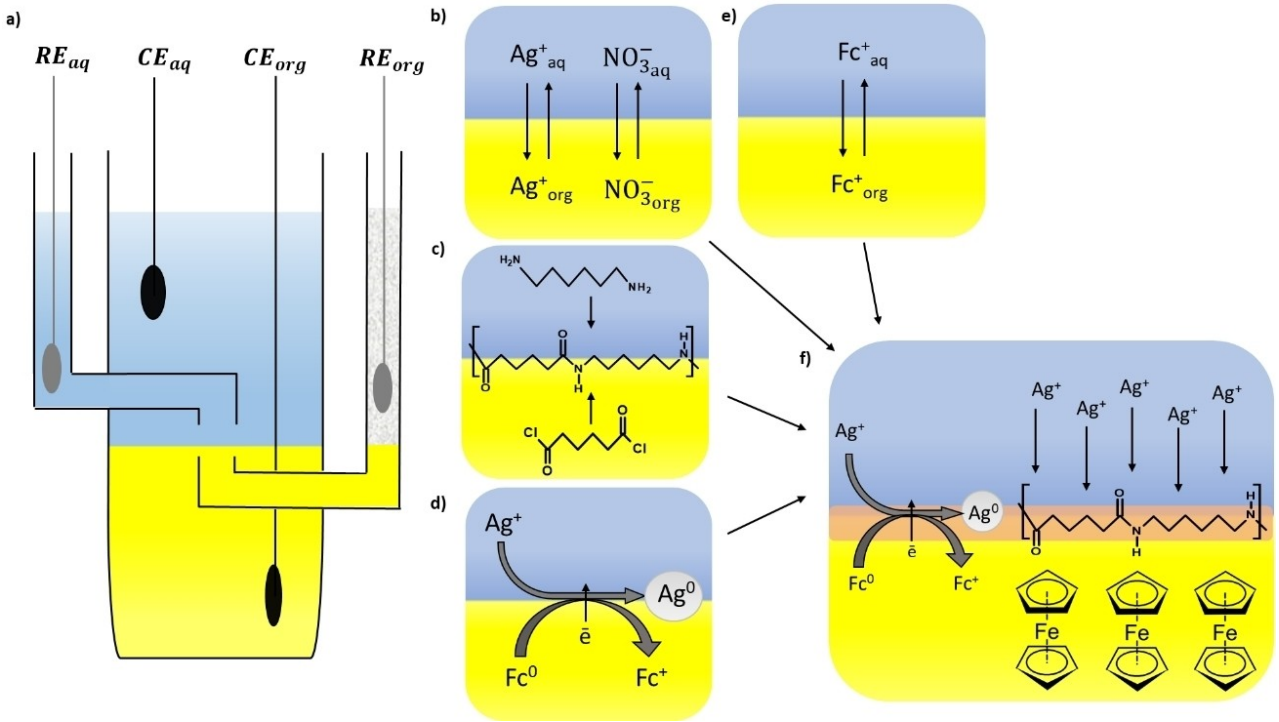

Figure 1. Scheme showing four-electrode electrochemical cell (a) used for the simultaneous deposition of Ag NPs and polyamide film (RE-reference electrode; CE–counter electrode; aq-the aqueous phase; org-the organic phase). Reactions happening in the cell during interfacial modification: simple ion transfer of Ag^+ and NO_3^- happening across the LLI (b); interfacial polycondensation happening between 1,6-DAH and AC resulting in the polyamide formation (c); interfacial electron transfer reaction from the organic phase to the aqueous phase originating from the reduction of Ag^+ to metallic Ag and ferrocene (Fc) oxidation to ferrocenium cations (Fc^+) (d); simple ion transfer of Fc^+ across the LLI (e). Scheme summarizing key interfacial charge transfer reaction leading to the formation of a polyamide film decorated with Ag NPs (f).

be defined as the Ag^+ transfer from the aqueous to the organic phase. Although for this cation the scheme (Figure 1b) depicts a simple ion transfer reaction, Sherburn et al. have found that the interfacial transfer of Ag^+ is affected by the nature of the organic phase background electrolyte anion shifting its Galvani potential of ion transfer from −0.01 V for tetraphenylborate anion to 0.17 V for tetrakis(4-chlorophenyl)borate.[37] This indicates that the interfacial transfer of Ag^+ is additionally facilitated by the negatively charged hydrophobic anions dissolved in the organic phase. Transfer of NO_3^- ($\Delta^{aq}_{org}\phi'_{NO_3^-} = -0.351\ V$)[5] from the aqueous to the organic phase will be recorded as the negative current. The interfacial polycondensation of two monomers, 1,6-DAH from the aqueous phase and AC from the organic phase is shown in Figure 1c. Previously, we have shown that at an appropriate pH value assuring the existence of 1,6-DAH in a partially protonated form we can introduce the electrochemically controlled step during interfacial polyamide formation. We have concluded that the partially protonated 1,6-DAH undergoing transfer from the aqueous to the organic phase can react with the acyl chloride group of the AC. Under such conditions, the resulting polyamide film formation was accelerated.[38] Figure 1d schematically depicts the interfacial electron transfer reaction between ferrocene (Fc) species from the organic phase and Ag^+ cations dissolved in the aqueous phase. Once the appropriate Galvani potential difference is applied to the ITIES the electron-donating Fc is being oxidized to ferrocenium cation (Fc^+) whereas Ag^+ is reduced to Ag^0 which resides at the ITIES in a form of Ag NPs. Interfacial reduction of Ag^+ to Ag^0 can be achieved with other electron donating hydrophobic reducing chemical species (e.g. ferrocene derivatives[39] or N-phenylpyrrole[40]). Finally, as shown in Figure 1e, Fc^+ formed during Ag NPs formation is also interfacially active and can be transferred from the organic to the aqueous phase below its $\Delta^{aq}_{org}\phi'_{Fc^+}$ which was reported to be 0.041 V.[41] Consequently, when all reagents needed to form polyamide film decorated with Ag NPs are present in biphasic system a number of mutually interconnected reactions may occur as shown in Figure 1f.

Figure 2A shows cyclic voltammograms (CVs) recorded before and after addition of $AgNO_3$ to the aqueous phase (pH = 7) at concentration equal to 100 μM. The series of CVs recorded at different [$AgNO_3$] are available as Figure S1A. In the absence of $AgNO_3$ in the aqueous phase, the available potential window was limited by the Na^+ transfer from the aqueous to the organic phase ($\Delta^{aq}_{org}\phi^0_{Na^+} = 0.591$ V; positive current on the more positive potential side)[5] and SO_4^{2-} transfer from the aqueous to the organic phase ($\Delta^{aq}_{org}\phi^0_{SO_4^{2-}}$ = f–0.509 V; negative current on the less positive potential side)[42] – see the red curve on Figure 2A. We have used Ag/Ag_2SO_4 as the aqueous phase

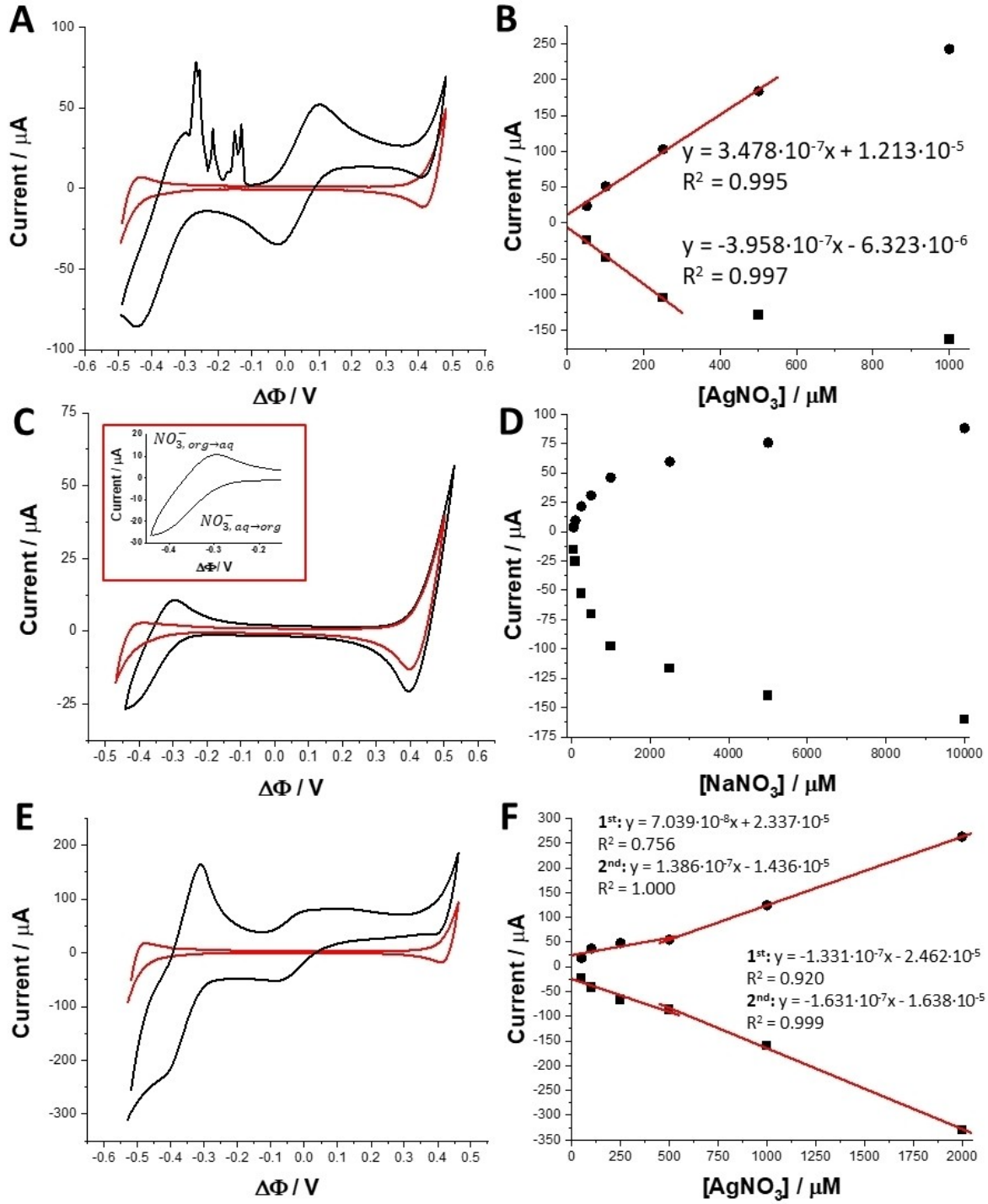

Figure 2. Cyclic voltammograms (A, C, E) recorded at different compositions of the aqueous and the organic phase. The aqueous phase (A): 10 mM Na_2SO_4 (pH = 7) with $[AgNO_3]$ = 100 μM; the organic phase: 5 mM BTPPATPBCl in 1,2-DCE. The aqueous phase (C): 10 mM Na_2SO_4 (pH = 7) with $[NaNO_3]$ from 100 μM; the organic phase: 5 mM BTPPATPBCl in 1,2-DCE. Inset: $[NaNO_3]$ = 100 μM. All CVs were recorded at 20 $mV \cdot s^{-1}$. The aqueous phase (E): 10 mM Na_2SO_4 (pH = 7) with $[AgNO_3]$ = 500 μM; the organic phase: 10 mM Fc and 5 mM BTPPATPBCl in 1,2-DCE. Calibration curve (B) plotted based on CVs from section A for the signals corresponding to Ag^+ transfer (from −0.1 till 0.3 V). Calibrations curves (D) plotted based on CVs from section C for the limiting current on the less positive potential window side. Calibration curves (F) plotted based on CVs from section E for the signals recorded in the range from −0.2 till 0.2 V.

reference electrodes[43] immersed into Na_2SO_4 solution. This was possible as we did not observe any precipitation of the Ag_2SO_4 since the concentration of used reagents were always below its molar solubility ($K_{sp} = 1.2 \cdot 10^{-5}$).[43] The presence of Ag^+ and NO_3^- in the aqueous phase resulted in the appearance of two extra pairs of signals. The negative end of the potential window was attributed to NO_3^- transfer as further confirmed by the increasing positive and negative currents in the potential range

from −0.5 to −0.1 V recorded for the increasing concentration of $NaNO_3$ added to the aqueous phase (see Figure 2C,D and Figure S1B from supporting information). Figure 2B shows the positive and negative peak current attributed to the Ag^+ interfacial transfer plotted in function of the $AgNO_3$ concentration. Obtained dependency deviates from the linear calibration curve expected for the simple ion transfer reaction. The ratio of the slopes for the first three studied concentrations obtained for the positive ($3.478 \cdot 10^{-7}$ A·M^{-1}) and negative ($-3.958 \cdot 10^{-7}$ A·M^{-1}) signals is equal to 0.88 which deviates from unity expected for fully reversible reaction. These observations are in line with what was reported by Sherburn et al. who indicated that Ag^+ transfer across the LLI is additionally facilitated by the organic phase background electrolyte salt anion–here $TPBCl^-$.[37] Occasionally, we were also recording current spikes (see negative potential ranges in Figure 2A and Figure S1A,B) characteristic for the phenomena studied by the group of Kakiuchi – electrochemical instability.[44,45] Most probably, the applied negative potentials are enough to trigger interfacial emulsification. Formed droplets of either aqueous phase containing background electrolyte ions or loaded organic phase release the cargo upon the collision with the eLLI followed by interfacial fusion.[46]

The interesting appearance of the recorded voltammetric curves was obtained when the organic phase composition was enriched by 10 mM Fc–see Figure 2E. Here, the CVs were recorded in the presence and the absence of $AgNO_3$. CVs recorded for the increasing concertation of $AgNO_3$ in the presence of Fc in the organic phase are available as Figure S1C. First pair of peaks with the $\Delta^{aq}_{org}\phi_{1/2}$ being equal to around −0.35 V was attributed to the transfer of NO_3^-. The negative signal with a peak maximum at −0.44 V (recorded at [$AgNO_3$] = 500 μM) is due to NO_3^- transfer from the aqueous to the organic phase.

Signals with $\Delta^{aq}_{org}\phi_{1/2}$ at around −0.05 V are complex and the governing currents are a mixture of a few processes, this is Ag^+ interfacial transfer [Eq. (1)], heterogenous electron transfer between Fc and Ag^+ [Eq. (2)], and the interfacial transfer of Fc^+ [Eq. (3)] and charge balancing anion [Eq. (4)] ; signals recorded below −0.15 V):[47]

$$Ag^+_{aq} \rightleftarrows Ag^+_{org} \quad (1)$$

$$Fc_{org} + Ag^+_{aq} + NO^-_{3,\,aq} \rightarrow Fc^+_{org} + Ag^0_{LLI} + NO^-_{3,\,org} \quad (2)$$

$$Fc^+_{org} \rightleftarrows Fc^+_{aq} \quad (3)$$

$$NO^-_{3,\,aq} \rightleftarrows NO^-_{3,\,org} \quad (4)$$

Reactions 1 and 2 [Eq. (1) and (2)] can be observed as the elongated positive peak (see Figure 2E) being a mixture of a current originating from the interfacial Ag^+ reduction (first signal forming a clear peak at 0 V), and Ag^+ transfer to the organic phase (shoulder of the positive signal that can be noticed in the potential difference range from 0.1 V till 0.3 V) where it can also be reduced to Ag^0 [Eq. (5) and (6)]. Also, the reduction of Ag^+ to metallic Ag^0 is associated with the formation of interfacially active Fc^+ that may give additional ionic current features [Eq. (3)] that are expected to occur at around $\Delta^{aq}_{org}\phi'_{Fc^+} = -0.016$ V.[48] Even in the absence of $AgNO_3$, the signal with a small intensity was observed at around 0 V which corresponds to the Fc^+ transfer formed upon spontaneous oxidation (the aqueous phase was not deprived from the oxygen during the experiments).[49–51]

$$Fc_{org} + Ag^+_{org} \rightarrow Fc^+_{aq} + Ag^0_{LLI} \quad (5)$$

$$Fc_{org} + Ag^+_{org} + NO^-_{3,\,aq} \rightarrow Fc^+_{org} + Ag^0_{LLI} + NO^-_{3,\,org} \quad (6)$$

The recorded positive signal (Figure 2E or Figure S1C) with a peak position at 0.05 V is shifted by around 100 mV to the lower potential difference values as compared with a positive peak from Figure 2A attributed to the Ag^+ transfer from the aqueous to the organic phase. This further confirms that the origin of the signals found within the range from −0.2 V to 0.2 V origin from a mixture of electron and ion transfer processes. Figure 2F shows the positive and negative peak currents plotted in function of the added $AgNO_3$ for the signals located at 0 V and −0.1 V, respectively. For fixed Fc concentration in the organic phase, and increasing $AgNO_3$ concentration added to the aqueous phase we have observed two linear dynamic ranges, first up to 500 μM and the second up to the last studied concentration point equal to 2 mM. According to our understanding, for the high Fc excess over Ag^+ the interfacial charge transfer reactions happening within the concerned potential range are mainly governed by the electron transfer between Fc and Ag^+, and Fc^+ crossing the interface. The ratio of the positive (0.704 A·M^{-1}) and negative (1.331 A·M^{-1}) slope for the first linear range is equal to 0.5 indicating that more charge is carried on the reverse voltammetry scanning. From [$AgNO_3$] = 500 μM we started observing second linear dynamic range that was attributed to the increasing fraction of current carried by the Ag^+ transfer either from the aqueous to the organic phase or from the organic to the aqueous phase. Also, we cannot exclude the possibility to reduce Ag^+ within the interfacial region on the organic phase side of the liquid-liquid interface by Fc species, as above $\Delta^{aq}_{org}\phi_{Ag^+}$ it will start partitioning to the organic phase (eq. 6). Figure S2 (see electronic supporting information) shows a photo of the macroscopic cell taken after voltammetric cycling displaying a LLI with a clearly visible thick film presumably being made of Ag NPs. We have also set a control experiments (see photos from Figure S2), where the flask was filled with the 5 mM $AgNO_3$ and 10 mM Na_2SO_4 (pH = 7) as the aqueous phase and the 10 mM Fc and 5 mM BTPPATPBCl as the organic phase. Already after 5 minutes we started noticing the formation of the precipitate within the interfacial region indicating that the Galvani potential difference of the formed LLI (open circuit potential) is sufficient to drive Ag^+ reduction by Fc from the organic phase.

In our previous work, we have shown that interfacial polycondensation of polyamide derived from the reaction between 1,6-DAH and AC can be studied and controlled at the ITIES.[38] Figure 3A shows the cyclic voltammograms recorded in the presence of 1,6-DAH added to the aqueous phase in the

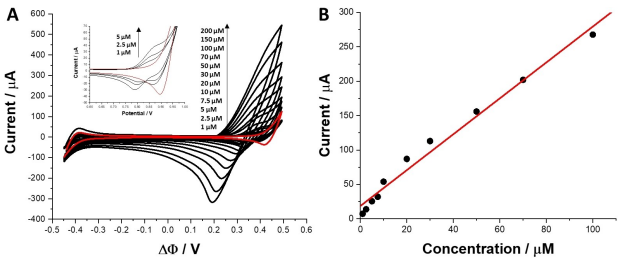

Figure 3. Ion transfer voltammograms (A) that were recorded for the increasing concentration of 1,6-DAH (1–200 µm) added to the aqueous phase (10 mM Na_2SO_4; pH = 11). The scan rate was 20 mV·s^{-1}. Calibration curve (B) plotted for the positive current signal corresponding to the transfer of 1,6-DAH from the aqueous to the organic phase.

concentration range from 1 to 200 µM. Background subtracted curves are additionally presented as Figure S3 (see electronic supporting information). At pH = 11, the ratio of monoprotonated (1,6-DAH$^+$) and doubly protonated (1,6-DAH^{2+}) diamines is 1:1 (pK_{a1} = 10.8 and pK_{a2} = 11.9).[38,52] This means that the currents making the signals at $\Delta^{aq}_{org}\phi_{1/2}$ = 0.35 V are governed by 1,6-DAH$^+$ and 1,6-DAH^{2+} transferring from the aqueous to the organic phase (positive currents) and due to their back transfer (negative currents). Linear increase of the positive peak current plotted in function of the increasing diamine concertation further confirms this behaviour. We have also recorded the cyclic voltammogram in the presence of the background electrolytes and 10 mM AC added to the organic phase (see Figure S5 from electronic supporting information). No additional signals were recorded within the available potential window. The interfacial reaction between acyl chloride and water molecules leading to the formation of carboxylic groups cannot be excluded. The formation of adipic acid, its partitioning to the aqueous phase where it should exists in the hydrolysed form was not observed during our experiments.

After individual study of all components needed to form polyamide film decorated with Ag-based NPs (at pH higher than 7 we cannot exclude the formation of silver hydroxide and silver oxide) the logical step was to formulate the ITIES composed of all needed reagents. Figure 4 shows CVs recorded under different composition of the organic and the aqueous phase. The pH of the later was set to be 11. The major chemical variable of the organic phase was the presence or the absence of 10 mM Fc, whereas for the aqueous phase it was the concentration of 1,6-DAH (either 5 or 10 mM) and the presence of $AgNO_3$. Interestingly, in the presence of 1,6-DAH we did not observe the formation of white or yellow precipitate being AgOH [Eq. (7)] or Ag_2O [Eq. (8)], respectively, indicating that silver can be dissolved in the alkaline media at given pH and the aqueous phase composition.

$$Ag^+ + OH^- \rightarrow AgOH\downarrow \quad (7)$$

$$2AgOH \rightarrow Ag_2O\downarrow + H_2O \quad (8)$$

According to the literature survey at relatively high pH and in the presence of compounds holding primary amine groups (in our case 1,6-DAH), AgOH can either dissolve to form silver hydroxy complexes-$Ag(OH)_j^{(j-1)-}$ [53] or can be stabilized in a form of Ag^+ – amine based complex [Eq. (9)].

$$Ag^+ + H_2N(CH_2)_6NH_2 \rightleftarrows Ag[H_2N(CH_2)_6NH_2]_2^+ \quad (9)$$

The dashed blue curve from Figure 4A was recorded in the presence of 5 mM 1,6-DAH at pH = 11. The transfer of 1,6-DAH is manifested as a broad signal limiting the potential window on the more positive potential difference side. Further addition of 10 mM Fc to the organic phase and 2 mM $AgNO_3$ to the aqueous phase resulted in the appearance of the additional signal shortening the potential window on the less positive potential side. This is attributed to the interfacial transfer of NO_3^- anions. To our surprise, the intensity of either positive or negative currents for E > 0.65 V and E = 0.57 V, respectively, in the presence or absence of Ag containing ions (in a form of hydroxy complexes or a complex formed with 1,6-DAH) in the aqueous phase and Fc species in the organic phase remained

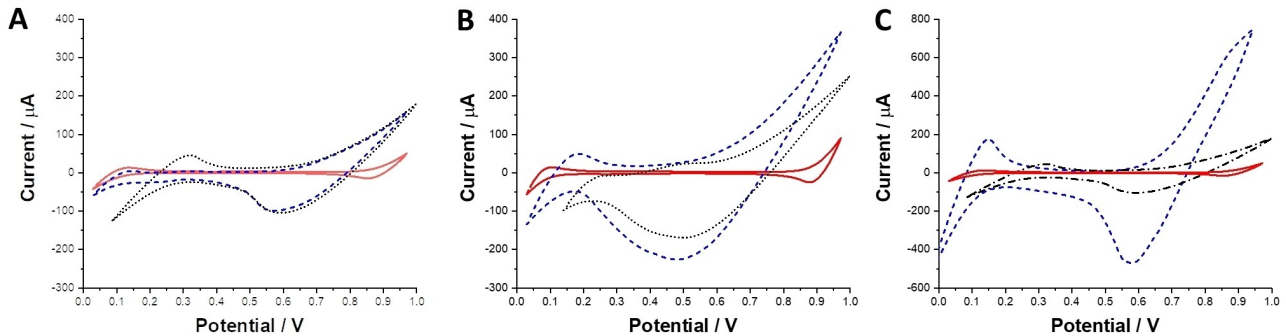

Figure 4. CVs recorded at ITIES under different experimental conditions which are depicted as cell I, II and III. In each section (A, B and C) red solid line corresponds to the cell I. CVs marked as blue dashed line were recorded in cell II with x = 5 mM and y = 0 mM for A; x = 10 mM and y = 0 mM for B; and x = 5 mM and y = 2 mM for C. CVs marked as black dotted line were recorded in cell II for z = 5 mM and h = 2 mM for A; z = 10 mM and h = 2 mM for B; and z = 5 mM and h = 2 mM for C. Scan rate was

nearly unaffected. We were expecting to observe additional fraction of current carried by charge transfer reactions discussed above and related to Ag-complex and Fc^+ ion transfer, and Ag-complex reduction. Even more surprising are the data plotted in Figure 4B with the only difference as comparted with the previously discussed data set (Figure 4A) being the increased concertation of 1,6-DAH (from 5 mM to 10 mM). First of all, the limiting current on the more positive side of the potential window increased from around 200 μA to 400 μA as the concentration of 1,6-DAH was doubled (see blue, dashed curve in Figure 4B). Addition of 10 mM Fc to the organic phase and 2 mM $AgNO_3$ to the aqueous phase is marked as the dotted black curve. Again we have noticed NO_3^- transfer on the less positive potential side shortening the available potential window, dropping current on the more positive potential side and a small signal recorded at around $E = 0.45$ V. The latter can be attributed to either electron transfer reaction related to Ag^+-complex reduction or Fc^+ interfacial transfer formed during the Ag-based NPs formation. Counter intuitive is the drop of the current recorded at $E > 0.6$ V or the drop of the negative peak with the centre at around 0.45 V. Initially we thought that the polyamide film makes a physical boundary which inhibits the transfer of small ions across the ITIES and even, function as a spacer between Ag^+-complexes and electron donating Fc, which in consequence do not contribute to recorded currents. To further verify this hypothesis, we have added the $AgNO_3$ to the aqueous in the absence of Fc in the organic phase. Obtained results are shown in Figure 4C as blue dashed curve. Here the concentrations of 1,6-DAH in the aqueous phase and AC in the organic phase were kept constant and were equal to 5 mM. Under such conditions, we are able to form compact polyamide film. Obtained positive signal recorded from 0.5 V to 0.9 V reaches nearly 800 μA and is 4 times higher as compared with the blue dashed curve from Figure 4A recorded for the same conditions with the only exception being a lack of $AgNO_3$. This clearly means that Ag^+-complexes can transfer across the ITIES modified with polyamide film. After Fc addition to the organic phase the currents on the more positive side of the potential window drops (see dotted black line in Figure 4C) by around 200%. We think that this behaviour is related to the formation of Ag-based NPs within the pinholes of the polyamide film that further inhibit charge transfer reactions across the ITIES. Also, at given pH of the aqueous phase forming polyamide film may be terminated with positively charged primary amine groups which do not react with acyl chloride functionalities of AC. As such, the electrostatic repulsion of positively charged Ag-complex and Fc^+ is possible.

We have adopted two methodologies allowing the voltammetric modification of the macroscopic ITIES with polyamide film and Ag-based NPs. In Figure 5A, the ITIES was modified during 40 consecutively recorded voltammetric scans with all reagents needed to form polyamide film and Ag-based NPs existing in the aqueous (10 mM 1,6-DAH and 2 mM $AgNO_3$) and the organic phase (5 mM AC and 10 mM Fc). In Figure 5B, during first 40 scans the aqueous phase was deprived from the 2 mM $AgNO_3$. It was added afterwards and 15 more cycles were recorded. We refer to two applied methodologies as simultaneous and sequential, respectively. Obtained voltammetric characteristic are similar to the one already described above (see the discussion pertaining to Figure 4). Additionally, as shown in Figure 5A, we have noticed that as we increase the number of voltammetric cycles the width of negative peak increases which may be correlated with the increasing concentration of Fc^+ whose ion transfer currents overlay with all other charge transfer reactions happening in the system. Figure 5C (see also Figure S5 from the electronic supporting information) shows the SEM image recorded for the polyamide film collected from the ITIES composed of the 5 mM organic phase electrolyte (BTPPATPBCl) and 5 mM AC used as the organic phase and 10 mM Na_2SO_4 and 10 mM 1,6-DAH used as the aqueous phase. Under such conditions, the film surface appears to be rather homogenous with craters and wrinkles possibly formed during drying process. The appearance of the polyamide film collected directly after recording voltammetric cycle number 40 is shown in Figure 5A and has changed significantly. Figure 5D and Figure S6 show that the analysed surface is uniformly decorated with particles assigned as Ag-based objects having a size up to a few tens of nm. We tried to record images with higher magnification but due to polyamide surface charging these attempts were not successful. Figure 5E and Figure S7 is the SEM image of a polyamide film prepared via sequential method (Ag NPs formation was done after polyamide film deposition). Here we have found that additional features exiting at the imaged surface were not as homogenous as for the films done according to simultaneous methodology. Figure S8 represents the IR spectra recorded for polyamide, polyamide synthesized in the presence of ferrocene in the organic phase, and polyamide electrochemically decorated with Ag-based NPs. In all cases, the characteristic absorption bands (3305, 2934, 2861, 1640, and 1539 cm^{-1}) typical for polyamide were present.[38,54] Eventual presence of ferrocene in the analysed sample can be confirmed based on absorption signals appearing in the region 1100–800 cm^{-1} due to out-of-plane vibrations of cyclopentadiene and at around 500 cm^{-1} due to asymmetric tensile vibrations of the metal ring. We have noticed that samples synthesized with ferrocene present in the organic phase and in the absence of $AgNO_3$ in the aqueous phase, provided the highest relative intensity of signals in the region of 1200–1000 cm^{-1}. Also, only for these samples we have observed additional signal at 875 cm^{-1}, which has disappeared in the presence of Ag-based NPs. Since all films formed at the macroscopic ITIES were collected with a rather crude method based on grabbing the deposit with tweezers, we had difficulties in defining the side of the film (either contacting the aqueous or the organic phase), and judging how the process of removing film from the liquid-liquid interface affects its appearance. Proposed workaround is based on using a membrane serving as a support for both, ITIES and formed deposits. In this respect, we have used the fiberglass membrane that was attached to the glass tube with a sealant (see Figure S9 for details). In this configuration, the organic phase was always in the upper compartment, as such, counteracting possible deposition originating from the sedimentation of the silver oxide particles formed in the volume of the aqueous phase.

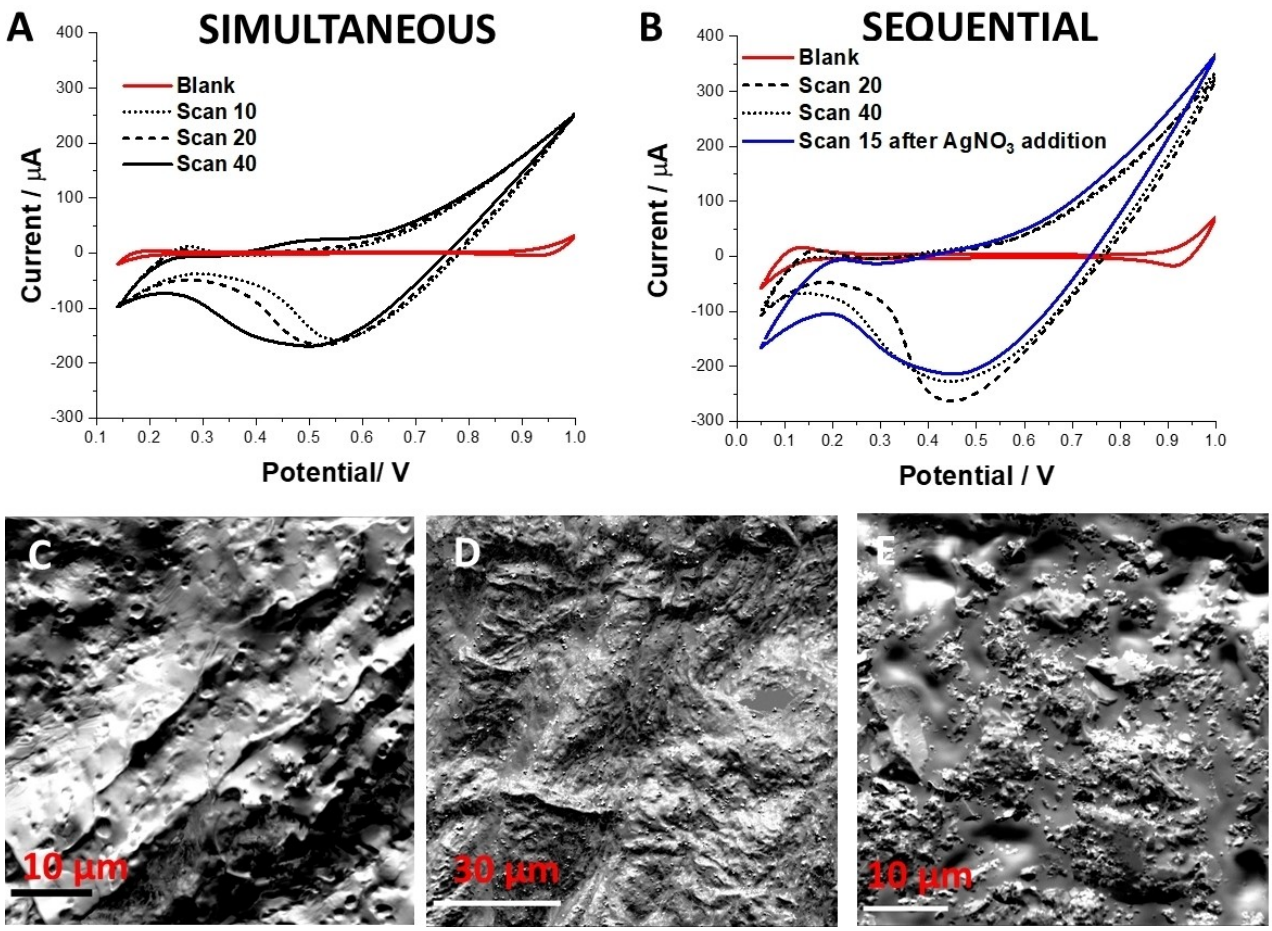

Figure 5. CVs recorded during LLI modification with polyamide and Ag-based NPs through simultaneous (A, Ag-complex reduction during interfacial polycondensation of polyamide film), and sequential (B, interfacial Ag-complex reduction after polyamide film formation) methodology. Red solid line is a blank recorded in cell I (see Figure 4). Other curves correspond to consecutively recorded CVs (see legend for details). The aqueous phase: 10 mM Na_2SO_4 (pH = 11) with 10 mM 1,6-DAH and 2 mM $AgNO_3$ (added before for A and after for B polyamide film formation). The organic phase: 5 mM BTPPATPBCl with 5 mM AC and 10 mM Fc in 1,2-DCE. Scan rate was 20 $mV \cdot s^{-1}$. SEM micrographs recorded for the polyamide film alone (C), polyamide film decorated with Ag NPs using "simultaneous" methodology (D), and polyamide film decorated with Ag NPs using "sequential" methodology.

Again, in the presence of the 1,6-DAH at pH 11 the addition of $AgNO_3$ to the aqueous phase resulted in faint white colour appearance rapidly dissolving after stirring.

In Figure 6 we have plotted the CVs recorded during ITIES supported with a fibre glass membrane modification. Once all reagents needed to form a polyamide film and Ag NPs were present in both phases we have recorded shared voltammetric features: (i) increasing capacitive current; (ii) positive; and (iii) negative limiting currents shifting towards lower and higher potential difference values, respectively. After recording appropriate amount of consecutively recoded CVs the fiberglass membrane were collected and analysed with SEM. Figure 6C is the membrane composed of a pressed glass fibres before modification. Figure 6D is a membrane decorated with the polyamide film and Ag NPs collected from the ITIES after recording CVs from Figure 6A. During interfacial modification, the shown side of the membrane was contacting the aqueous phase. The inspection of the membrane surface with a naked eye revealed the presence of grey surface expected for the forming Ag NPs. These can be further visualized as the island-like domain present within the membrane surface decorated with a number of particles (see Figure S10A). The situation has changed completely as we move to the fiberglass membrane modified sequentially. The initially formed polyamide film most probably form a compact layer in between the glass fibres which inhibits the formation of Ag NPs. The frequency of occurrence of the corresponding white spots has dropped from clearly visible aggregates (Figure 6D) to a single and rarely noticeable points distributed among the analysed surface. In future we plan to extend our study focused on electrochemical modification of the interracially formed polyamide film with other nanomaterials. We also plan to investigate the applicability of the form material in textile industry after scaling up the entire platform.

Conclusion

In this work, we studied the possibility to form polyamide film further decorated with Ag NPs at the electrified liquid-liquid interface. Interfacial polycondensation was controlled via parti-

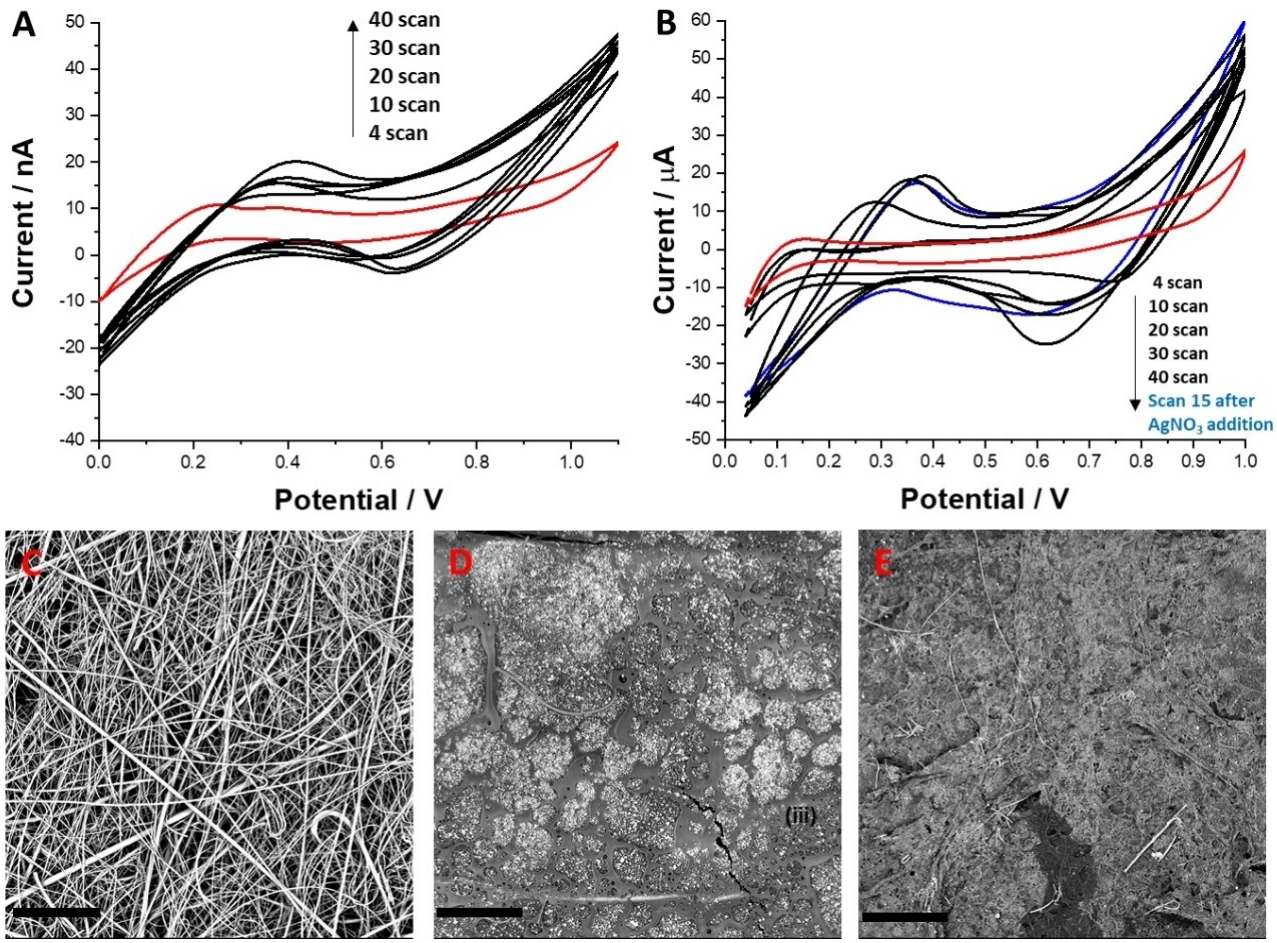

Figure 6. CVs recorded at the ITIES supported with a fiberglass membrane. Simultaneous (A, Ag^+ reduction during interfacial polycondensation of polyamide film), and sequential (B, interfacial Ag^+ reduction after polyamide film formation) methodology. Red solid lines correspond to a blank recorded in cell I (see Figure 4). Other curves correspond to consecutively recorded CVs (see legend for details). The aqueous phase: 10 mM Na_2SO_4 (pH = 11) with 10 mM 1,6-DAH and 2 mM $AgNO_3$ (added before for A and after for B polyamide film formation). The organic phase: 5 mM BTPPATPBCl with 5 mM AC and 10 mM Fc in 1,2-DCE. Scan rate was 20 $mV \cdot s^{-1}$. SEM micrographics recorded for the fiberglass membrane before modification (C), fiberglass membrane modified with polyamide film and Ag NPs formed during simultaneous (D), and sequential (E) modification. For the SEM images: the scale bars correspond to 50 μm.

ally protonated 1,6-diaminohexane transfer from the aqueous phase to the LLI where it reacted with adipoyl chloride. Ag nanoparticles were formed either during interfacial polycondensation of polyamide or after initial polymerization using cyclic voltammetry. As such, the Ag^+ cations initially dissolved in the aqueous phase were reduced to Ag(0) by the electron donating Fc dissolved in the organic phase. All possible charge transfer reactions happening across the electrified liquid-liquid interface were studied individually and later in a complex system (all reagents were placed in the electrochemical cell). Formation of Ag nanoparticles was confirmed with SEM. Polyamide decorated with Ag nanoparticles was formed as a freestanding film at the electrified liquid-liquid interface and within the fiberglass membrane used as a support of both, the liquid-liquid interface and forming deposit.

Acknowledgements

The presented research was financed by the National Science Centre Poland as part of the PRELUDIUM 19 project (UMO-2020/37/N/ST4/00270). Magdalena Karpińska is acknowledge for performing initial experiments.

Conflict of Interest

Authors declare no conflict of interests.

Data Availability Statement

The data that support the findings of this study are openly available in Zenodo at 10.5281/zenodo.6467222, reference number 6467222.

Keywords: Electrochemistry · Interfacial electron transfer · Interfacial polycondensation · ITIES · Materials Science

[1] J. Koryta, *Electrochim. Acta* **1979**, *24*, 293–300.
[2] F. Reymond, D. Fermin, H. J. Lee, H. H. Girault, *Electochim. Acta* **2000**, *45*, 2647–2662.
[3] K. Rudnicki, L. Poltorak, S. Skrzypek, E. J. R. Sudhölter, *Anal. Chem.* **2018**, *90*, 7112–7116.
[4] P. Vanysek, L. Basaez Ramirez, *J. Chil. Chem. Soc.* **2008**, *2*, 1455–1464.
[5] Z. Samec, *Pure Appl. Chem.* **2004**, *76*, 2147–2180.
[6] S. Liu, Q. Li, Y. Shao, *Chem. Soc. Rev.* **2011**, *40*, 2236–53.
[7] G. C. Lillie, R. A. W. Dryfe, S. M. Holmes, *Analyst* **2001**, *126*, 1857–1860.
[8] B. Liu, M. V. Mirkin, *Electroanalysis* **2000**, *12*, 1433–1446.
[9] H. Hu, S. Xie, X. Meng, P. Jing, M. Zhang, L. Shen, Z. Zhu, M. Li, Q. Zhuang, Y. Shao, *Anal. Chem.* **2006**, *78*, 7034–7039.
[10] N. Younan, M. Hojeij, L. Ribeaucourt, H. H. Girault, *Electrochem. Commun.* **2010**, *12*, 912–915.
[11] P. S. Toth, A. K. Rabiu, R. A. W. W. Dryfe, *Electrochem. Commun.* **2015**, *60*, 153–157.
[12] M. C. Collins, M. Hébrant, G. Herzog, *Electrochim. Acta* **2018**, *282*, 155–162.
[13] L. Poltorak, A. Gamero-Quijano, G. Herzog, A. Walcarius, *Appl. Mater. Res.* **2017**, *9*, 533–550.
[14] P. S. Toth, Q. M. Ramasse, M. Velický, R. A. W. W. Dryfe, *Chem. Sci.* **2015**, *6*, 1316–1323.
[15] B. Sefer, R. Gulaboski, V. Mirčeski, *J. Solid State Electrochem.* **2011**, *16*, 2373–2381.
[16] K. Lepková, J. Clohessy, V. J. Cunnane, *Electochim. Acta* **2008**, *53*, 6273–6277.
[17] A. Trojánek, J. Langmaier, Z. Samec, *J. Electroanal. Chem.* **2007**, *599*, 160–166.
[18] U. Evans-Kennedy, J. Clohessy, V. J. Cunnane, *Macromolecules* **2004**, *37*, 3630–3634.
[19] R. Knake, A. W. Fahmi, S. A. M. Tofail, J. Clohessy, M. Mihov, V. J. Cunnane, *Langmuir* **2005**, *21*, 1001–1008.
[20] M. Vignali, R. Edwards, V. J. Cunnane, *J. Electroanal. Chem.* **2006**, *592*, 37–45.
[21] A. W. Fahmi, S. A. M. Tofail, J. Clohessy, M. Mihov, V. J. Cunnane, N. Ng, **2005**, 1001–1008.
[22] K. Sipa, K. Kowalewska, A. Leniart, S. Skrzypek, L. Poltorak, *Electrochem. Commun.* **2021**, *123*, 106910.
[23] K. Kowalewska, K. Sipa, B. Burnat, S. Skrzypek, L. Poltorak, *Materials (Basel).* **2022**, *15*, 2196.
[24] A. Gamero-Quijano, M. Dossot, A. Walcarius, M. D. Scanlon, G. Herzog, *Langmuir* **2021**, *37*, 4033–4041.
[25] L. Poltorak, M. Hébrant, M. Afsharian, M. Etienne, G. Herzog, A. Walcarius, *Electrochim. Acta* **2016**, *188*, 71–77.
[26] L. Poltorak, G. Herzog, A. Walcarius, *Electrochem. Commun.* **2013**, *37*, 76–79.
[27] S. Tan, M. Hojeij, B. Su, G. Meriguet, N. Eugster, H. H. Girault, *J. Electroanal. Chem.* **2007**, *604*, 65–71.
[28] M. D. Scanlon, E. Smirnov, T. J. Stockmann, P. Peljo, *Chem. Rev.* **2018**, *118*, 3722–3751.
[29] A. N. J. Rodgers, R. A. W. Dryfe, **2016**, 472–479.
[30] T. J. Stockmann, J. Zhang, J. C. Wren, Z. Ding, *Electochim. Acta* **2012**, *62*, 8–18.
[31] D. W. M. Arrigan, *Annu. Reports Sect. "C" Physical Chem.* **2013**, *109*, 167; Physical Chem. **2013**, 109, 167.
[32] A. N. J. Rodgers, S. G. Booth, R. A. W. Dryfe, *Electrochem. Commun.* **2014**, *47*, 17–20.
[33] M. Arooj, D. W. M. Arrigan, R. L. Mancera, *J. Phys. Chem. B* **2019**, *123*, 7436–7444.
[34] R. Matsui, T. Sakaki, T. Osakai, *Electroanalysis* **2012**, *24*, 1164–1169.
[35] C. J. Collins, C. Lyons, J. Strutwolf, D. W. M. Arrigan, *Talanta* **2010**, *80*, 1993–1998.
[36] D. W. M. Arrigan, M. J. Hackett, R. L. Mancera, *Curr. Opin. Electrochem.* **2018**, *12*, 27–32.
[37] A. Sherburn, M. Platt, D. W. M. Arrigan, N. M. Boag, R. A. W. Dryfe, *Analyst* **2003**, *128*, 1187–1192.
[38] K. Kowalewska, K. Sipa, A. Leniart, S. Skrzypek, L. Poltorak, *Electrochem. Commun.* **2020**, *115*, 106732.
[39] J. Guo, T. Takahira, R. Othman, P. R. Unwin, *Electrochem. Commun.* **2003**, *5*, 1005–1010.
[40] C. Johans, J. Clohessy, S. Fantini, Kyosti Kontturi, V. J. Cunnane, *Electrochem. Commun.* **2002**, *4*, 227–230.
[41] V. J. Cunnane, G. Geblewicz, D. J. Schiffrin, *Electrochim. Acta* **1995**, *40*, 3005–3014.
[42] N. E. A. Cousens, A. R. Kucernak, *Electrochem. Commun.* **2011**, *13*, 1539–1541.
[43] M. Velický, K. Y. Tam, R. A. W. Dryfe, *Anal. Methods* **2012**, *4*, 1207–1211.
[44] T. Kakiuchi, *J. Electroanal. Chem.* **2004**, *569*, 287–291.
[45] Y. Kitazumi, T. Kakiuchi, *J. Electroanal. Chem.* **2010**, *648*, 8–14.
[46] E. Laborda, A. Molina, V. F. Espin, F. Martinez-Ortiz, J. Gracia de la Torre, R. G. Compton, *Angew. Chem. Int. Ed.* **2017**, *56*, 782–785; *Angew. Chem.* **2017**, *129*, 800–803.
[47] F. Scholz, U. Hasse, *Electrochem. Commun.* **2005**, *7*, 541–546.
[48] T. J. Stockmann, H. Deng, P. Peljo, K. Kontturi, M. Opallo, H. H. Girault, *J. Electroanal. Chem.* **2014**, *729*, 43–52.
[49] B. Su, I. Hatay, A. Trojánek, Z. Samec, T. Khoury, C. P. Gros, J. M. Barbe, A. Daina, P. A. Carrupt, H. H. Girault, *J. Am. Chem. Soc.* **2010**, *132*, 2655–2662.
[50] R. Partovi-Nia, B. Su, F. Li, C. P. Gros, J. M. Barbe, Z. Samec, H. H. Girault, *Chem. A Eur. J.* **2009**, *15*, 2335–2340.
[51] I. Hatay, B. Su, F. Li, M. A. Méndez, T. Khoury, C. P. Gros, J. M. Barbe, M. Ersoz, Z. Samec, H. H. Girault, *J. Am. Chem. Soc.* **2009**, *131*, 13453–13459.
[52] D. R. Lide, *Handb. Chem. Phys.* **2003**, *53*, 2616.
[53] H. B. Jonassen, T. F. Fagley, C. C. Rolland, P. C. Yates, **1985**, 864–868.
[54] K. Sipa, K. Kowalewska, A. Leniart, A. Walcarius, G. Herzog, S. Skrzypek, L. Poltorak, *Electrochem. Commun.* **2021**, *123*, DOI 10.1016/j.elecom.2020.106910.

Manuscript received: April 18, 2022
Revised manuscript received: July 15, 2022
Accepted manuscript online: July 21, 2022

Characterization of microITIES modified with polyamides

Karolina Kowalewska[a*], Karolina Kwaczyński[a], Madjid Tarabet[b], Karolina Sobczak[a], Andrzej Leniart[a], Sławomira Skrzypek[a], Manuel Dossot[b], Gregoire Herzog[b], Łukasz Półtorak[a*]

a. *Electrochemistry@Soft Interfaces Team, Department of Inorganic and Analytical Chemistry, Faculty of Chemistry, University of Lodz, Tamka 12, 91-403 Lodz, Poland.*
b. *Université de Lorraine, CNRS, LCPME, 54000 Nancy, France*

***Corresponding authors:** lukasz.poltorak@chemia.uni.lodz.pl
karolina.kowalewska@chemia.uni.lodz.pl*

Abstract

In this work, we present the possibility to electrochemically assist and study interfacial polycondensation derived from the reactions between 1,6-diaminohexane or *p*-phenylenediamine used as the diamine (always initially present in the aqueous phase) and acyl chlorides in a form of 1,3,5-benzenetricarbonyl trichloride, terephthaloyl chloride or adipoyl chloride (present in the organic phase – 1,2-dichloroethane solution). Synthesized polyamides are formed at the polarized liquid – liquid interfaces (or the interface between two immiscible electrolyte solutions – ITIES) as a consequence of the partly protonated diamine transfer from the aqueous to the organic phase. In this respect, we have defined the aqueous phase pH assuring availability of the amine groups ($-NH_2$) for the reaction with the acyl chloride and protonated amine groups ($-NH_3^+$) defining the electrochemical interfacial activity of chosen compounds. The possibility to electrochemically assist the interfacial formation of polyamides was first tested using the macroscopic ITIES. Formed polyamides were collected and analysed using scanning electron microscopy, energy dispersive x-ray spectroscopy and Raman spectroscopy. Next, we have employed the microscopic ITIES (microITIES) based system formed using fused silica microcapillaries. Cyclic voltammetry was employed for the polyamide modified microITIES assessment (evolution of molecular sieving properties using a model ion - tetramethylammonium cation).

Keywords: polyamides, interfacial polycondensation, polarized liquid – liquid interface, Kevlar, Nylon, acyl chlorides, diamine.

1. Introduction

Polyamides belong to the large group of polymers having an amide bond present in their structure. Polyamides can be divided into aliphatic (straight-chain), aromatic (aramids) and semi-aromatic (polyphthalamides). Aliphatic polyamides form straight chain monomers. Whenever two monomers, each containing an aromatic ring in its structure react, we obtain aramid. Polyphthalamides are formed as the result of the reaction between aromatic and aliphatic monomers. Polyamides hold valuable commercial importance. They have many industrial applications, primarily in the textile industry for the production of clothes, but are also a component of ropes, lines, toothbrushes or tights [1,2]. Polyamide based materials are also frequently applied in R&D laboratories due to the high resistivity to organic solvents. These class of materials is especially useful as membranes [3], but also find applications as adsorbents [4] or for labware fabrication [5]. One can obtain polyamides by interfacial polymerization derived from a reaction between compounds containing multiple amine and acid chloride groups [6]. The substrates are dissolved in the aqueous and the organic phases (based on their solubility) and react at the junction formed between two immiscible liquids to form a polyamide material. The interfacial deposit is formed until (i) one of the reactants is exhausted, or (ii) the compactness of the formed polymer inhibits the transfer of the reactants to the soft junction. The reaction can be also impeded by the proton formed upon amide bond formation. Very popular example of a polyamide derived from the interfacial polycondensation is Nylon-6.6 [7]. It can be obtained quickly, spontaneously and easily in a spectacular manner, known as the "nylon rope trick" [8]. Since the protons are formed as by-products of the reaction between amine and acyl chloride groups, the interfacial polycondensation can be electrochemically assisted at the polarized liquid – liquid interfaces (the presence of protons allows the protonation of the amine groups triggering the interfacial electrochemical activity of the concerned compounds) [9].

Electrochemistry at the Interface between Two Immiscible Electrolyte Solutions (ITIES) is a platform that when combined with electroanalytical techniques allows the study of interfacial phenomena under the influence of an applied potential difference [10]. ITIES-based

systems are defect-free and self-healing, take the shape of the container, and can be studied with all available electrochemical techniques. The intrinsic properties of the ITIES are frequently employed to study purely ion interfacial charge transfer, providing an alternative to solid electrodes [11]. Macroscopic ITIES can be studied in a classical electrochemical cell equipped with two Luggin capillaries. Usually, the volume of each phase (either aqueous or organic) equals to a few mL. In the vast majority of reports, the ITIES is formed between an aqueous phase (highly hydrophilic salt (e.g. NaCl, HCl, LiCl) dissolved in water) and an organic phase (hydrophobic salt (e.g. bistriphenylphosphoranyldiene tetrakis(4-chlorophenydiene)borate) dissolved in a solvent like 1,2-dichloroethane, α,α,α-trifluorotoluene) [12–14]. A lot of attention is also given to miniaturize polarized liquid – liquid interfaces to ensure greater stability of the soft junction (aided by the employed supports with predesigned surface wettability/capillary forces) and allow the reduction in consumption of toxic chemicals (and chemicals in general) [15]. The liquid-liquid interface downscaling can be achieved with the supports made of polymer [16], silicon [17,18], or fiberglass membranes [19]. MicroITIES systems are also created by using glass tubes, or single/double barrel capillaries with a dimensionality ranging from few tens of nm to a few tens of μm [20,21]/ In this work, the microITIES was formed by placing a short piece of silica microcapillary tubing having 25 μm in diameter into a micropipette tip, further secure via heat treatment [22]. Resulting platforms allowed for the rapid fabrication that was beneficial for the microITIES modification with the polyamide material.

New properties of polarized liquid – liquid interfaces can be obtained by means of different materials placement at the soft junction. *In situ*-based modification methodology can be followed by (i) interfacial ion transfer, (ii) interfacial electron transfer, (iii) spontaneous adsorption to the interfacial region or (iv) interfacial polycondensation. An example of the interfacial deposition assisted by the ion transfer reaction of a surfactant molecules initially dissolved in the organic phase to the aqueous phase containing silanol species may lead to the electrochemically controlled synthesis of silica [23,24]. Moreover, the polarized liquid – liquid interfaces can be modified with metallic nanoparticles, which are formed as a result of interfacial electron transfer (e.g. from electron donor dissolved in the organic phase, to the aqueous reservoir of metallic NPs precursors) [25–28]. Examples cover the electrochemically controlled synthesis of Pd nanoparticles using an alumina membrane as a support [29], synthesis of gold nanofilm [27,30], or silver nanoparticles [31] at the ITIES. Several elegant

papers by Cunnane's team describe the interfacial formation of methyl and phenyl – pyrrole oligomers [32] and electropolymerization of 2,2':5',2''-terthiophene [33], the polymeric materials was controlled by interfacial electron transfer. Recent works discuss the formation of electrosynthesized poly(2,5-dimercapto-1,3,4-thiadiazole) films [34] or poly(3,4-ethylenedioxythiophene) thin films (the latter displaying exceptional biocompatibility) [35] at the polarized water-α,α,α-trifluorotoluene. Interfacial polycondensation defines a vast amount of growth polymerization reactions originating from a reaction between two or more monomers separated based on their solubility in the contacted immiscible phases. Vast amount of reactions can be rediscovered at the ITIES, especially when charged/ionisable function groups can be found within the structure of involved monomers. Recently we have shown, that polyamide interfacial polycondensation can be studied and assisted at the ITIES by the electrochemical control leading to a simple methodology allowing the LLI modification [9,25].

In this work, the electrochemically controlled synthesis of different polyamide materials was carried out. We modified ITIES with the polyamide films derived from the reaction between 1,6-diaminohexane or *p*-phenylenediamine used as the diamine (always initially present in the aqueous phase) and acyl chlorides in a form of 1,3,5-benzenetricarbonyl trichloride, terephthaloyl chloride or adipoyl chloride (present in the organic phase – 1,2-dichloroethane solution). Selected chemical species are popular monomers used for different polyamides formation, and hence, were also chosen to be studied at the ITIES. Polymers were formed at the macroscopic and miniaturized ITIES. Cyclic voltammetry was employed to assist the deposition process and to characterize modified ITIES permeability to ionic species. The materials extracted from ITIES were characterized using Raman spectroscopy and SEM – EDX.

2. Methods and materials

2.1.Chemicals

Sodium chloride (NaCl, ≥99,5%, Fisher Chemicals), acetic acid (CH_3COOH, 99.5 – 99.9%, POCh), phosphoric acid (H_3PO_4, 80%, for analysis, ChemPur), boric acid (H_3BO_3, for analysis, ChemPur) were used to prepare the Britton – Robbinson buffer. Sodium hydroxide (NaOH, for analysis, POCH) were used to prepare 1M solution that were further employed for pH adjustment. Demineralized water (Hydrolab®) was used in all cases to prepare the aqueous solutions. The organic phase was hydrophobic salt ($BTPPA^+TPBCl^-$) dissolved in 1,2 – dichloroethane (1,2-DCE, for analysis, POCH). The organic phase electrolyte $BTPPA^+TPBCl^-$

(Bis(triphenylphosphoranylidiene)ammonium tetrakis(4-chlorophenylborate)) was synthesized using bis(triphenylphosphoranylidiene)ammonium chloride ($BTPPA^+Cl^-$, 97%, Sigma-Aldrich) and potassium tetrakis(4-chlorophenyl) ($KTPB^+Cl^-$, ≥98%, Sigma-Aldrich) salt via mixing equimolar amounts of both reagents in methanol:water mixture (2:1). Resulting precipitate was than filtrated and recrystallized from acetone. The following compounds of diamines and di- or tri-acid chlorides were used for the synthesis of polyamide materials: p-phenylenediamine (PPD, 98%, Sigma – Aldrich), 1,6 – diaminohexane (1,6-DAH, ≥99,5%, Acros Organics), 1,3,5-benzenetricarbonyl trichloride (1,3,5,BTCTCl, for analysis, Apollo Scientific), terephthaloyl chloride (TCl, ≥99%, Sigma – Aldrich), and adipoyl chloride (AC, 98%. Alfa Aesar). A quaternary amine - tetramethylammonium chloride (TMACl, >98%, Acros Organics) was used to test molecular sieving properties of polyamide modified microITIES. The fused silica capillary tubing having the internal diameter equal to 25 µm was purchased from VWR.

2.2.Electrochemical experiments

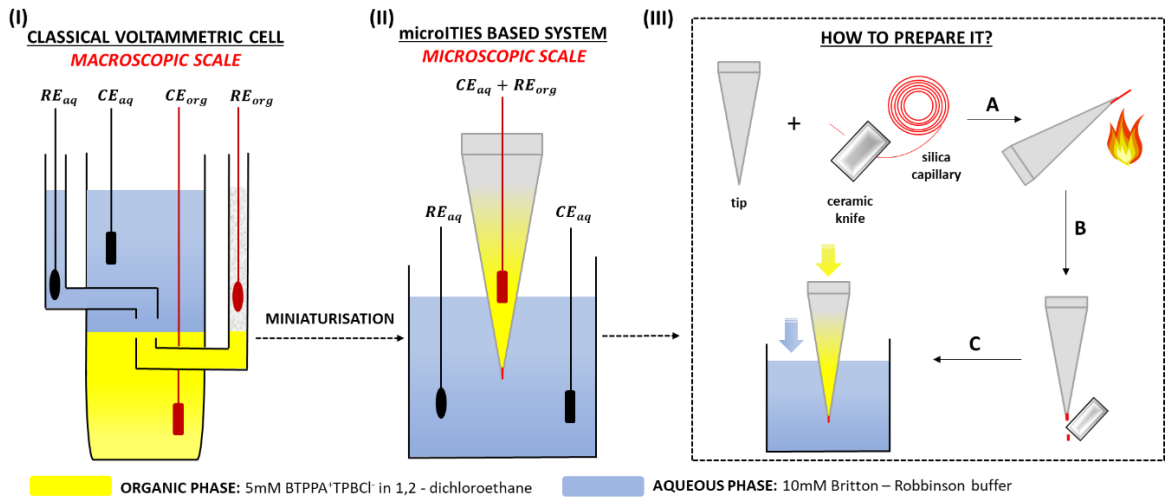

Figure 1. Scheme showing classical voltammetric cell (**I**) used for macroITIES polarization and modification, (**II**) used for microITIES modification and electroanalytical characterization. The organic phase is marked in yellow, whereas the aqueous phase is marked in blue. Set of electrodes being in contact with the organic phase are marked in red, and for the water phase in black. $RE_{aq/org}$= Ag/AgCl wire, $CE_{aq/org}$= platinum electrode (Pt). The third part of figure **(III)** shows the preparation protocol of the microITIES based system by embedding (**A**) a silica capillary in a micropipette tip, (**B**) removing excess capillary using a ceramic knife, and (**C**) filling the created system with the organic phase followed by a set of electrodes placement.

Electrochemical studies were carried out on macroscopic and microscopic scale. In macroscopic scale (see Fig.1-(**I**)) a classical voltammetric glass cell (interface radii equal to 0.7 cm) equipped with a set of four electrodes was used. Two Ag/AgCl reference electrodes and two Pt counter electrodes were involved. In microscopic scale (Fig. 1-(**II**)), the ITIES was supported with a micropipette tip finished with the silica capillary tubing having a diameter equal to around 25 µm. The created microtip was filled with the organic phase and immersed in the aqueous phase. Here, the platinum, and the Ag/AgCl electrodes were used as the aqueous phase counter and reference electrodes, respectively. The platinum wire electrode contacted with the organic phase served as both: the organic phase counter and reference electrode. MicroITIES support was fabricated following procedure reported elsewhere.[22] All experiments were conducted using Autolab 108 (Metrohm®) with Nova 1.11 software.

2.3.SEM - EDX

The scanning electron microscopy (SEM, a Phenom G2 Pure, FEI Company, the Netherlands) was used to examine the morphology of polyamide material formed at the macroscopic and microscopic LLI. SEM images were acquired using a high sensitivity backscatter electron detector (BSD) with an accelerating voltage of 5 kV.

SEM - EDX was also used for local analysis and mapping of manufactured polyamide materials using the JEOL JMS-IT500HR microscope (JEOL, Japan) equipped with the Ultim Max 170 EDS detector (Oxford Instruments, UK).

2.4.Raman Spectroscopy

Raman spectra have been taken with a Renishaw Qontor set-up equipped with a Peletier cooled CCD camera, a laser of 785 nm wavelength working at 50 mW and an edge filter to separate the Rayleigh from the Raman scattered light. A grating with 1200 grooves/mm was used, leading to a spectral resolution of 1 cm^{-1}. The laser light was focused on the microscope stage using a X50 objective with long working distance (11 mm) and a numerical aperture of 0.75. Typical experiments required an average of 4 acquisitions with 5 s of integration time on the detector.

3. Result and discussion

3.1 Polyamides synthesis at macroscopic polarized liquid-liquid interface

We have studied the possibility to assist electrochemically the synthesis of polyamides at the macroscopic ITIES. The possible reaction routes between the various monomers dissolved in either aqueous or the organic phase that we have studied are shown in Fig. 2. The polyamides synthesised are derived from the reaction between one out of two employed diamines and one out of three selected di- or tri-acyl chlorides. As shown in Fig. 2, the investigated pair of monomers are (aq stands for the aqueous phase; org stands for the organic phase): **I** - *p*-phenylenediamine (aq) and 1,3,5-benzenetricarbonyl trichloride (org), **II** - *p*-phenylenediamine (aq) and terephthaloyl chloride (org), **III** - *p*-phenylenediamine (aq) and adipoyl chloride (org), **IV** - 1,6-diaminohexane (aq) and 1,3,5-benzenetricarbonyl trichloride (org), **V** - 1,6-diaminohexane (aq) and terephthaloyl chloride (org). The numbering **I-V** is adopted and refer to resulting polyamides in all section of this manuscript. The interfacial polycondensation of nylon-6,6 (**VI**; reaction between 1,6-diaminohexane and adipoyl chloride) is purposely not marked as it was investigated previously by our group (see [9]).

For *p*-phenylenediamine and 1,6-diaminohexane we have plotted concentration distribution diagrams (Fig. S1). *p*-phenylenediamine pK_a's values are pK_{a1} = 2.8 and pK_{a2} = 6.2 [36]. For 1,6-diaminohexane, these values are pK_{a1} = 10.8 and pK_{a2} = 11.9 [9]. Both monomers soluble in the aqueous phase, have two amine groups located at the periphery of the aromatic ring or alkyl chain. As such, for each diamine, we can distinguish three possible species that may exist in the aqueous phase depending on its pH: this is neutral diamine (A^0); monoprotonated diamine (A^+) or diprotonated diamine (A^{2+}). To form a amide bond, a fraction of compounds providing amine groups with a lone pair of electrons need to be available to attack carbon atom (with a net positive charge). A fraction of protonated amine groups, which are deprived from a lone electron pair, will provide the interfacial electrochemical activity of the amine monomers. In other words, we need charged species that may undergo electrochemically controlled ion transfer from the aqueous to the organic phase being reservoir of the monomers equipped with acyl chloride functionalities. The inspection of the concentration distribution diagrams revealed that the optimal aqueous phase pH for the electrochemically assisted interfacial polycondensation reaction is pH = 6.2 for the *p*-phenylenediamine pH = 11.3 for the 1,6-diaminohexane. Further information taken from the

concentration fraction diagrams indicates that at pH = 6.2 (*p*-phenylenediamine; Fig. S1A) the aqueous phase contains 50% of A^0; 50% of A^+; and 0% of A^{2+}. For 1,6-diaminohexane we have selected the aqueous phase pH = 11.3 (see Fig. S1B) that fixed its composition to 64% of A^+; 18% of A^{2+}, and 18% of A^0. The reason why the pH of the aqueous phase solution of the 1,6-diaminohexane was not elevated (lowered fraction of the doubly protonated species – A^{2+}) is related to OH^- concentration, which when too high could limit the available potential window during voltammetric scanning used for the ITIES modification.

With the pH of the aqueous phase fixed, we have designed the experiment to study the effect of the diamine concentration added to the aqueous phase, in the absence of the acyl chloride in the organic phase, on the shape of the cyclic voltammograms. Fig. S2A and Fig. S2B show the resulting current-potential dependencies for *p*-phenylenediamine and 1,6-diaminohexane in the concentration range from 20 µM to 3 mM, respectively. In both cases we have observed that starting from around 20 µM we can distinguish a pair of signals (positive and negative currents) located on the positive potential difference side of the available potential window. As the concentration of diamine increases (> 500 µM) the current intensity at E > 0.6V grows (as expected) and overlaps with the current linked to the transfer of the background electrolyte, which limits the potential window on more positive side (Na^+ transfer from the aqueous to the organic phase). Our understanding is that, for *p*-phenylenediamine at pH = 6.2, the positive currents are due to A^+ transfer from the aqueous to the organic phase, whereas for 1,6-diaminohexane at pH = 11.3, the positive current is a mixture of the A^+ and A^{2+} transfer from the aqueous to the organic phase. By analogy, the negative currents are due to A^+ or A^+/A^{2+} back transfer to the aqueous phase. We also found, that all employed acyl chlorides soluble only in the organic phase, this is 1,3,5-benzenetricarbonyl trichloride (Fig. S2C), terephthaloyl chloride (Fig. S2D) and adipoyl chloride (Fig. S2E), at relatively high concentration fixed to 5 mM of each, do not provide any additional current variation within the available potential window. Acyl chloride functional group may react with water to form carboxylic acid groups and hydrochloric acid as a side product. This means that small fraction of monoanionic or dianionic species with hydrolysed carboxylic groups (high pH) may exist within the interfacial region. Nevertheless, the voltammetric insights do not reveal the presence of such compounds.

Fig. 2 further depicts the ion transfer voltammograms recorded in the presence of different pair of diamines and di- or tri-acyl chlorides dissolved in the aqueous and the organic phase, respectively. For all cases I-V (for the numbering refer to Fig. 2A) the concentration of

acyl chloride dissolved in the organic phase was fixed and equal to 5 mM, whereas the concentration of diamine was an experimental variable progressively increasing from 100 µM to 5 mM.

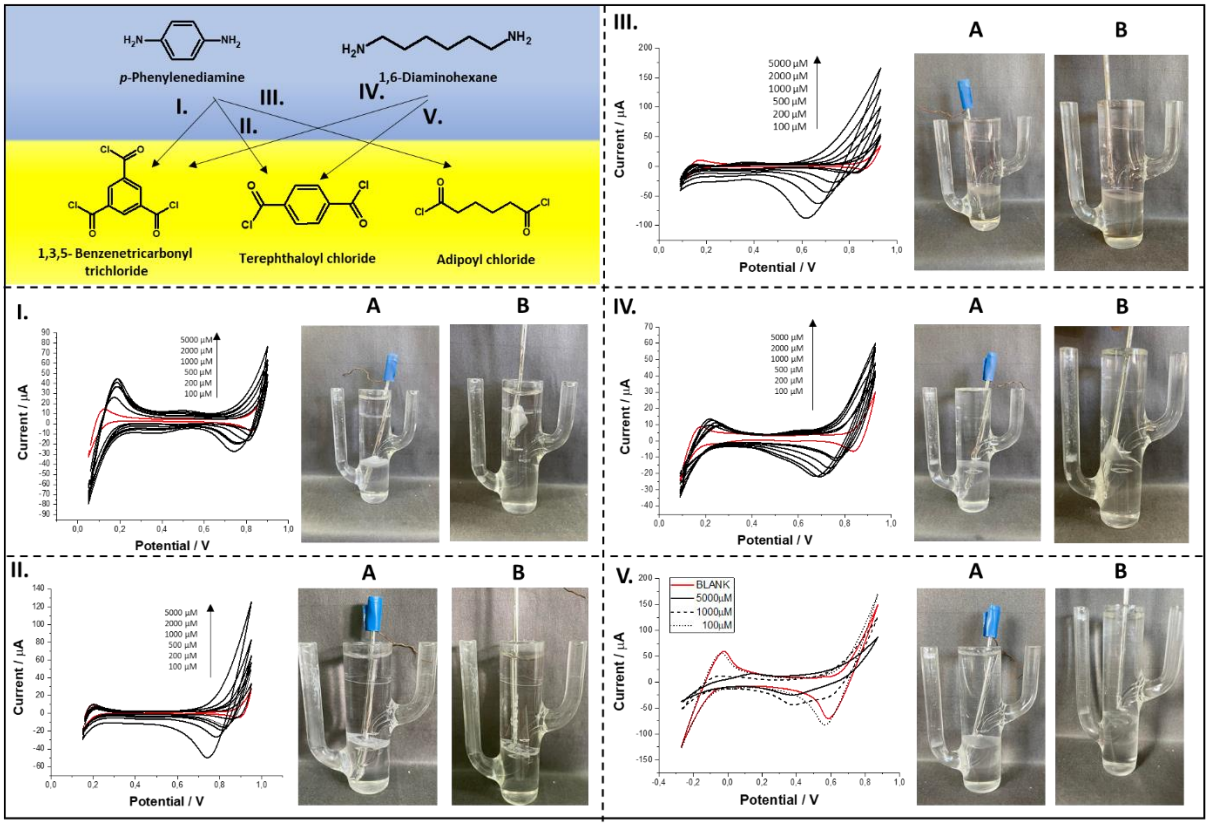

Figure 2. Left upper corner: Scheme displaying all possible reactions between acyl chlorides and di-amines studied at the ITIES. The numbers of reaction routes from I to V refer to the corresponding cyclic voltammograms recorded during the electrochemically assisted polyamides deposition at the macroscopic ITIES. Concentration of acyl chloride was fixed (5 mM), whereas the concentration of di-amine dissolved in the aqueous phase was increased from 100 to 5000 µM. The photos on the right from cyclic voltammograms are recorded after the interfacial polycondensation reaction occurred. The image **(A)** shows the polyamide material formed at the ITIES. In the second picture **(B)**, the material is pulled from the interface using a counter electrode from the organic phase.

From Fig. 2 we can notice that reactions I, II, III and IV provide similar features, this is, as the concentration of *p*-phenylenediamine (I, II and II) and 1,6-diaminohexane (IV) increase we can observe the increase in the positive current limiting the potential window on the more positive potential difference side of the cyclic voltammogram. Also, we have noticed additional pair of

peaks located between +0.2V and +0.5V (especially visible in Fig. 2-I, $E_{1/2}$ around 0.41V) for *p*-phenylenediamine and between +0.5V and +0.8V (see Fig. 2-IV, $E_{1/2}$ around 0.58V) for 1,6-diaminohexane. In the presence of the aqueous and the organic phase monomers, a number of electrochemical and chemical reactions can occur: (i) the electrochemically controlled transfer of either A^+ or A^{2+} from the aqueous to the organic phase giving positive current; (ii) reaction of the nitrogen atom having a lone pair of electrons with the carbon atom of the acyl chloride functionality occurring either at the ITIES or on the organic phase side of the ITIES after A^+ transfer or A^0 partitioning to the interfacial region; (iii) the A^+ or A^{2+} dissociation in the organic phase followed by the ion transfer reaction providing new amine groups for the reaction with acyl chloride; (iv) acidification of the aqueous phase side of the ITIES as the interfacial polycondensation proceeds (release of protons) that may affect the distribution of $A^0/A^+/A^{2+}$ further affecting the shape of the cyclic voltammograms; and finally, (v) the formation of charged dimers/trimers that may transfer back from the organic phase to the aqueous phase. As a matter of fact, for the latter, we believe that the extra pair of signals recorded before the prominent limiting current obtained for the higher diamine concentration originates from these complex species transfer. This is in line with the prediction, as the formed amides (dimers, trimers) should be more hydrophobic as compared with the charged diamine species shifting their ion transfer potentials to less positive potential difference values. Reaction between 1,6-diaminohexane and terephthaloyl chloride (V) gave rise to initially increasing signals attributed to the amine transfer from the aqueous to the organic phase (up to 100 µM), followed by a visible current drop, even these attributed to the transfer of the aqueous phase background electrolyte ions. This is especially visible on the cyclic voltammogram from Fig. 2-V, marked with a black solid line and attributed to the 5 mM 1,6-diaminohexane and 5 mM terephthaloyl chloride. The intensity of the peak current located at E = +0.05 V is nearly unaffected after addition of 100 µM of 1,6-diaminohexane and drops by around 85% when final concentration of diamine equal to 5 mM is present in the aqueous phase. This clearly demonstrates that the permeability of the formed polyphthalamide terephthaloyl/1,6-diaminohexane film is low, and hence, should display efficient ionic sieving properties. Each pair of monomers, after excessive cycling (>20 cycles) resulted in the formation of the deposit at the ITIES. Visual inspection of the formed polymeric films is additionally depicted on the photos taken for the cell after voltammetric cyclic (see Fig. 2, photos on the right from the cyclic voltammograms). First photo was taken for the cell with the intact ITIES whereas the second shows the film after lifting the

organic phase counter electrode. By doing this, we observed that compact and relatively thick films were obtained via reaction route I and IV (reaction between 1,3,5-benzenetricarbonyl trichloride and *p*-phenylenediamine or 1,6-diaminohexane, respectively). In both cases, the film could be lifted from the ITIES after the voltammetric deposition. Most probably, formed polyamide films hold a relatively open and cross linked structure originating from the existence of three acyl chloride substituents in 1,3,5-benzenetricarbonyl trichloride monomer, which do not inhibit the mass transfer of diamine from the aqueous to the organic phase. This is in line with the increasing ionic currents growing along with the increasing aqueous phase monomer concentration. For the reaction route II and III we have obtained films that were breaking easily once the organic phase counter electrode was moved. Similar features were attributed to the reaction route V, which displayed significant blocking effect on the transfer of all ions present in the cell (see Fig. 2-V). The fragile polyamide film could be easily disrupt, most probably meaning that this thin film is not permeable to either of the monomers already at the initial deposition time.

Fig. 3 shows the data obtained for the polyamide materials extracted from the macroscopic ITIES after electrochemically assisted deposition process. With scanning electron microscopy, we have noticed that different polyamides, as expected, exhibit different surface morphologies.

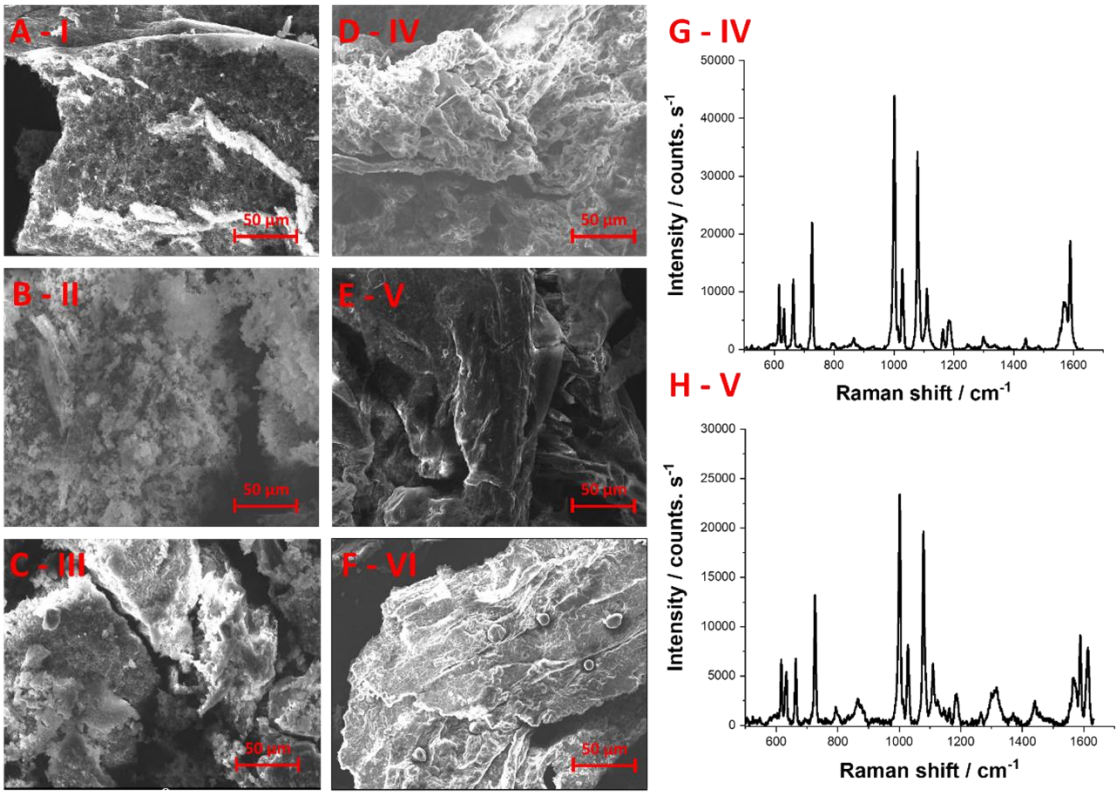

Figure 3. SEM images recorded for polyamide films synthesized and collected from the ITIES. A-I – *p*-phenylenediamine and 1,3,5-benzenetricarbonyl trichloride, B-II – *p*-phenylenediamine and terephthaloyl chloride, C-III – *p*-phenylenediamine and adipoyl chloride, D-IV – 1,6-diaminohexane and 1,3,5-benzenetricarbonyl trichloride, E-V – 1,6–diaminohexane and terephthaloyl chloride, F-VI – 1,6- diaminohexane and adipoyl chloride. G-IV and H-V are the Raman spectra recorded for polyamides derived from a reaction between 1,6-diaminohexane and 1,3,5-benzenetricarbonyl trichloride; and 1,6–diaminohexane and terephthaloyl chloride, respectively. 50% red laser (785nm) intensity was used.

The inspection of the SEM images reveals that polyamides formed via route I, II and III are rather spongy with the debris existing at the material surface whereas the remaining polymers obtained in reaction IV, V and VI display significantly less fine features. Fig. S3 available in the electronic supporting information provide more SEM images recorded at three different magnifications. All collected materials were also examined using Raman spectroscopy. Obtained spectra are not identical to the spectra already reported in the literature for e.g. polyamide-6,6 or polyaramid fibres like Kevlar.[37–41] The results obtained using Raman spectroscopy were similar for all interfacially formed deposits and most probably correspond to the background electrolyte which apparently is entrapped in the film upon interfacial synthesis (the recorded Raman spectra for BTPPACl – data not shown – is very similar to the spectra depicted in Fig. 3G and Fig. 3H). . EDX analysis has shown that in addition to carbon, nitrogen, and oxygen polymeric films contain other elements at non negligible % contribution. We have found sodium, phosphate, and chloride indicating that the background electrolyte salts (from both phases) may be entrapped within the polyamide material during the interfacial polycondensation process. We have found that on average, more background electrolyte ions are present in the polyamides derived from reactions IV, V and VI (e.g. up to 11.20% of Na^+ found in film IV). Also, we have compared the %composition of C, N and O in the films formed at the ITIES with the expected (theoretical) %composition of the pure films. Obtained correlation holds expected order of magnitude (see Table 1).

Table 1. %Composition of the polyamide films collected from the ITIES. I – *p*-phenylenediamine + 1,3,5-benzenetricarbonyl trichloride, II – *p*-phenylenediamine + terephtaloyl chloride, III – *p*-phenylenediamine + adipoyl chloride, IV – 1,6-diaminohexane + 1,3,5-benzenetricarbonyl trichloride , V – 1,6–diaminohexane + terephtaloyl chloride, VI – 1,6- diaminohexane + adipoyl chloride.

TESTED COMPOSITION

NAME / ELEMENT [%]	I	II	III	IV	V	VI
C	66	73	71	66	73	65
N	4	12	10	4	6	7
O	10	11	15	9	13	16
Na	9	0	1	11	4	7
P	2	0	1	0	1	2
Cl	9	4	2	10	3	3

THEORETICAL COMPOSITION

NAME / ELEMENT [%]	I	II	III	IV	V	VI
C	68	71	66	61	68	64
N	15	12	13	10	11	12
O	13	13	15	17	13	14

3.2. Microscopic liquid-liquid interface modified with different polyamides

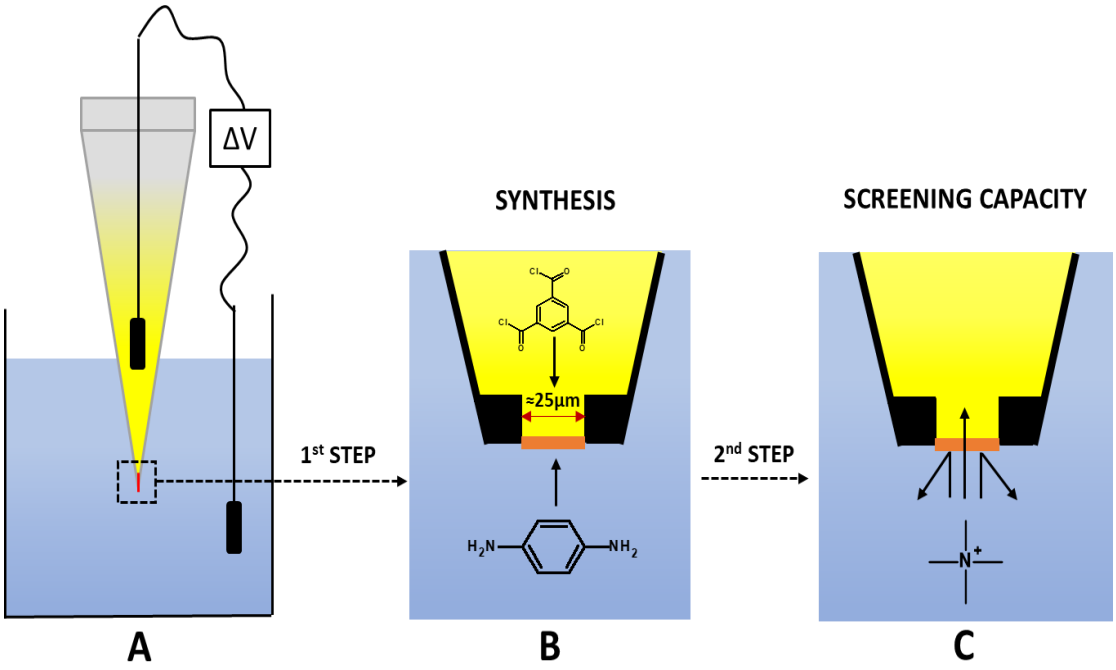

Figure 4. Experimental sequence aiming at (**A**) bare microITIES characterization; (**B**) microITIES modification with the chosen polyamide (example shows the reaction between *p*-phenylenediamine (aq) and 1,3,5-benzenetricarbonyl trichloride (org) and (**C**) modified microITIES characterization with quaternary ammonium cations.

In order to test polyamides compactness formed at the ITIES the entire system was miniaturized using fused silica capillaries serving as the soft junctions supports. **Fig. 4** shows the typical processing route applied for all studied polyamides. The **1st step** (**A**) accounts for the microITIES preparation (see procedure reported elsewhere [22]) and the resulting supports electroanalytical evaluation with the cyclic voltammetry in the presence of the model ion. The currents originating from the tetramethylammonium (TMA^+) cation transfer from the aqueous to the organic phase were used to calculate the diameter of the supported ITIES [42]. As it will be shown for all voltammograms displayed below, the mass transfer of TMA^+ from the aqueous to the organic phase follows the hemispherical diffusion layer profile providing sigmoidal current response. The back transfer happening inside the capillary is limited by the linear diffusion, and hence, the negative, peak like signal is recorded. Only the tips having 24.5 µm +/- 1.0 µm were used for further processing. **Fig. 4B** shows the electrochemically assisted microITIES modification step. The concentration of monomers was set to 10 mM and 5 mM for

diamine and di-/tri-acyl chloride dissolved in the aqueous and the organic phase, respectively. For given concentrations we were obtaining enough material for further analysis, and we also found that these concentration provided films affecting the interfacial charge transfer reactions. The interfacial polycondensation was assisted by cyclic voltammetry with the experiential variable being the number of recorded voltammetric cycles: 5, 10, 15 or 20. In the last step (Fig. 4C), the microITIES modified with polyamide film with the predefined number of voltammetric cycles was removed from the aqueous phase containing diamine. The tip was rinsed with demineralized H_2O and was further inserted into a fresh cell to which the quaternary ammonium model ion (TMA^+) was added. The outcome of the molecular sieving properties for each formed polyamide film are presented and discussed below.

(I) *p*—phenylenediamine and 1,3,5,benzenetricarbonyl trichloride

First, we have investigated the polyamide (I) created using *p*-phenylenediamine and 1,3,5-benzenetricarbonyl trichloride. Fig. 5A and 5B shows the monomer structures used during electrochemically assisted interfacial polycondensation. Before ITIES modification the composition of both phases was set to: the aqueous phase - 10 mM *p*-phenylenediamine dissolved in a 10mM BRB at pH = 6.2; the organic phase – 5 mM 1,3,5-benzenetricarbonyl trichloride dissolved in a 5 mM $BTPPA^+TPBCl$ in 1,2-DCE. As shown in Fig. 5C, formed material covers a surface being slightly greater than the surface of the pore (around 25 µm in diameter) indicating that: (i) the material grows towards the aqueous phase side of the ITIES as the reaction time pass by; or (ii) the drop in the ITIES interfacial tension caused by the adsorbing dimers/trimers/oligomers affects the position of the soft junction going into the aqueous phase during the electrochemically assisted modification. In Fig. 5D or Fig. S5 one can notice that obtained film is not homogenous. Analysis of the image suggests that the formed polyamide holds surface heterogeneity which is difficult to assess with SEM analysis. Fig. 5E – 5H are the cyclic voltammograms recorded in the absence and in the presence of TMA^+ (in the aqueous phase) at the ITIES modified with polyamide (I) after indicated number of voltammetric cycles. We have observed that in the absence of the TMA^+ in the aqueous phase, the positive and the negative limiting currents are becoming more resistive for the longer deposition process, although still being permeable for Na^+ ions (more positive potential difference side of the potential window) and the aqueous phase background electrolyte anions (Cl^-, phosphate, borate or CH_3COO^-; more negative side of the potential window). The inspection of the positive

currents (sigmoidal wave corresponding to the transfer of the TMA^+ from the aqueous to the organic phase) reveals that up to 10 cycles the signal intensity for 180 µM TMACl remains rather unaffected, after 15 cycles it drops by around 93%, whereas after 20 cycles the signal is missing. This suggests that the film compactness do not allow for the TMA^+ transfer or its thickness affects the TMA^+ diffusivity across the modified ITIES.

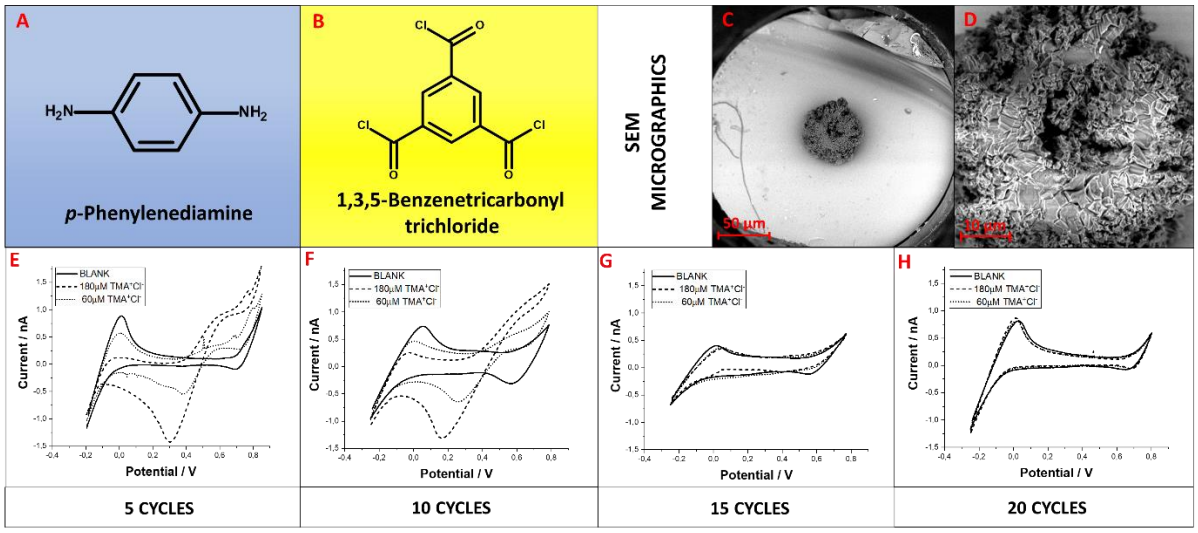

Figure 5. The figure shows structural formulas of *p*-phenylenediamine and 1,3,5-benzenetricarbonyl trichloride dissolved in the aqueous (A) and the organic (B) phase, respectively. C and D shows SEM micrographics taken for the polyamide modified microITIES formed after 20 consecutively recorded voltammetric scans. E, F, G and H are the voltammograms recorded at modified microITIES in the presence of [TMA^+] = 60 or 180 µM after different amounts of voltammetric cycle recorded during polyamide film formation at the ITIES. The recorded blank reading corresponds to the bold cyclic voltammogram recorded at modified microITIES in the absence of TMA^+.

(II) *p*—phenylenediamine and terephtaloyl chloride

The same characterization procedure was applied to all studied pairs of monomers. Analogical set of data for polyamide (II) is depicted in Fig. 6 and Fig. S5-II. SEM micrographies indicate the formed film entirely covers the pore. The morphology of the interfacial formed material is distinct from the polyamide (I) as not clear pinholes and holes are visible at its surface. Also, from Fig. S5-II (the SEM image recorded for the highest magnification) one can notice a clear boundary between the film and the edge of the pore, which indicates that the film formation

occurs within the capillary ingress. With the exception of the sigmoidal wave intensity attributed to 180 µM TMA^+ for the film formed with 5 voltammetric scans, we have observed that the polyamide (II) decreases the sigmoidal wave positive current 0.90 nA for 10 cycles, 0.56 nA for 15 cycles, and 0.16 nA for 20 cycles.

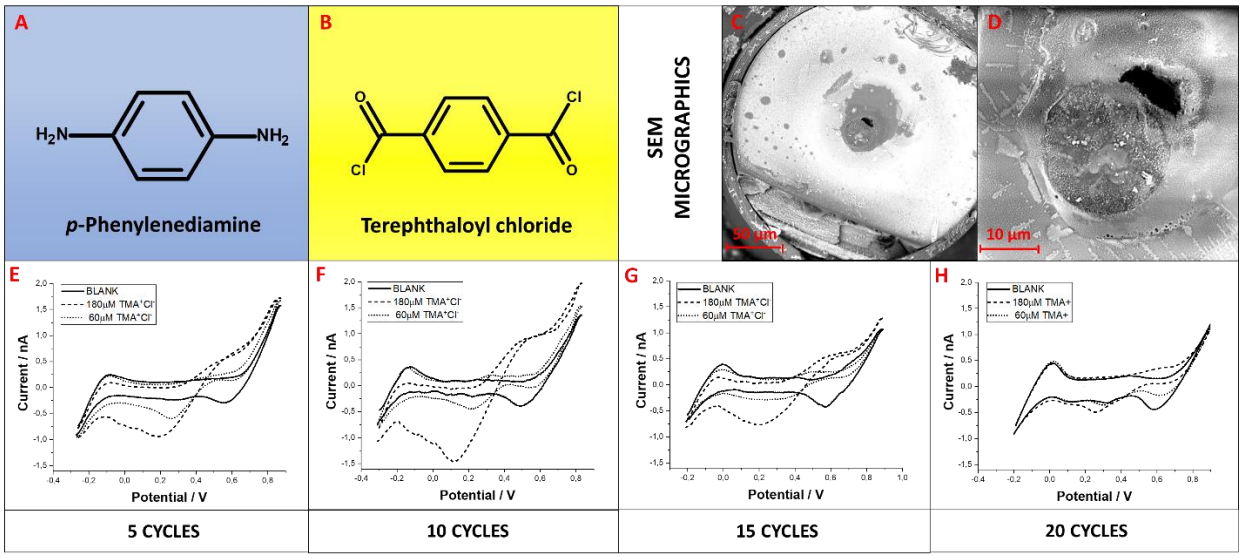

Figure 6. The figure shows structural formulas of *p*-phenylenediamine and terephthaloyl chloride dissolved in the aqueous (A) and the organic (B) phase, respectively. C and D shows SEM micrographics taken for the polyamide modified microITIES formed after 20 consecutively recorded voltammetric scans. E, F, G and H are the cyclic voltammograms recorded at modified microITIES in the absence (blank) and in the presence of [TMA^+] = 60 or 180 µM after indicated amount of the consecutively applied cycles. The recorded blank reading corresponds to the bold cyclic voltammogram recorded at modified microITIES in the absence of TMA^+.

(III) *p*-phenylenediamine and adipoyl chloride

The polyamide (III) gave a material with very interesting surface properties. SEM images from Fig. 7C and 7D clearly indicate that the film surface packed with a number of black spots which we have attributed to the film intrinsic porosity. Similar to other capillaries the film was formed within the pore and was slightly covering its edges. The biggest pores of the polyamide (III) are having up to a few hundred of nanometres (see Fig. S5-III; SEM micrographie recorded at highest magnification), and hence, our expectation was that the film will be permeable to TMA^+. Our prediction was confirmed with the voltammetric data shown in Fig. 7E – 7H. As a material with a pore size being a few order of magnitude larger than the hydrodynamic radius of the

TMA^+, the drop of the positive ionic current attributed to the studied model ion was equal to around 20% when comparing the film formed with 5 and 20 voltammetric cycles.

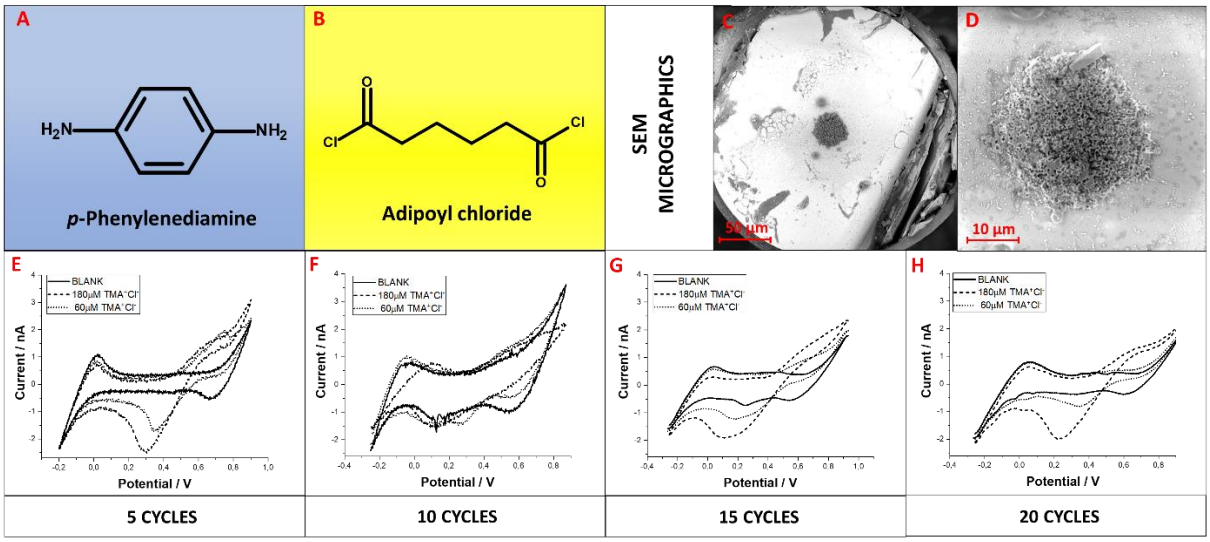

Figure 7. The figure shows structural formulas of *p*-phenylenediamine and adipoyl chloride dissolved in the aqueous (A) and the organic (B) phase, respectively. C and D shows SEM micrographics taken for the polyamide modified microITIES formed after 20 consecutively recorded voltammetric scans. E, F, G and H are the voltammograms recorded at modified microITIES in the presence of $[TMA^+]$ = 60 or 180 µM after different amounts of voltammetric cycles recorded during polyamide formation at the ITIES. The recorded blank reading corresponds to the bold cyclic voltammogram recorded at modified microITIES in the absence of TMA^+.

The third pair of monomers to synthesis of polyamide material were *p*-phenylenediamine and adipoyl chloride. **Figure 7** shows the monomer structures used for the synthesis reaction, voltammograms recorded for the modified microITIES systems for a given number of scanning cycles and selected SEM images for x1000 and x5000 magnification. The remaining images recorded using SEM were placed in supporting information (**SI Fig. S5).** The 10mM *P*-phenylenediamine was in a 10mM BRB at pH=6.2 and 5mM adipoyl chloride was in a 5mM $BTPPA^+Cl^-$ in 1,2-dichloroethane. The visible blank in the graph shows the voltammogram recorded for the modified microITIES system. Polyamide is formed at the miniaturized liquid – liquid interface in an electrochemically controlled manner, but it is very brittle and the model ion easily passes through it. A decrease in the signal of the model ion transition from the

aqueous phase to the organic phase and back is visible, but it was not possible to obtain an effectively blocked interface with the polyamide material.

(IV) 1,6-diaminohexane and 1,3,5,benzenetricarbonyl trichloride

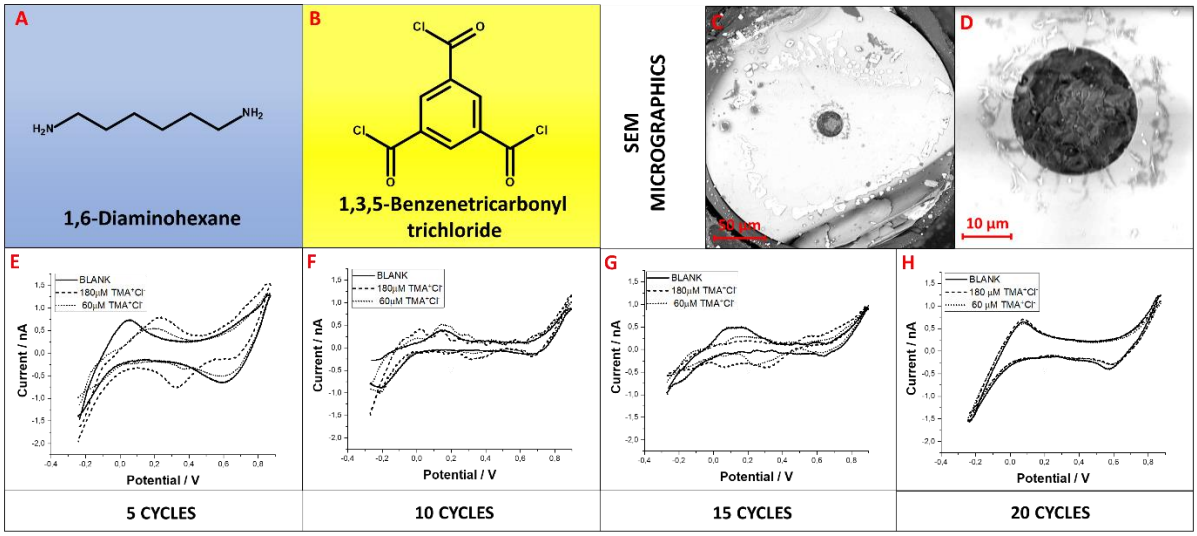

Figure 8. The figure shows structural formulas of 1,6-diaminohexane and 1,3,5-benzenetricarbonyl trichloride dissolved in the aqueous (A) and the organic (B) phase, respectively. C and D shows SEM micrographics taken for the polyamide modified microITIES formed after 20 consecutively recorded voltammetric scans. E, F, G and H are the voltammograms recorded at modified microITIES in the absence and in the presence of [TMA^+] = 60 or 180 µM after different number of applied voltammetric cycles. The recorded blank reading corresponds to the bold cyclic voltammogram recorded at modified microITIES in the absence of TMA^+.

The 4th pair of tested monomers (1,6-diaminohexane and 1,3,5-benzenetricarbonyl trichloride) gave a set of data depicted in **Fig. 8.** SEM images from Fig. 8C and 8D (also **Fig. S5-IV)** indicate that: (i) the film is compact; (ii) wrinkles exists at the surface and probably are the artefact of the drying process, and (iii) the surrounding of the capillary pore is decorated with a fibrous features which suggests that some fibres may grow on the aqueous phase side during interfacial polycondensation, and further collapse and remain at the surface of the capillary as the polyamide is dried. Interestingly, polyamide (IV) started to become an obstacle for the TMA^+ transfer either from the aqueous to the organic or from the organic to the aqueous phase

already after first five deposition cycles (see Fig. 8E). MicroITIES modified with polyamide (IV) with five deposition cycles gave additional voltammetric features located within less positive potential difference side (see positive peak signal at around +0.2V), that we think can be attributed to the anionic species (being the aqueous phase background electrolyte) transfer from the organic (inside of the capillary, where the mass transfer is governed by the linear diffusion) to the aqueous phase. Further increase in the number of deposition cycles blocked the interface, and even triggered the electrochemical instability manifested by the irregular current patterns as shown in Fig. 8F and Fig. 8G. The film formed after 20 modification cycles was entirely impermeable for the TMA^+ transfer.

(V) 1,6-diaminohexane and terephthaloyl chloride

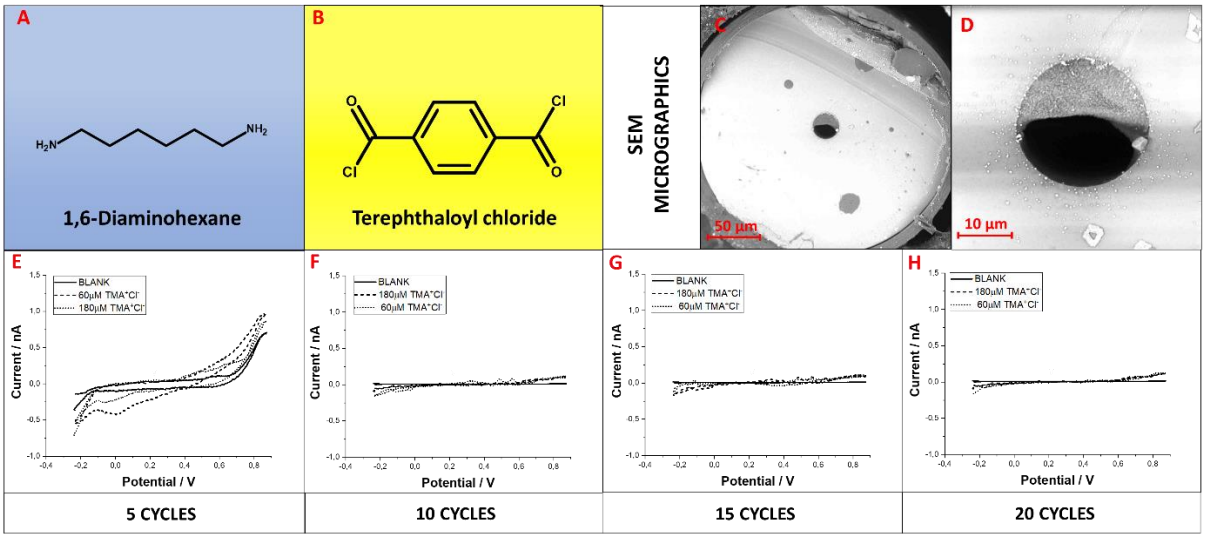

Figure 9. The figure shows structural formulas of 1,6-diaminohexane and terephthaloyl chloride dissolved in the aqueous (A) and the organic (B) phase, respectively. C and D shows SEM micrographics taken for the polyamide modified microITIES formed after 20 consecutively recorded voltammetric scans. E, F, G and H are the voltammograms recorded at modified microITIES in the absence and in the presence of $[TMA^+]$ = 60 or 180 µM after different number of applied voltammetric cycles. The recorded blank reading corresponds to the bold cyclic voltammogram recorded at modified microITIES in the absence of TMA^+.

The last studied deposit was derived from a reaction between 1,6-diaminohexane and terephthaloyl chloride. SEM images from Fig. 9C, 9D and Fig. S5-V are in line with the observations we have made when performing the experiments at the macroscopic ITIES. The

formed film covers only part of the micropore, which suggest its high fragility. The film formed at the macroscopic ITIES could not be lifted with the organic phase counter electrode as it was breaking and remaining as a broken flakes within soft junction. Fig. 9D shows that film covers only part of the pore ingress and probably has broken when both phases were removed from the film neighbourhood. The very high compactness of the film was already visible during the macroITIES modification process as the ionic currents originating from the 1,6-diaminohexane transfer were dropping as the film thickness was increasing. MicroITIES modified with polyamide (V) with 5 voltammetric cycles gave a curves with potential window elongated at the more negative potential difference side (anionic species transfer blocking effect) and blocked transfer of the TMA^+ from the aqueous to the organic phase (significantly reduced positive current signals). Also, the signal of the TMA^+ back transfer was shifted towards negative potential difference values indicating that additional portion of the energy must be supplied to the system to cross the ITIES modified with polyamide (V). Fig. 9F, 9G and 9H shows that the microITIES is not permeable to any ions present in both phases indicating that the ITIES is entirely blocked by the interfacially formed material.

Based on our screening study, we have concluded that in all cases the polyamide deposits were formed within the capillary ingress. For most deposits (I – IV) it was obvious that the reaction proceeds over time as the formed polymeric material could be found at the pore surroundings. In case of reaction (V) the film was found to be thin and located only within the pore, which further suggests that the compactness of the deposited polymer self-inhibited its further growth. Finally, the interfacially formed polyamides can be attributed to three classes of materials: (i) deposits with pores being significantly bigger than the size of the employed model ions – reaction - III; (ii) deposits that display a sieving effect – reaction I, II and IV; and (iii) deposit that entirely block the liquid-liquid interface – reaction V.

4. Conclusions

In this work, we have used the voltammetry to study and assist the interfacial polycondensation of a number of polyamides formed at the electrified liquid-liquid interface. Optimized soft junction modification conditions were chosen to form polymeric materials derived from reactions between aqueous phase soluble 1,6-diaminohexane or *p*-phenylenediamine and acyl chlorides dissolved in the organic phase, this is 1,3,5-

benzenetricarbonyl trichloride, terephthaloyl chloride or adipoyl chloride. Formed materials were characterized using SEM, EDX and Raman Spectroscopy. Next, the microscopic liquid-liquid interface supported with a fused silica capillary was modified with all studied polyamide materials and the resulting platforms were characterized in terms of their molecular sieving properties. The effect of the deposition conditions on the ionic currents being attributed to the tetramethylammonium cation interfacial transfer were investigated. We have found that the polyamide formed as a result of the reaction between *p*-phenylenediamine and adipoyl chloride gave a porous deposit being permeable even when longer deposition times (number of applied voltammetric deposition cycles) were applied. The film formed using 1,6-diaminohexane and terephthaloyl chloride entirely blocked the interface, whereas for the other pairs the model ion (tetramethylammonium cation) transfer was inhibited only for thicker films, still being permeable to the background electrolyte ions. We believe, that proposed platform can be used as the model system for the evolution of the polymeric films derived from the interfacial polycondensation reactions.

5. Conflicts of interest

There are no conflicts to declare.

6. Acknowledgements

The presented research was financed by the National Science Centre Poland as part of the PRELUDIUM 19 project (UMO-2020/37/N/ST4/00270). The authors are also grateful to Polish National Agency For Academic Exchange and Campus France for financing PHC Polonium Project (BPN/BFR/2021/1/00006).

7. References

[1] K. Marchildon, Polyamides - Still strong after seventy years, Macromol. React. Eng. 5 (2011) 22–54. https://doi.org/10.1002/mren.201000017.

[2] J.A. Reglero Ruiz, M. Trigo-López, F.C. García, J.M. García, Functional aromatic polyamides, Polymers (Basel). 9 (2017). https://doi.org/10.3390/polym9090414.

[3] L. Shen, R. Cheng, M. Yi, W.S. Hung, S. Japip, L. Tian, X. Zhang, S. Jiang, S. Li, Y. Wang, Polyamide-based membranes with structural homogeneity for ultrafast molecular sieving, Nat. Commun. 13 (2022) 1–11. https://doi.org/10.1038/s41467-022-28183-1.

[4] Y. Wen, H. Chen, X. Zhou, Q. Deng, C. Zhao, X. Gong, A polyamide resin based method for adsorption of anthocyanins from blackberries, New J. Chem. 40 (2016) 3773–3780. https://doi.org/10.1039/c6nj00054a.

[5] X. Zhang, W. Fan, T. Liu, Fused deposition modeling 3D printing of polyamide-based composites and its applications, Compos. Commun. 21 (2020) 100413. https://doi.org/10.1016/j.coco.2020.100413.

[6] K. Piradashvili, E.M. Alexandrino, F.R. Wurm, K. Landfester, Reactions and polymerizations at the liquid-liquid interface, Chem. Rev. 116 (2016) 2141–2169. https://doi.org/10.1021/acs.chemrev.5b00567.

[7] E.L. Wittbecker, P.W. Morgan, Interfacial polycondensation. I., J. Polym. Sci. Part A Polym. Chem. 34 (1996) 521–529. https://doi.org/10.1002/pola.1996.815.

[8] K. Kowalewska, Nylon Rope Trick, Https://Www.Youtube.Com/Watch?V=S6asCwVG8zU&t=14s. (2020). https://www.youtube.com/watch?v=S6asCwVG8zU.

[9] K. Kowalewska, K. Sipa, A. Leniart, S. Skrzypek, L. Poltorak, Electrochemistry at the liquid–liquid interface rediscovers interfacial polycondensation of nylon-6,6, Electrochem. Commun. 115 (2020) 106732. https://doi.org/10.1016/j.elecom.2020.106732.

[10] D. Fermı, H.J. Lee, H.H. Girault, Electrochemistry at liquid/liquid interfaces: methodology and potential applications, Electrochim. Acta. 45 (2000) 2647–2662. https://doi.org/10.1016/S0013-4686(00)00343-1.

[11] Petr Vanysek and Luis Basaez Ramirez, Interface Between Two Immiscible Liquid Electrolytes: A Review, J. Chil. Chem. Soc. 2 (2008) 1455–1464. https://doi.org/10.4067/S0717-97072008000200002.

[12] A. Gamero-Quijano, J.A. Manzanares, S.M.B.H. Ghazvini, P.J. Low, M.D. Scanlon, Potential-Modulated Ion Distributions in the Back-to-Back Electrical Double Layers at a

Polarised Liquid|Liquid Interface Regulate the Kinetics of Interfacial Electron Transfer, ChemElectroChem. 202201042 (2022). https://doi.org/10.1002/celc.202201042.

[13] J. Strutwolf, M.D. Scanlon, D.W.M. Arrigan, Electrochemical ion transfer across liquid/liquid interfaces confined within solid-state micropore arrays - Simulations and experiments, Analyst. 134 (2009) 148–158. https://doi.org/10.1039/b815256j.

[14] R. Chen, K. Xu, M. Shen, Avocado oil, coconut oil, walnut oil as true oil phase for ion transfer at nanoscale liquid/liquid interfaces, Electrochim. Acta. 357 (2020) 136788. https://doi.org/10.1016/j.electacta.2020.136788.

[15] Z. Samec, Electrochemistry at the interface between two immiscible electolyte solutions (IUPAC technical report), Pure Appl. Chem. 76 (2004) 2147–2180. https://doi.org/10.1351/pac200476122147.

[16] S. Amemiya, Y. Kim, R. Ishimatsu, B. Kabagambe, Electrochemical heparin sensing at liquid/liquid interfaces and polymeric membranes, Anal. Bioanal. Chem. 399 (2011) 571–579. https://doi.org/10.1007/s00216-010-4056-2.

[17] R. Zazpe, C. Hibert, J. O'Brien, Y.H.Y.H. Lanyon, D.W.M.M.D.W.M. Arrigan, Ion-transfer voltammetry at silicon membrane-based arrays of micro-liquid-liquid interfaces, Lab Chip. 7 (2007) 1732–1737. https://doi.org/10.1039/b712601h.

[18] R. Ishimatsu, J. Kim, P. Jing, C.C. Striemer, D.Z. Fang, P.M. Fauchet, J.L. McGrath, S. Amemiya, Ion-selective permeability of an ultrathin nanoporous silicon membrane as probed by scanning electrochemical microscopy using micropipet-supported ITIES tips., Anal. Chem. 82 (2010) 7127–34. https://doi.org/10.1021/ac1005052.

[19] P. Borgul, K. Rudnicki, L. Chu, A. Leniart, S. Skrzypek, E.J.R. Sudhölter, L. Poltorak, Layer-by-layer (LbL) assembly of polyelectrolytes at the surface of a fiberglass membrane used as a support of the polarized liquid–liquid interface, Electrochim. Acta. 363 (2020). https://doi.org/10.1016/j.electacta.2020.137215.

[20] S. Liu, Q. Li, Y. Shao, Electrochemistry at micro- and nanoscopic liquid/liquid interfaces, Chem. Soc. Rev. 40 (2011) 2236–2253. https://doi.org/10.1039/c0cs00168f.

[21] H. Hu, S. Xie, X. Meng, P. Jing, M. Zhang, L. Shen, Z. Zhu, M. Li, Q. Zhuang, Y. Shao,

Fabrication and characterization of submicrometer- and nanometer-sized double-barrel pipets, Anal. Chem. 78 (2006) 7034–7039. https://doi.org/10.1021/ac060773r.

[22] K. Rudnicki, L. Poltorak, S. Skrzypek, E.J.R. Sudhölter, Fused silica micro-capillaries used for a simple miniaturization of the electrified liquid – liquid interface, Anal. Chem. 90 (2018) 7112–7116. https://doi.org/10.1021/acs.analchem.8b01351.

[23] L. Poltorak, A. Gamero-quijano, G. Herzog, A. Walcarius, Decorating soft electrified interfaces : From molecular assemblies to nano-objects, Appl. Mater. Today. 9 (2017) 533–550. https://doi.org/10.1016/j.apmt.2017.10.001.

[24] M.C. Collins, M. Hébrant, G. Herzog, Ion transfer at polarised liquid-liquid interfaces modified with adsorbed silica nanoparticles, Electrochim. Acta. 282 (2018) 155–162. https://doi.org/10.1016/j.electacta.2018.06.036.

[25] K. Kowalewska, K. Sipa, K. Kaczmarek, S. Skrzypek, L. Poltorak, Interfacial Synthesis of Nylon-6,6 and Its Modification with Silver-Based Nanoparticles at the Electrified Liquid-Liquid Interface, ChemElectroChem. 9 (2022). https://doi.org/10.1002/celc.202200435.

[26] N. Younan, M. Hojeij, L. Ribeaucourt, H.H. Girault, Electrochemical properties of gold nanoparticles assembly at polarised liquid|liquid interfaces, Electrochem. Commun. 12 (2010) 912–915. https://doi.org/10.1016/j.elecom.2010.04.019.

[27] M.D. Scanlon, E. Smirnov, T.J. Stockmann, P. Peljo, Gold Nanofilms at Liquid-Liquid Interfaces: An Emerging Platform for Redox Electrocatalysis, Nanoplasmonic Sensors, and Electrovariable Optics, Chem. Rev. 118 (2018) 3722–3751. https://doi.org/10.1021/acs.chemrev.7b00595.

[28] A.N.J. Rodgers, S.G. Booth, R.A.W. Dryfe, Particle deposition and catalysis at the interface between two immiscible electrolyte solutions (ITIES): A mini-review, Electrochem. Commun. 47 (2014) 17–20. https://doi.org/10.1016/j.elecom.2014.07.009.

[29] M. Platt, R.A.W. Dryfe, E.P.L. Roberts, Electrodeposition of palladium nanoparticles at the liquid-liquid interface using porous alumina templates, Electrochim. Acta. 48 (2003) 3037–3046. https://doi.org/10.1016/S0013-4686(03)00373-6.

[30] E. Smirnov, P. Peljo, M.D. Scanlon, H.H. Girault, Gold Nanofilm Redox Catalysis for

Oxygen Reduction at Soft Interfaces, Electrochim. Acta. 197 (2016) 362–373. https://doi.org/10.1016/j.electacta.2015.10.104.

[31] A. Uehara, S.G. Booth, S.Y. Chang, S.L.M. Schroeder, T. Imai, T. Hashimoto, J.F.W. Mosselmans, R.A.W. Dryfe, Electrochemical Insight into the Brust-Schiffrin Synthesis of Au Nanoparticles, J. Am. Chem. Soc. 137 (2015) 15135–15144. https://doi.org/10.1021/jacs.5b07825.

[32] V.J. Cunnane, U. Evans, Formation of oligomers of methyl- and phenyl-pyrrole at an electrified liquid/liquid interface, Chem. Commun. (1998) 2163–2164. https://doi.org/10.1039/a806365f.

[33] K. Gorgy, F. Fusalba, U. Evans, K. Kontturi, V.J. Cunnane, Electropolymerization of 2,2′:5′,2″ terthiophene at an electrified liquid-liquid interface, Synth. Met. 125 (2001) 365–373. https://doi.org/10.1016/S0379-6779(01)00474-X.

[34] M.F. Suárez-Herrera, A. Gamero-Quijano, M.D. Scanlon, Electrosynthesis of poly(2,5-dimercapto-1,3,4-thiadiazole) films and their composites with gold nanoparticles at a polarised liquid|liquid interface, Electrochim. Acta. 424 (2022) 140677. https://doi.org/10.1016/j.electacta.2022.140677.

[35] R.A. Lehane, A. Gamero-Quijano, S. Malijauskaite, A. Holzinger, M. Conroy, F. Laffir, A. Kumar, U. Bangert, K. McGourty, M.D. Scanlon, Electrosynthesis of Biocompatible Free-Standing PEDOT Thin Films at a Polarized Liquid|Liquid Interface, J. Am. Chem. Soc. 144 (2022) 4853–4862. https://doi.org/10.1021/jacs.1c12373.

[36] A. Meyer, K. Fischer, Oxidative transformation processes and products of para-phenylenediamine (PPD) and para-toluenediamine (PTD)—a review, Environ. Sci. Eur. 27 (2015). https://doi.org/10.1186/s12302-015-0044-7.

[37] S.M. Shebanov, I.K. Novikov, A. V. Pavlikov, O.B. Anańin, I.A. Gerasimov, IR and Raman Spectra of Modern Aramid Fibers, Fibre Chem. 48 (2016) 158–164. https://doi.org/10.1007/s10692-016-9761-y.

[38] J. V. Miller, E.G. Bartick, Forensic analysis of single fibers by Raman spectroscopy, Appl. Spectrosc. 55 (2001) 1729–1732. https://doi.org/10.1366/0003702011954099.

[39] N.E. Triggs, J.J. Valentine, Raman Studies of Hydrogen Bonding in Polyamides, Isr. J. Chem. 34 (1994) 89–93. https://doi.org/10.1002/ijch.199400013.

[40] B.H. Stuart, Polymer crystallinity studied using Raman spectroscopy, Vib. Spectrosc. 10 (1996) 79–87. https://doi.org/10.1016/0924-2031(95)00042-9.

[41] N. Tong, C. Zhu, C. Zhang, Y. Zhang, Study on Raman spectra of aliphatic polyamide fibers, Optik (Stuttg). 127 (2016) 21–24. https://doi.org/10.1016/j.ijleo.2015.09.180.

[42] T. Hinoue, E. Ikeda, S. Watariguchi, Y. Kibune, Thermal modulation voltammetry with laser heating at an aqueous|nitrobenzene solution microinterface: Determination of the standard entropy changes of transfer for tetraalkylammonium ions, Anal. Chem. 79 (2007) 291–298. https://doi.org/10.1021/ac061315l.

Supporting Information

Characterization of microITIES modified with polyamides

Karolina Kowalewska[a*], Karolina Kwaczyński[a], Madjid Tarabet[b], Karolina Sobczak[a], Andrzej Leniart[a], Sławomira Skrzypek[a], Manuel Dossot[b], Gregoire Herzog[b], Łukasz Półtorak[a]*

a. *Electrochemistry@Soft Interfaces Team, Department of Inorganic and Analytical Chemistry, Faculty of Chemistry, University of Lodz, Tamka 12, 91-403 Lodz, Poland.*
b. *Université de Lorraine, CNRS, LCPME, 54000 Nancy, France*

***Corresponding authors:** lukasz.poltorak@chemia.uni.lodz.pl*
karolina.kowalewska@chemia.uni.lodz.pl

Table of Content

1. Concentration fractions diagrams

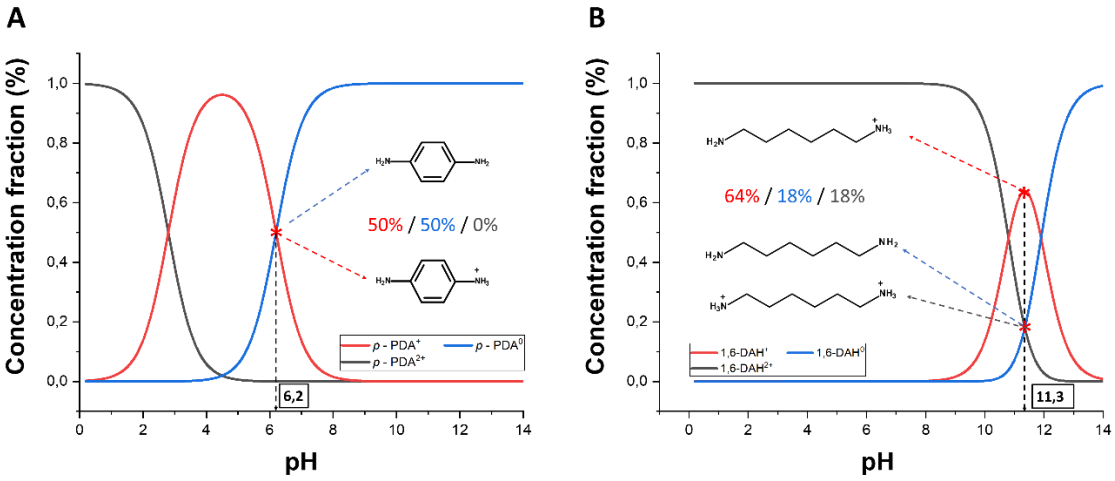

Figure S1. Concentration fraction diagrams plotted for: **A** – *p*-phenylenediamine (PPD, $pK_{a_1} = 2.8$ $pK_{a_2} = 6.2$ [1]) and **B** – 1,6-diaminohexane (1,6-DAH, $pK_{a_1} = 10.8$ $pK_{a_2} = 11.9$ [2]).

2. Electrochemical activity of monomers

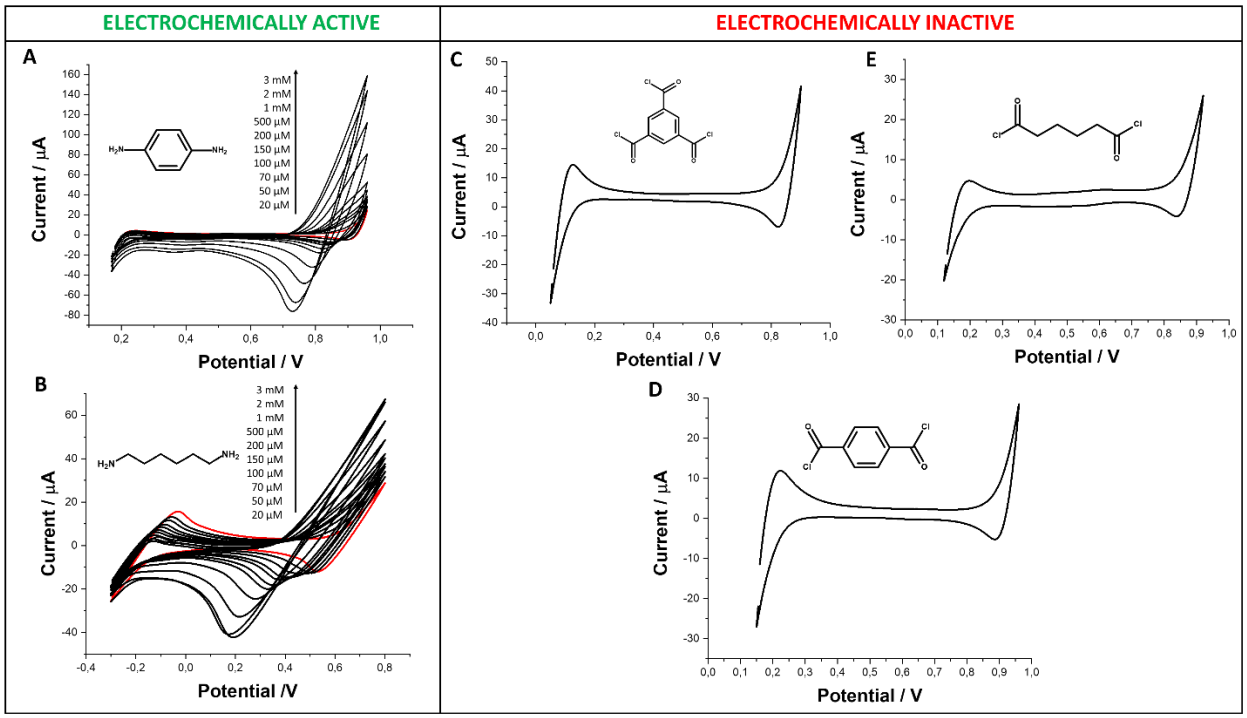

Figure S2. Cyclic voltammograms recorded in the presence of different monomers (studied alone) used during interfacial polyamides synthesis. **A** - Cyclic voltammograms corresponding to *p*-phenylenediamine recorded in the concentration range 20 µM – 3 mM. The aqueous phase: 10 mM Britton-Robbinson buffer (BRB) pH = 6.2; 20 µM – 3 mM PPD. The organic phase**:** 5 mM OE in DCE. **B** - Cyclic voltammograms corresponding to 1,6-diaminohexane recorded in the concentration range 20 µM – 3 mM. The aqueous phase: 10 mM BRB pH= 11; 20 µM – 3 mM 1,6-DAH. The organic phase**:** 5 mM OE in DCE. **C, D,** and **E** – Cyclic voltammograms recorded for 5 mM 1,3,5-benzenetricarbonyl

trichloride (C), terephtaloyl chloride (D) and adipoyl chloride (E) dissolved in organic phase. The aqueous phase: 10 mM BRB pH = 6.2. The organic phase: 5 mM OE and 5 mM acyl chloride. OE stands for the organic electrolyte. The scan rate was set to 20 $mV \cdot s^{-1}$.

3. Scanning Electron Microscopy – polyamide synthesized at macroITIES

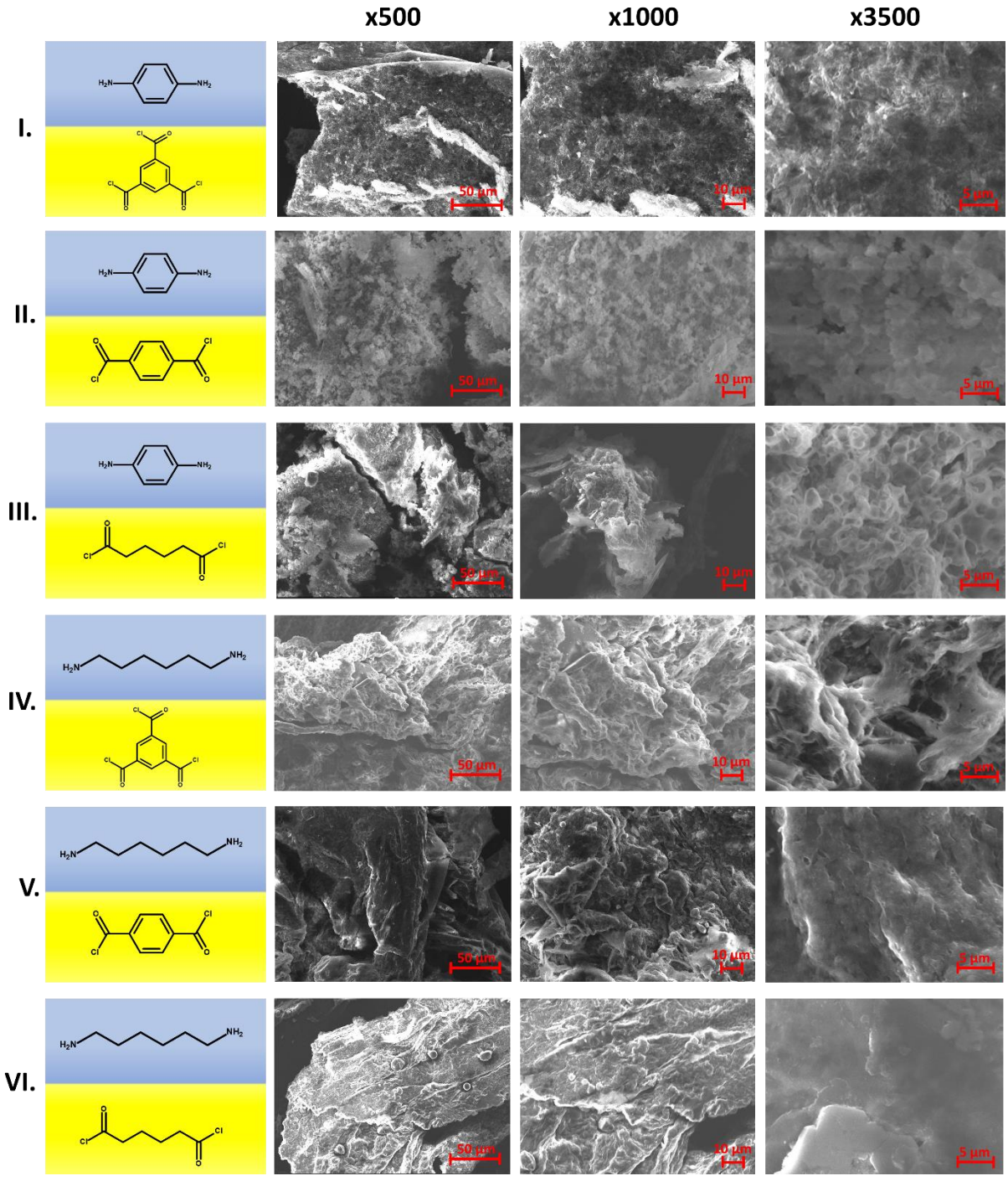

Figure S3. SEM micrographics recorded for six polyamide materials synthesized and collected from the macroITIES. 1st column shows the composition of the aqueous and the organic phase. 2nd, 3rd, and 4th columns are the SEM micrographics recorded at three different magnification: x500, x1000 and x3500, respectively. Lines provide the composition of the used monomers: **I** – *p*-phenylenediamine (aq) and 1,3,5-benzenetricarbonyl trichloride (org), **II** – *p*-phenylenediamine (aq) and terephtaloyl chloride

(org), **III** – *p*-phenylenediamine (aq) and ddipoyl chloride (org), **IV** – 1,6-diaminohexane (aq) and 1,3,5-benzenetricarbonyl trichloride (org), **V** – 1,6–diaminohexane (aq) and terephtaloyl chloride (org), **VI** – 1,6- diaminohexane (aq) and adipoyl chloride (org). The organic phase was: 5mM acyl chloride dissolve in 5mM $BTPPA^{+}TPBCl^{-}$ in 1,2 – dichloroethane, a the water phase was: 10mM diamine dissolve in 10mM Britton Robbinson Buffer in appropriate pH (PPD pH= 6.2, 1,6-DAH pH=11.0.

4. EDX

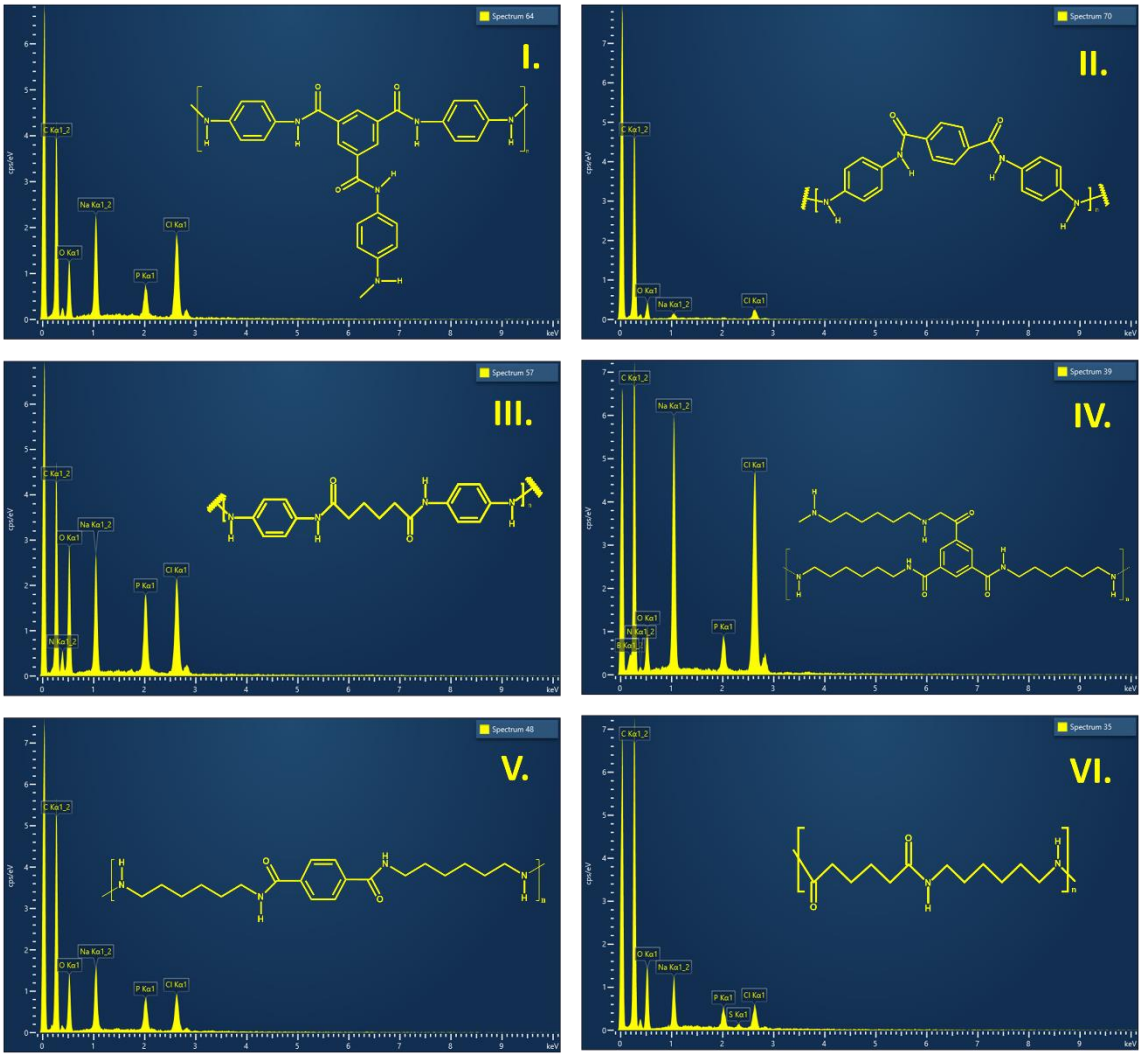

Figure S4. EDX spectra for a given polyamides (see structures) collected from the macroITIES: **I** – *p*-phenylenediamine + 1,3,5-benzenetricarbonyl trichloride, **II** – *p*-phenylenediamine + terephtaloyl chloride, **III** – *p*-phenylenediamine + adipoyl chloride, **IV** – 1,6-diaminohexane + 1,3,5-benzenetricarbonyl trichloride , **V** – 1,6–diaminohexane + terephtaloyl chloride, **VI** – 1,6-diaminohexane + adipoyl chloride.

5. Scanning Electron Microscopy – µITIES

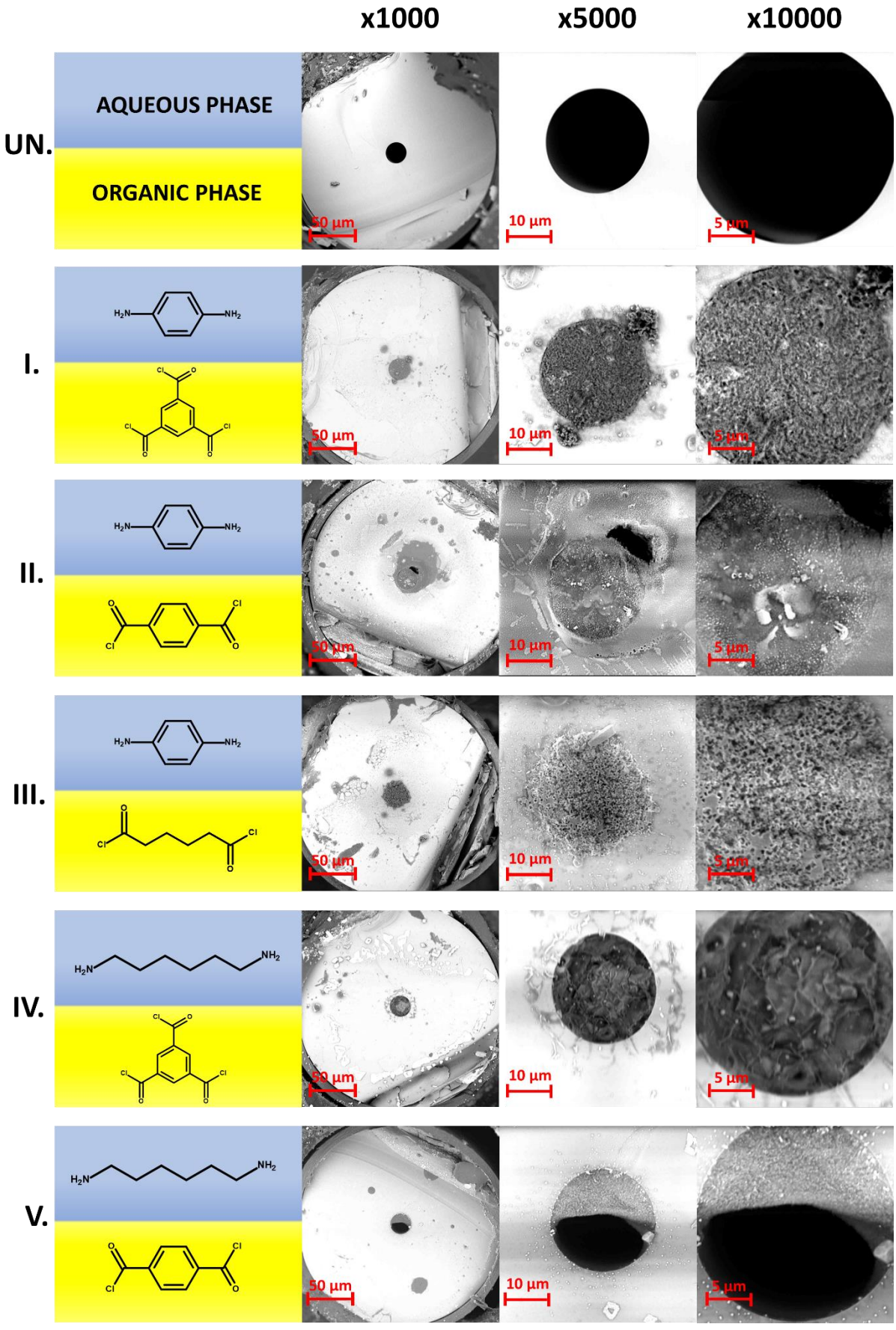

Figure S5. Micrographics recorded using scanning electron microscope (SEM) for micro-ITIES system with modified µ-LLI by polyamides materials. **UN** – unmodified µITIES system, **I** – *p*-phenylenediamine + 1,3,5-benzenetricarbonyl trichloride, **II** – *p*-phenylenediamine + terephtaloyl chloride, **III** – *p*-phenylenediamine + adipoyl chloride, **IV** – 1,6-diaminohexane + 1,3,5-benzenetricarbonyl trichloride , **V** – 1,6–diaminohexane + terephtaloyl chloride, **VI** – 1,6- diaminohexane + adipoyl chloride.

[1] A. Meyer, K. Fischer, Oxidative transformation processes and products of para-phenylenediamine (PPD) and para-toluenediamine (PTD)—a review, Environ. Sci. Eur. 27 (2015). https://doi.org/10.1186/s12302-015-0044-7.

[2] K. Kowalewska, K. Sipa, A. Leniart, S. Skrzypek, L. Poltorak, Electrochemistry at the liquid–liquid interface rediscovers interfacial polycondensation of nylon-6,6, Electrochem. Commun. 115 (2020) 106732. https://doi.org/10.1016/j.elecom.2020.106732.

Oświadczenia współautorów

STATEMENT OF THE CO-AUTHORS

We hereby declare that Karolina Kowalewska contribution to the publication, entitled "Electrochemistry at the liquid – liquid interface rediscovers interfacial polycondensation of nylon-6,6" (Electrochem. Commun. **2020**, 115, 106732) preparation process is major. Following list describes the input of all co-authors:

Karolina Kowalewska: Investigation (all electrochemical experiments), Formal analysis.

Karolina Sipa: Investigation (reproducibility study), Formal analysis.

Andrzej Leniart: Investigation (SEM analysis), Formal analysis.

Sławomira Skrzypek: Supervision, Writing – review & editing.

Łukasz Półtorak: Methodology, Visualization, Supervision, Project administration, Funding acquisition, Writing – review & editing, Writing -original draft.

Karolina Kowalewska

Łukasz Półtorak

Karolina Kwaczyński (Sipa

Andrzej Leniart

Sławomira Skrzypek

STATEMENT OF THE CO-AUTHORS

We hereby declare that Karolina Kowalewska contribution to the publication, entitled "Electroanalytical study of five carbosilane dendrimers at the interface between two immiscible electrolyte solutions" (Analyst **2021**, 146, 1376) preparation process is major. Following list describes the input of all co-authors:

Karolina Kowalewska: Investigation (all electrochemical experiments), Formal analysis, Data curation, Writing -original draft, Writing – review & editing.

Tamara Rodriguez-Prieto: Investigation (synthesis of the compounds), Writing – review & editing.

Sławomira Skrzypek: Supervision, Writing – review & editing.

Jesús Cano: Methodology, Supervision, Project administration, Writing – review & editing.

Rafael Gómez Ramírez: Methodology, Supervision , Project administration, Funding acquisition, Writing – review & editing

Łukasz Półtorak: Methodology, Visualization, Supervision, Project administration, Conceptualization, Funding acquisition, Writing – review & editing, Writing -original draft.

Karolina Kowalewska

Łukasz Półtorak

Sławomira Skrzypek

STATEMENT OF THE CO-AUTHORS

We hereby declare that Karolina Kowalewska contribution to the publication, entitled "Electroanalytical study of five carbosilane dendrimers at the interface between two immiscible electrolyte solutions" (Analyst **2021**, 146, 1376) preparation process is major. Following list describes the input of all co-authors:

Karolina Kowalewska: Investigation (all electrochemical experiments), Formal analysis, Data curation, Writing -original draft, Writing – review & editing.

Tamara Rodriguez-Prieto: Investigation (synthesis of the compounds), Writing – review & editing.

Sławomira Skrzypek: Supervision, Writing – review & editing.

Jesús Cano: Methodology, Supervision, Project administration, Writing – review & editing.

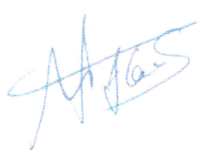

Rafael Gómez Ramírez: Methodology, Supervision , Project administration, Funding acquisition, Writing – review & editing

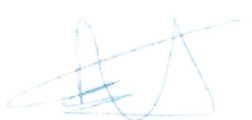

Łukasz Półtorak: Methodology, Visualization, Supervision, Project administration, Conceptualization, Funding acquisition, Writing – review & editing, Writing -original draft.

STATEMENT OF THE CO-AUTHORS

We hereby declare that Karolina Kowalewska contribution to the publication, entitled "Interfacial Deposition of Titanium Dioxide at the polarized liquid – liquid interface" (Materials, **2022**, 15, 2196) preparation process is major. Following list describes the input of all co-authors:

Karolina Kowalewska: Conceptualization, Methodology, Validation, Formal analysis, Investigation all electrochemical experiments, Data curation, Writing -original draft preparation, Writing – review & editing, Visualization, Project administration, Funding acquisition.

Karolina Sipa: Methodology, Formal analysis, Investigation, Data curation, Writing – review & editing.

Barbara Burnat: Formal analysis, Investigation (SEM analysis), Writing – review & editing.

Sławomira Skrzypek: Supervision, Writing – review & editing.

Łukasz Półtorak: Conceptualization, Methodology, Resources, Supervision, Project administration, Writing -original draft preparation, Writing – review & editing.

Karolina Kowalewska

Łukasz Półtorak

Karolina Kwaciński (Sipa

Barbara Burnat

Sławomira Skrzypek

STATEMENT OF THE CO-AUTHORS

We hereby declare that Karolina Kowalewska contribution to the publication, entitled "Interfacial synthesis of nylon-6,6 and its modification with silver-based nanoparticles at the electrified liquid – liquid interface" (ChemElectroChem **2022**, 9, e202200435) preparation process is major. Following list describes the input of all co-authors:

Karolina Kowalewska: Conceptualization, Methodology, Validation, Investigation (all electrochemical experiments), Formal analysis, Data curation, Writing -original draft preparation, Visualization, Writing – review & editing, Project administration, Funding acquisition.

Karolina Sipa: Formal analysis, Writing – review & editing.

Katarzyna Kaczmarek: Investigation (SEM analysis), Data curation, Writing – review & editing.

Sławomira Skrzypek: Writing – review & editing.

Łukasz Półtorak: Conceptualization, Supervision, Visualization, Project administration, Writing – review & editing.

Karolina Kowalewska

Łukasz Półtorak

Karolina Kwaczyński (Sipa

Katarzyna Kaczmarek

Sławomira Skrzypek

STATEMENT OF THE CO-AUTHORS

We hereby declare that Karolina Kowalewska contribution to the publication, entitled "Molecular sieving properties of microITIES modified with polyamides " (under review) preparation process is major. Following list describes the input of all co-authors:

Karolina Kowalewska: Conceptualization, Methodology, Validation, Investigation (all electrochemical experiments, characterisation), Formal analysis, Data curation, Writing - original draft preparation, Visualization, Writing – review & editing, Project administration, Funding acquisition.

Karolina Kwaczyński: Supervison, Validation, Writing – review & editing.

Madjid Tarabet: Formal analysis, Data curation (SEM analysis), Writing – review & editing.

Karolina Sobczak: Investigation (reproducibility study).

Andrzej Leniart: Data curation (SEM analysis), Writing – review & editing.

Sławomira Skrzypek: Writing – review & editing.

Manuel Dossot: Supervision, Writing – review & editing.

Gregoire Herzog: Supervision, Project administration, Writing – review & editing.

Łukasz Półtorak: Supervision, Visualization, Project administration, Writing – review & editing.

Karolina Kowalewska

Łukasz Półtorak

Karolina Kwaczyński

Karolina Sobczak

Andrzej Leniart

Sławomira Skrzypek

STATEMENT OF THE CO-AUTHORS

We hereby declare that Karolina Kowalewska contribution to the publication, entitled "Molecular sieving properties of microITIES modified with polyamides " (under review) preparation process is major. Following list describes the input of all co-authors:

Karolina Kowalewska: Conceptualization, Methodology, Validation, Investigation (all electrochemical experiments, characterisation), Formal analysis, Data curation, Writing - original draft preparation, Visualization, Writing – review & editing, Project administration, Funding acquisition.

Karolina Kwaczyński: Supervison, Validation, Writing – review & editing.

Madjid Tarabet: Formal analysis, Data curation (SEM analysis), Writing – review & editing.

Karolina Sobczak: Investigation (reproducibility study).

Andrzej Leniart: Data curation (SEM analysis), Writing – review & editing.

Sławomira Skrzypek: Writing – review & editing.

Manuel Dossot: Supervision, Writing – review & editing.

Gregoire Herzog: Supervision, Project administration, Writing – review & editing.

Łukasz Półtorak: Supervision, Visualization, Project administration, Writing – review & editing.

Grégoire Herzog

10/2/23

Manuel DOSSOT

13/02/2023

Madjid TARABET

13/02/2023